AD-A207 569 FINAL REPORT: HIGH POWER SEMICONDUCTOR LASER SOURCES 1/1
(U) CALIFORNIA INST OF TECH PASADENA A YARIV 1989
N00014-85-K-0211

UNCLASSIFIED F/G 20/12 NL

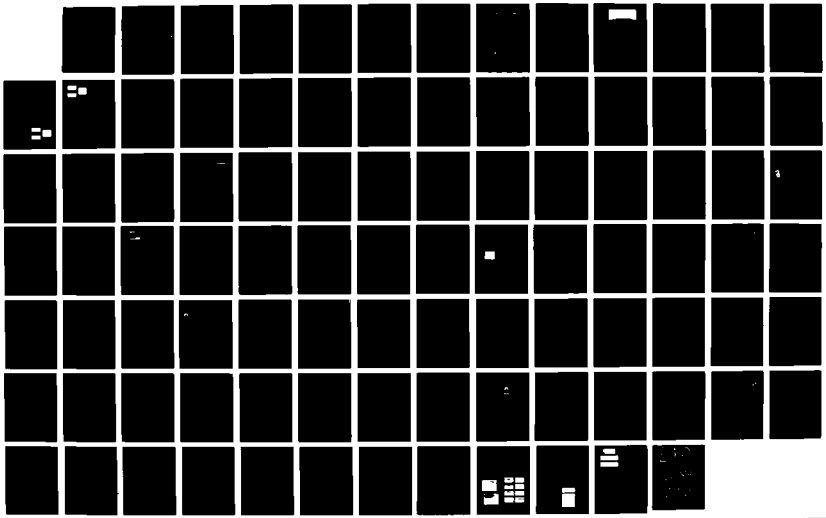

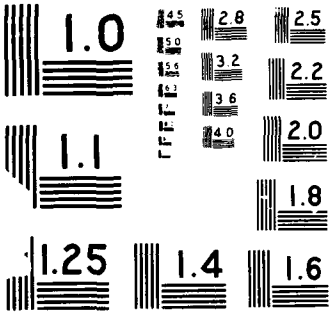
1.0
2.8
2.5
3.2
2.2
3.6
4.0
2.0
1.1
1.8
1.25
1.4
1.6

Unclassified

AD-A207 569

DOCUMENTATION PAGE

Form Approved
OMB No. 0704-0188

Unclassified	1b RESTRICTIVE MARKINGS
2a. SECURITY CLASSIFICATION AUTHORITY	3. DISTRIBUTION/AVAILABILITY OF REPORT Approved for public release; distribution unlimited.
2b. DECLASSIFICATION/DOWNGRADING SCHEDULE	
4. PERFORMING ORGANIZATION REPORT NUMBER(S) N00014-85-K-0211	5. MONITORING ORGANIZATION REPORT NUMBER(S)
6a. NAME OF PERFORMING ORGANIZATION California Institute of Technology 6b. OFFICE SYMBOL (If applicable)	7a. NAME OF MONITORING ORGANIZATION Office of Naval Research
6c. ADDRESS (City, State, and ZIP Code) Pasadena, California 91125	7b. ADDRESS (City, State, and ZIP Code) 565 S. Wilson Pasadena, California 91106-3212
8a. NAME OF FUNDING/SPONSORING ORGANIZATION Office of Naval Research 8b. OFFICE SYMBOL (If applicable)	9. PROCUREMENT INSTRUMENT IDENTIFICATION NUMBER P00001
8c. ADDRESS (City, State, and ZIP Code) 800 N. Quincy Street Arlington, VA 22217	10. SOURCE OF FUNDING NUMBERS PROGRAM ELEMENT NO. / PROJECT NO. / TASK NO / WORK UNIT ACCESSION NO

11. TITLE (Include Security Classification)
Final Report: High Power Semiconductor Laser Sources

12. PERSONAL AUTHOR(S)
A. Yariv

13a. TYPE OF REPORT	13b. TIME COVERED	14. DATE OF REPORT (Year, Month, Day)	15. PAGE COUNT
Reprint	FROM _____ TO _____		

16. SUPPLEMENTARY NOTATION The view, opinions and/or findings contained in this report are those of the author(s) and should not be construed as an official Department of the Navy position, policy, or decision unless so designated by other documentation.

17. COSATI CODES			18. SUBJECT TERMS (Continue on reverse if necessary and identify by block number)
FIELD	GROUP	SUB-GROUP	Semiconductors and quantum well lasers

19. ABSTRACT (Continue on reverse if necessary and identify by block number)

The main purpose of the research was to design and fabricate a surface emitting semiconductor laser based on multi quantum well amplification. During the contract period we have succeeded in improvement of the basic quantum well active medium so as to result in maximum gain for a given inversion density and have analyzed the fabrication of GaAs/GaAlAs multilayer dielectric reflectors for providing the optical feedback to the surface emitting semiconductor laser. We have also made significant progress in the development of diffusion techniques to provide the p and n regions adjacent to the active region for carrier injection. The progress was slower than hoped for due to the fickle nature of "mother research" but we have made considerable systematic progress. With continued effort and support we should stand a fair chance of realizing an operating surface emitting semiconductor laser.

20. DISTRIBUTION/AVAILABILITY OF ABSTRACT ☐ UNCLASSIFIED/UNLIMITED ☐ SAME AS RPT. ☐ DTIC USERS	21. ABSTRACT SECURITY CLASSIFICATION
22a. NAME OF RESPONSIBLE INDIVIDUAL	22b. TELEPHONE (Include Area Code) / 22c. OFFICE SYMBOL

DD Form 1473, JUN 86 — Previous editions are obsolete. — SECURITY CLASSIFICATION OF THIS PAGE

OFFICE OF NAVAL RESEARCH

FINAL REPORT

FOR

CONTRACT N00014-85-K-0211

TASK NO. 696-002

HIGH POWER SEMICONDUCTOR LASER SOURCES

Amnon Yariv, Principal Investigator
California Institute of Technology
Pasadena, California 91125

Reproduction in whole, or in part, is permitted for any purpose of the United States Government.

*This document has been approved for public release and sale; its distribution is unlimited.

TABLE OF CONTENTS

I. INTRODUCTION. 1

II. REPORT OF RESEARCH RESULTS. 1

III. RECOMMENDATIONS FOR FUTURE WORK 3

IV. LIST OF PROJECT RELATED REPRINTS. 7

A-1

QUALITY INSPECTED 4

I. INTRODUCTION:

The main purpose of the research supported by this grant was to design and fabricate a surface emitting semiconductor laser (SESL) based on multi quantum well amplification.

This work was to be accomplished in a number of stages:

(1) improvement of the basic quantum well active medium so as to result in maximum gain for a given inversion density;

(2) the analysis and fabrication of GaAs/GaAlAs multilayer dielectric reflectors for providing the optical feedback to the SESL.

(3) the development of diffusion techniques to provide the p and n regions adjacent to the active region for carrier injection.

(4) final operation of the whole device.

During the contract period we have succeeded in tasks (1) and (2) and have made significant progress in category (3). The progress was slower than hoped for due to the fickle nature of "mother research" but we have made considerable systematic progress. With continued effort (and support) we should stand a fair chance of realizing an operating surface emitting semiconductor laser.

The main items of progress achieved during the contract period are summarized in what follows. A list of references supported (in part) by this contract is appended.

II. REPORT OF RESEARCH RESULTS:

A. The Quantum Well Material:

We have spent a great deal of effort and resources in learning how to grow high quality MBE material for the active region (gain). This is a crucial element in the system since the total short distance of

amplification (~2μm) requires maximal gain. A parallel theoretical effort led to prediction of practical available gain of ~10^3 cm^{-1} with an injected carrier density of n~$2x10^{18}$ cm^{-3} (see Figure 1).

There are two basic approaches to designing a SEL. One method uses an optical cavity in the plane of the substrate with output coupling perpendicular to the cavity and the other method involves the formation of a vertical cavity. The latter approach is taken here. One of the main difficulties in creating a vertical cavity surface emitter is achieving sufficient gain. Due to the small cavity length (a few microns as compared to a few hundred microns for conventional structures) a very high gain coefficient is required. For this reason we are experimenting with both multiple quantum well and bulk gallium arsenide active regions. To inject carriers, two diffusions are performed: a silicon diffusion which gives an N-doped region and a zinc diffusion which gives a p doped region (see Figure 1), sandwiched between the n and p regions in an intrinsic active region into which electrons and holes are injected laterally. Both diffusions enhance the interdiffusion of gallium and aluminum to cause impurity induced disordering of the multiple quantum well in the diffused region and leave a doped region with uniform aluminum concentration which serves as both a waveguide and a source for electrons or holes.

The figure shows the proposed SESL, and the Bragg end reflectors as well as the proposed p and n diffusion to the active region.

Figure 2 shows the theoretical plot of the reflectivity of the GaAs/GaAlAs Bragg reflector stack while Figure 2 also shows the experimental data on the Bragg reflector.

We have grown Bragg reflectors with high reflectivity (>96%) and we can control the position of this reflection peak. Also, the effect of the cavity enclosed by the two Bragg reflectors has been observed through Fabry-Perot transmission peaks in the reflectance spectrum of the entire SEL structure (see Figure 2).

For electrically pumping the SEL, we have tried schemes involving Zn and Si diffusions and regrowth by LPE for the contact regions. We believe the most promising solution involves an LPE regrowth for the N-region and either another regrowth for the P-region or a Zn diffusion. Both of these current injection schemes are being pursued. When the technological problems involved in this processing have been solved, the SEL has a good chance of lasing.

An SEM of the complete laser structure including the active regions and the diffused p and n contact regions is shown in Figure 3.

The work was terminated at this stage.

II. Recommendation for Future Work:

We believe the most challenging technical problem remaining before the realization of a current injection surface emitting semiconductor laser is the problem of doped contact regions. We have made substantial progress in this direction and recommend that work in this direction continue.

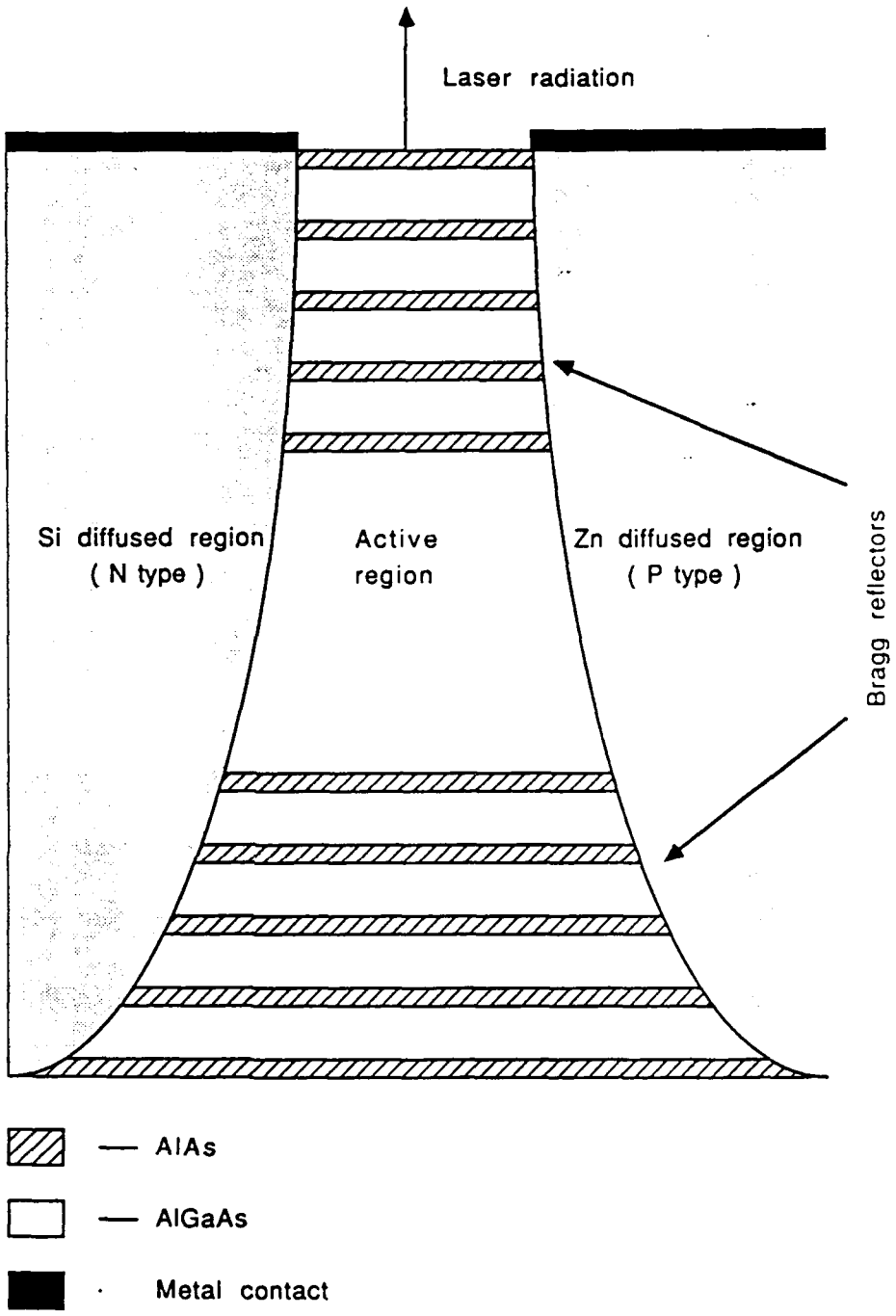

Figure 1
A schematic cross section of the device. The substrate is toward the bottom of the page and the surface is toward the top. Electrons and holes are injected laterally into the active region.

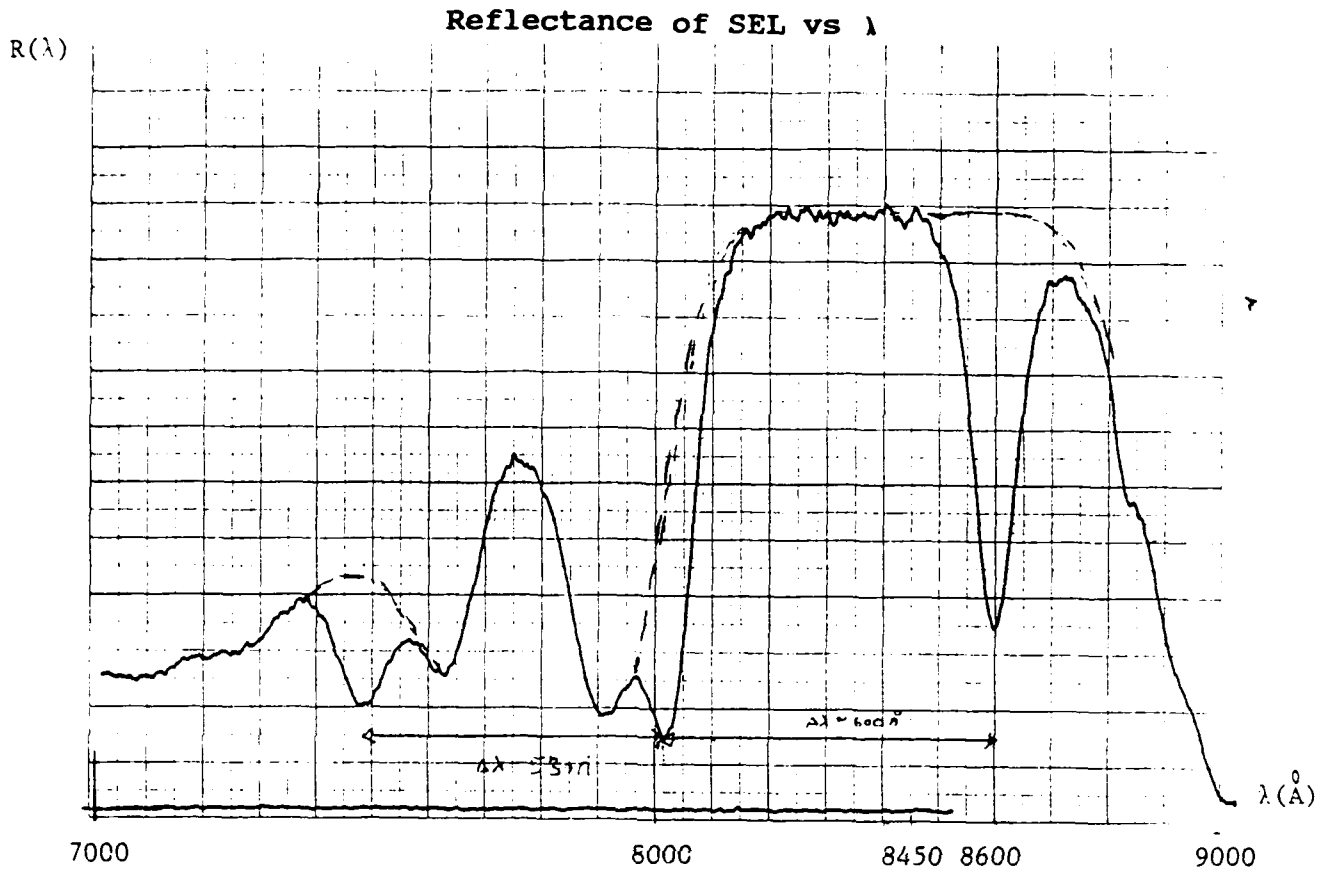

Figure 2
Reflectance curve shows Fabry-Perot transmission peaks at λ=8600Å, l=8000Å.

Dashed curve shows expected R(λ) for one Bragg reflector.

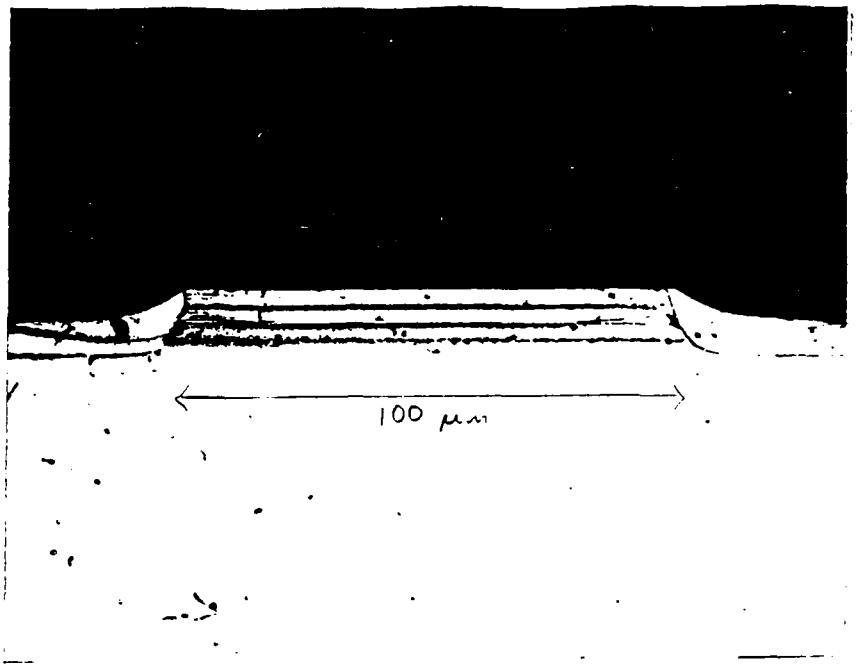

Figure 3
Cross section of an SEL structure consisting of two 25 x $(Al_{0.2}Ga_{0.8}As)_{\lambda/4}$ Bragg reflectors with a 2.4 μm GaAs active region. On both sides of the 100 μm mesa, N-AlGaAs has been regrown by LPE.

B. Reprints

The following list of reprints represent work supported partially by the subject grant.

A. Yariv, "Scaling laws and minimum threshold currents for quantum-confined semiconductor lasers," Appl. Phys. Lett. 53 (12), 1033 (Sept. 1988).

D. Mehuys, K. Mitsunaga, L. Eng, W. K. Marshall and A. Yariv, "Supermode control in diffraction-coupled semiconductor laser arrays," Appl. Phys. Lett. 53 (13) 1165 (Sept. 1988).

P. L. Derry, H. Z. Chen, H. Morkoc, A. Yariv, K. Lau, N. Bar-Chaim, K. Lee and J. Rosenberg, "Ultralow threshold graded-index separate-confinement heterostructure single quantum well (Al,Ga)As lasers," J. Vac. Sci. Technol. B 6 (2) (Mar/Apr 1988).

H. Z. Chen, A. Ghaffari, H. Morkoc, and A. Yariv, "Effect of substrate tilting on molecular beam epitaxial grown AlGaAs/GaAs lasers having very low threshold current densities," Appl. Phys. Lett. 51 (25) 2094 (Dec. 1987).

D. Mehuys, R. J. Lang, M. Mittelstein, J. Salzman, and A. Yariv, "Self-stabilized nonlinear lateral modes of broad area lasers," IEEE JQE QE-23 (11) 1909 (November 1987).

M. Mittelstein, Y. Arakawa, A. Larsson and A. Yariv, "Second quantized state lasing of a current pumped single quantum well laser," Appl. Phys. Lett. 49 (25) 1689 (Dec. 1986).

Y. Arakawa and A. Yariv, "Quantum well lasers--gain, spectra, dynamics," IEEE JQE QE-22 (9) 1887 (Sept. 1986).

R. Lang and A. Yariv, "Intermodal stability of a coupled-cavity Semiconductor Laser," IEEE JQE QE-22 (5) 631 (May 1986).

Y. Arakawa, K. Vahala and A. Yariv, "Dynamic and spectral properties of semiconductor lasers with quantum-well and quantum-wire effects," Surface Science 174, 155 (1986).

Y. Arakawa, A. Larsson, J. Paslaski and A. Yariv, "Active Q switching in a GaAs/AlGaAs multiquantum well laser with an intracavity monolithic loss modulator," Appl. Phys. Lett. 48 (9) 561 (March 1986).

Y. Arakawa and A. Yariv, "Theory of gain, modulation response and spectral linewidth in AlGaAs quantum well lasers," IEEE JQE QE-21 (10) 1666 (Oct. 1985).

Unclassified
SECURITY CLASSIFICATION OF THIS PAGE

REPORT DOCUMENTATION PAGE

Form Approved
OMB No. 0704-0188

1a. REPORT SECURITY CLASSIFICATION Unclassified	1b. RESTRICTIVE MARKINGS
2a. SECURITY CLASSIFICATION AUTHORITY	3. DISTRIBUTION/AVAILABILITY OF REPORT Approved for public release; distribution unlimited.
2b. DECLASSIFICATION/DOWNGRADING SCHEDULE	
4. PERFORMING ORGANIZATION REPORT NUMBER(S) N00014-85-K-0211	5. MONITORING ORGANIZATION REPORT NUMBER(S) 696-002
6a. NAME OF PERFORMING ORGANIZATION California Institute of Technology 6b. OFFICE SYMBOL (If applicable)	7a. NAME OF MONITORING ORGANIZATION Office of Naval Research
6c. ADDRESS (City, State, and ZIP Code) Pasadena, California 91125	7b. ADDRESS (City, State, and ZIP Code) 565 S. Wilson Pasadena, California 91106-3212
8a. NAME OF FUNDING/SPONSORING ORGANIZATION Office of Naval Research 8b. OFFICE SYMBOL (If applicable)	9. PROCUREMENT INSTRUMENT IDENTIFICATION NUMBER
8c. ADDRESS (City, State, and ZIP Code) 800 N. Quincy Street Arlington, VA 22217	10. SOURCE OF FUNDING NUMBERS PROGRAM ELEMENT NO. / PROJECT NO. / TASK NO / WORK UNIT ACCESSION NO

11. TITLE (Include Security Classification)
Supermode control in diffraction-coupled semiconductor laser arrays

12. PERSONAL AUTHOR(S)
D. Mehuys, K. Mitsunaga, L. Eng, W. K. Marshall and A. Yariv

13a. TYPE OF REPORT	13b. TIME COVERED	14. DATE OF REPORT (Year, Month, Day)	15. PAGE COUNT
Reprint	FROM _____ TO _____	1988 September	3

16. SUPPLEMENTARY NOTATION The view, opinions and/or findings contained in this report are those of the author(s) and should not be construed as an official Department of the Navy position, policy, or decision unless so designated by other documentation.

17. COSATI CODES			18. SUBJECT TERMS (Continue on reverse if necessary and identify by block number)
FIELD	GROUP	SUB-GROUP	Semiconductors

19. ABSTRACT (Continue on reverse if necessary and identify by block number)

Supermode control is demonstrated theoretically and experimentally in diffraction-coupled semiconductor laser arrays. A linear theory is presented to determine the supermode threshold gain as a function of the coupling cavity length. By fabricating devices with different coupling cavity lengths, array operation in both the fundamental and highest order supermodes is achieved.

20. DISTRIBUTION/AVAILABILITY OF ABSTRACT ☐ UNCLASSIFIED/UNLIMITED ☐ SAME AS RPT ☐ DTIC USERS	21. ABSTRACT SECURITY CLASSIFICATION unclassified
22a. NAME OF RESPONSIBLE INDIVIDUAL	22b. TELEPHONE (Include Area Code) / 22c. OFFICE SYMBOL

DD Form 1473, JUN 86 Previous editions are obsolete SECURITY CLASSIFICATION OF THIS PAGE

Supermode control in diffraction-coupled semiconductor laser arrays

P. Mehuys, K. Mitsunaga,[a] L. Eng, W. K. Marshall, and A. Yariv
Department of Applied Physics, 128-95, California Institute of Technology, Pasadena, California 91125

(Received 29 April 1988; accepted for publication 19 July 1988)

464

Supermode control is demonstrated theoretically and experimentally in diffraction-coupled semiconductor laser arrays. A linear theory is presented to determine the supermode threshold gain as a function of the coupling cavity length. By fabricating devices with different coupling cavity lengths, array operation in both the fundamental and highest order supermodes is achieved.

Conventional semiconductor laser arrays are formed by placing many single-mode waveguides in close proximity, so that the dominant coupling mechanism is evanescent overlap. In practice, unfortunately, the eigenmode with the highest modal gain is not the fundamental supermode, but that which has adjacent array elements coupled π radians out-of-phase. The result is an undesirable double-lobed far field.

Diffraction-coupled arrays represent one approach towards achieving fundamental supermode operation, and consequently have received growing attention.[1-6] In this geometry, illustrated in Fig. 1, the channels are optically isolated for some length L, and then are allowed to couple by "diffraction" in a common end region of length D. Thus the coupling is discrete, rather than distributed, and the phase of the coupling constant is determined by D. If D is chosen so that the phase difference between the self-reflection and that from nearest neighbors is 2π, for example, adjacent elements are expected to lock in phase and the array should operate in the fundamental supermode. In this letter, we investigate control of the lasing supermode by optimization of the length of the diffraction region. We present both analysis and experimental results for the device of Fig. 1.

For the purpose of analysis, consider an array with N channels of suitable width w and effective index step to support a single waveguide mode $e_n(x)$, where x is the lateral dimension. Let $\mathbf{e}$ be an $N \times 1$ column vector whose elements are the complex amplitude of the field in each channel at the left-hand edge of the array region. This vector is then propagated down the length of the array and reflected at its interfaces by suitable matrices $\mathbf{P}$, $\mathbf{R}_l$, and $\mathbf{R}_r$, as indicated in Fig. 1. Requiring $\mathbf{e}$ to reproduce itself after one round trip gives the oscillation condition

$$\mathbf{e} = \mathbf{R}_l\mathbf{P}\mathbf{R}_r\mathbf{P}\mathbf{e}, \tag{1}$$

where $\mathbf{P}$ is the propagation matrix in the channeled section and $\mathbf{R}_l$, $\mathbf{R}_r$ are effective reflectivity matrices at the left- and right-hand edges of the *array* region (i.e., $\mathbf{R}_r$ includes the effect of the diffraction region). Assuming identical channels of length L, the propagation matrix is simply $\mathbf{P} = \exp(i\sigma L)I$, where I is the identity matrix, and σ, the unknown propagation constant, is given by $\sigma = (n_0/c)\omega - i(\gamma/2)$. Here ω is the radian frequency, γ is the required threshold gain, n_0 is the effective index of the channel, and c is the speed of light in free space. The left-hand reflection matrix is simply $\mathbf{R}_l = r_0 I$, where r_0 is the amplitude reflectivity of the TE mode at the GaAs-air interface ($r_0 \simeq \sqrt{R}$, $R \simeq 0.3$). The round-trip condition (1) can then be written as

$$(r_0 e^{i2\sigma L}\mathbf{R}_r - I)\mathbf{e} = 0. \tag{2}$$

Hence, $r_0^{-1}\exp(-i2\sigma L)$ is an eigenvalue of the matrix $\mathbf{R}_r$ and the array supermodes are its eigenvectors. It remains only to compute the effective reflection matrix $\mathbf{R}_r$ of the diffraction region.

We model the diffraction region as a cavity of width W which supports a large number, M, of "slab waveguide" modes $c_m(x)$. Their amplitudes can be described by an $M \times 1$ column vector $\mathbf{c}$. To compute the reflection matrix $\mathbf{R}_r$, we first couple the channel modes $\mathbf{e}$ into the cavity basis $\mathbf{c}$ via an $N \times M$ coupling matrix $\mathbf{V}$: $\mathbf{e} = \mathbf{V}\mathbf{c}$. The cavity modes can then be propagated and reflected from a planar mirror (using their known propagation constants β_m) via the $M \times M$ matrix $\mathbf{P}'$ whose elements are $P'_{mn} = r_0 \exp(i2\beta_m D)\delta_{mn}$, where δ_{mn} is the Kronecker delta. After projecting back onto the channel basis with the transpose $\mathbf{V}^t$ of the coupling matrix, $\mathbf{e}_{\text{after}} = \mathbf{V}\mathbf{P}'\mathbf{V}^t\mathbf{e}_{\text{before}}$, so that the reflection matrix for the diffraction region is

$$\mathbf{R}_r = \mathbf{V}\mathbf{P}'\mathbf{V}^t. \tag{3}$$

Note that $\mathbf{V}\mathbf{V}^t \simeq I$ (small radiation loss), but $\mathbf{V}^t\mathbf{V} \neq I$ (reflecting significant coupling loss). For our calculations, we have assumed strong effective index guiding for both the array and diffraction regions, so that

$$e_n(x) = \sqrt{2/w}\cos[\pi(x - nl)/w], \quad x \in (nl \pm w/2)$$
$$c_m(x) = \sqrt{2/W}\sin[m\pi(x + W/2)/W], \quad x \in (\pm W/2). \tag{4}$$

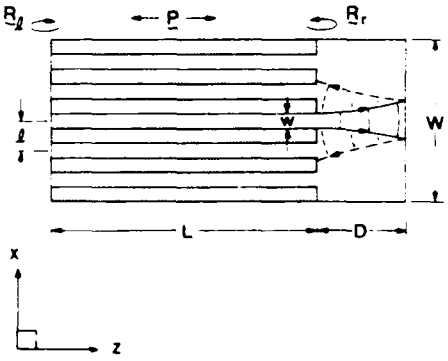

FIG. 1. Diffraction-coupled array geometry. The shaded areas represent optical isolation. The array channels have width w and length L while the diffraction region is of width W and length D. The array period is l.

[a] On leave from Mitsubishi Electric Corporation, Amagasaki, Hyogo, Japan.

 © 1988 American Institute of Physics

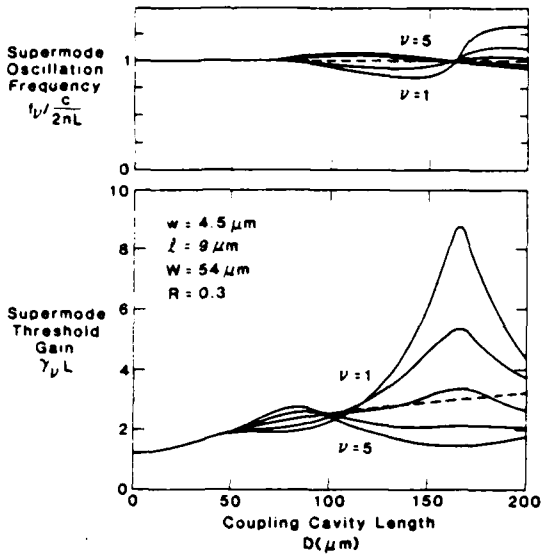

FIG. 2. Theoretical threshold gain and oscillation frequency for the supermodes of a five-element diffraction-coupled array, as a function of coupling length, D. The $\nu = 1$ mode is the fundamental supermode. The dashed line gives the result for uncoupled lasers.

and the propagation constants β_m in the diffraction region are approximately $\beta_m^2 = k_0^2 n_0^2 - m^2\pi^2/W^2$, where $k_0 = 2\pi/\lambda$ is the free-space propagation constant. The elements of the coupling matrix are therefore given by

$$v_{nm} = \frac{2}{\sqrt{wW}} \int_{nl-w/2}^{nl+w/2} dx \times \cos\left(\pi \frac{x - nl}{2}\right) \sin\left(m\pi \frac{x + W/2}{W}\right). \quad (5)$$

After calculating $\mathbf{R}_\nu$, the eigenvalue problem (2) is solved numerically. Figure 2 illustrates the threshold gains and oscillation frequencies as a function of the diffraction region length for a five-element array with channel width $w = 5$ μm, diffraction region width $W = 54$ μm, and array period $l = 9$ μm. The number of cavity modes $c_m(x)$ used was $M = 50$.

Firstly, we observe periodic oscillations in the threshold gains as a function of D. This corresponds to the variation in phase of the coupling constants. Secondly, these oscillations are bounded by an envelope whose width increases from zero at $D = 0$ to a very large value. This is only partly due to the increase in absolute value of the coupling constant as D is increased; the primary mode discrimination arises due to the varied losses experienced by the supermodes as they couple back from the diffraction region into the array. The fundamental supermode ($\nu = 1$) has the lowest threshold gain at a length of $D = 80$ μm while the highest order supermode ($\nu = 5$) has the lowest threshold gain for $D = 160$ μm. The dashed line indicates the result for uncoupled lasers. According to Basov,[7] supermodes with diffraction losses higher than those of uncoupled lasers are unstable.

We have fabricated seven-element diffraction-coupled arrays from GaAs/GaAlAs graded-index separate confinement multiple quantum well material grown in our laboratory by molecular beam epitaxy. The array elements were 4.5-μm-wide ridge waveguides formed by wet chemical etching through the contact and upper cladding layers to within 0.1–0.2 μm of the active region. This provides strong effective index guiding, and by further placing the elements on relatively wide centers of 9 μm, optical isolation between the waveguides was achieved. A Cr/Au contact evaporated over the device formed ohmic contacts to the top of the ridge waveguides and to the diffraction region (i.e., to the p^+-GaAs contact layer), while a Schottky barrier was formed between the ridges where the p-AlGaAs cladding layer was exposed.[1]

The effect of the diffraction region length was observed experimentally by cleaving devices with D varying up to 150 μm. The array region length was approximately 250 μm long for all devices. Arrays with no diffraction region showed no evidence of coherence between elements, as inferred from far fields and spectrally resolved nearfields. Figures 3 and 4 show the near fields at both facets and the far field (which is the same on both sides) for devices with diffraction regions of $D = 80$ μm and $D = 150$ μm, respectively. The output power level is 100 mW in both cases. The near field on the array side shows the number of lasing channels, while on the coupling cavity side, the two-dimensional diffraction pattern of the lasing supermode is visible. The far field of Fig. 3 has a strong central lobe at 0°, indicating operation in the fundamental supermode, but also exhibits first and second diffraction orders. The far-field lobe spacing corresponds closely to the theoretically predicted value of 5.5° for channels on 9 μm centers, and the width of each lobe is about twice the diffraction limit. The overall envelope is about 15° in width, corresponding to the spot size of about 3 μm for each individual channel. The far field of Fig. 4 has no lobe at 0°; however, but is primarily double lobed with higher diffraction orders visible as well, indicating operation in a higher order supermode. The near-field pattern on the diffraction side is the signature of the highest order supermode. Note that the higher diffraction orders can be suppressed by increasing the ratio w/l.

The threshold and differential quantum efficiency of

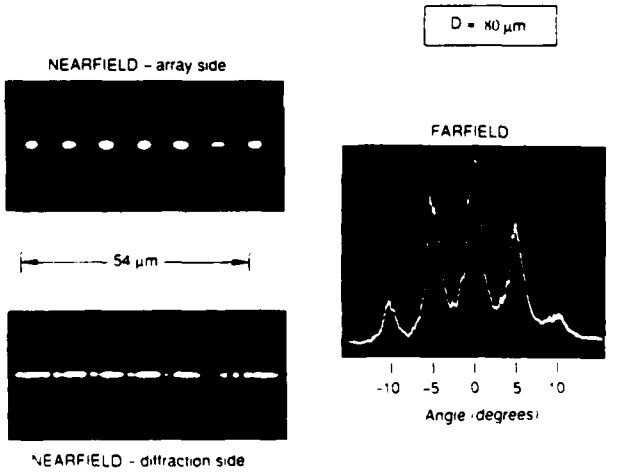

FIG. 3. Experimental results for a seven-element array with $D = 80$ μm. Near fields on the array and diffraction sides, plus the far field at an output power of 100 mW.

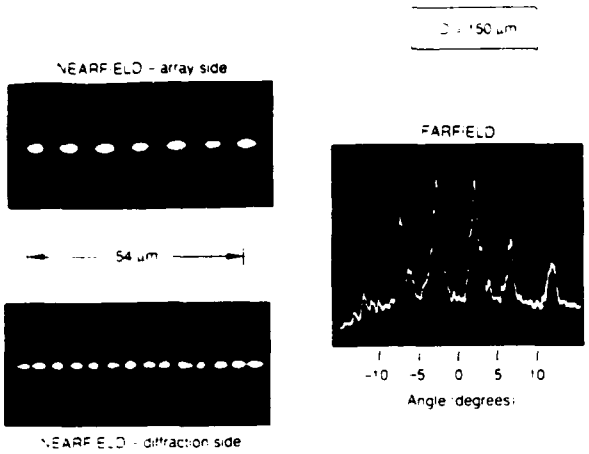

FIG. 4. Experimental results for a seven-element array with $D = 150\ \mu m$. Near fields on the array and diffraction sides, plus the far field at an output power of 100 mW.

these devices were 400 mA and 42%, respectively. This is to be compared with 200 mA and 66% for broad area lasers of comparable size fabricated from the same wafer. The simultaneous appearance of increased threshold, lower differential quantum efficiency, and clean near fields and far fields compared with broad-area lasers is closely correlated with achieving a good etch to within 0.1–0.2 μm of the active region. This is necessary to strongly confine the light to the channels of the array region, thereby minimizing evanescent overlap between the channels. At this point the coupling loss between the diffraction region and the array region becomes significant. Consequently a strong asymmetry in the output power is achieved, with roughly 50% more power output through the diffraction region.

In summary, we have demonstrated theoretically and experimentally the effect of the length of the diffraction region in controlling the lasing supermode in diffraction-coupled semiconductor laser arrays. Operation in the fundamental and highest order supermodes at an output power level of 100 mW was achieved by optimizing the length of the diffraction region. The research described in this letter was conducted in the Applied Physics department, California Institute of Technology, with the support of the Office of Naval Research and the National Science Foundation. Mr. Marshall was supported in part by a fellowship from Caltech's Program in Advanced Technologies, supported by Aerojet-General, General Motors, and TRW. The authors appreciate helpful discussions with M. Mittelstein.

[1] J. Katz, S. Margalit, and A. Yariv, Appl. Phys. Lett. **42**, 554 (1983).
[2] T. R. Chen, K. L. Yu, B. Chang, A. Hasson, S. Margalit, and A. Yariv, Appl. Phys. Lett. **43**, 136 (1983).
[3] J. J. Yang and M. Jansen, Electron. Lett. **22**, 2 (1986).
[4] S. Wang, J. Z. Wilcox, M. Jansen, and J. J. Yang, Appl. Phys. Lett. **48**, 1770 (1986).
[5] J. Z. Wilcox, M. Jansen, J. J. Yang, S. S. Ou, M. Sergant, and W. Simmons, Appl. Phys. Lett. **50**, 1319 (1987).
[6] J. Z. Wilcox, M. Jansen, J. Yang, G. Peterson, A. Silver, W. Simmons, S. S. Ou, and M. Sergant, Appl. Phys. Lett. **51**, 631 (1987).
[7] N. Basov, F. Belenov, and V. Letokhov, Sov. Phys. Tech. Phys. **10**, 845 (1965).

Unclassified
SECURITY CLASSIFICATION OF THIS PAGE

REPORT DOCUMENTATION PAGE

Form Approved
OMB No. 0704-0188

1a. REPORT SECURITY CLASSIFICATION Unclassified	1b. RESTRICTIVE MARKINGS
2a. SECURITY CLASSIFICATION AUTHORITY	3. DISTRIBUTION/AVAILABILITY OF REPORT Approved for public release; distribution unlimited.
2b. DECLASSIFICATION/DOWNGRADING SCHEDULE	
4. PERFORMING ORGANIZATION REPORT NUMBER(S) N00014-85-K-0211	5. MONITORING ORGANIZATION REPORT NUMBER(S) 696-002
6a. NAME OF PERFORMING ORGANIZATION California Institute of Technology 6b. OFFICE SYMBOL (If applicable)	7a. NAME OF MONITORING ORGANIZATION Office of Naval Research
6c. ADDRESS (City, State, and ZIP Code) Pasadena, California 91125	7b. ADDRESS (City, State, and ZIP Code) 565 S. Wilson Pasadena, California 91106-3212
8a. NAME OF FUNDING/SPONSORING ORGANIZATION Office of Naval Research 8b. OFFICE SYMBOL (If applicable)	9. PROCUREMENT INSTRUMENT IDENTIFICATION NUMBER p00001
8c. ADDRESS (City, State, and ZIP Code) 800 N. Quincy Street Arlington, VA 22217	10. SOURCE OF FUNDING NUMBERS PROGRAM ELEMENT NO. / PROJECT NO. / TASK NO / WORK UNIT ACCESSION NO.

11. TITLE (Include Security Classification)
Scaling laws and minimum threshold currents for quantum-confined semiconductor lasers

12. PERSONAL AUTHOR(S)
A. Yariv

13a. TYPE OF REPORT	13b. TIME COVERED	14. DATE OF REPORT (Year, Month, Day)	15. PAGE COUNT
Reprint	FROM _____ TO _____	1988 September	3

16. SUPPLEMENTARY NOTATION The view, opinions and/or findings contained in this report are those of the author(s) and should not be construed as an official Department of the Navy position, policy, or decision unless so designated by other documentation.

17. COSATI CODES			18. SUBJECT TERMS (Continue on reverse if necessary and identify by block number)
FIELD	GROUP	SUB-GROUP	Semiconductor Lasers

19. ABSTRACT (Continue on reverse if necessary and identify by block number)

Basic scaling laws are derived for bulk, two-dimensional (quantum well) and one-dimensional (quantum wire) semiconductor lasers. Starting from quantum derivation of the optical properties of confined carriers, the dimensional dependencies of the scaling laws are made explicit. Threshold currents of ∿100 and 2-3μA are predicted for single quantum well and quantum wire lasers, respectively. The basic considerations of this analysis were used recently to obtain ultralow threshold quantum well lasers (P.L. Derry, A. Yariv, K. Lau, N. Bar-Chaim, K. Lee and J. Rosenberg, Appl. Phys. Lett. 50, 1773 (1987)).

20. DISTRIBUTION/AVAILABILITY OF ABSTRACT ☒ UNCLASSIFIED/UNLIMITED ☐ SAME AS RPT. ☐ DTIC USERS	21. ABSTRACT SECURITY CLASSIFICATION unclassified
22a. NAME OF RESPONSIBLE INDIVIDUAL	22b. TELEPHONE (Include Area Code) (818)356-4821 / 22c. OFFICE SYMBOL

DD Form 1473, JUN 86 Previous editions are obsolete. SECURITY CLASSIFICATION OF THIS PAGE

Scaling laws and minimum threshold currents for quantum-confined semiconductor lasers

Amnon Yariv
California Institute of Technology, Pasadena, California 91125

(Received 3 May 1988; accepted for publication 11 July 1988)

Basic scaling laws are derived for bulk, two-dimensional (quantum well) and one-dimensional (quantum wire) semiconductor lasers. Starting from quantum derivation of the optical properties of confined carriers, the dimensional dependencies of the scaling laws are made explicit. Threshold currents of ~ 100 and 2–3 μA are predicted for single quantum well and quantum wire lasers, respectively. The basic considerations of this analysis were used recently to obtain ultralow threshold quantum well lasers [P. L. Derry, A. Yariv, K. Lau, N. Bar-Chaim, K. Lee, and J. Rosenberg, Appl. Phys. Lett. **50**, 1773 (1987)].

In semiconductor lasers the separate and precise control of electronic (gain) and optical confinement made possible by epitaxial crystal growth and fine lithography make for a rich interplay between "physics" and "geometry"—an interplay which determines the laser threshold. In this letter we show, starting with the fundamental confinement physics, how the threshold currents of conventional bulk (three-dimensional), two-dimensional (quantum well), and one-dimensional (quantum wire) lasers depend on the respective geometrical and physical parameters, and then derive the relevant basic scaling laws for the threshold currents of each class.

The basic generic laser configuration is illustrated in Fig. 1. The active region is a rectangular prism with dimensions $L_z \times L_y \times L$ which is embedded within the optical mode volume $d \times W \times L$. In the case of quantum wells and quantum wires we take the potential well depth as infinite (this puts a limit, in practice, on the smallest well dimensions) and assume that only the first quantized states ($n = 1$) are involved.

The first major consideration is that of the transparency density. It is defined as the injected carrier density which renders the active region transparent. Clearly, the maintenance of these densities establishes a lower limit on the threshold currents. As an example, we will calculate the transparency density of a quantum wire with equal electron and hole effective masses ($m_e = m_h$) whose energy diagram is shown in Fig. 2. The transparency condition for an inverted population of Fermions obtains when the condition

$$\hbar\omega = E_{FC} - E_{FV}$$

at the frequency ω of maximum gain, where E_{FC} and E_{FV} are the quasi-Fermi levels for the conduction band and valence band, respectively, since maximum gain is exercised by $\hbar\omega = E_g + (\epsilon_{1,1})_C + (\epsilon_{1,1})_V$. The transparency condition in the case $m_C = m_V$ is obtained when the quasi-Fermi level in the conduction band E_{FC} coincides with the first quantized level $\epsilon_{1,1}$ and E_{FV} with the first quantized level in the valence band. The total number of electrons (or holes) per unit length at transparency is then obtained by integrating the product of the density of states function and the Fermi distribution function from $\epsilon_{1,1}$ to infinity. We neglect contributions from higher subbands which are effectively cut off by the Fermi function:

$$N_{1D}^{tr}\left(\frac{\text{electrons}}{m}\right) = \frac{\sqrt{2m_C}}{\pi\hbar}\int_{\epsilon_{1,1}}^{\infty}\frac{(E_c-\epsilon_{1,1})^{-1/2}}{e^{(E_c-\epsilon_{1,1})/kT}+1}\,dE_c \tag{1}$$

$$= (\sqrt{2m_C}/\pi\hbar)\times 1.072(kT)^{1/2}. \tag{2}$$

The key observation as far as scaling is concerned is that N_{1D}^{tr} is the *lineal* (electrons per unit length) density and that it is *independent* of the cross-sectional dimensions L_z and L_y of the quantum wire. Similar considerations in the case of a quantum well lead to a transparency (area) density

$$N_{2D}^{tr}\left(\frac{\text{electrons}}{m^2}\right) = \frac{m_C}{\pi\hbar^2}\int_{\epsilon_1}^{\infty}\frac{dE_c}{e^{(E_c-\epsilon_1)/kT}+1} = \frac{m_C kT}{\pi\hbar^2}\ln 2, \tag{3}$$

which is independent of the quantum well thickness L_z.

Numerical calculation of the transparency densities using the actual values of m_C and m_V in, say, GaAs, gives values three to four times larger than the values of Eqs. (2) and (3). The transparency requirements[1] can be summarized in

$$\begin{aligned} N_{3D}^{tr} &\sim 1.5\times 10^{18}\ \text{cm}^{-3},\\ N_{2D}^{tr} &\sim 1.5\times 10^{12}\ \text{cm}^{-2},\\ N_{1D}^{tr} &\sim 1.5\times 10^{6}\ \text{cm}^{-1}. \end{aligned} \tag{4}$$

The key point to reemphasize is the independence of the above values of N^{tr} of the confinement geometry and the *different* physical dimension of the transparency density in each generic case.

The bulk gains, i.e., gains experienced by a hypothetical optical wave which is completely confined to the active region, can be expressed near the transparency condition by

$$(3D)g_{3D} = g'_{3D}(N_{3D} - N_{3D}^{tr}).$$

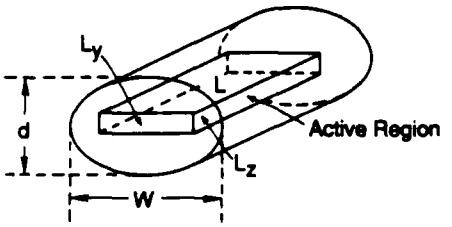

FIG. 1. Basic electron confinement and optical mode geometries.

 © 1988 American Institute of Physics

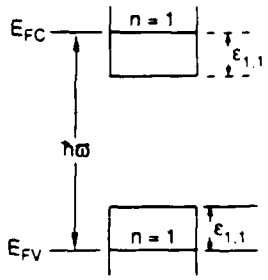

FIG. 2. Energy level diagram of the quantum-confined carriers.

The corresponding expressions for the 2D and 1D cases require some thought. Consider the 2D case. Transparency occurs when $N_{2D} = N_{2D}^{tr}$ (electrons/cm^2). The bulk gain, on the other hand, depends on the *volumetric density* of carriers.[1] We can satisfy both requirements by writing the bulk gain as

$$(2D)g_{2D} = g'_{2D}\left(\frac{N_{2D}}{L_z}\right) - \frac{N_{2D}^{tr}}{L_z}, \tag{5}$$

where g'_{2D} is a constant. In a similar fashion,

$$(1D)g_{1D} = g'_{2D}\left(\frac{N_{1D}}{L_z L_y} - \frac{N_{1D}^{tr}}{L_z L_y}\right).$$

The g's are constant specific to the material and the dimension of the confinement. They are called the differential gain constant, the differential gain constants, and the explicit dimensional dependencies (i.e., on L_z and L_y) of the three cases follow from basic quantum-induced transition rate considerations. This dependence, as well as those expressed by Eq. (4), is central to what follows.

We will next derive expressions for the threshold current densities for lasers whose modes propagate along the axis x of the active region. First consider the three-dimensional case. The threshold condition is

$$\Gamma g'_{3D}(N - N_{3D}^{tr}) = \Gamma\alpha_{fc} + (1/L)\ln R^{-1} + \alpha_{scatt}, \tag{6}$$

where $\Gamma \sim L_z/d$ is the optical confinement factor, $\alpha_{fc} = bN_{3D}$ is the bulk free-carrier absorption coefficient of the active region material, and α_{scatt} is the scattering loss of the mode. Solving for N and taking the threshold current as $(N_{3D}eV_a/\tau)$, where $V_a = WL_zL$ is the volume of the active region and τ the carrier lifetime, leads to

$$(I_{th})_{3D}\left(\frac{\eta\tau}{e}\right) = N_{3D}^{tr}(WL_zL) + \left(\frac{Wd}{g'_{3D}}\right)\ln R^{-1} + \frac{(WLd)}{g'_{3D}}\alpha_{scatt}, \tag{7}$$

where $\eta \equiv 1 - b/g'_{3D}$.

A similar calculation for a quantum well, but taking $\alpha_{fc} = bN_{2D}/L_z$ and, as before $\Gamma = L_z/d$, gives

$$(I_{th})_{2D}\left(\frac{\eta\tau}{e}\right) = N_{2D}^{tr}(WL) + \frac{(Wd)}{g'_{2D}}\ln R^{-1} + \frac{(WLd)}{g'_{2D}}\alpha_{scatt}. \tag{8}$$

In the quantum wire case we take $\Gamma = L_zL_y/dW$, leading to

$$(I_{th})_{1D}\left(\frac{\eta\tau}{e}\right) = N_{1D}^{tr}L + \frac{(Wd)}{g'_{1D}}\ln R^{-1} + \frac{(WLd)}{g'_{1D}}\alpha_{scatt}. \tag{9}$$

Equations (7)–(9) are the basic scaling relations for the three generic laser classes. The quantum confinement physics is now represented explicitly by the appropriate geometry-independent transparency densities.

The scaling laws explain some basic observations and act as design guides. For example, in a conventional (three-dimensional) laser the first term on the right side of Eq. (7) dominates, which explains the length (L) and active region thickness (L_z) dependence of I_{th} in such lasers. In the quantum well (two-dimensional) laser for conventional lengths, say $L < 500\,\mu$m, it is the second term on the right side of Eq. (8) which dominates. This explains why the (total) threshold current of high quality material uncoated quantum well lasers is independent of the length L.[2] Since this dominant term can be reduced to near zero with $R \to 1$, we would expect a major reduction of I_{th} as the facet reflectivity is increased. Indeed, the recent demonstration of submilliampere threshold currents exploited exactly this point and values of $R \sim 0.8$ resulted in nearly an order of magnitude lowering of I_{th} (0.55 mA) from those of uncoated lasers ($R \sim 0.31$). The relative insignificance of the second term on the right side in the three-dimensional case Eq. (7) explains why the same strategy does not work in conventional (three-dimensional) lasers. We also note that when, in the process of evaluating intrinsic quantum well material, we compare the threshold current densities (I_{th}/WL) of quantum well lasers made from the material, the dominant second term varies as L^{-1}. The only meaningful comparison is thus of very long lasers and/or lasers with $R \to 1$ where the reflectivity term is negligible. The minimum threshold current density of a quantum well laser in the limit $R \to 1$ and $\alpha_{scatt} = 0$ is

$$\frac{(I_{min})_{2D}}{(WL)} = \frac{N_{2D}^{tr}e}{\tau\eta} \sim 60\ \text{A/cm}^2$$

for $\eta \simeq 1$, $\tau = 4\times10^{-9}$ s, and $N_{2D}^{tr} = 1.5\times10^{12}$ cm^{-2}. This shows that recently achieved values of 88 A/cm^2 in our laboratory are approaching the theoretical limit. In a practical laser with, say, $W = 1.5\,\mu$m, $L = 120\,\mu$m, the value of the I_{th} comes out to $\sim$0.1 mA. We note that the lowest reported result is $I_{th} \sim 0.55$ mA.

In a quantum wire laser the situation is similar to that of a quantum well laser. The second term on the right side of Eq. (9) will dominate unless reduced by allowing $R \to 1$. If we neglect α_{scatt}, then the threshold current of a laser with $R \simeq 1$ and, say, $L = 100\,\mu$m will be

$$(I_{th})_{1D} \sim (N_{1D}^{tr})\frac{eL}{\tau} \sim 0.6\,\mu\text{A},$$

where we use $N_{1D}^{tr} \sim 1.5\times10^6$ cm^{-1}, $\eta \simeq 1$, and $\tau \sim 4\times10^{-9}$ s. Such a laser can only muster a maximum modal gain[3]

$$(\gamma_{max})_{1D} = \frac{\Gamma_z\Gamma_y}{L_zL_y}\frac{k^2\mu^2}{n^2\epsilon_0\hbar^{3/2}}\sqrt{m_rT_2}, \tag{10}$$

where L_z and L_y are the quantum wire cross-sectional dimension, μ the transition matrix element, Γ_z and Γ_y the optical confinement factors, m_r the reduced mass, and T_2 the carrier dephasing time. Equation (10) leads to a maximum gain $\gamma_{max} \sim 7\ cm^{-1}$, which might not be sufficient to overcome losses in pratical lasers. In this case, an array of parallel quantum wires can be used to obtain the needed total gain.

In summary, the basic scaling laws for the threshold current of quantum confined lasers are derived and are used to explain basic observations as well as serve as a guide in designing ultralow threshold lasers. Using the above considerations, we find that threshold currents of 100 μA from present generation quantum well lasers and of 2–3 μA in quantum wire lasers are possible. Further improvements, possibly by a factor of ~4–5, can be anticipated if we succeed in reducing the hole mass in GaAs wells and wires to near that of the electron.

Fruitful discussions with M. Mittelstein and P. Derry are gratefully acknowledged. This work was supported by the Office of Naval Research and the Defense Advanced Research Projects Agency.

[1] Y. Arakawa and A. Yariv, IEEE J. Quantum Electron. QE-21, 1666 (1985).
[2] P. S. Zory, A. R. Reisinger, L. J. Mawst, G. Costrini, C. A. Zmudzinski, M. A. Emanuel, M. E. Givens, and J. J. Coleman, Electron. Lett. 22, 9 (1986); also H. Chen (private communication).
[3] P. L. Derry, A. Yariv, K. Lau, N. Bar-Chaim, K. Lee, and J. Rosenberg, Appl. Phys. Lett. 50, 1773 (1987); also K. Lau, P. L. Derry, and A. Yariv, Appl. Phys. Lett. 52, 88 (1988).

Unclassified
SECURITY CLASSIFICATION OF THIS PAGE

REPORT DOCUMENTATION PAGE

Form Approved
OMB No. 0704-0188

1a. REPORT SECURITY CLASSIFICATION Unclassified	1b. RESTRICTIVE MARKINGS
2a. SECURITY CLASSIFICATION AUTHORITY	3. DISTRIBUTION/AVAILABILITY OF REPORT Approved for public release; distribution unlimited.
2b. DECLASSIFICATION/DOWNGRADING SCHEDULE	
4. PERFORMING ORGANIZATION REPORT NUMBER(S) N00014-85-K-0211	5. MONITORING ORGANIZATION REPORT NUMBER(S) 696-002
6a. NAME OF PERFORMING ORGANIZATION California Institute of Technology 6b. OFFICE SYMBOL (If applicable)	7a. NAME OF MONITORING ORGANIZATION Office of Naval Research
6c. ADDRESS (City, State, and ZIP Code) Pasadena, California 91125	7b. ADDRESS (City, State, and ZIP Code) 565 S. Wilson Pasadena, California 91106-3212
8a. NAME OF FUNDING/SPONSORING ORGANIZATION Office of Naval Research 8b. OFFICE SYMBOL (If applicable)	9. PROCUREMENT INSTRUMENT IDENTIFICATION NUMBER P00001
8c. ADDRESS (City, State, and ZIP Code) 800 N. Quincy Street Arlington, VA 22217	10. SOURCE OF FUNDING NUMBERS PROGRAM ELEMENT NO. / PROJECT NO. / TASK NO / WORK UNIT ACCESSION NO

11. TITLE (Include Security Classification)
Ultralow threshold graded-index separate-confinement heterostructure single quantum well (Al,Ga)As lasers

12. PERSONAL AUTHOR(S)
P. L. Derry, H. Z. Chen, H. Morkoc, A. Yariv, K. Lau, N. Bar-Chaim, K. Lee, J. Rosenberg

13a. TYPE OF REPORT	13b. TIME COVERED	14. DATE OF REPORT (Year, Month, Day)	15. PAGE COUNT
Reprint	FROM _____ TO _____	1988 Mar/Apr	3

16. SUPPLEMENTARY NOTATION The view, opinions and/or findings contained in this report are those of the author(s) and should not be construed as an official Department of the Navy position, policy, or decision unless so designated by other documentation.

17. COSATI CODES			18. SUBJECT TERMS (Continue on reverse if necessary and identify by block number)
FIELD	GROUP	SUB-GROUP	quantum well lasers

19. ABSTRACT (Continue on reverse if necessary and identify by block number)

Broad area graded-index separate-confinement heterostructure single quantum well lasers grown by molecular-beam epitaxy (MBE) with threshold current density as low as 93 A/cm^2 (520 μm long) have been fabricated. Buried lasers formed from similarly structured MBE material with liquid phase epitaxy regrowth had threshold currents at submilliampere levels when high reflectivity coatings were applied to the end facets. A cw threshold current of 0.55 mA was obtained for a laser with facet reflectivities of ∿80%, a cavity length of 120 μm, and an active region stripe width of 1 μm. These devices driven directly with logic level signals have switch-on delays <50 ps without any current prebias. Such lasers permit fully on-off switching while at the same time obviating the need for bias monitoring and feedback control.

20. DISTRIBUTION/AVAILABILITY OF ABSTRACT ☐ UNCLASSIFIED/UNLIMITED ☐ SAME AS RPT. ☐ DTIC USERS	21. ABSTRACT SECURITY CLASSIFICATION
22a. NAME OF RESPONSIBLE INDIVIDUAL	22b. TELEPHONE (Include Area Code) / 22c. OFFICE SYMBOL

DD Form 1473, JUN 86 Previous editions are obsolete. SECURITY CLASSIFICATION OF THIS PAGE

Ultralow threshold graded-index separate-confinement heterostructure single quantum well (Al,Ga)As lasers

451

P. L. Derry, H. Z. Chen, H. Morkoç,[a] and A. Yariv
California Institute of Technology, Pasadena, California 91125

K. Y. Lau, N. Bar-Chaim, K. Lee, and J. Rosenberg
ORTEL Corporation, Alhambra, California 91803

(Received 9 September 1987; accepted 17 November 1987)

Broad area graded-index separate-confinement heterostructure single quantum well lasers grown by molecular-beam epitaxy (MBE) with threshold current density as low as 93 A/cm^2 (520 μm long) have been fabricated. Buried lasers formed from similarly structured MBE material with liquid phase epitaxy regrowth had threshold currents at submilliampere levels when high reflectivity coatings were applied to the end facets. A cw threshold current of 0.55 mA was obtained for a laser with facet reflectivities of $\sim$80%, a cavity length of 120 μm, and an active region stripe width of 1 μm. These devices driven directly with logic level signals have switch-on delays $<$ 50 ps without any current prebias. Such lasers permit fully on–off switching while at the same time obviating the need for bias monitoring and feedback control.

Semiconductor lasers are being considered for future generations of supercomputers. The number of lasers that may be involved is so large that a major premium is placed on a reduction of the threshold current of such lasers. Lasers which can be modulated at high speed without current prebias and a feedback circuit are also highly desirable for optical interconnects and/or optical computing work. Lasers with submilliampere threshold currents will meet these requirements since with a modest current pulse ($\sim$30 mA) they can be modulated at high speed without substantial delay between the application of a current pulse and the onset of lasing. Buried heterostructure graded-index separate-confinement heterostructure single quantum well (BH GRIN-SCH SQW) lasers are capable of meeting these requirements as recently demonstrated.[1,2]

The suitability of BH GRIN-SCH SQW lasers for submilliampere operation can easily be seen by considering the threshold current density J_{th},[3]

$$J_{th} = J_o + \frac{\alpha de}{B\tau\Gamma} + \frac{de}{2LB\tau\Gamma} \ln \frac{1}{R_1 R_2}, \qquad (1)$$

where J_o is the transparency current density, α is the internal loss (active region and waveguiding), d is the active region thickness, e is the absolute value of the electron charge, τ is the effective recombination time near transparency, B is the differential gain constant, Γ is the optical confinement factor, L is the laser cavity length, and R_1 and R_2 are the end facet reflectivities. In a GRIN-SCH SQW α can be expected to be small ($<$2 cm^{-1}).[4] The transparency carrier density for a SQW is nearly the same as that for a conventional double heterostructure (DH),[5] but the active region volume is much smaller in a SQW than in a DH so J_o is much smaller for a SQW. This means that a SQW with appropriate optical confinement will have a much lower threshold than a DH; furthermore, decreasing the end losses will lead to a much more significant reduction in threshold current for a SQW than for a DH laser, because the end losses account for a much greater fraction of the threshold gain for the SQW. We can take advantage of this experimentally by evaporating high reflectivity dielectric coatings on the cleaved facets of GRIN-SCH SQW lasers to reduce the end losses. In this article we report on extremely high quality molecular-beam epitaxy (MBE) growth of GRIN-SCH SQW lasers necessary for improvement in BH GRIN-SCH SQW lasers and report on results with BH GRIN-SCH SQW lasers with high reflectivity coatings.

GRIN-SCH SQW structures were grown on (100) GaAs substrates doped with Si to a level of about 5×10^{17} cm^{-3}. After the standard wafer preparation and oxide desorption, a 1.5-μm-thick buffer layer of n-GaAs was grown at 600 °C followed by a 1.5-μm-thick n-$Al_{0.5}Ga_{0.5}As$ cladding layer grown at 700 °C. (In some samples a five period short period superlattice was grown between the buffer layer and cladding layers to impede impurity diffusion.) The n-AlGaAs was graded in composition from 50% to 20% AlAs over 1750 Å before the growth of a SQW with a thickness that varied between 40 and 100 Å. Following the quantum well, a p-AlGaAs layer graded from 20% to 50% AlAs over 1750 Å was grown, and was capped with a 1.5 μm p-$Al_{0.5}Ga_{0.5}As$ cladding layer. A 0.5 μm p^+-GaAs layer was then grown on top to facilitate contact formation. A schematic diagram of the structure is shown in Fig. 1.

Broad area lasers (110 μm wide) from structures with quantum well thicknesses of 40, 60, 80, and 100 Å were fabricated and tested for their spectrum and current-light characteristics. Cavity lengths ranging from $\sim$500 to 3000 μm were examined. The best results were achieved for a 520-μm-long device with an 80-Å-wide quantum well which had a threshold current density of 93A/cm^2. Table I details the laser threshold current densities for long (longer than 3 mm) devices obtained from the onset of lasing emission atop spontaneous emission. In the range of lengths (3.09–3.29 mm) examined, length differences should not affect the threshold current density appreciably, while with shorter devices (400–600 μm) length differences would change

 © 1988 American Vacuum Society

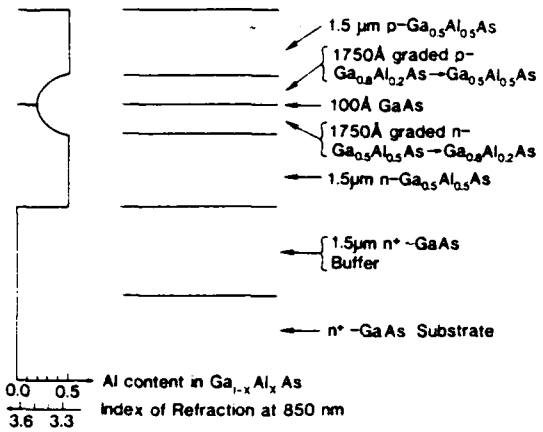

FIG. 1. Schematic diagram of a GRIN-SCH SQW laser showing layers and their indexes of refraction.

threshold current density significantly. Therefore with long devices we can determine the dependence of threshold current density on quantum well width more easily. A striking observation is that the threshold current density is not appreciably dependent on the quantum well thickness in the range studied. This is attributed to the optical modal gain being proportional to the quantum well thickness, whereas the quantum well medium gain is inversely proportional to the quantum well size. The results indicate that these two effects nearly cancel each other over a certain range.[6] In the limit of very thin (< 20 Å) and very wide (> 200 Å) quantum wells however, substantially higher threshold currents are expected, due to loss of carrier confinement in the former and the onset of three-dimensional density of states in the latter.

Some of the GRIN-SCH 100 Å SQW structures were then used to fabricate buried lasers. Broad area devices 450 μm long and 100 Å wide fabricated from this earlier material had threshold current densities of $\sim$450 A/cm^2. Mesas 2 μm wide were etched through the MBE layers down to the substrate. A 1 μm p-$Al_{0.3}Ga_{0.7}As$ layer and a 3 μm n-$Al_{0.3}Ga_{0.7}As$ layer were grown by liquid phase epitaxy (LPE) to provide current confinement. A shallow Zn diffusion was performed to facilitate formation of an Ohmic contact on the p side of the device, and Ohmic contacts were applied. Finished devices had an active layer stripe width of 1 μm. These devices were found to have average internal losses (including waveguiding losses) of $\sim$13 cm^{-1}.

The modal gain g for a semiconductor laser is given by

$$g = \alpha + \frac{1}{2L} \ln \frac{1}{R_1 R_2}. \tag{2}$$

Using this relationship, the measured value of the loss, and

TABLE I. Laser characteristics vs quantum well width.

Well width	Cavity length	Lasing wavelength	J_{th}
100 Å	3.29 mm	8702 ± 30 Å	115 A/cm^2
80 Å	3.21 mm	8640 ± 25 Å	93 A/cm^2
60 Å	3.09 mm	8578 ± 21 Å	120 A/cm^2
40 Å	3.24 mm	8363 ± 24 Å	117 A/cm^2

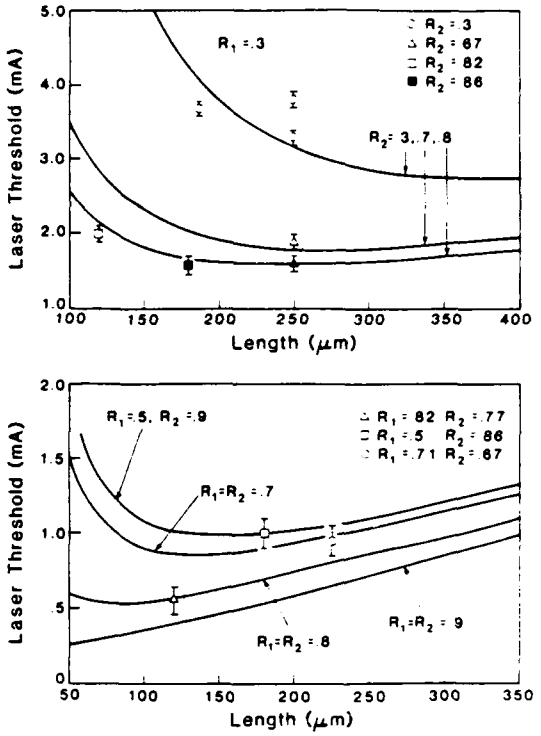

FIG. 2. Calculated threshold current for a BH GRIN-SCH SQW laser with various cavity lengths and facet reflectivities. Experimental points are also shown.

the gain versus current relationship calculated in the manner of Arakawa and Yariv,[7] expected values of threshold current for various cavity lengths and facet reflectivities were calculated. These theoretical results are shown in Fig. 2. Experimental results for cavity lengths of 250, 180, and 120 μm are also shown in Fig. 2. Threshold currents were measured cw at room temperature. The most dramatic threshold reductions with high reflectivity coatings were obtained for short lasers since end losses are more significant for shorter cavities. As shown in Fig. 3(b) with no high reflectivity coatings a 120-μm-long laser had a threshold of 5.5 mA. When both end facets were coated to $\sim$80% reflectivity the threshold current for the same laser was reduced to 0.55 mA as shown in Fig. 3(a). This value represents a substantial benchmark for lasers intended for optical computing.

The delay time for the onset of lasing following a current pulse of amplitude I assuming a constant carrier lifetime τ_s is given by[8]

$$\tau_d = \tau_s \ln\left(\frac{I}{I - I_{th}}\right) \rightarrow \tau_s \frac{I_{th}}{I}, \tag{3}$$

for large I, where I_{th} is the cw threshold current. Clearly lasers with small I_{th} will have shorter delay times for pulses of equal amplitude. We have measured the delay time for a BH GRIN-SCH SQW laser with a cavity length of 250 μm, $\sim$70% reflectivity coatings on both facets and a cw threshold current of 0.95 mA. A direct pulse current without bias was applied to the laser. The drive pulse amplitude was controlled by a broadband continuously variable rf attenuator. The pulse shape was maintained in all measurements. To accurately measure the switch-on delay down to < 50 ps

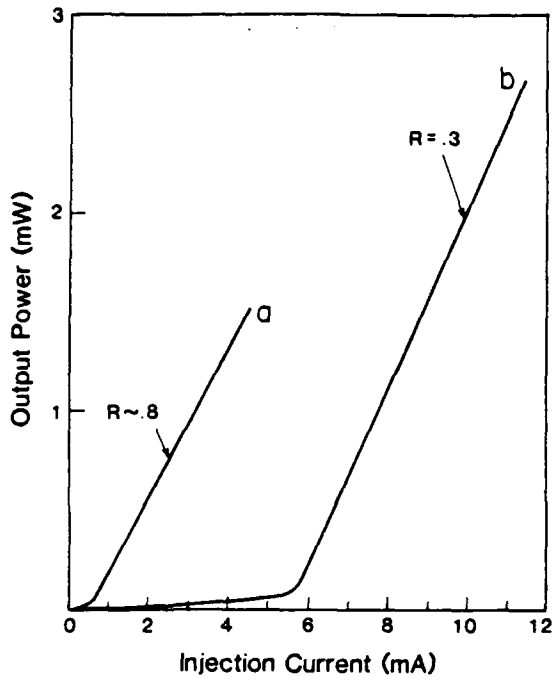

FIG. 3. Light output vs current curve for a 120-μm-long BH GRIN-SCH SQW laser with (a) high reflectivity coated cleaved facets and (b) uncoated cleaved facets. Both curves are for the same laser.

time scale it was assumed that the laser turns off without delay at the termination of the current pulse; this assumption was well supported by the observed data. The results, shown in Fig. 4, demonstrate that the laser had a switch-on delay of between 20 and 50 ps with a modest 30 mA pulse drive.

In cases where a laser is modulated by a real digital pulse stream, the starting condition for each pulse is affected by the charge leftover from the previous pulse if one existed.[9,10]

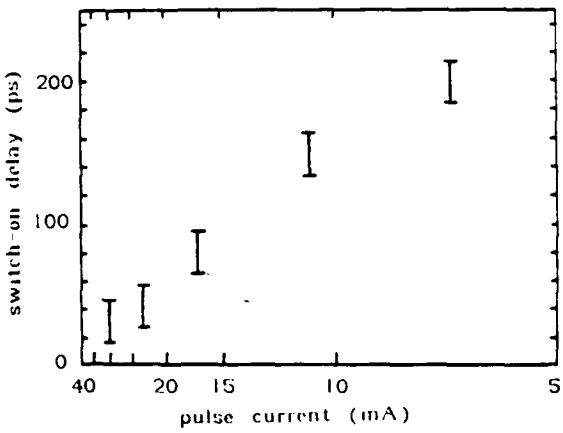

FIG. 4. Measured switch-on delay vs pulse current amplitude for a 250-μm-long BH GRIN-SCH SQW with ~70% reflectivity facet coatings and a cw threshold current of 0.95 mA.

The charge density typically stays at slightly below the threshold level following an optical pulse, and decays with a time constant equal to the carrier lifetime. The second of two consecutive optical pulses will have a higher amplitude: this is called the pattern effect. When driven by two consecutive current pulses separated by as little as 200 ps (limited by the rise time of the pulser) the present BH GRIN-SCH SQW lasers, however, showed no pattern effect.

In conclusion, we have demonstrated very low current density broad area lasers which can be applied to fabricating submilliampere buried GRIN-SCH SQW. We have fabricated BH GRIN-SCH SQW (Al,Ga)As lasers with high reflectivity coatings which have cw threshold currents as low as 0.55 mA. We have also demonstrated that these lasers can be modulated directly at high speed with logic-level drives without the need for current prebias. The lasers exhibit truly on–off switching with switch-on delays of <50 ps; the pattern effect is eliminated. Since our best GRIN-SCH SQW lasers were not used for making buried lasers and the regrowth was not optimized for limiting current leakage (which was significant) we expect that threshold currents as low as 0.2 mA should be realizable with optimized devices.

Acknowledgments: The Caltech portion of this work was supported by the National Science Foundation, the Office of Naval Research, and the Air Force Office of Scientific Research. H. M. was partially supported by SDIO-IST through the Jet Propulsion Laboratory. The ORTEL portion was supported by the Defense Advanced Research Projects Agency under the Optical Computing Program and Naval Research Laboratory.

[a)] On leave from the University of Illinois at Urbana–Champaign, Coordinated Science Laboratory, 1101 West Springfield Avenue, Urbana, Illinois 61801.

[1] P. L. Derry, A. Yariv, K. Y. Lau, N. Bar-Chaim, K. Lee, and J. Rosenberg, Appl. Phys. Lett. **50**, 1773 (1987).
[2] K. Y. Lau, N. Bar-Chaim, P. L. Derry, and A. Yariv, Appl. Phys. Lett. **51**, 69 (1987).
[3] H. C. Casey, Jr. and M. B. Panish, *Heterostructure Lasers Part A: Fundamental Principles* (Academic, Orlando, 1978), p. 183.
[4] M. Mittelstein, Y. Arakawa, A. Larsson, and A. Yariv, Appl. Phys. Lett. **49**, 1689 (1986).
[5] M. Mittelstein, A. Larsson, and A. Yariv (unpublished results).
[6] H. Z. Chen, A. Ghaffari, H. Morkoç, and A. Yariv, Appl. Phys. Lett. **25**, 2094 (1987).
[7] Y. Arakawa and A. Yariv, IEEE J. Quantum Electron. **21**, 1666 (1985).
[8] H. C. Casey, Jr. and M. B. Panish, *Heterostructure Lasers Part B: Materials and Operating Characteristics* (Academic, Orlando, 1978), p. 228.
[9] P. M. Boers and M. T. Vlaadingerbroek, Electron. Lett. **11**, 206 (1975).
[10] J. E. Bowers, B. R. Hemenway, A. H. Gnauck, and D. P. Wilt, IEEE J. Quantum Electron. **22**, 833 (1986).

Unclassified
SECURITY CLASSIFICATION OF THIS PAGE

REPORT DOCUMENTATION PAGE

Form Approved
OMB No. 0704-0188

1a. REPORT SECURITY CLASSIFICATION Unclassified	1b. RESTRICTIVE MARKINGS
2a. SECURITY CLASSIFICATION AUTHORITY	3. DISTRIBUTION/AVAILABILITY OF REPORT Approved for public release; distribution unlimited.
2b. DECLASSIFICATION/DOWNGRADING SCHEDULE	
4. PERFORMING ORGANIZATION REPORT NUMBER(S) N00014-85-K-0211	5. MONITORING ORGANIZATION REPORT NUMBER(S) 696-002
6a. NAME OF PERFORMING ORGANIZATION California Institute of Technology 6b. OFFICE SYMBOL (If applicable)	7a. NAME OF MONITORING ORGANIZATION Office of Naval Research
6c. ADDRESS (City, State, and ZIP Code) Pasadena, California 91125	7b. ADDRESS (City, State, and ZIP Code) 565 S. Wilson Pasadena, California 91106-3212
8a. NAME OF FUNDING/SPONSORING ORGANIZATION Office of Naval Research 8b. OFFICE SYMBOL (If applicable)	9. PROCUREMENT INSTRUMENT IDENTIFICATION NUMBER P00001
8c. ADDRESS (City, State, and ZIP Code) 800 N. Quincy Street Arlington, VA 22217	10. SOURCE OF FUNDING NUMBERS PROGRAM ELEMENT NO. / PROJECT NO. / TASK NO / WORK UNIT ACCESSION NO.

11. TITLE (Include Security Classification)
Effect of substrate tilting on molecular beam epitaxial grown AlGaAs/GaAs lasers having very low threshold current densities

12. PERSONAL AUTHOR(S)
H. Chen, A. Ghaffari, H. Morkoc and A. Yariv

13a. TYPE OF REPORT	13b. TIME COVERED	14. DATE OF REPORT (Year, Month, Day)	15. PAGE COUNT
Reprint	FROM _____ TO _____	1987 December	3

16. SUPPLEMENTARY NOTATION The view, opinions and/or findings contained in this report are those of the author(s) and should not be construed as an official Department of the Navy position, policy, or decision unless so designated by other documentation.

17. COSATI CODES			18. SUBJECT TERMS (Continue on reverse if necessary and identify by block number)
FIELD	GROUP	SUB-GROUP	Molecular beam epitaxy AlGaAs/GaAs lasers

19. ABSTRACT (Continue on reverse if necessary and identify by block number)

Single quantum well, graded refractive index separate confinement heterostructure (SQW GRINSCH) lasers with well thicknesses in the range of 65-480 Å have been grown by molecular beam epitaxy (MBE) on (100) and off of (100) by 4° toward (111) A substrates. The threshold current density appears to be independent of the well thickness in the range of 65-165 Å due to the compensating effects of volume of inversion and optical confinement. Under optimum growth conditions, the tilted substrates led to lower threshold current densities, the lowest value being 93 A/cm^2 for a 520-μm-long cavity laser with a 125-Å-thick well. To our knowledge, this is by far the best ever reported threshold current density obtained in a semiconductor injection laser. Deviations from optimum growth conditions drastically increased the threshold current density on (100) substrates whereas the degradation for those on the tilted substrates was much less pronounced.

20. DISTRIBUTION/AVAILABILITY OF ABSTRACT ☐ UNCLASSIFIED/UNLIMITED ☐ SAME AS RPT. ☐ DTIC USERS	21. ABSTRACT SECURITY CLASSIFICATION
22a. NAME OF RESPONSIBLE INDIVIDUAL	22b. TELEPHONE (Include Area Code) / 22c. OFFICE SYMBOL

DD Form 1473, JUN 86 Previous editions are obsolete. SECURITY CLASSIFICATION OF THIS PAGE

Effect of substrate tilting on molecular beam epitaxial grown AlGaAs/GaAs lasers having very low threshold current densities

H. Z. Chen, A. Ghaffari, H. Morkoç,[a] and A. Yariv
California Institute of Technology, Pasadena, California 91125

(Received 21 August 1987; accepted for publication 5 October 1987)

Single quantum well, graded refractive index separate confinement heterostucture (SQW GRINSCH) lasers with well thicknesses in the range of 65–480 Å have been grown by molecular beam epitaxy (MBE) on (100) and off of (100) by 4° toward (111) *A* substrates. The threshold current density appears to be independent of the well thickness in the range of 65–165 Å due to the compensating effects of volume of inversion and optical confinement. Under optimum growth conditions, the tilted substrates led to lower threshold current densities, the lowest value being 93 A/cm^2 for a 520-μm-long cavity laser with a 125-Å-thick well. To our knowledge, this is by far the best ever reported threshold current density obtained in a semiconductor injection laser. Deviations from optimum growth conditions drastically increased the threshold current density on (100) substrates whereas the degradation for those on the tilted substrates was much less pronounced.

Properties of heterojunction GaAs/AlGaAs devices and quantum wells depend strongly on the quality of GaAs layers sandwiched between two AlGaAs layers. Two heterointerfaces thus formed are not necessarily identical because the inverted interface is formed between the GaAs grown on AlGaAs, and the normal interface is a result of AlGaAs grown on GaAs.[1] Due to the small surface migration rate of Al and/or the enhanced impurity surface segregation in AlGaAs, the inverted interface is generally believed to be rough which causes excessive scattering and loss, and contains larger amounts of impurities.[2,3] In the case of molecular beam epitaxy (MBE), this problem is alleviated somewhat by growing the AlGaAs layer at substrate temperatures slightly higher than 700 °C where the surface mobility of Al is satisfactory. At these elevated temperatures it has also been suggested that the As_4 (often used) is cracked at the surface to As_2 which has a much higher sticking coefficient, thus leading to enhanced structural and electronic properties.[4]

In a more recent investigation, Tsui *et al.*[5] have reported on the optical and morphological quality of AlGaAs using As_4, grown below 700 °C on tilted substrates. Tsui *et al.*[6] also extended their work to include GaAs/AlGaAs single quantum well heterostructures, which are very sensitive to the quality of the AlGaAs buffer layer where a substantial sharpening of the photoluminescence linewidths on tilted substrates was observed. The improved results in both investigations were obtained only when the (100) substrates were cut at an angle ranging from 2.53° to 7° towards one of the nearest (111) *A* planes.

In this letter we report on AlGaAs/GaAs lasers grown on (100) GaAs substrates tilted toward (111)*A* by 4°, and show that the tilted substrates produce lasers with consistently lower threshold current densities than the nominal (100) substrates. The improvements became very substantial when growth conditions other than those found to be optimal for (100) growth are used.

Structures studied were grown by MBE on GaAs substrates with straight (100) surfaces and on those tilted 4° toward one of the nearest (111)*A* planes. In order to avoid any experimental errors, straight and tilted substrates were mounted side by side on the same wafer holder. Graded index separate confinement heterostructure single quantum well (GRINSCH SQW) lasers were used as a test for the investigation of the substrate tilting. The lasers consisted of a 1.5-μm *n*-type GaAs buffer layer, then a 1.5-μm *n*- and *p*-cladding layer on each side of the GRINSCH region which is a 0.35-μm graded waveguide with a single quantum well at the center, and capped with a 0.5-μm GaAs p^+ layer for ohmic contact. In one series, the growth condition optimum for the (100) growth, i.e., 700 °C substrate temperature, was used with quantum well thicknesses of 65, 95, 125, 165, 300, and 480 Å. In another series, the 125-Å structure was used as a test where the growth temperature was changed from 700 to 680 °C and then to 660 °C, nonoptimum for the straight (100) substrates. Broad area lasers with a stripe width of 110 μm and cleaved cavity length ranging from 500 to 3300 μm were fabricated from the 16 samples grown. The lasing threshold current and emission wavelength were determined by the observation of a sharp spike in the spectrum atop the spontaneous emission background using an optical multichannel analyzer, and then compared to the light-current plot which yielded identical results.

Figure 1 summarizes the threshold current densities for the six different quantum well widths (65, 95, 125, 165, 300, 480 Å) used on both tilted and straight (100) substrates, whereas the lasing wavelength and cavity lengths associated with this series of lasers are tabulated in Table I. The cavity lengths listed in Table I were chosen to be long enough (≈ 3 mm) such that the mirror loss can be neglected, and the threshold current densities will reflect the intrinsic optical quality of the structures. It is clear from the results that the

[a] On leave from Coordinated Science Laboratory, University of Illinois, 1101 W Springfield Ave., Urbana, IL 61801.

 © 1987 American Institute of Physics

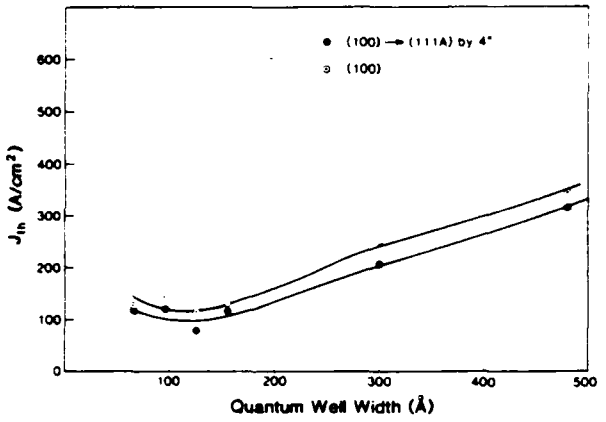

FIG. 1. Laser threshold current density vs the quantum well thickness in GaAs/AlGaAs GRINSCH SQW lasers grown on straight (100) (open circles) and on (100) tilted towards (111)A by 4° (closed circles).

TABLE I. Laser characteristics versus quantum well width grown at 700 °C.

Substrate	L_z (Å)	L (mm)	λ_{av}	J_{th}
(100)	480	3.15	8860 ± 17 Å	343 A/cm²
4°→(111)A	480	3.01	8867 ± 22 Å	316 A/cm²
(100)	300	3.28	8870 ± 25 Å	238 A/cm²
4°→(111)A	300	3.14	8850 ± 18 Å	203 A/cm²
(100)	165	3.20	8712 ± 26 Å	130 A/cm²
4°→(111)A	165	3.29	8692 ± 31 Å	115 A/cm²
(100)	125	3.26	8652 ± 26 Å	114 A/cm²
4°→(111)A	125	3.30	8628 ± 17 Å	80 A/cm²
(100)	95	3.18	8582 ± 19 Å	148 A/cm²
4°→(111)A	95	3.09	8574 ± 23 Å	120 A/cm²
(100)	65	3.19	8378 ± 20 Å	124 A/cm²
4°→(111)A	65	3.24	8349 ± 18 Å	117 A/cm²

threshold densities are consistently lower for lasers grown on the tilted substrates.

Drastic changes in the performance of lasers on both tilted and straight (100) substrates are observed when the substrate temperature is dropped to 680 °C in one experiment and to 660 °C in another, as shown in Table II. For the 680 °C growth, the difference in surface morphologies between two substrates clearly favored the tilted ones. Threshold current density measurements further showed that the lasers on straight (100) substrates exhibited threshold current density (J_{th} = 472 A/cm²), three times higher than that on the tilted one (J_{th} = 163 A/cm³). For the 660 °C growth, the surface morphology of growth on the straight (100) substrate was significantly worse than that on the tilted one, and as a result, the lasers on the straight (100) substrate failed to lase at a current density as high as 6000 A/cm² while the lasers on the tilted substrate lased with J_{th} of 403 A/cm². In addition, GRINSCH lasers with a 35-Å quantum well size were also used to study the effect of excessive outgasing of the GaAs substrates before growth (loss of As stabilized surface). The tilted substrate led to a threshold current density of about 205 A/cm² while the straight one produced 545 A/cm². This is also a clear indication that the tilted substrates provide a wider range of growth temperature where good results can be obtained. These observations are extraordinary not only in the sense that the threshold current densities obtained on both tilted and straight (100) substrates are the lowest ever reported by nearly a factor of 2,[7] but also in that the tilted substrates always produced much better results, and were far more tolerant to deviations from the optimum conditions. This means that extensive trial and error type of time consuming procedures can be eliminated since there is no reliable method of MBE substrate temperature measurement.

The enhanced results on tilted substrates can be attributed in part to the fact that tilted surfaces have steps terminated with Ga. As a result, As incident on the surface can form three bonds, two to the Ga atoms on (100) surface, and one to the Ga atom on the (111) face of the step. Thus, an increased As sticking probability is obtained which, as the results suggest, will lead to smooth AlGaAs layer surfaces. In addition, a second mechanism suggested by Rode *et al.*,[8] that the stepped surfaces minimize energetic instabilities at the growing surface, may also be responsible.

In conclusion, we have demonstrated that tilted substrates result in improved optical quality and lower threshold current densities in quantum well lasers grown on GaAs substrates. More important, the surface morphology of growth on the tilted (100) substrates is less sensitive to the growth conditions, making it easier to grow low threshold current laser material. In the process of this study, the threshold current density in GRINSCH lasers has been reduced to 93 A/cm² for a cavity length of 520 μm (80 A/cm² was obtained for a 3.3-mm-long cavity). In addition, the threshold current density has been observed to be insensitive to quantum well thickness in the range of 65–125 Å.

TABLE II. Laser characteristics versus substrate temperature during growth and outgasing conditions.

Substrate	T_{sub} (°C)	L_z (Å)	L (mm)	λ_{av}	J_{th}
(100)	680	125	3.08	8636 ± 7 Å	472 A/cm²
4°→(111)A	680	125	3.06	8670 ± 20 Å	163 A/cm²
(100)	660	125	3.14	···	not lasing
4°→(111)A	660	125	3.16	8675 ± 21 Å	403 A/cm²
(100)*	700	35	3.10	8017 ± 29 Å	548 A/cm²
4°→(111)A*	700	35	3.17	8075 ± 31 Å	205 A/cm²

* The substrate was outgassed at extremely high temperatures.

This work is supported by the Office of Naval Research, the Air Force Office of Scientific Research, and the National Science Foundation. One of us, H.M., is also a disinguished visiting scientist at Caltech Jet Propulsion Laboratory and is supported partially by SDIO-IST.

[1]H. Morkoç, L. C. Witkowski, T. J. Drummond, C.M. Stanchak, A. Y. Cho, and B. G. Streetman, Electron. Lett. **37**, 1933 (1980).

[2]H. Morkoç, T. J. Drummond, W. Kopp, and R. Fischer, J. Electrochem. Soc. **129**, 824 (1982).

[3]H.Morkoç, T.J. Drummond, and R. Fischer, J. Appl. Phys. **53**, 1030 (1982).

[4]L. P. Erickson, T. J. Mattord, P. W. Palmberg, R. Fischer, and H. Morkoç, Electron. Lett. **19**, 632 (1983).

[5]R.K. Tsui, J. A. Curless, G. D. Kramer, M. S. Peffley, and D. L. Rode, J. Appl. Phys. **58**, 2570 (1985).

[6]R. K. Tsui, G. D. Kramer, J. A. Curless, and M. S. Peffley, Appl. Phys. Lett. **48**, 940 (1986).

[7]O. Wada, T. Sanada, M. Kuno, and T. Fujii, Electron. Lett. **21**, 1205 (1985).

[8]D. L. Rode, W. R. Wagner, and N. E. Schumaker, Appl. Phys. Lett. **30**, 75 (1977).

Unclassified
SECURITY CLASSIFICATION OF THIS PAGE

REPORT DOCUMENTATION PAGE

Form Approved
OMB No. 0704-0188

1a. REPORT SECURITY CLASSIFICATION Unclassified	1b. RESTRICTIVE MARKINGS
2a. SECURITY CLASSIFICATION AUTHORITY	3. DISTRIBUTION/AVAILABILITY OF REPORT Approved for public release; distribution unlimited.
2b. DECLASSIFICATION/DOWNGRADING SCHEDULE	
4. PERFORMING ORGANIZATION REPORT NUMBER(S) N00014-85-K-0211	5. MONITORING ORGANIZATION REPORT NUMBER(S) 696-002
6a. NAME OF PERFORMING ORGANIZATION California Institute of Technology 6b. OFFICE SYMBOL (If applicable)	7a. NAME OF MONITORING ORGANIZATION Office of Naval Research
6c. ADDRESS (City, State, and ZIP Code) Pasadena, California 91125	7b. ADDRESS (City, State, and ZIP Code) 565 S. Wilson Pasadena, California 91106-3212
8a. NAME OF FUNDING/SPONSORING ORGANIZATION Office of Naval Research 8b. OFFICE SYMBOL (If applicable)	9. PROCUREMENT INSTRUMENT IDENTIFICATION NUMBER P00001
8c. ADDRESS (City, State, and ZIP Code) 800 N. Quincy Street Arlington, VA 22217	10. SOURCE OF FUNDING NUMBERS PROGRAM ELEMENT NO. / PROJECT NO. / TASK NO / WORK UNIT ACCESSION NO.

11. TITLE (Include Security Classification)
Self-Stabilized Nonlinear Lateral Modes of Broad Area Lasers

12. PERSONAL AUTHOR(S)
D. Mehuys, R. J. Lang, M. Mittelstein, J. Salzman and A. Yariv

13a. TYPE OF REPORT	13b. TIME COVERED	14. DATE OF REPORT (Year, Month, Day)	15. PAGE COUNT
Reprint	FROM _____ TO _____	1987 November	12

16. SUPPLEMENTARY NOTATION The view, opinions and/or findings contained in this report are those of the author(s) and should not be construed as an official Department of the Navy position, policy, or decision unless so designated by other documentation.

17. COSATI CODES			18. SUBJECT TERMS (Continue on reverse if necessary and identify by block number)
FIELD	GROUP	SUB-GROUP	broad area lasers

19. ABSTRACT (Continue on reverse if necessary and identify by block number)

The lateral modes of broad area lasers are investigated theoretically. The nonlinear interaction between optical field and effective refractive index leads to a saturable nonlinearity in the governing field equation, so that self-modulated solutions are found to be stable with increased current injection above saturation intensity. We derive approximate analytical solutions for traveling wave fields within the broad area laser. The field amplitude consists of a small ripple superimposed on a large dc value. Matching fields at the boundary determines the modulation depth and imparts an overall phase curvature to the traveling wave mode. There are multiple lateral modes for a given set of operating conditions, and modes with successively more lobes in the ripple have greater overall phase curvature. In contrast to the linear problem, several lateral modes can achieve the same modal gain for a given injected current density, by saturating the gain to a different extent. Thus, these modes would exhibit slightly different optical powers.

20. DISTRIBUTION/AVAILABILITY OF ABSTRACT ☐ UNCLASSIFIED/UNLIMITED ☐ SAME AS RPT ☐ DTIC USERS	21. ABSTRACT SECURITY CLASSIFICATION
22a. NAME OF RESPONSIBLE INDIVIDUAL	22b. TELEPHONE (Include Area Code) / 22c. OFFICE SYMBOL

DD Form 1473, JUN 86 Previous editions are obsolete. SECURITY CLASSIFICATION OF THIS PAGE

J-QE 23 11 16666

Self-Stabilized Nonlinear Lateral Modes of Broad Area Lasers

D. Mehuys
R.J. Lang
M. Mittelstein
J. Salzman
A. Yariv

Reprinted from
IEEE JOURNAL OF QUANTUM ELECTRONICS
Vol. QE-23, No. 11, November 1987

Self-Stabilized Nonlinear Lateral Modes of Broad Area Lasers

DAVID MEHUYS, STUDENT MEMBER, IEEE, ROBERT J. LANG, MEMBER, IEEE, MICHAEL MITTELSTEIN, JOSEPH SALZMAN, AND AMNON YARIV, FELLOW, IEEE

Abstract—**The lateral modes of broad area lasers are investigated theoretically. The nonlinear interaction between optical field and effective refractive index leads to a saturable nonlinearity in the governing field equation, so that self-modulated solutions are found to be stable with increased current injection above saturation intensity. We derive approximate analytical solutions for traveling wave fields within the broad area laser. The field amplitude consists of a small ripple superimposed on a large dc value. Matching fields at the boundary determines the modulation depth and imparts an overall phase curvature to the traveling wave mode. There are multiple lateral modes for a given set of operating conditions, and modes with successively more lobes in the ripple have greater overall phase curvature. In contrast to the linear problem, several lateral modes can achieve the same modal gain, for a given injected current density, by saturating the gain to different extent. Thus, these modes would exhibit slightly different optical powers.**

I. Introduction

In principle, the most direct way to increase the optical power available from a semiconductor laser is to increase the volume of the lasing mode. It is not sufficient merely to increase the pump level because the resonator facets are susceptible to catastrophic damage at high optical powers. The simplest practical recourse is to increase the lateral dimension. In the past, stripe geometry lasers wider than about 10 μm exhibited filamentary near fields that were not stable with respect to increased current injection and gave rise to equally unstable far-field patterns. Thus stripe geometry lasers were fabricated to support only a single "filament," [1] and the high-power effort shifted toward building phased arrays of such lasers. It was difficult, however, to fabricate arrays in which adjacent elements were coupled in-phase. In fact, twin-lobed far-field patterns were the rule rather than the exception, because the preferred lasing mode in uniform arrays is not the fundamental supermode [2] of the array. Subsequently, many schemes have been proposed to favor the fundamental supermode, and several groups have reported laser arrays oscillating into a single-lobed far field [3]–[13]. However, all of the above require an additional degree of complexity in array design and fabrication, and true single lateral mode operation remains difficult to achieve over a large range of injected current density. More elaborate schemes such as unstable resonator geometries [14] show promise but are still technologically immature.

Recently, our group demonstrated [15] wide (≥ 100 μm) uniform gain broad area quantum well lasers that oscillate coherently into a nearly diffraction-limited single-lobed far-field pattern. The emission was stable over a large range of injected current, and a gradual broadening of the far field with increasing power level was the only apparent degradation. The near field was characterized by a relatively flat amplitude with a small (≈ 10 percent) superimposed ripple; the ripple period was close to 10 μm. Such a field cannot be explained by the simple linear theory of gain-guided structures. This led to renewed interest on our part in the basic properties and expected performance of such devices. In this paper, we investigate the theoretical behavior of these broad area lasers.

In particular, we intend to characterize the optical modes consistent with a heavily saturated gain profile. Our devices were driven up to 60 times threshold [16], so we are most interested in characterizing the high-power regime. In this regime, the intensity dependence of the carrier density and the resulting changes in the refractive index *must* be included in the analysis. They provide the positive feedback between the field and the material which forms its confining waveguide. It is well-known that this feedback is the basis of the regenerative self-focusing mechanism that leads to filamentation [17]. In regions of high optical intensity, the local gain is depressed by stimulated emission. Through the band-edge effect, this depression leads to a local increase in refractive index, which tends to further confine the light and increase the local field intensity. Thompson, in 1972, analyzed optical nonlinearities due to carrier depletion and found them to introduce a third-order nonlinearity in the field equation [17]. His solutions in unbounded media were either solitary "filaments," or periodic solutions consisting of adjacent "filaments" coupled either in phase or in antiphase. A serious limitation of his approach was the restriction to real refractive index variations only. As he pointed out, this restriction makes it impossible to match

Manuscript received February 23, 1987; revised June 11, 1987. The research described in this work was conducted in the Department of Applied Physics, California Institute of Technology, and was supported in part by the Office of Naval Research and by the National Science Foundation.

D. Mehuys, M. Mittlestein, and A. Yariv are with the Department of Applied Physics, California Institute of Technology, Pasadena, CA 91125.

R. J. Lang is with the Standard Elektrik Lorenz Research Centre, 7000 Stuttgart 40, West Germany.

J. Salzman is with Bell Communications Research, Red Bank, NJ 07701.

IEEE Log Number 8716666.

0018-9197/87/1100-1909$01.00 © 1987 IEEE

his multifilament solutions to lossy boundaries, and thus excludes the eigenfunctions of gain-guided lasers (which we introduce).

Since then, much of the work in the literature [18]–[21] has focused on analyzing the stability of solitary filaments and providing design guidelines [22] for narrow stripe-geometry lasers. In this work, we focus on the "multifilament" solutions which are important in broad area lasers. However, since the modulation depth of our solutions is relatively small, it is inaccurate to characterize these solutions as "coupled filaments." In fact, to the contrary, these modes evolve in a smooth way from higher order modes of the complex linear waveguide. Further, we show that gain saturation is responsible for the stabilization of "filament" size. Lateral carrier diffusion does not play a significant role in this stabilization.

II. Carrier-Dependent Refractive Index

In this section the complex refractive index is written to include the carrier dependence. Throughout this work we consider traveling waves of the form

$$\mathcal{E}(x, y, z, t) = E(x)\, F(x, y)\, e^{i(\beta z - \omega t)} \tag{1}$$

where x is the lateral dimension, y the transverse dimension, and z the direction of propagation. The propagation constant is β and the angular frequency ω. $E(x)$ is the unknown lateral mode, and $F(x, y)$ gives the transverse mode field distribution. As the problem cannot be solved exactly by separation of variables, the transverse mode shape contains a slowly-varying dependence on the lateral coordinate [23].

Under these approximations, the lateral mode $E(x)$ satisfies the Helmholtz equation

$$\frac{d^2E(x)}{dx^2} + k_0^2\left\{n_{\text{eff}}^2(x) - \eta^2\right\} E(x) = 0, \tag{2}$$

where $n_{\text{eff}}^2(x)$ is the usual effective index determined by solving the transverse eigenmode problem at each value of x. The eigenvalue, η^2, is defined by the longitudinal propagation constant $\beta = k_0\eta$, and k_0 is the free-space propagation constant.

The physical origin of the self-focusing mechanism lies in the local depression of the gain profile by stimulated emission (spatial hole-burning), and this is what we shall quantify first. It will then be incorporated into the effective refractive index. Fig. 1(a) shows a broad area device of the type we shall consider. The laser shown is a single quantum well separate confinement heterostructure known to give very low threshold densities [24]. Fig. 1(b) and (c) show representative optical modes of the transverse and lateral waveguides, respectively. The transverse mode is index-guided, and for the single quantum well of thickness L_y, it is characterized by a small optical confinement factor Γ.

The lateral waveguide is formed by the current stripe and the lateral mode depends on the gain and index profiles introduced by the steady-state carrier distribution. In

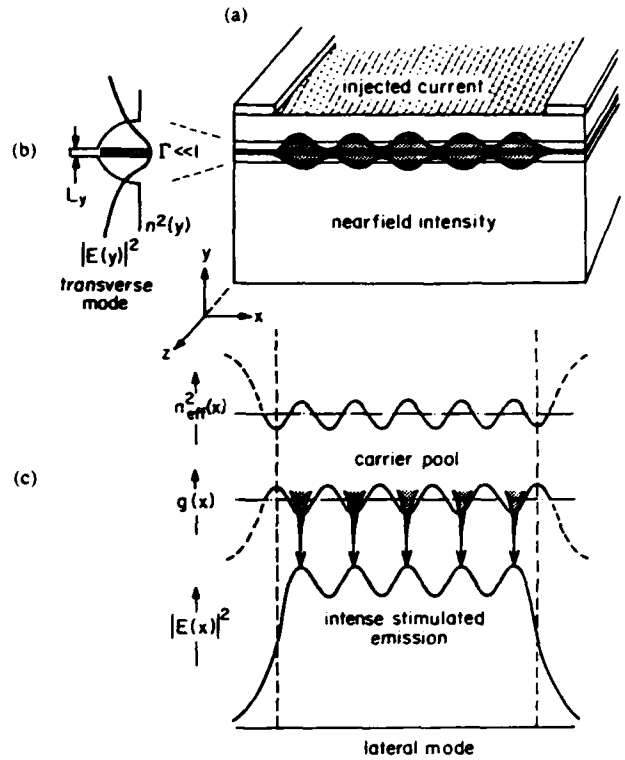

Fig. 1. (a) Stripe-geometry broad area laser with coordinate system used in this analysis. (b) Fundamental transverse mode of graded index single quantum well structure, showing very small optical confinement factor. (c) Nonlinear lateral mode as observed from our best devices. The gain is locally depleted by stimulated emission in the high intensity regions, leading to an increase in the local refractive index and the phenomenon of self-focusing.

the carrier rate equation we shall consider one-dimensional variables, since we have separated out the longitudinal dependence and integrated out the transverse dependence. When the lateral mode "sees" an effective index n_{eff}, the steady-state rate equation becomes [19], [20]

$$\frac{J(x)}{e} = \left(\frac{c}{n_{\text{eff}}}\right)\Gamma g(N(x))\, P(x) + \frac{N(x)}{\tau_{\text{sp}}} - D\frac{d^2N(x)}{dx^2} \tag{3}$$

where

$J(x)$ = injected current density [$\text{cm}^{-2}\,\text{s}^{-1}$]
$N(x)$ = carrier density [cm^{-2}]
$P(x)$ = photon density in lateral mode $E(x)$ [cm^{-2}]
$g(x)$ = spatial gain profile in the quantum well [cm^{-1}]
τ_{sp} = spontaneous lifetime [s]
D = lateral diffusion coefficient [$\text{cm}^2\,\text{V}^{-1}\,\text{s}^{-1}$].

Equation (3) states that at a given position x, the carriers gained by injected current are balanced in steady state by losses due to stimulated and spontaneous emission and by

lateral diffusion. Nonradiative recombination processes can be lumped into the spontaneous emission lifetime τ_{sp}. We define a normalized saturated gain profile as

$$\gamma(x) \equiv \frac{g(x) - g_{th}}{g_{th}} = \frac{g'_{th}}{g_{th}}(N(x) - N_{th}). \tag{4}$$

where, as is customary [17], we have linearized about the threshold gain $g_{th} \equiv g(N_{th})$. g'_{th} is the differential gain (with respect to carrier density) at threshold. The dimensionless quantity $\gamma(x)$ quantifies the spatial hole-burning, giving the deviation from threshold gain in units of the threshold gain. Equation (3) can now be expressed as a second-order linear ordinary differential equation in the normalized saturated gain profile:

$$L_{sp}^2 \frac{d^2\gamma(x)}{dx^2} - \left[1 + \frac{P(x)}{P_{sat}}\right]\gamma(x) = \frac{P(x)}{P_{sat}} - \frac{J(x) - J_{th}}{J_{sat}}, \tag{5}$$

where the following definitions have been made:

$$L_{sp}^2 \equiv D\tau_{sp} \tag{6a}$$

$$P_{sat} \equiv \frac{n_{eff}/c}{\Gamma g'_{th}\tau_{sp}} \tag{6b}$$

$$J_{th} \equiv \frac{eN_{th}}{\tau_{sp}} \tag{6c}$$

$$J_{sat} \equiv \frac{eg_{th}}{\tau_{sp}g'_{th}}. \tag{6d}$$

L_{sp} is the diffusion length when the carrier lifetime is determined solely by spontaneous emission and J_{th} is the threshold current density. The equation has no simple solution, as the diffusion operator L is x-dependent:

$$L(x) \equiv L_{sp}^2 \frac{d^2}{dx^2} - \left[1 + \frac{P(x)}{P_{sat}}\right], \tag{7}$$

and $P(x)$ is still unknown. We can, however, find an approximate solution in terms of $P(x)$. Since $P(x) \geq 0$ for all x, it is appropriate to find a WKB approximation for the Green's function of $L(x)$ [25]:

$$G_{WKB}(x, x') = \frac{1}{2L_{sp}} \frac{\exp\left\{-\frac{1}{L_{sp}}\left|\int_{x'}^{x}\sqrt{1 + \frac{P(t)}{P_{sat}}}\,dt\right|\right\}}{\left[\left(1 + \frac{P(x)}{P_{sat}}\right)\left(1 + \frac{P(x')}{P_{sat}}\right)\right]^{1/4}}. \tag{8}$$

The Green's function is integrated against the right-hand side of (5) and the integral is expanded asymptotically in powers of the diffusion length. The result for the saturated gain profile is as follows:

$$\gamma(x) \sim \gamma_0(x) + \frac{L_{sp}^2}{1 + \frac{P(x)}{P_{sat}}}\frac{d^2\gamma_0(x)}{dx^2} + O\left\{\frac{L_{sp}^4}{\left(1 + \frac{P(x)}{P_{sat}}\right)^2}\right\} \tag{9}$$

where

$$\gamma_0(x) = \frac{\frac{J(x) - J_{th}}{J_{sat}} - \frac{P(x)}{P_{sat}}}{1 + \frac{P(x)}{P_{sat}}} \tag{10}$$

is the solution when diffusion is neglected. Consider a saturated gain profile that reflects a self-modulated near field. While the level of the losses determines the average gain level, regions of relatively high (low) optical intensity cause regions of local depression (elevation) in the gain. This effect, due to stimulated emission, is dominant and is represented by the first term in (9). In addition, diffusion will cause some of the carriers to shift from regions of high gain to regions of low gain—filling in the gaps—and this effect is represented by the second term in (9); it is a correction to the first term.

Now, suppose that $\gamma(x)$ oscillates about zero with a periodicity defined by transverse wave vector k_t. Compared to the first term in (9), the diffusion term is of order $k_t^2 L_{sp}^2/(1 + (P(x)/P_{sat}))$. If $k_t L_{sp}$ is small compared to one, then $k_t^2 L_{sp}^2 << 1$, and the diffusion correction is small; as the power increases over P_{sat}, it becomes smaller yet. That is, the diffusion length, being proportional to the square root of the carrier lifetime, is reduced in the presence of stimulated emission. Note that P_{sat} can be interpreted as the photon density at which the stimulated emission rate equals the spontaneous emission rate, since at this intensity the carrier lifetime is reduced by a factor of two. This is in accordance with other definitions of the saturation intensity [17], [26].

Since modulation in $P(x)$ occurs only on spatial scales longer than L_{sp} and the effects of diffusion become vanishingly small at high power, we neglect them. As a result, we take (10) as the saturated gain profile. It remains to incorporate this expression into the complex refractive index. Observing the traveling wave convention (1) leads to the relationship

$$n_{eff}^2(x) = n_0^2 - \frac{n_0}{k_0}\Gamma g_{th}(b + i)\gamma(x) \tag{11}$$

where n_0 is the effective index of refraction corresponding to the threshold gain level, and b is the antiguiding factor [positive, with convention (1)]. In our model, b is identical to the linewidth enhancement factor α at threshold

carrier density. Finally, we establish the dependence of n_{eff}^2 on field $E(x)$ by making use of the following relation:

$$|E(x)|^2 = \frac{2\hbar\omega}{n_0^2}\frac{\Gamma P(x)}{L_y} \tag{12}$$

where $\hbar\omega$ is the lasing transition energy and L_y is the previously mentioned active layer thickness. The field strength at saturation is then [from (6b) and (12)]

$$E_{\text{sat}}^2 = \frac{2\hbar\omega}{n_0^2}\frac{n_{\text{eff}}}{c}\frac{1}{g'_{\text{th}}L_y\tau_{\text{sp}}}. \tag{13}$$

We further define

$$\epsilon_{\text{sat}} \equiv \frac{n_0}{k_0} b\Gamma g_{\text{th}}, \tag{14}$$

and note for future reference that ϵ_{sat} is proportional to the threshold gain. Equation (11) for the carrier-dependent dielectric constant becomes

$$n_{\text{eff}}^2(x) = n_0^2 + \epsilon_{\text{sat}}\left(1 + \frac{i}{b}\right) \cdot \frac{|E(x)|^2 - E_{\text{sat}}^2\dfrac{J(x) - J_{\text{th}}}{J_{\text{sat}}}}{|E(x)|^2 + E_{\text{sat}}^2}. \tag{15}$$

Equation (15) predicts, as expected, an increase in both the real and imaginary parts of n_{eff}^2 in regions where $|E(x)|^2$ is large. That is, the gain is decreased while the refractive index is increased. Furthermore, at threshold, $J = J_{\text{th}}$ and $P = 0$, which gives $n_{\text{eff}}^2 = n_0^2$ as desired. At low-field intensity, $|E(x)|^2 << E_{\text{sat}}^2$, this expression is of the form common to the nonlinear optics literature [27]: $n^2(x) = n_0^2 + n_2 \cdot I(x)$, where I is the optical intensity. However, in our case, the nonlinearity in the effective index is *saturable*. As seen from (15) the maximum local increase in dielectric constant occurs in the saturated limit $|E(x)|^2 >> E_{\text{sat}}^2$, and is given by ϵ_{sat}. It can be appreciated from (14) that the parameter ϵ_{sat} represents the depression in dielectric constant in pumping from transparency to threshold current density. To minimize self-focusing, it should be as small as possible. Equation (14) indicates that to accomplish this, small values for the antiguiding factor, optical confinement factor, and threshold gain are desired. All of these quantities are generally regarded as smaller in quantum well (QW) lasers than in regular double heterostructure (DH) lasers, and thus we conclude that the nonlinear action is weaker in QW lasers. ϵ_{sat} has been measured in both QW and DH lasers and is known to be smaller by a factor of 2 in the case of the QW lasers [28]. In very low threshold QW lasers, this improvement may be doubled again.

III. Complex-Valued Nonlinear Field Equation

Incorporating the complex effective refractive index (15) into the Helmholtz equation (2) gives the following second-order, nonlinear, nonanalytic, complex eigenvalue problem to be solved for the modes of the broad area laser:

$$\frac{1}{k_0^2}\frac{d^2E(x)}{dx^2} + \left\{n_0^2 - \eta^2 + \left(1 + \frac{i}{b}\right)\epsilon_{\text{sat}} \cdot \frac{|E(x)|^2 - E_{\text{sat}}^2\dfrac{J(x) - J_{\text{th}}}{J_{\text{sat}}}}{|E(x)|^2 + E_{\text{sat}}^2}\right\} E(x) = 0 \tag{16}$$

As can be deduced from phase-plane arguments, (16) supports periodic solutions of the form $E(x) = E_0(1 + me(x))$ where E_0 represents the average field amplitude and $e(x)$ is a periodic function that contains the filamentary self-modulation. Here m is a modulation depth small compared to unity, so the composite solution has no nulls. Thompson identified such "multifilament" solutions in his treatise, and it is evident that corresponding solutions exist in the complex case for a laser of infinite width. For our laser of finite width, we take a solution of the form

$$E \equiv E_0 e^{a + i\phi} \tag{17}$$

so that amplitude variations appear in a and phase variations in ϕ. As such, small modulation solutions are characterized by small a, in which case appropriate linearizations can be easily made. Let ξ be a dimensionless position co-ordinate: $x \equiv \xi d$, where d is the half-width of the laser. Since $E(0) \neq 0$, we consider only even solutions for $E(\xi)$, and thus our task is to solve the problem on the interval $0 < \xi < 1$. In the normalized coordinates, equation (16) becomes

$$a'' + i\theta' + a'^2 + i2a'\theta - \theta^2 + L(a) = 0 \tag{18}$$

where $\theta(\xi) \equiv \phi'(\xi)$ (note that the equation depends only on the phase gradient θ, not on the absolute phase ϕ). The intensity-dependent refractive index term is included in the last term of (18):

$$L(a) \equiv k_0^2 d^2 \left\{n_0^2 - \eta^2 + \left(1 + \frac{i}{b}\right)\epsilon_{\text{sat}} \cdot \frac{E_0^2 e^{2a} - E_{\text{sat}}^2\dfrac{J - J_{\text{th}}}{J_{\text{sat}}}}{E_0^2 e^{2a} + E_{\text{sat}}^2}\right\}. \tag{19}$$

The term $L(a)$ can be linearized for the case of $|a| << 1$ (small modulation depth):

$$L(a) = L_0 + L_1 \cdot a + O(a^2) \tag{20}$$

with

$$L_0 \equiv k_0^2 d^2 (n_0^2 - \eta^2) + \frac{1}{2}\left(1 + \frac{i}{b}\right) k_0^2 d^2 \epsilon_{\text{sat}}(1 - \sigma) \tag{21a}$$

$$L_1 = \left(1 + \frac{i}{b}\right) q_0^2 \tag{21b}$$

and where the following definitions have been made:

$$\sigma \equiv \frac{\dfrac{J - J_{\text{th}}}{J_{\text{sat}}} + 1}{\dfrac{E_0^2}{E_{\text{sat}}^2} + 1} \tag{22a}$$

$$\mu \equiv \frac{E_0^2}{E_0^2 + E_{\text{sat}}^2} \tag{22b}$$

$$q_0^2 \equiv 2k_0^2 d^2 \sigma \mu \epsilon_{\text{sat}} \tag{22c}$$

Here σ is a dimensionless quantity related to the ratio between pump and field intensities, and in our model, is constrained by energy conservation to be an $O(1)$ term. On the other hand, μ gives the approximate ratio of stimulated to stimulated + spontaneous emission, and saturates smoothly towards unity in the high-power limit. q_0^2 is proportional to the $\sigma\mu$ product, and (as we shall see) corresponds to the squared filament wave vector.

We have solved (18) [subject to the linearization (20)] analytically. The bulk of the derivation appears as Appendix A. At this point, we merely summarize the result.

In addition to the filamentary self-modulation, we allow for a global phase curvature and a slowly-varying amplitude variation to satisfy the loss requirement of the amplified mode. We separate the two as

$$a = a_f + a_s \tag{23a}$$

$$\theta = \theta_f + \theta_s \tag{23b}$$

where f denotes "fast" (or "filament") and s denotes "slow."

The fast and slow variables are decoupled by an appropriate averaging procedure. The fast, or self-modulation terms, are

$$a_f = m(\xi) \cos \int q_r d\xi \tag{24a}$$

$$\theta_f = m(\xi) \left[-\frac{q_0^2}{bq_r} \cdot \sin \int q_r d\xi - 2\theta_s \cos \int q_r d\xi \right] \tag{24b}$$

$$\phi_f(\xi) = m(\xi) \left[-\frac{q_0^2}{bq_r^2} \cdot \cos \int q_r d\xi - 2\frac{\theta_s}{q_r} \sin \int q_r d\xi \right] \tag{24c}$$

where m and q_r are the slowly-varying modulation depth and filament wavenumber, given by

$$m(\xi) = m_0 \left(1 + \rho \sinh^2 (\chi_0 \xi)\right)^{1/2\rho},$$

$$\rho \equiv 1 + \frac{4b^2\chi_0^2}{q_0^2} \tag{25a}$$

$$\int q_r d\xi = q_0 \xi + \frac{2b^2\chi_0}{q_0} \cdot \left(\chi_0 \xi - \tanh(\chi_0 \xi)\right) \tag{25b}$$

and m_0 is the modulation depth at the center of the device.

The slow amplitude and phase variations are

$$a_s = \frac{b^2\chi_0^2}{q_0^2} \tanh^2 (\chi_0 \xi) - \frac{1}{2}\left(m^2(\xi) - m_0^2\right) \tag{26a}$$

$$\theta_s = b\chi_0 \tanh (\chi_0 \xi) \tag{26b}$$

$$\phi_s = b \ln \cosh (\chi_0 \xi). \tag{26c}$$

These solutions are parameterized by m_0 and χ_0. Later it will be shown how these quantities are related to the real and imaginary parts of the eigenvalue, η.

The parameter χ_0 appears throughout, and we pause to discuss its significance. Locally, the angle between the optical axis and the direction of phase and energy propagation is, for small angles (in radians),

$$\Theta(\xi) = \frac{1}{\text{Re}(\beta)} \frac{d\phi}{dx} = \frac{\lambda_0}{2n\pi d} \theta(\xi) \tag{27}$$

where n is the real refractive index and $\theta = \theta_s + \theta_f$, as before. Thus $\lambda_0 b\chi_0/2n\pi d$ is the maximum slowly-varying angle of off-axis propagation, while d/χ_0 is the lateral position of the "knee" of the hyperbolic tangent. The value of χ_0 is set by matching to the fields outside of the gain stripe. As a rule, the larger the change in n_{eff} is, the larger χ_0 must be to accommodate it. Note that solutions in media of infinite extent are obtained by putting $\chi_0 = 0$, while m_0 is unspecified.

Thus, depending on the magnitude of χ_0 compared to unity, the phase front can be approximately parabolic over the width of the device ($\chi_0 < 1$), or else quickly approach a linear asymptote on either side ($\chi_0 >> 1$). The important consequence of this fact is that in the former case, the far field will be essentially single-lobed, while in the latter case a sharply-defined double-lobed far field will result. Consequently, it is desirable to minimize the change in n_{eff} at the edge of the gain stripe to reduce χ_0 and get a narrow far field.

The primary structure in the near-field pattern is the self-modulation. Its wavenumber in the center of the laser is q_0, defined by (22c) as

$$q_0^2 = 2\sigma k_0^2 d^2 \epsilon_{\text{sat}} \frac{E_0^2}{E_0^2 + E_{\text{sat}}^2}. \tag{28}$$

This is an intensity-dependent quantity, small at low intensity, but quickly increasing to a limiting value. Hence the filament spacing becomes stable as saturation intensity is surpassed.

Since the filament width saturates, the number of filaments must also stabilize. From (24a) we see that the

number of lobes in the near field is

$$N = \left\lceil 1 + \int_0^1 \frac{q_r}{\pi} d\xi \right\rceil \geq \left\lceil 1 + \frac{q_0}{\pi} \right\rceil \tag{29}$$

where $\lceil \cdots \rceil$ denotes the greatest integer less than or equal to the argument. The variable q_r is always greater than or equal to q_0 (25b), which establishes a lower bound for N. The squared wavenumber q_0^2 saturates to $2\sigma k_0^2 d^2 \epsilon_{sat}$. Recall that σ is an $O(1)$ quantity and can be taken as unity for purposes of discussion. As we mentioned earlier, ϵ_{sat} is the difference in real dielectric constant between transparency and threshold. This difference comes from unsaturable losses (chiefly mirror losses). For a laser of width W, we have

$$N \geq \lceil 1 + W/W_f \rceil \tag{30}$$

where W_f is a saturated filament spacing given by

$$W_f \equiv \sqrt{\frac{\pi \lambda_0 L}{\mathrm{Re}\,(n_0)\, b[\alpha L + \ln(1/R)]}}. \tag{31}$$

where L is the laser length, R is the facet reflectivity, and α is the distributed loss constant. Thus, unsaturable losses in addition to the mirror losses decrease the saturated filament spacing and increase the number of filaments.

In order to quantify this analysis, we choose ϵ_{sat} to characterize the wafers grown in our laboratory by molecular beam epitaxy. For a single quantum well device with threshold current density 250 A/cm^2, the relevant values are $\Gamma g_{th} = 30$ cm^{-1} and $b = 2$ [29]. The value of b has been estimated for AlGaAs lasers to lie in the range 2–6 [30] with the lower values more appropriate for quantum well lasers. At $\lambda = 0.845$ μm, this gives $\epsilon_{sat} = 2.7 \times 10^{-3}$, and a saturated filament spacing of ~ 12 μm. This value justifies our decision to neglect diffusion effects in formulating (15). For a device 100 μm wide, the estimated lower bound on filament number is $N = 9$.

At this point, the solutions are parameterized by the modulation depth m_0, phase gradient χ_0, and the field amplitude E_0. It remains to relate m_0 and χ_0 to the eigenvalue, η. We make implicit definitions of $\Delta_{r,i}$ in terms of η as follows:

$$k_0^2 d^2 (n_0^2 - \eta^2) \doteq 2 n_0 k_0^2 d^2 (n_0 - \eta) \equiv \frac{1}{2}\left(\Delta_r + i\frac{\Delta_i}{b}\right). \tag{32}$$

Thus, $\Delta_{r,i}$ gives the deviation of the eigenvalue from the effective index at threshold. From (21a) we have

$$L_0 \equiv L_0^r + iL_0^i \tag{33a}$$

$$L_0^r = \frac{1}{2}(\Delta_r + k_0^2 d^2 \epsilon_{sat}(1 - \sigma)) \tag{33b}$$

$$L_0^i = \frac{1}{2b}(\Delta_i + k_0^2 d^2 \epsilon_{sat}(1 - \sigma)). \tag{33c}$$

Using (A7), (A24)–(A25) (from Appendix A) leads to

$$\Delta_r = k_0^2 d^2 \epsilon_{sat}(\sigma - 1) - m_0^2 q_0^2 \tag{34a}$$

$$\Delta_i = k_0^2 d^2 \epsilon_{sat}(\sigma - 1) - 2m_0^2 q_0^2 - 2b^2 \chi_0^2. \tag{34b}$$

Thus, solving for the physically meaningful quantities of modulation depth m_0 and the slow phase gradient χ_0 by boundary matching is equivalent to determining the eigenvalues Δ_r and Δ_i.

A physically important parameter is the modal gain G_m, defined to be the rate at which the traveling wave solution grows. For purposes of discussion, we allow the modal gain to be different from the threshold gain Γg_{th} and thus examine all traveling wave solutions. Since $G_m - \Gamma g_{th} = -2k_0 \Im m(\eta - n_0)$, we have

$$G_m = \Gamma g_{th} + \frac{\Delta_i}{2b\,\mathrm{Re}\,(n_0)\, k_0 d^2}. \tag{35}$$

Ultimately, energy conservation requires $\Delta_i = 0$ for a lasing mode, and this determines the unknown field amplitude E_0 in terms of m_0 and χ_0 via (34b). The three terms in Δ_i correspond to three physical mechanisms that affect the gain. The first is proportional to $\sigma - 1$. Recall that σ is related to the ratio of pump intensity to field intensity. An increase in σ indicates an increase in the pump level (or decrease in the optical power) which reduces the amount of gain saturation. The second term, proportional to m_0^2, reflects the inefficiency introduced by modulation in the near-field pattern. In comparison of a field with a modulated near field to one without, where both experience the same *modal* gain, the *average* gain level consistent with the modulated field is increased by an amount proportional to the square of the modulation depth; that amount appears here. The third term, proportional to χ_0^2, reflects the losses due to phase curvature, or off-axis propagation. Energy propagating at an angle to the optical axis is absorbed by the lossy boundaries; this effect also reduces the gain.

IV. The Outer Solution and Boundary Matching

Beyond the gain stripe ($\xi \geq 1$), the pump current is zero. However, several processes conspire to prevent the gain from immediately taking on its unpumped value. Current spreading will cause the current injected into the active region to taper off at the edge of the gain stripe. Optical pumping also occurs, which partially bleaches the unpumped material. Our model of n_{eff} is based on a linearization of the gain about the threshold gain, and extension of this model into the unpumped region would be clearly inaccurate. In addition, the roll-off rate of n_{eff} would be of the same order of magnitude as q_0. Consequently, the separation of scales we used in the previous portion of this paper would be inappropriate.

However, the exact shape of the gain distribution outside the gain stripe affects only slightly the rate at which the field grows or decays at the edge of the gain stripe, which determines the values that the inner solution must take on there. For our model, we will assume that the

effective index of refraction outside the stripe has a functional form that satisfies the following criteria:

1) $n_{\text{eff}} = n_0$ at the edge of the gain stripe.

2) n_{eff} rolls off smoothly to its full absorption value, defined to be n_1.

In addition, we would like the specific functional form to allow for a closed-form analytic solution. These criteria are satisfied if we take

$$n_{\text{eff}}^2 \equiv n_0^2 + B \tanh \kappa(\xi - 1) + C \tanh^2 \kappa(\xi - 1) \tag{36}$$

where

$$B + C = n_1^2 - n_0^2 \tag{37}$$

and κ characterizes the roll-off rate.

Our approximate solution outside the gain stripe is the solution of the Helmholtz equation (2) with this effective index; that is,

$$E = E_1 e^{-D(\xi - 1)} \operatorname{sech}^{F/\kappa} \kappa(\xi - 1) \tag{38}$$

where the complex constants D and F satisfy

$$F^2 + \kappa F + 2DF = -(n_1^2 - n_0^2) \tag{39a}$$

$$D^2 - \kappa F = -\frac{1}{2}\left(\Delta_r + i\frac{\Delta_i}{b}\right). \tag{39b}$$

The appropriate branches to select are Re $(D) \geq 0$ and Re $(F) \geq 0$. The eigenvalues are determined by the requirement that the field E and its first derivative E' be continuous at the edge of the gain stripe ($\xi = 1$). Both conditions can be met by the requirement

$$\left.\frac{E'}{E}\right|_{\xi = 1^-} = \left.\frac{E'}{E}\right|_{\xi = 1^+}. \tag{40}$$

Consequently, the transcendental equation which determines the eigenvalues and modal gain is:

$$a'(1) + i\theta(1) = -D. \tag{41}$$

V. Discussion

We can now solve the eigenvalue equation for m_0 and χ_0 and substitute the results into our expressions for the lateral mode. In Fig. 2(a) and (b) we have plotted the lateral power distribution and local phase angle, respectively, for a 10-filament mode of a 100 μm wide device, for current pumping $J = 6J_{\text{th}}$, $J_{\text{th}}/J_{\text{sat}} = 3$, $b = 2$, and $\epsilon_{\text{sat}} = 2.7 \times 10^{-3}$. The unsaturated (amplitude) loss outside the gain stripe is taken to be 90 cm^{-1}, and κ corresponds to a 10–90 percent roll-off distance of 20 μm in n_{eff}. The number of lobes in the near-field pattern, 10, is higher than our estimate, reflecting the additional contributions to q_r that come from χ_0. As we said, χ_0 is set by boundary effects; consequently, lossier boundaries on the gain stripe will increase the number of lobes in the near field. This pattern is very similar to the experimental trace reported in [15] [reproduced in Figure 2(c)] in the size

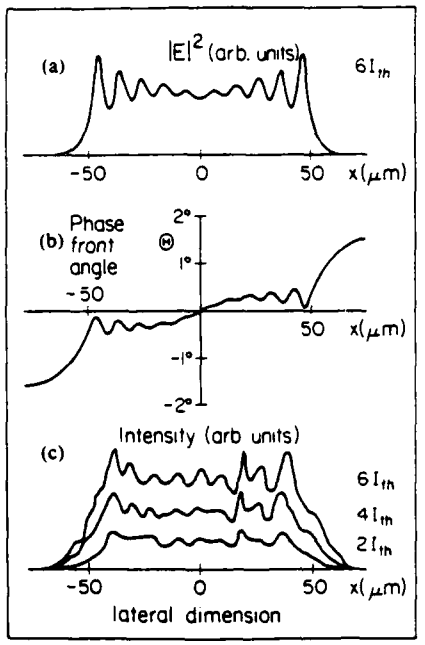

Fig. 2. Our analytical solution for the lowest-σ 10-filament mode of a device with half-width $d = 50$ μm, $\epsilon_{\text{sat}} = 2.7 \times 10^{-3}$ and $\Gamma g_{\text{th}} = 30$ cm^{-1}. The spreading parameter at the edges is $\kappa^{-1} = 20$ μm. (a) Near-field intensity. (b) Local phase front angle. The slow component of the phase front angle reaches 0.32° at the lossy boundary, corresponding to emission off-axis of about 1.1° outside the facet. (c) Experimental trace of near-field intensity of 100 μm wide device at several points above threshold [15].

and spacing of the lobes and the increase in modulation depth towards the edge of the stripe. In addition, we can estimate the width of the far field from the largest local average phase angle under the gain stripe. In Fig. 2(a), the average phase angle (inside the facet) is approximately, from (38), 0.32°, which yields a far-field width of 2.1° outside the laser; that, too, is in agreement with [15].

Next, let us consider the lateral mode spectrum. In the linear case, this spectrum is characterized by a finite set of modes, each with a distinct modal gain. The mode with the highest modal gain is deemed to be the lasing mode at threshold. However, the situation is more complex in the associated nonlinear problem. In addition to modal gain G_m, each mode must also be characterized by a field amplitude E_0, at a given injected current density. This added degree of freedom allows a finite set of lateral modes to have the same modal gain by allowing the individual amplitudes to vary.

This multiplicity is illustrated in Fig. 3. Here we plot the modal gain as a function of σ for modes containing 8–13 filaments. If the resonator losses are 30 cm^{-1}, then all solutions with matching modal gain are candidates for lasing modes. For comparison, the gain of a uniform plane wave of the same E_0 is also plotted. None of the lateral modes is as efficient as a plane wave in extracting gain. That is to be expected because the lateral modes have the absorbing boundaries to contend with. The boundaries introduce losses in two ways. First, they induce a spatial modulation, which lowers the extraction efficiency by an

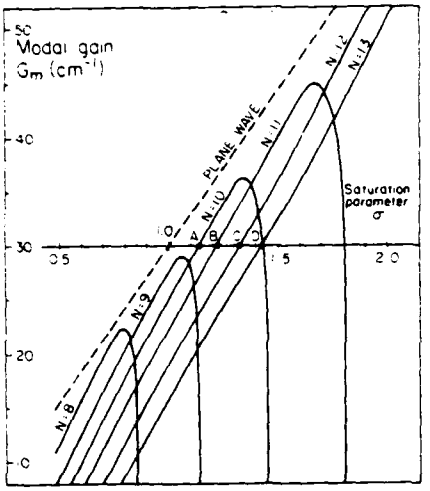

Fig. 3. Traces of the $N = 8$ through 13 filament solutions in the modal gain versus σ plane, with conditions as in Fig. 2. All modes have lower modal gain than the plane wave, as a result of the modulation depth and phase curvature induced by the boundaries. For a resonator with threshold gain of 30 cm^{-1}, allowable modes must satisfy the steady-state condition $G_m = \Gamma g_{th}$ ($\Delta_t = 0$).

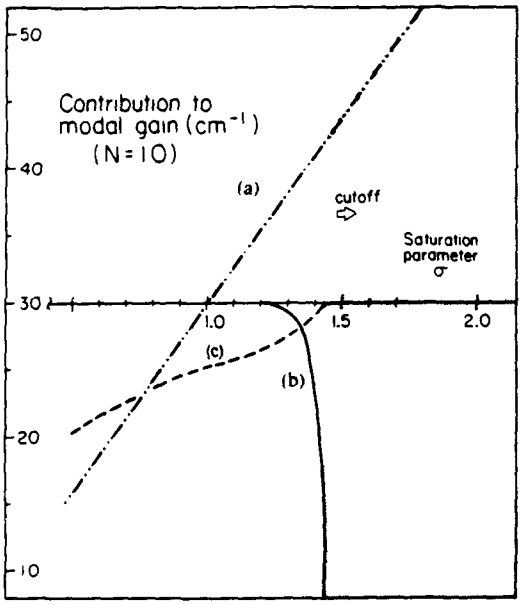

Fig. 4. Relative contribution to modal gain from (a) pumping ($\sigma - 1$), (b) modulation depth (m), and (c) phase curvature (χ) for the $N = 10$ filament solution in Fig. 3. Huge losses incurred by increasing modulation lead to an upper "cutoff" in σ. The $N = 10$ solution does not exist beyond cutoff.

amount proportional to m_0^2. Secondly, as we have said, they impart an overall phase curvature to the field, which directs energy off of the axis of propagation and into the absorbing walls. The relative contributions of these two mechanisms are plotted in Fig. 4 for the lowest-σ mode (i.e., the 10-filament mode). Their explicit contribution to the modal gain can be seen in (34)–(35). The two contributions combine to give each mode an upper cutoff in σ. As σ increases (and thus power decreases), the modal gain for any given lateral mode will tend to increase as well, because the gain is becoming less and less saturated. However, the saturated filament spacing is becoming ever smaller, and the penalty that the mode pays is an increased modulation depth. Eventually, the modulation penalty overwhelms the benefits of gain saturation: the modal gain falls off again, and the cutoff appears. Fortunately, higher order modes (meaning more filaments) have successively higher cutoff-σ's, so higher modal gains are always possible with higher order modes.

We have made the assumption that, for a given Γg_{th}, the field pattern with the greatest power (lowest σ) is the actual lasing mode. However, at a given threshold gain, solutions exist for all the lateral modes that are above cutoff. In Fig. 5 we plot the lateral power distribution for the 4 lowest order modes with modal gains of 30 cm^{-1}. Successively higher order modes have more lobes, smaller modulation depth, and more phase curvature [as can be inferred from the correction to the filament wavenumber given in equation (25b)].

Finally, we comment briefly on the issue of modal selection. In linear theory, the rule is: the mode with the most gain wins. In a nonlinear system, the lasing mode is determined not by modal gain, but by a stability analysis. It is possible (but not likely) that the mode with the smallest σ is unstable, while a mode with a higher σ is stable. Alternatively, for certain operating points there may be multiple stable points (as is the case in coupled-cavity lasers, for example [31]).

The plausibility of the latter scenario may become more apparent by considering longitudinal variations within the laser. In a Fabry–Perot laser, the average optical intensity is not a constant, but is minimized somewhere between the two facets. Likewise, the material gain is maximized in the central region. According to our analysis, different modes may be favored in different regions of the resonator. The round-trip σ of a lateral/longitudinal mode combination would thus be a weighted average of local σ, and this average would be the arbiter of which mode lases.

Concerning stability, we remark that in the unsaturated case where $|E(x)|^2 << E_{sat}^2$, the Helmholtz equation can be expressed in the form of the nonlinear Schrödinger equation. This equation is one of a class which admits soliton-like solutions, which are known to be unstable against many types of perturbation [32]. Thus, in the low-power regime, the laser may exhibit instability. Above saturation intensity, however, the nonlinearity is much weaker and the self-guiding mechanism is stabilized.

Until recently, stable, uniform near-field patterns have not been commonly observed, as an excellent crystal growth over the entire laser is required to realize spatially uniform gain and index profiles. We can see from Fig. 3 that the different longitudinal modes differ in modal gain by only a few cm^{-1}. Furthermore, in numerical calculations we have found that variations in local gain of a fraction of a cm^{-1} will disrupt the smooth lateral structure. To some degree, the effects of longitudinal propagation can smooth out the effects of inhomogeneities. Nevertheless, the broad area laser will remain extremely sensitive to such effects. Possibly, the destabilizing effect of material defects can be overcome by structures such as the recently demonstrated "controlled filament" laser [33]. In this structure, the effective mirror reflectivity is mod-

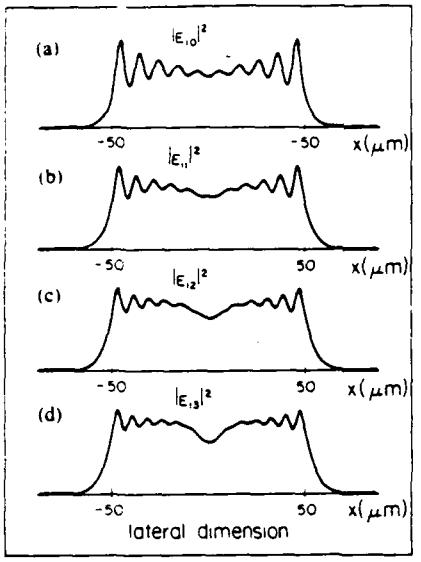

Fig. 5. Near-field intensities for the $N = 10, 11, 12$, and 13 filament solutions for the 30 cm^{-1} loss resonator. Parts (a)–(d) correspond to modes A–D in Fig. 3.

ulated in the lateral dimension in order to induce filaments at prescribed positions. The present analysis indicates that this structure can be optimized if the reflectivity modulation is chosen with the same periodicity as the saturated filament spacing of the parent broad area laser.

VII. Appendix A

This appendix details the solution of (18), (20), and (23). After dividing into real and imaginary parts, (18) becomes

$$a_f'' + a_s'' + (a_f' + a_s')^2 - (\theta_f + \theta_s)^2 + L_0^r + L_1^r(a_f + a_s) = 0 \quad \text{(A1a)}$$

$$\theta_f' + \theta_s' + 2(a_f' + a_s')(\theta_f + \theta_s) + L_0^i + L_1^i(a_f + a_s) = 0 \quad \text{(A1b)}$$

where, for example, L_0^r denotes the real part of L_0. The fast variables a_f, θ_f, are those which vary on a spatial scale of $O(\pi/q_0)$; the slow variables a_s, θ_s vary on a spatial scale of $O(1)$. To exploit the existence of two distinct length scales, we spatially average equations (A1) over a distance long compared to $2\pi/q_0$, but short compared to 1, leaving

$$a_s'' + a_s'^2 - \theta_s^2 + L_0^r + L_1^r a_s + \langle a_f'^2 - \theta_f^2 \rangle = 0 \quad \text{(A2a)}$$

$$\theta_s' + 2a_s'\theta_s + L_0^i + L_1^i a_s + 2\langle a_f'\theta_f \rangle = 0. \quad \text{(A2b)}$$

$\langle \cdots \rangle$ denotes spatial averaging over the fast scale; (A2a)–(A2b) vary on the slow scale. They determine the slowly-varying quantities a_s and θ_s.

Keeping highest order terms (dropping $a_s'^2$, a_s'') leads to the following two coupled equations for the slowly-varying amplitude and phase gradient:

$$-\theta_s^2 + L_0^r + L_1^r a_s + \langle a_f'^2 - \theta_f^2 \rangle = 0 \quad \text{(A3a)}$$

$$\theta_s' + 2a_s'\theta_s + L_0^i + L_1^i a_s + 2\langle a_f'\theta_f \rangle = 0. \quad \text{(A3b)}$$

Noting from (21b) that $L_1^r = bL_1^i$, we can eliminate a_s easily from these equations, leaving the following equation in θ_s:

$$b\theta_s' + \theta_s(\theta_s + 2ba_s') = b^2\chi^2(\xi) \quad \text{(A4a)}$$

where

$$b^2\chi^2(\xi) \equiv L_0^r - bL_0^i + \langle a_f'^2 - \theta_f^2 \rangle - 2b\langle a_f'\theta_f \rangle. \quad \text{(A4b)}$$

Neglecting $2ba_s'$ with respect to θ_s, (A4) becomes

$$b\theta_s' = b^2\chi^2(\xi) - \theta_s^2. \quad \text{(A5)}$$

We choose initial conditions $a_s(0) = 0$, $a_s'(0) = 0$, $\theta_s(0) = 0$, which together with (A3a) implies

$$L_0^r + \langle a_f'^2 - \theta_f^2 \rangle|_0 = 0. \quad \text{(A6)}$$

Then

$$b\chi^2(0) = -L_0^i - 2\langle a_f'\theta_f \rangle|_0. \quad \text{(A7)}$$

By approximating $\chi \simeq \chi(0) \equiv \chi_0$ (to be checked in Appendix B), we can integrate (A5) for the slowly-varying phase gradient, and then determine the slowly-varying amplitude from (A3a):

$$\theta_s = b\chi_0 \tanh(\chi_0\xi) \quad \text{(A8a)}$$

$$a_s = \frac{1}{L_1^r}\left(\tanh^2(\chi_0\xi) - L_0^r - \langle a_f'^2 - \theta_f^2 \rangle\right). \quad \text{(A8b)}$$

We spatially-averaged (A1) to obtain the slow equations, (A2). Upon subtracting (A2) from (A1), we are left with the fast equations:

$$a_f'' + (a_f'^2 - \langle a_f'^2 \rangle) + 2a_f'a_s' - (\theta_f^2 - \langle \theta_f^2 \rangle) - 2\theta_f\theta_s + L_1^r a_f = 0 \quad \text{(A9a)}$$

$$\theta_f' + 2(a_f'\theta_f - \langle a_f'\theta_f \rangle) + 2a_f'\theta_s + 2a_s'\theta_f + L_1^i a_f = 0. \quad \text{(A9b)}$$

Equations (A9a)–(A9b) describe a harmonic oscillator system with a slowly-varying resonance frequency. The terms in parentheses act as driving terms at double the resonant frequency; their corresponding response will be smaller than the fundamental, and we neglect them in favor of the fundamental response. Of the remaining terms, we keep only those of $O(q_0^2)$ and neglect the $O(q_0)$ and $O(1)$ terms. Equation (A9) then simplifies to

$$a_f'' - 2\theta_s\theta_f + L_1^r a_f = 0 \quad \text{(A10a)}$$

$$\theta_f' + 2\theta_s a_f' + L_1^i a_f = 0. \quad \text{(A10b)}$$

In view of the slowly-varying coefficients, we form a WKB-type solution

$$a_f \sim c_1 e^{i\int q\,d\xi} \quad \text{(A11a)}$$

$$\theta_f \sim c_2 e^{i\int q\,d\xi} \quad \text{(A11b)}$$

with slowly-varying $q(\xi)$. Together, (A10) becomes the following eigenvalue system

$$\begin{bmatrix} -q^2 + q_0^2 & -2\theta_s \\ \frac{q_0^2}{b} + iq2\theta_s & iq \end{bmatrix} \begin{pmatrix} c_1 \\ c_2 \end{pmatrix} = \begin{pmatrix} 0 \\ 0 \end{pmatrix} \quad \text{(A12)}$$

The characteristic equation is

$$q^2 = q_0^2 + 4\theta_s^2 - i\frac{q_0^2 2\theta_s}{bq}. \quad \text{(A13)}$$

Taking q to be of the form $q_r - iq_i$, then $q^2 = q_r^2 - q_i^2 - i2q_rq_i$. Assuming $q_r^2 >> q_i^2$, we take

$$q^2 = q_r^2 - i2q_rq_i. \quad \text{(A14)}$$

Comparing (A13) and (A14) gives

$$q_r^2 = q_0^2 + 4\theta_s^2 \quad \text{(A15a)}$$

$$q_i = \frac{\theta_s}{b}\frac{q_0^2}{q_0^2 + 4\theta_s^2}. \quad \text{(A15b)}$$

There are two solutions for q_r (equal magnitude, opposite sign), and one for q_i. Thus the two solutions of (A13) for the propagation constant are

$$q_\pm = \pm q_r - iq_i \quad \text{(A16)}$$

where henceforth q_r is understood to be the positive root of (A15a). Note that $q_i << q_r$, as assumed. Now, a_f and θ_f are real quantities. Symmetry dictates the choice of a_f as

$$a_f = \frac{m_0}{2}\left(e^{i\int q_+ d\xi} + e^{i\int q_- d\xi}\right)$$

$$= m_0 e^{\int q_i d\xi}\cos\int q_r\, d\xi. \quad \text{(A17)}$$

The quantity $m(\xi) \equiv m_0 \exp\int q_i\, d\xi$ is the slowly-varying modulation depth. The phase θ_f is then determined by the eigenvector of (A12). We have

$$\left.\frac{c_2}{c_1}\right|_\pm = i\frac{q_0^2}{bq_\pm} - 2\theta_s \approx \pm i\frac{q_0^2}{bq_r} - 2\theta_s. \quad \text{(A18)}$$

Then

$$\theta_f = \frac{m_0}{2}\left[\left.\frac{c_2}{c_1}\right|_+ e^{i\int q_+ d\xi} + \left.\frac{c_2}{c_1}\right|_- e^{i\int q_- d\xi}\right]$$

$$= m(\xi)\left(-\frac{q_0^2}{bq_r}\sin\int q_r\, d\xi - 2\theta_s\cos\int q_r\, d\xi\right). \quad \text{(A19)}$$

Finally, let us estimate how the modulation depth and filament wavenumber vary across the half-width of the device. From (A15b) and (A8a) we have

$$\int q_i\, d\xi = \frac{q_0^2}{b}\int\frac{\theta_s}{q_0^2 + 4\theta_s^2}\, d\xi$$

$$= \frac{1}{2\rho}\ln\left(1 + \rho\sinh^2(\chi_0\xi)\right) \quad \text{(A20a)}$$

where

$$\rho \equiv 1 + \frac{4b^2\chi_0^2}{q_0^2}. \quad \text{(A20b)}$$

Hence the modulation depth is

$$m(\xi) = m_0 e^{\int q_i d\xi} = m_0\left(1 + \rho\sinh^2(\chi_0\xi)\right)^{1/2\rho}. \quad \text{(A21)}$$

Thus, the modulation depth is at a minimum, m_0, at the center of the device, and increases monotonically towards the boundary. For the filament wave vector, we will find that $2\theta_s \le q_0$, so $q_r = \sqrt{q_0^2 + 4\theta_s^2} \approx q_0 + 2\theta_s^2/q_0$. Then

$$\int q_r\, d\xi = q_0\xi + \frac{2b^2\chi_0}{q_0}\left(\chi_0\xi - \tanh(\chi_0\xi)\right). \quad \text{(A22)}$$

At the middle of the device, the wave vector is simply q_0 and it, too, increases monotonically towards the boundary.

Finally, recalling the slow equations (A3), we can now evaluate the averaged quantities that depend on the fast solutions a_f and θ_f:

$$\langle\theta_f^2\rangle = \frac{m^2}{2}\left(\frac{q_0^2}{b^2}\frac{q_0^2}{q_0^2 + 4\theta_s^2} + 4\theta_s^2\right) \quad \text{(A23a)}$$

$$\langle a_f'^2\rangle = \frac{m^2}{2}\left(\frac{\theta_s^2}{b^2}\left(\frac{q_0^2}{q_0^2 + 4\theta_s^2}\right)^2 + q_0^2 + 4\theta_s^2\right) \quad \text{(A23b)}$$

$$\langle a_f'\theta_f\rangle = \frac{m^2}{2}\left(\frac{q_0^2}{b} - \frac{2\theta_s^2}{b}\frac{q_0^2}{q_0^2 + 4\theta_s^2}\right). \quad \text{(A23c)}$$

This enables explicit evaluation of the slowly-varying amplitude; together (A23) and (A8b) give

$$a_s = \frac{1}{q_0^2}\left[b^2\chi_0^2\tanh^2\chi_0\xi - L_0^r - \frac{m^2}{2}q_0^2\right] \quad \text{(A24)}$$

where terms of relative order $1/b^2$ have been neglected. This equation can be simplified further. By imposing the condition $a_s(0) = 0$, we infer from (A24) that $L_0^r = -\frac{1}{2}m_0^2q_0^2$. Equation (A24) becomes

$$a_s = \frac{b^2\chi_0^2}{q_0^2}\tanh^2\chi_0\xi - \frac{1}{2}\left(m^2(\xi) - m_0^2\right). \quad \text{(A25)}$$

The last calculation we need is the quantity χ. From (A4b) we have

$$b^2\chi^2 = L_0^r - bL_0^i + \frac{m^2}{2}\frac{q_0^2}{q_0^2 + 4\theta_s^2}$$

$$\cdot\left[\frac{\theta_s^2q_0^2}{b^2(q_0^2 + 4\theta_s^2)} - q_0^2\left(1 + \frac{1}{b^2}\right)\right]. \quad \text{(A26)}$$

To a good approximation (lowest order in $1/b^2$),

$$b^2\chi^2 \approx L_0^r - bL_0^i - \frac{m^2}{2}\frac{q_0^4}{q_0^2 + 4\theta_s^2}. \quad \text{(A27)}$$

APPENDIX B

In the solution of (A5)

$$b\theta_s' = b^2\chi^2(\xi) - \theta_s^2 \tag{B1}$$

we made the approximation that $\chi(\xi)$ was a constant, χ_0. The actual expression for $\chi(\xi)$ is

$$\chi^2(\xi) - \chi_0^2 = \frac{1}{2b^2}\left[m_0^2 - m^2(\xi))\, q_0^2 + m^2(\xi)\, q_0^2\left(\frac{4\theta_s^2}{q_r^2}\right)\right]. \tag{B2}$$

While $\chi(\xi) = \chi_0$ at $\xi = 0$, the difference could conceivably become significant when $m(\xi) >> m_0$. We can make an estimate of the error by taking

$$\theta_s = \theta_{s0} + \theta_{s1}, \qquad \theta_{s1} << \theta_{s0}, \tag{B3}$$

where θ_{s0} satisfies (A8). Substituting (B3) into (B2) gives

$$b\theta_{s1}' + 2\theta_{s0}\theta_{s1} + \theta_{s1}^2 = b^2(\chi^2(\xi) - \chi_0^2). \tag{B4}$$

We neglect θ_{s1}^2 (we are assuming the error is small) and substitute (B1) for $\chi^2(\xi) - \chi_0^2$, to get

$$\theta_{s1}' + \frac{2}{b}\theta_{s0}\theta_{s1} = \frac{q_0^2}{2b^2}\left(m_0^2 - m^2(\xi)\frac{q_0^2}{q_r^2}\right). \tag{B5}$$

(B5) has the solution

$$\theta_{s1} = \frac{m_0^2 q_0^2}{2b}\operatorname{sech}^2\chi_0\xi \int_0^\xi d\zeta \cosh^2\chi_0\zeta \cdot \left[1 - \frac{q_0^2(1 + \rho\sinh^2\chi_0\zeta)^{1/\rho}}{q_0^2 + 4b^2\chi_0^2\tanh^2\chi_0\zeta}\right]. \tag{B6}$$

The integral in (B6) does not have a simple closed-form expression, but we are only interested in determining the approximate size of θ_{s1} relative to θ_{s0}. We asymptotically expand (B6) for large and small χ_0, yielding

$$\frac{\theta_{s1}}{\max(\theta_{s0})} = \frac{\theta_{s1}}{b\chi_0} \sim \frac{m_0^2 q_0^2}{4b^2\chi_0^2} \quad \text{as} \quad \chi_0 \to \infty \tag{B7a}$$

$$\frac{\theta_{s1}}{b\chi_0} \sim -\frac{m_0^2 q_0^2}{6b}\chi_0\xi^3 \quad \text{as} \quad \chi_0 \to 0 \tag{B7b}$$

While θ_{s1} undergoes a sign change at some intermediate value of χ_0, neither expression becomes $O(1)$ for reasonable values of m_0, q_0, and χ_0. Therefore, the original approximation is valid.

REFERENCES

[1] J. C. Dyment, "Hermite-Gaussian mode patterns in GaAs junction lasers," *Appl. Phys. Lett.*, vol. 10, pp. 84–86, 1967.

[2] E. Kapon, J. Katz, and A. Yariv, "Supermode analysis of phase-locked arrays of semiconductor lasers," *Opt. Lett.*, vol. 10, no. 4, pp. 125–127, 1984.

[3] J. Katz, E. Kapon, C. Lindsey, J. S. Smith, S. Margalit, U. Shreter, and A. Yariv, "Phase-locked semiconductor laser array with separate contacts," *Appl. Phys. Lett.*, vol. 43, pp. 1257–1260, 1984.

[4] E. Kapon, C. Lindsey, J. Katz, S. Margalit, and A. Yariv, "Chirped arrays of diode lasers for supermode control," *Appl. Phys. Lett.*, vol. 45, pp. 200–202, 1984.

[5] D. Ackley, "Phase-locked injection laser arrays with non-uniform stripe spacing," *Electron Lett.*, vol. 20, pp. 695–697, 1984.

[6] L. Figueroa, C. Morrison, H. D. Law, and F. Goodwin, "Twin-channel laser with high cw power and low beam divergence," *J. Appl. Phys.*, vol. 56, pp. 3357–3359, 1984.

[7] Y. Twu, A. Dienes, S. Wang, and J. R. Whinnery, "High power coupled-ridge waveguide semiconductor laser arrays," *Appl. Phys. Lett.*, vol. 45, pp. 709–711, 1984.

[8] S. Mukai, C. Lindsey, J. Katz, E. Kapon, Z. Rav-noy, S. Margalit, and A. Yariv, "Fundamental mode oscillation of a buried ridge waveguide laser arrays," *Appl. Phys. Lett.*, vol. 45, pp. 834–835, 1984.

[9] C. Lindsey, E. Kapon, J. Katz, S. Margalit, and A. Yariv, "Single-contact tailored gain phased array of semiconductor lasers," *Appl. Phys. Lett.*, vol. 45, pp. 722–724, 1984.

[10] C. Lindsey, P. Derry, and A. Yariv, "Tailored gain broad area semiconductor laser with single-lobed diffraction-limited farfield pattern," *Electron Lett.*, vol. 21, pp. 671–673, 1985.

[11] D. Welch, D. Scifres, P. Cross, H. King, W. Streifer, R. D. Burnham, J. Yaeli, and T. Paoli, "High power cw operation of phased array diode lasers with diffraction-limited output beam," *Appl. Phys. Lett.*, vol. 47, pp. 1134–1136, 1985.

[12] L. Goldberg, H. F. Taylor, J. F. Welles, and D. Scifres, "Injection locking of coupled-stripe diode laser arrays," *Appl. Phys. Lett.*, vol. 46, pp. 236–238, 1985.

[13] J. P. Hohimer, A. Owyoung, and G. R. Hadley, "Single-channel injection locking of a diode laser array with a cw dye laser," *Appl. Phys. Lett.*, vol. 47, pp. 1244–1246, 1985.

[14] J. Salzman, T. Venkatesan, R. Lang, M. Mittelstein, and A. Yariv, "Unstable resonator cavity semiconductor lasers," *Appl. Phys. Lett.*, vol. 46, pp. 218–220, 1985.

[15] A. Larsson, M. Mittlestein, Y. Arakawa, and A. Yariv, "High efficiency broad area single quantum well lasers with narrow single-lobed farfield pattern prepared by MBE," *Electron Lett.*, vol. 22, no. 2, pp. 79–81, 1986.

[16] M. Mittlestein, J. Salzman, A. Larsson, and A. Yariv, unpublished.

[17] G. H. B. Thompson, "A theory for filamentation in semiconductor lasers," *Optoelectronics*, vol. 4, pp. 257–310, 1972.

[18] F. R. Nash, "Mode guidance parallel to the junction plane of double heterostructure GaAs lasers," *J. Appl. Phys.*, vol. 44, pp. 4696–4707, 1973.

[19] P. A. Kirkby, A. R. Goodwin, G. H. B. Thompson, and P. R. Selway, "Observations of self-focusing in stripe geometry semiconductor lasers and the development of a comprehensive model of their operation," *IEEE J. Quantum Electron.*, vol. QE-13, pp. 705–719, 1977.

[20] R. Lang, "Lateral transverse mode instability and its stabilization in stripe-geometry injection lasers," *IEEE J. Quantum Electron.*, vol. QE-15, pp. 718–726, 1979.

[21] S. Wang, C. Y. Chen, A. Liao, and L. Figueroa, "Control of mode behavior in semiconductor lasers," *IEEE J. Quantum Electron.*, vol. QE-17, pp. 453–468, 1981.

[22] L. Figueroa, T. Holcomb, K. Burghard, D. Bullock, C. Morrison, L. Zinkiewicz, and G. A. Evans, "Modeling of the optical characteristics for twin-channel laser structures," *IEEE J. Quantum Electron.*, vol. QE-22, pp. 2141–2149, 1986.

[23] W. Streifer and E. Kapon, "Application of the equivalent index method to DH diode lasers," *Appl. Opt.*, vol. 18, no. 22, pp. 3724–3725, 1979.

[24] W. Tsang, "Extremely low threshold AlGaAs graded-index waveguide separate confinement heterostructure lasers grown by molecular beam epitaxy," *Appl. Phys. Lett.*, vol. 40, pp. 217–219, 1982.

[25] C. Bender and S. Orszag, *Advanced Mathematical Methods for Scientists and Engineers*. New York: McGraw-Hill, 1978, p. 499.

[26] A. Yariv, *Optical Electronics*, 3rd ed. New York: Holt, Rinehart and Winston, 1985, p. 142.

[27] G. Stegeman and C. Seaton, "Nonlinear integrated optics," *J. Appl. Phys.*, vol. 58, pp. R57–R78, 1985.

[28] N. Dutta, N. Olsson, and W. Tsang, "Carrier-induced refractive index change in AlGaAs quantum well lasers," *Appl. Phys. Lett.*, vol. 45, pp. 836–837, 1984.

[29] A. Arakawa and A. Yariv, "Theory of gain, modulation response, and spectral linewidth in AlGaAs quantum well lasers," *IEEE J. Quantum Electron.*, vol. QE-21, no. 10, pp. 1666–1674, 1985.

[30] J. Buus, "Principles of semiconductor laser modelling," *IEE Proc.*, vol. 132-J, no. 1, pp. 42–51, 1985.

[31] R. J. Lang and A. Yariv, "Intermodal stability of a coupled-cavity laser," *IEEE J. Quantum Electron.*, vol. QE-22, pp. 631–636, 1986.

[32] M. Ablowitz and A. Segur, *Solitons and the Inverse Scattering Transform*. Studies in Applied Mathematics, Siam, 1981, pp. 271-273.
[33] J. Salzman, A. Larsson and A. Yariv, "Phase locked controlled filament laser," *Appl. Phys. Lett.*, vol. 49, pp. 611-613, 1986.

David Mehuys (S'85), for a photograph and biography, see p. 787 of the June 1987 issue of this JOURNAL.

Robert J. Lang (S'83-M'86), for a photograph and biography, see p. 399 of the April 1987 issue of this JOURNAL.

Michael Mittelstein was born in Hamburg, West Germany, in 1956. He received the Vordiploms (B.S. degrees) in physics and computer science, both in 1977, and the Diploma (M.S. degree) in physics in 1983, all from the University of Hamburg.

In 1981 he joined the Laser Physics Department under Prof. F.P. Schäfer, at the Max-Planck-Institute of Biophysical Chemistry, Göttingen, West Germany. During the course of his work there he was exposed to several types of laser systems and became specialized in the field of excimer lasers. Since 1983 he has been working towards the Ph.D. degree in applied physics with Prof. A. Yariv at the California Institute of Technology, Pasadena. He has been involved in various aspects of semiconductor lasers. After exploring unstable resonators and other configurations, he is currently investigating quantum well lasers. Major topics studied include nonlinear gain and the index of refraction, as well as spectral characteristics. He examines their effects on waveguiding and resonator requirements and their consequences on fundamental properties of high-performance devices.

Joseph Salzman, for a photograph and biography, see p. 400 of the April 1987 issue of this JOURNAL.

Amnon Yariv (S'56-M'59-F'70), for a photograph and biography, see p. 399 of the April 1987 issue of this JOURNAL.

Unclassified
SECURITY CLASSIFICATION OF THIS PAGE

REPORT DOCUMENTATION PAGE

Form Approved
OMB No. 0704-0188

1a. REPORT SECURITY CLASSIFICATION Unclassified	1b. RESTRICTIVE MARKINGS
2a. SECURITY CLASSIFICATION AUTHORITY	3. DISTRIBUTION/AVAILABILITY OF REPORT Approved for public release; distribution unlimited.
2b. DECLASSIFICATION/DOWNGRADING SCHEDULE	
4. PERFORMING ORGANIZATION REPORT NUMBER(S) N00014-85-K-0211	5. MONITORING ORGANIZATION REPORT NUMBER(S) 696-002
6a. NAME OF PERFORMING ORGANIZATION California Institute of Technology 6b. OFFICE SYMBOL (If applicable)	7a. NAME OF MONITORING ORGANIZATION Office of Naval Research
6c. ADDRESS (City, State, and ZIP Code) Pasadena, California 91125	7b. ADDRESS (City, State, and ZIP Code) 565 S. Wilson Pasadena, California 91106-3212
8a. NAME OF FUNDING/SPONSORING ORGANIZATION Office of Naval Research 8b. OFFICE SYMBOL (If applicable)	9. PROCUREMENT INSTRUMENT IDENTIFICATION NUMBER P00001
8c. ADDRESS (City, State, and ZIP Code) 800 N. Quincy Street Arlington, VA 22217	10. SOURCE OF FUNDING NUMBERS PROGRAM ELEMENT NO. / PROJECT NO. / TASK NO / WORK UNIT ACCESSION NO.

11. TITLE (Include Security Classification)
Second quantized state lasing of a current pumped single quantum well laser

12. PERSONAL AUTHOR(S)
M. Mittelstein, Y. Arakawa, A. Larsson and A. Yariv

13a. TYPE OF REPORT	13b. TIME COVERED	14. DATE OF REPORT (Year, Month, Day)	15. PAGE COUNT
Reprint	FROM _____ TO _____	86 December	3

16. SUPPLEMENTARY NOTATION The view, opinions and/or findings contained in this report are those of the author(s) and should not be construed as an official Department of the Navy position, policy, or decision unless so designated by other documentation.

17. COSATI CODES			18. SUBJECT TERMS (Continue on reverse if necessary and identify by block number)
FIELD	GROUP	SUB-GROUP	single quantum well laser

19. ABSTRACT (Continue on reverse if necessary and identify by block number)

Newly observed features of quantum well lasers are presented and explained with the aid of a simple model. These involve lasing with gain contributions not only from the fundamental (n=1) state, but simultaneously from the second quantized (n=2) state as well. Experimental data for current pumped GaAlAs/GaAs single quantum well lasers are presented. Very high resonator losses ($\gtrsim 100$ cm^{-1}) force the lasers to augment their gain with major contributions from the second quantized state. The main signature of n=2 lasing, a sudden and large increase in the lasing photon energy, is observed and explained by the theory.

20. DISTRIBUTION/AVAILABILITY OF ABSTRACT ☐ UNCLASSIFIED/UNLIMITED ☐ SAME AS RPT ☐ DTIC USERS	21. ABSTRACT SECURITY CLASSIFICATION
22a. NAME OF RESPONSIBLE INDIVIDUAL	22b. TELEPHONE (Include Area Code) / 22c. OFFICE SYMBOL

DD Form 1473, JUN 86 Previous editions are obsolete. SECURITY CLASSIFICATION OF THIS PAGE

Second quantized state lasing of a current pumped single quantum well laser

Michael Mittelstein, Yasuhiko Arakawa,[a] Anders Larsson,[b] and Amnon Yariv
California Institute of Technology, Pasadena, California 91125

412

(Received 7 July 1986; accepted for publication 27 October 1986)

Newly observed features of quantum well lasers are presented and explained with the aid of a simple model. These involve lasing with gain contributions not only from the fundamental ($n = 1$) state, but simultaneously from the second quantized ($n = 2$) state as well. Experimental data for current pumped GaAlAs/GaAs single quantum well lasers are presented. Very high resonator losses ($\gtrsim 100\ \mathrm{cm}^{-1}$) force the lasers to augment their gain with major contributions from the second quantized state. The main signature of $n = 2$ lasing, a sudden and large increase in the lasing photon energy, is observed and explained by the theory.

In this letter we report on an experimental and theoretical investigation of the gain of quantum well lasers and present experimental evidence of lasing involving the second quantized ($n = 2$) level.[1] Lasing at a higher energy is induced by increasing the losses in a single quantum well laser, which is attained by decreasing the cavity length of Fabry–Perot lasers. In addition, however, a substantial increase in threshold current was observed. This feature was predicted by Arakawa and Yariv[2] and by McIlroy *et al.*[3] and also observed by Zory *et al.*[4] but was not specifically related to the second quantized state lasing.

The experimental approach utilizes the fact that at lasing the modal gain constant g is equal to the modal losses; that is, in Fabry–Perot resonators

$$g = \alpha_i + (1/L)\ln(1/R). \tag{1}$$

Cleaved, uncoated, broad-area, gain-guided lasers are used and a reflectivity of $R = 0.3$ is assumed. Our single quantum well (SQW) devices grown by molecular beam epitaxy[5] show very low internal losses measured to be $\alpha_i \leqslant 2\ \mathrm{cm}^{-1}$. Therefore, the modal gain at lasing can be selected by simply cleaving devices to the appropriate length L.[1]

A set of lasers was characterized and then cleaved to progressively shorter lengths, resulting in lasers with lengths spanning 70 to 470 μm. In Fig. 1 the measured wavelength at threshold is shown as a function of the modal gain (loss) constant. The vertical bar indicates the spread of the data while the horizontal bar gives the average value. The curve shows results from a theoretical model which is discussed in the following part of this letter. The most striking feature of the data is the very abrupt change of lasing wavelength in the vicinity of 100 cm^{-1}, which we identify with the onset of second quantized state ($n = 2$) lasing.

We employ a simple model to describe the essential characteristics of a quantum well laser and their implications with respect to our measurements. The one-dimensional carrier confinement in a quantum well leads to a staircase density of states function. Considering the $n = 1$ and $n = 2$ states only, the modal gain at photon energy E is calculated from

$$g(E) = C \sum_{n=1}^{2} H\left[(E - E_g)S - E_n\right]\left[2f_c(E) - 1\right]. \tag{2}$$

The constant C, the maximum available modal gain per quantized state, is estimated from our data to be 100 cm^{-1}. The conduction-band offset as a fraction of the total band-gap offset S, is taken to be 0.85.[6] The staircase nature of the density of states function is represented by the Heaviside function H. For E_g we use the band-gap energy of bulk GaAs 1.42 eV. The Fermi function for the electrons with the quasi-Fermi energy E_{fc} is

$$f_c(E) = \frac{1}{\exp\left(\left[(E - E_g)S - E_{fc}\right]/kT\right) + 1}. \tag{3}$$

With $m_c^* = 0.067\, m_e$, where m_e is the electron mass, a 100-Å infinite wall well implies that the first quantized energy is $E_1 = 0.056$ eV and that E_2 is four times as large. In the particular structure used in our experiments (as described in Ref. 5) the actual values are computed by numerical solution of the Schrödinger equation to be $E_1 = 0.0314$ eV and $E_2 = 0.1196$ eV. In this solution we use $E_g(X) = (1.42 + 1.247X)$ eV where X is the Al mole fraction. The expression (2) is a slight simplification that ignores some of the specific hole features and does not include collision broadening.

Figure 2 shows the electron density distribution and gain spectrum of our model for two conditions: Fig. 2(a) is

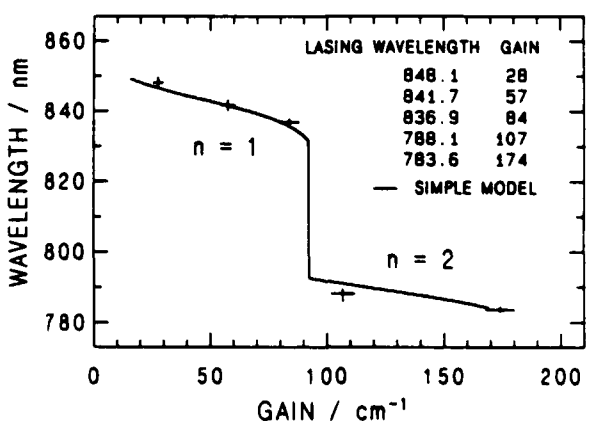

FIG. 1. Lasing wavelength vs modal gain measurements are shown in comparison to predictions of our simple model.

[a] Present address: University of Tokyo, Tokyo 106, Japan.
[b] Present address: Chalmers University of Technology, Göteborg, Sweden.

 © 1986 American Institute of Physics

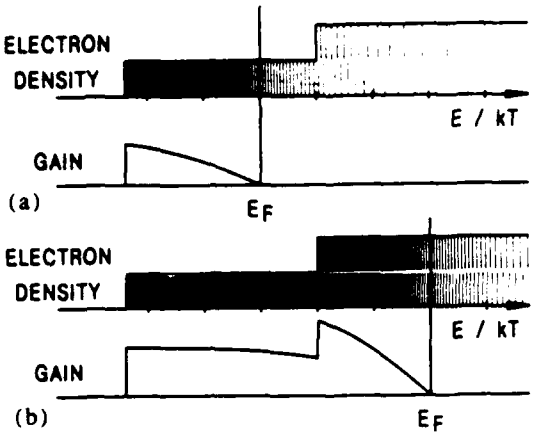

FIG. 2. Gain spectra as computed using (2) from the shown electron density. The occupation of the staircase density of states function is indicated by shading. The vertical bar indicates the quasi-Fermi energy, and the energy is drawn to scale for room temperature. Part (a) shows conditions of high pump density, part (b) of very high pump density resulting in the gain maximum at the onset energy of the second quantized state.

for the case of a high pump current density, several times the threshold current density of a normal SQW laser; Fig. 2(b) is at an even higher current density. The gain spectrum at the higher pumping level is very wide and shows a new peak at the onset energy of the second quantized state. Especially notable is the doubling of the gain at the onset energy of the second quantized state where its gain adds to that of the first one. Furthermore, in this model considerably higher quasi-Fermi energies (as obtained in very short lasers) lead to nearly double the gain in the high-energy region with respect to the maximum value obtainable from the $n = 1$ state alone.

For more realistic quantitative results, broadening is incorporated via an effective smearing of the steps in the density of states function in the basic model by an amount $\Delta E \simeq \hbar/\tau$, where τ is the intraband scattering time of the electrons. A value of $\Delta E = 6.6$ meV corresponding to $\tau = 0.1$ ps is used. The broadening is altered to have exponential tails rather than a Lorentzian shape. Including broadening, the modal gain expression becomes

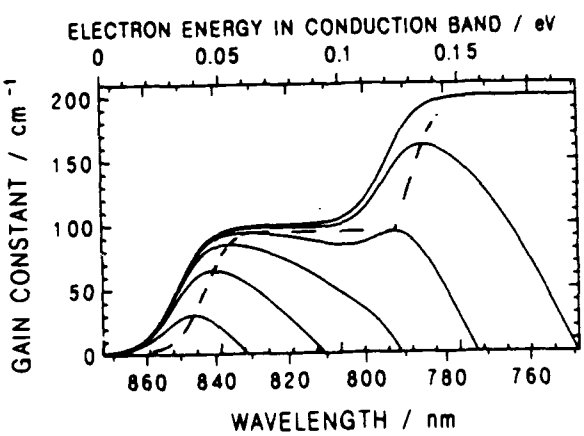

FIG. 3. Gain spectra as computed using (4) for various quasi-Fermi energies are shown as solid lines. The top solid curve gives the maximum available gain, which is limited by the density of states function. The broken curve traces the maximum gain of the spectra with varying quasi-Fermi energy.

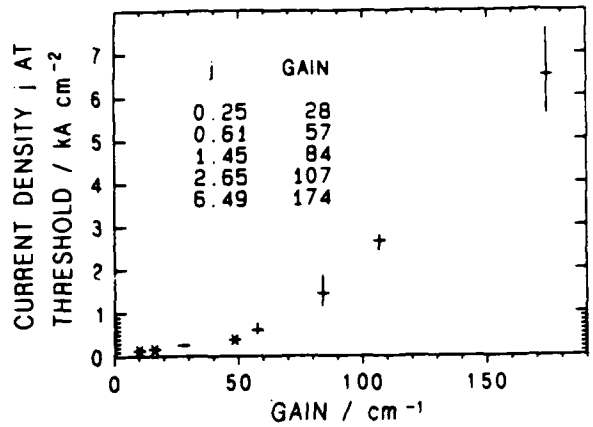

FIG. 4. Threshold current density vs lasing gain measurements. For explanation see text.

$$g(E) = C \sum_{n=1}^{2} \frac{1}{\exp([E_n - E]\, S/\Delta E) + 1} \, [2f_c(E) - 1] \, . \tag{4}$$

This equation gives gain spectra as shown in Fig. 3 for different quasi-Fermi energies. In this model the gain curve crosses zero at the quasi-Fermi energy of the conduction electrons. The higher quasi-Fermi energies (corresponding to higher pump densities) are associated with the short cavity lasers. The calculations show a wide gain spectrum which leads to a high level of recombination radiation even as threshold is approached. We verified this by measuring gain spectra of short lasers below threshold which indicated fairly flat gain over a region extending over more than 50 nm.

The uppermost curve in Fig. 3 shows the maximum available gain as a function of photon energy, that is, the value which would result from an infinite pumping current in this model. Therefore, the gain needed to overcome very high losses ($\gtrsim 100$ cm^{-1} in our case) can only be obtained from a SQW laser by enlisting the added contribution of a second ($n = 2$) quantized state. Consequently, the lasing wavelength must shift to shorter wavelengths as the required gain (i.e., the loss of the cavity) is increased. By tracing the peak of the gain spectrum (4) for varying quasi-Fermi energies as indicated in Fig. 3 the lasing wavelength as a function of modal gain is obtained in this model. This result is the curve shown together with the experimental data in Fig. 1.

The qualitative agreement of our results with this model is good, and leaves little doubt concerning the participation of the second quantized state in the lasing.

The lasing wavelength characteristics explained above are accompanied by an extraordinary increase in threshold current with increasing gain (that is, decreasing length). The observed dependence of threshold current density on the laser gain is shown in Fig. 4. Again, the vertical bar indicates the spread of the data while the horizontal bar gives the average value. The threshold current was determined from the first rapid change in intensity of any longitudinal mode with small increases in current. This was necessary since the short devices exhibit a high spectrally integrated light intensity at threshold (about 10 mW for 100 μm width caused by the wide gain spectrum as explained above). Furthermore, their very high threshold current densities limit

measurements far above threshold. Thus the conventional method of linearly extrapolating the light-current curve would be inaccurate for the short devices. This restriction does not apply for longer devices, and results of some individual test lasers are shown as asterisks in Fig. 4.

Our model is consistent with the qualitative features of the data shown in Fig. 4. The theoretical treatment of the threshold current density as a function of gain is more complicated than that described above to explain the dependence of the oscillation wavelength on the gain. For the high loss devices it must take into account the density of states function at energies above the quantum well and is thus a sensitive function of the band profile outside the well region. Such an analysis is now in progress and will be described in a more detailed account of the work.

The considerations and data presented in this letter have a strong bearing on the design for extremely short quantum well lasers and on the quest for short-wavelength semiconductor lasers.

In conclusion, the lasing of a current pumped single quantum well laser from the second quantized state was demonstrated. A simple model explains the threshold current and spectral characteristics of the effect, especially the discontinuous change in lasing wavelength.

The authors thank a reviewer for a helpful critique. The research reported in this letter was supported by the National Science Foundation, Office of Naval Research, and Rockwell International Corporation.

[1]M. Mittelstein, Y. Arakawa, A. Larsson, and A. Yariv, XIV International Quantum Electronics Conference, June 1986, PD16.

[2]Y. Arakawa and A. Yariv, IEEE J. Quantum Electron. **QE-21**, 1666 (1985).

[3]P. W. A. McIlroy, A. Kurobe, and Y. Uematsu, IEEE J. Quantum Electron. **QE-21**, 1958 (1985).

[4]P. S. Zory, A. R. Reisinger, L. J. Mawst, G. Costrini, C. A. Zmudzinski, M. A. Emanuel, M. E. Givens, and I. J. Coleman, Electron. Lett. **22**, 475 (1986).

[5]A. Larsson, M. Mittelstein, Y. Arakawa, and A. Yariv, Electron. Lett. **22**, 79 (1986).

[6]The effect of changing S is primarily a vertical shift of the curve in Fig. 1, while leaving its characteristic features unchanged. We are aware that a value of $S = 0.6$ is more consistent with the majority of recent determinations; we use 0.85 because it provides the best fit to our data. However, our model is too simple to draw conclusions regarding the appropriate value of S.

Unclassified
SECURITY CLASSIFICATION OF THIS PAGE

REPORT DOCUMENTATION PAGE

Form Approved
OMB No. 0704-0188

1a. REPORT SECURITY CLASSIFICATION Unclassified	1b. RESTRICTIVE MARKINGS
2a. SECURITY CLASSIFICATION AUTHORITY 2b. DECLASSIFICATION / DOWNGRADING SCHEDULE	3. DISTRIBUTION / AVAILABILITY OF REPORT Approved for public release; distribution unlimited.
4. PERFORMING ORGANIZATION REPORT NUMBER(S) N00014-85-K-0211	5. MONITORING ORGANIZATION REPORT NUMBER(S) 696-002
6a. NAME OF PERFORMING ORGANIZATION California Institute of Technology 6b. OFFICE SYMBOL (If applicable)	7a. NAME OF MONITORING ORGANIZATION Office of Naval Research
6c. ADDRESS (City, State, and ZIP Code) Pasadena, California 91125	7b. ADDRESS (City, State, and ZIP Code) 565 S. Wilson Pasadena, California 91106-3212
8a. NAME OF FUNDING / SPONSORING ORGANIZATION Office of Naval Research 8b. OFFICE SYMBOL (If applicable)	9. PROCUREMENT INSTRUMENT IDENTIFICATION NUMBER P00001
8c. ADDRESS (City, State, and ZIP Code) 800 N. Quincy Street Arlington, VA 22217	10. SOURCE OF FUNDING NUMBERS PROGRAM ELEMENT NO. / PROJECT NO. / TASK NO / WORK UNIT ACCESSION NO.

11. TITLE (Include Security Classification)
Quantum Well Lasers--Gain, Spectra, Dynamics

12. PERSONAL AUTHOR(S)
Y. Arakawa and A. Yariv

13a. TYPE OF REPORT	13b. TIME COVERED	14. DATE OF REPORT (Year, Month, Day)	15. PAGE COUNT
Reprint	FROM _____ TO _____	1986 September	13

16. SUPPLEMENTARY NOTATION The view, opinions and/or findings contained in this report are those of the author(s) and should not be construed as an official Department of the Navy position, policy, or decision unless so designated by other documentation.

17. COSATI CODES			18. SUBJECT TERMS (Continue on reverse if necessary and identify by block number)
FIELD	GROUP	SUB-GROUP	quantum well lasers

19. ABSTRACT (Continue on reverse if necessary and identify by block number)

We discuss a number of theoretical and experimental issues in quantum well lasers with emphasis on the basic behavior of the gain, the field spectrum, and the modulation dynamics. It is revealed that the use of quantum well structures results in improvement of these properties and brings several new concepts to optical semiconductor devices.

20. DISTRIBUTION / AVAILABILITY OF ABSTRACT ☐ UNCLASSIFIED/UNLIMITED ☐ SAME AS RPT. ☐ DTIC USERS	21. ABSTRACT SECURITY CLASSIFICATION
22a. NAME OF RESPONSIBLE INDIVIDUAL	22b. TELEPHONE (Include Area Code) / 22c. OFFICE SYMBOL

DD Form 1473, JUN 86 Previous editions are obsolete. SECURITY CLASSIFICATION OF THIS PAGE

Quantum Well Lasers—Gain, Spectra, Dynamics

Y. ARAKAWA, MEMBER, IEEE, AND A. YARIV, FELLOW, IEEE

(Invited Paper)

Abstract—**We discuss a number of theoretical and experimental issues in quantum well lasers with emphasis on the basic behavior of the gain, the field spectrum, and the modulation dynamics. It is revealed that the use of quantum well structures results in improvement of these properties and brings several new concepts to optical semiconductor devices.**

I. Introduction

THE ability to fabricate single quantum well (SQW) and multiple quantum well (MQW) devices has given rise to new optical and electronic devices as well as to new physical phenomena [1]. Since the first investigation of optical properties in quantum wells by Dingle *et al.*, [2] the application of quantum well structures to semiconductor laser diodes [3], [4] has received considerable attention because of physical interest as well as its superior characteristics, such as low threshold current density [5], [6], low temperature dependence of threshold current [7]–[9], lasing wavelength tunability, and excellent dynamic properties [10]–[12]. By controlling the width of the quantum wells, one can modify the electron and hole wavefunctions, which leads to the modification of material parameters. This results in improvements of the laser characteristics, as well as introduction of new concepts to semiconductor optical devices.

In this paper, we describe the basic properties of the quantum well laser with emphasis on its dynamic and spectral properties as well as gain characteristics. We also discuss new device concepts including a Q-switched quantum well laser [13] and a quantum wire laser [9], [10].

II. Gain and Threshold Current

A. Density of States

In a quantum well (QW) structure, a series of energy levels and associated subbands are formed due to the quantization of electrons in the direction of the QW thickness. The density of states (per unit energy and area) of such confined electrons in a SQW structure is given by

$$\rho_c(E) = \sum_{n=1}^{\infty} \frac{m_c}{\pi\hbar^2} H[E - \epsilon_n] \tag{1}$$

where $H[x]$, m_c, $\hbar$, and ϵ_n are the Heaviside function, the effective mass of electrons, Planck's constant (h) divided by 2π, and the quantized energy level of electrons in the nth subband of the QW, respectively. When the barriers are sufficiently high and the barrier thickness is sufficiently large, ϵ_n is equal to

$$\epsilon_n = \frac{(n\pi\hbar)^2}{2m_c L_z^2} \tag{2}$$

where L_z is the thickness of the QW.

If we use a MQW structure instead of the SQW, the density of states is modified. When barrier layers between wells are thick enough, each well is independent. In this case, the density of states is just N times density of states of electrons in an SQW.

$$\rho_c(E) = N \sum_{n=1}^{\infty} \frac{m_c}{\pi\hbar^2} H[E - \epsilon_n] \tag{3}$$

where N is the number of QW's. On the other hand, if the barrier is sufficiently thin or its barrier height is small enough so that coupling between adjacent wells is substantial, the quantized energy levels are no longer degenerate, and each single well level splits into N different energy levels. In this case, the density of states (per unit energy and area) is expressed by

$$\rho_c(E) = \sum_{n=1}^{\infty} \sum_{k=1}^{N} \frac{m_c}{\pi\hbar^2} H[E - \epsilon_{nk}] \tag{4}$$

where ϵ_{nk} ($k = 1, \cdots, N$) are the energy levels which split from a single well energy level. Kroemer *et al.* [14] and Yariv *et al.* [15] analytically estimated the energy broadening due to this coupling. The coupling is important for obtaining a uniform carrier distribution in the MQW structure. However, strong coupling leads to the smearing of the configuration of the density of states and a resulting reduction in the two-dimensional character of the wells. We can characterize the smearing due to coupling by ΔE ($\equiv \max \epsilon_{nk} - \min \epsilon_{nk}$). This ΔE corresponds to the degree to which the smearing in the density of states occurs. Since the tunneling time τ_t of electrons through a barrier is on the order of $\hbar/\Delta E$, the following relations

Manuscript received January 5, 1986; revised April 11, 1986. This work was supported by the U.S. Air Force Office of Scientific Research, the U.S. Office of Naval Research, the I.T.T. Corporation, and the Japan Society for the Promotion of Science.

Y. Arakawa is with the California Institute of Technology, Pasadena, CA 91125, on leave from the Institute of Industrial Science, University of Tokyo, Minato-ku, Tokyo 106, Japan.

A. Yariv is with the California Institute of Technology, Pasadena, CA 91125.

IEEE Log Number 8609366.

0018-9197/86/0900-1887$01.00 © 1986 IEEE

are required for obtaining good uniformity of carrier concentration and maintaining the two-dimensional properties [14]:

$$\hbar/\tau_r \ll \Delta E(=\hbar/\tau_t) \ll \hbar/\tau_{in} \tag{5}$$

where τ_r is the carrier recombination time at lasing and τ_{in} is the intraband relaxation time (i.e., T_2 time). The first inequality indicates that the tunneling time for uniform carrier distribution should be much smaller than the recombination time. The second one implies that the smearing due to the coupling should be much smaller than the smearing due to the carrier relaxation effects. A localization effect in two slightly asymmetric wells is also discussed by Lang *et al.* [16] and Yariv *et al.* [15]. In order to simplify the discussion in this paper, we assume that the coupling in an MQW is weak enough that the density of states can be described by (3).

B. Linear Gain

The gain properties in QW lasers have been investigated using different theoretical treatments [17]–[23]. The main features of the gain properties in QW lasers are the gain flattening effect, dependence on the number and the thickness of the QW's and the anisotropy of the momentum matrix element. When the recombination is dominated by the band-to-band radiative process [24], [25], the linear bulk gain derived under k-selection rule is given by [26]

$$g(E, n) = \frac{\omega}{n_r^2} \chi_I(E, n) \tag{6}$$

$$\chi_I(E, n) = \int \sum_{n=0}^{\infty} \sum_{j=l,h} \rho^j_{\mathrm{red}_n}(\epsilon)(f_c(E_{c_n}) - f_v(E_{v_n}))\, \hat{\chi}_I^{n,j}(E, \epsilon)\, d\epsilon. \tag{7}$$

The bulk gain is the gain exercised by an electromagnetic field if it were completely confined to the QW (i.e., a confinement factor of unity). E is the photon energy, j designates either light holes (l) or heavy holes (h), $\rho^j_{\mathrm{red}_n}$ is the reduced density of states which is defined by $\rho^j_{\mathrm{red}_n} = ((\rho_{c_n})^{-1} + (\rho^j_{v_n})^{-1})^{-1}$, $\rho^j_{v_n}$ is the density of states of light holes ($j = l$) or heavy holes ($j = h$), and f_c (f_v) is the quasi Fermi–Dirac distribution function for electrons (holes) in the conduction band (the valence band) with the Fermi-energy ϵ_{f_c} (ϵ_{f_v}). E_{c_n} and $E^j_{v_n}$ are equal to $(m_c\epsilon^j_{v_n} + m^j_v E + m^j_v\epsilon_{cn})/(m_c + m^j_v)$ and $(m_c\epsilon^j_{v_n} - m_c E + m^j_v\epsilon_{cn})/(m_c + m^j_v)$, respectively, where m^j_v and $\epsilon^j_{v_n}$ are the effective mass and the energy level of the nth subband of light holes ($j = l$) or heavy holes ($j = h$). $\chi_I(E, n)$ is the imaginary part of the susceptibility and $\hat{\chi}_I^{n,j}(E, \epsilon)$ is the susceptibility of each electron–heavy hole pair (or electron–light hole pair) in the nth subband and is given by

$$\hat{\chi}_I^{n,j}(E, \epsilon) = \frac{\pi e^2 h}{m_0^2 c n_r E_g} |M_{n,j}(\epsilon)|^2_{\mathrm{ave}} \frac{\hbar/\tau_{in}}{(E - \epsilon)^2 + (\hbar/\tau_{in})^2} \tag{8}$$

where n_r is the refractive index of the active layer, e is the electron charge, m_0 is the mass electrons, c is the light velocity, and E_g is the bandgap. Although the possibility of the transition with no k-selection rule [19] and a violation of the $\Delta n = 0$ selection rule have been discussed, we will adopt the formula with k-selection rule with $\Delta n = 0$ selection rule.

In QW structures, it was observed by Kobayashi *et al.* [27] that the internal gain depends on the polarization of the light. Asada *et al.* [28] and Yamanishi *et al.* [29] discussed this phenomenon using the $\boldsymbol{k} \cdot \boldsymbol{p}$ perturbation method developed by Kane [30]. For instance, $|M_{n,j}|^2_{\mathrm{ave}}$ for the TE mode (polarized parallel to the layers) due to an electron–heavy hole transition is given by

$$|M_{n,h}|^{2\mathrm{TE}}_{\mathrm{ave}} = |M_0|^2_{\mathrm{ave}} (1 + E/(\epsilon_{c_n} - \epsilon^h_{v_n})) \tag{8}$$

where $|M_0|^2_{\mathrm{ave}}$ is the square of the dipole matrix element of conventional double heterostructure (DH) lasers and is approximately equal to $1.33\, m_0 E_g$. For more precise discussion on this matrix element, nonparabolicity and anisotropy of valence band should be considered, which is discussed elsewhere. The calculated results shown below are, however, on the basis of the above simple model.

The quasi-Fermi energy levels ϵ_{F_c} and ϵ_{F_v} in a laser are determined by both the charge neutrality condition and the condition that the modal gain $g_{\mathrm{mod}}(E) = \Gamma_g(E)$ where Γ is the optical confinement factor) at the photon energy E_l for the laser oscillation is equal to the total losses α_{total} as follows:

$$g_{\mathrm{mod}}(E_l) = \Gamma_g(E) = \alpha_{\mathrm{total}} = \Gamma\alpha_{\mathrm{ac}} + (1 - \Gamma)\, \alpha_{\mathrm{ex}} + L^{-1} \ln (1/R) \tag{9}$$

where α_{ac}, α_{ex}, R, and L are the loss in the active region, the loss in the cladding layers, the reflectivity, and the cavity length, respectively.

Once the Fermi energy levels are fixed, the injected current density J is determined by the following equation:

$$J = eN \left(\iint \frac{8\pi n_r^2 E_g^2}{c^2 h} \sum_{n=0}^{\infty} \sum_{j=l,h} \rho_{\mathrm{red}_j}(\epsilon) f_c(E_{c_n}) \cdot (1 - f_v(E_{c_n}))\, \hat{\chi}_I^{n,j}(E, \epsilon)\, d\epsilon\, dE \right). \tag{10}$$

The optical confinement factor Γ depends strongly on the structure. If we use the separate confinement structure, Γ can be expressed approximately by the following simple formulas [11]:

$$\Gamma = 0.3N \frac{L_z}{L_0} \tag{11}$$

where N is the number of QW's, L_0 is equal to 1000 Å, and the following structure is assumed: the MQW laser has $Ga_{0.75}Al_{0.25}As$ barriers and $Ga_{0.75}Al_{0.25}As$ waveguide layers, and the dimension of the waveguide layers is determined so that the total thickness, including QW's, barriers, and waveguide layers, is equal to 2000 Å. The cladding layers are made of p-$Ga_{0.6}Al_{0.4}As$ and n-$Ga_{0.6}Al_{0.4}As$. In the following calculation, we will ignore

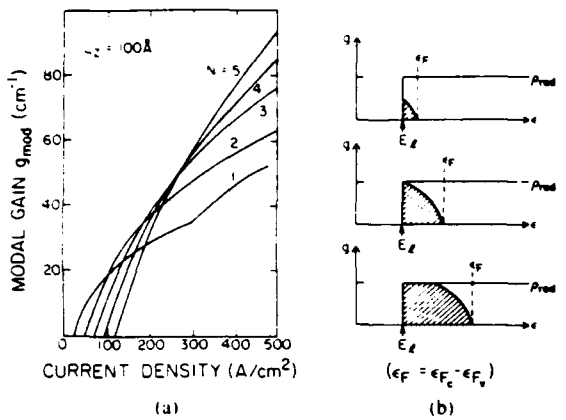

Fig. 1. (a) The modal gain g_{mod} ($=\Gamma g$) as a function of the injected current density with various number of quantum wells N. The thickness of each quantum well is assumed to be 100 Å. (b) An illustration which explains how the gain flattening effect occurs with the increase of the Fermi energy levels.

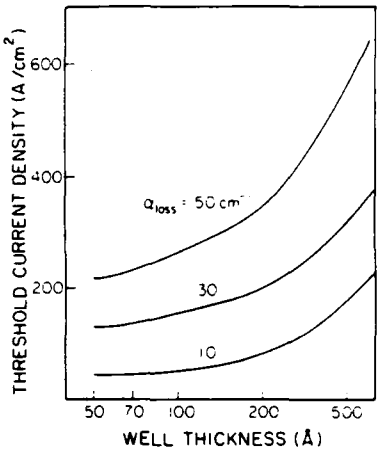

Fig. 2. The threshold current as a function of the quantum well thickness with various total loss α loss. The number of quantum wells is optimized so that the threshold current is minimum.

nonradiative effects such as the Auger recombination and the intervalence band effect [31]–[34].

If the carrier density, hence the quasi-Fermi energy level, in each QW is the same, the modal gain with N QW's, $g^N_{mod}(E_l)$, is given by

$$g^N_{mod}(E_l) = N g^{(N=1)}_{mod}(E_l) \tag{12}$$

where E_l is the lasing photon energy. But, this, of course, happens at

$$J^N = N J^{(N=1)} \tag{13}$$

or, stated in words, the modal gain available from N QW's is N times that of an SQW and is obtained at a current density which is N times that of an SQW laser. Fig. 1(a) shows the calculated modal gain $g^N_{mod}(E_l)$ as a function of the injected current density in a QW laser with N QW's on the basis of (12) and (13). We notice a very marked flattening ("saturation") of the gain at high injected currents, especially in an SQW ($N = 1$). This gain flattening effect is due to the step-like shape of the density of states functions, and the fact that once the quasi-Fermi energy levels penetrate into the conduction band and valence band, which happens at high injected currents, the product $\rho_{red}(\epsilon)(f_c - f_v)$, which determines the gain, becomes a constant and no longer increases with the current. This is illustrated in Fig. 1(b). This flattening effect was evidenced recently by Arakawa *et al.* [35] in a systematic measurement of the threshold current of high-quality GRIN-SCH (graded index waveguide-separate confinement heterostructure) SQW lasers of different cavity length. They observed the jump of the lasing wavelength with the decrease of the cavity length from the wavelength corresponding to $n = 1$ transition to the wavelength corresponding to $n = 2$ transition, which demonstrates the existence of discrete quantized energy levels.

Owing to this gain flattening effect, there exits an optimum number of QW's for minimizing the threshold current for a given total loss α_{total}. From Fig. 1(a), we see that, for low losses, the injected threshold current is minimum with $N = 1$. On the other hand, if $\alpha_{total} = 20$ cm^{-1}, the threshold current with $N = 1$ is larger than that of $N = 2$. At higher values of α_{total} which call for larger laser modal gain, a larger number of wells is needed. When α_{total} is 50 cm^{-1}, a five-well structure ($N = 5$) will have the lowest threshold current.

Fig. 2 shows the threshold current as a function of the QW thickness for various α_{total}. In this calculation, the number of QW's is optimized for each QE thickness so that the threshold current is minimum. The results indicate that the threshold current of thinner QW lasers (L_z = 50–100 Å) is much lower than that of thicker QW lasers. We also notice that the threshold current is minimized with $L_z \approx 60$ Å when α_{loss} is low (α_{loss} = 10–30 cm^{-1}). This is mainly due to the fact that the current for transparency (gain equals to zero) is minimized at the thickness of $L_z \approx 60$ Å in the case of $N = 1$ and also due to the fact that the optimum N in QW lasers with each thickness is 1 in the case of low α_{total} for thin QW structures.

C. Experiment

Many experiments on GaAs/GaAlAs QW laser [5], [7], [36]–[43], InGaAsP/InP QW lasers [44]–[47], InGaAlAs QW lasers [48], and AlGaSb QW lasers [49] have been reported. Fuji *et al.* [5] reported a very low threshold current density as low as 175 A/cm^2 with 480 μm cavity length in a GaAs/AlGaAs GRIN-SCH SQW laser. This demonstrates the realization of high gain with lower spontaneous emission rate owing to the step-like density of states.

sulting in a red shift of the excitonic absorption energy. The band discontinuities prevent the ionization of the exciton, allowing excitonic resonances to be observed at room temperature with large applied fields ($> 10^5$ V/cm).

The concept of the size effect modulation proposed by Yamanishi *et al.* [74] also utilizes the application of electric field. This causes the spatial of the electron distribution and hole distribution in a well, which leads to the modulation of the matrix elements.

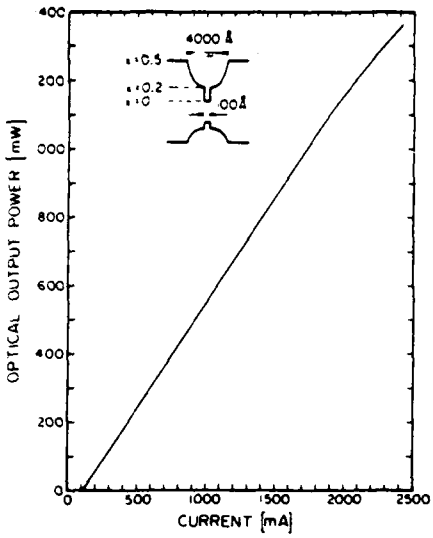

Fig. 3. The light output power versus injection current under pulsed condition of a 100 μm wide and 480 μm broad area GaAs/AlGaAs GRIN-SCH laser (400 ns, 25 Hz).

Fig. 4. The far-field pattern parallel to the injection plane of a 100 μm wide broad area GaAs/AlGaAs GRIN-SCH laser at $I = 1.2I_{th}$. The measured full width at half maximum is 0.8° which is quite close to the diffraction limit of 0.4°.

Recently, in MBE-grown broad area GaAs/AlGaAs GRIN-SCH SQW lasers, a quantum efficiency around 70 percent with a single far-field lobe as narrow as 0.8° has been achieved by Larsson *et al.* [50]. Fig. 3 shows the measured light output power versus injection current under pulsed condition (400 ns, 25 Hz) using calibrated Si photodiodes and filters. The threshold current is 110 mA, which corresponds to a threshold current density of 230 A/cm^2. The maximum output power of 1.35 W from one mirror was limited by the available current from current source. The high external quantum efficiency is a combined result of the low threshold current density and the high differential quantum efficiency of 84 percent. This can be explained in terms of the step-like density of states associated with the quasi-two-dimensional structure of the SQW, enhanced carrier and optical confinement in the GRIN region, and optimized growth conditions. The internal loss estimated by measuring the differential quantum efficiency of the lasers with various cavity length is as low as 1.8 cm^{-1}. Fig. 4 shows the far-field pattern parallel to the junction plane for a 100 μm wide laser at $I = 1.2I_{th}$ where I_{th} is the threshold current. The measured full width at half maximum (FWHM) is 0.8°, to be compared to the diffraction limit of 0.4°. This extremely narrow far field is a result of increased lateral coherence produced by uniformly distributed and phase-locked filaments.

III. Differential Gain and Modulation Bandwidth

A. Relaxation Oscillation Frequency and Differential Gain

The direct modulation of a semiconductor laser has been a subject of active research for the past 20 years [51]–[55]. Experiments have shown the existence of a resonance peak in the modulation response. In the early stage of the semiconductor laser development, the principal concern was in optimizing structures for realizing low threshold currents and high quantum efficiencies. With the increasing sophistication of the laser and the maturing of the technology, their high-speed dynamic characteristics became a subject of increasing importance. Many efforts have been devoted to realizing a wide bandwidth in conventional DH semiconductor lasers by changing the laser geometry. Another approach is to modify the basic material properties through the use of QW structures. In this section, we discuss the possibility of the improvement of these characteristics.

The relaxation oscillation corner frequency f_r gives the useful direct modulation bandwidth of a semiconductor laser. The simple rate equation for laser dynamics can be described as follows:

$$\frac{dn}{dt} = \frac{J(t)}{eL_z} - \frac{n_r}{c} g(n, E_l) P - \frac{n}{\tau_s} \tag{14}$$

$$\frac{dP}{dt} = \Gamma \frac{n_r}{c} g(n, E_l) P + \beta \frac{n}{\tau_s} - \frac{P}{\tau_p} \tag{15}$$

where P is the photon density, β is the spontaneous emission coefficient into the lasing mode, τ_s is the carrier lifetime, $J(t)$ (cm^{-2}) is the injected current density, n is the carrier concentration, and $g(n, E_l)$ (cm^{-2}) is the bulk gain, while $\Gamma g(n, E_l)$ is the modal gain as a function of the carrier density n at the lasing photon energy E_l. To emphasize the dependence of the gain on carrier concentration, we denote the gain as $g(E, n)$ hereafter. When we discuss the carrier density in QW structures, we usually use the two-dimensional density (per cm^2). However, the proper "bookkeeping" of photons and carriers requires that n stand for carrier density per unit volume. The relaxation resonance frequency f_r is determined by a small-signal analysis of (14) and (15). The result can simply be expressed by [53]

$$f_r = \frac{1}{2\pi} \sqrt{\frac{n_r g'(E_l, n)}{c} \frac{P_0}{\tau_p}} \tag{16}$$

where P_0 is the stationary photon density in the cavity and $g'(E_l, n)$ is the differential gain (i.e., $g'(E, n) = \partial g(E, n)/\partial n$). This result suggests several ways to improve f_r: larger $g'(E_l, n)$, smaller τ_p, and larger P_0. The reduction of τ_p and the increase of P_0 are realized with the use of short cavity lasers [53] and window-type lasers [54]. To

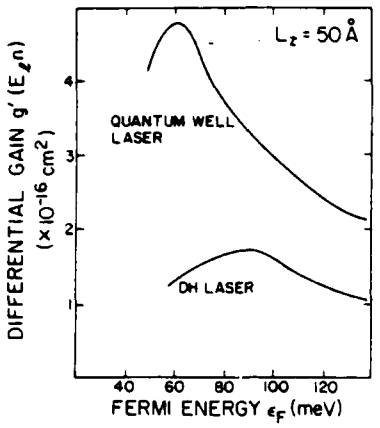

Fig. 5. The differential gain as a function of the conduction band quasi-Fermi energy level in a conventional double heterostructure laser and a quantum well laser with 50 Å well thickness.

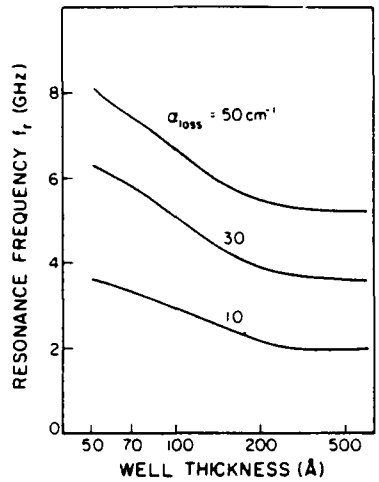

Fig. 6. The relaxation resonance frequency in a quantum well laser as a function of the well thickness. The number of quantum wells and quantum wires is optimized for each quantum well thickness.

increase $g'(E_l, n)$, operation at low temperatures [55] and the use of coupled cavity lasers [56] have been considered.

The basic quantum mechanical expression for $g'(E, n)$ suggests yet another way to increase $g'(E, n)$: changing the electron density of states with the use of QW's [10], [11]. Since the gain $g(E, n)$ is proportional to the imaginary part $\chi_I(E, n)$, as shown in (6), $g'(E, n)$ can be expressed by the following equation:

$$g'(E, n) = \frac{\partial}{\partial n}\left(\frac{\omega}{n_r^2}\chi_I(E, n)\right). \tag{17}$$

It is easily seen from this equation that the density of states plays an important role in determining the properties of $g'(E, n)$ as well as $g(E, n)$. The step-like density of states narrows the gain spectrum compared to that in the bulk material, which leads to an increase of $g'(E, n)$.

Fig. 5 shows the calculated differential gain $g'(E_l, n(\epsilon_{F_c}))$ for a conventional DH laser and a QW laser as a function of the conduction band quasi-Fermi energy level ϵ_{F_c} (measured from the lowest subband energy level). The thickness of the QW structures is equal to 50 Å. The quasi-Fermi energy level for the holes is determined by the charge neutrality condition. The result predicts an enhancement of $g'(E, n)$ for the QW active layer. Note that since $g'(E_l, n)$ is a bulk parameter, it is independent of the number of QW's.

This figure also shows that $g'(E_l, n)$ depends strongly on ϵ_{F_c} (i.e., necessary excitation for laser oscillation). The Fermi energy dependence of $g'(E_l, n)$ implies that there is an optimum number N of QW's in a laser structure which causes the largest enhancement of f_r. To see this, consider, again, the threshold condition for lasing in (9). For simplicity, we ignore the dependence of α_{total} on the structure. Since the gain is a monotonically increasing function of ϵ_{F_c}, the required ϵ_{F_c} for laser oscillation decreases monotonically with the increase of N. Consequently, there exits an optimum N for realizing $\epsilon_{F_c}^{\max}$, defined to yield the maximum $g'(E_l, n)$. It is easily shown that the ϵ_{F_c} at lasing threshold for $N = 1$ is much larger than $\epsilon_{F_c}^{\max}$. Therefore, the largest $g'(E_l, n)$ and the fastest modulation speeds are achieved for the MQW cases ($N \geq 2$). Fig. 6 shows the calculated f_r as a function of L_z (the QW width); α_{total} is assumed to be 50 cm^{-1}. At each L_z, the number of wells is optimized and f_r is normalized by f_r of a conventional DH laser (i.e., $L_z \to \infty$). The results suggest that by optimizing N, f_r can be enhanced by a factor of two in thin QW lasers.

B. Experiment

The enhancement of f_r was experimentally demonstrated by Uomi *et al.* [57]. They used an MQW laser with a self-aligned structure grown by MOCVD and measured the relaxation oscillation observed in the transient characteristics without dc bias at room temperature. f_r was measured as a function of (P/P_c) where P is the output power and P_c is the power for catastrophic optical damage. It was found that f_r of the MQW laser is about twice as large as that of a DH laser with the same structure. They estimated the modulation frequency to be 11 GHz near the catastrophic optical damage limit. This experimental result supports the above theoretical calculations. Iwamura *et al.* [58] measured the longitudinal mode behavior in MQW lasers under modulation, and they obtained a result which suggest that the narrower gain spectrum of an MQW laser causes fewer longitudinal modes under modulation.

IV. Spectral Noise Properties

A. Spectral Linewidth

Recently, the subject of semiconductor laser noise has received considerable attention. The deviation of conventional DH laser noise characteristics from well-established norms was demonstrated by Fleming *et al.* [59]. They found that the linewidth varies inversely with output power, as predicted by the modified Schawlow–Townes formula. The coefficient of the power dependence, however, was significantly larger than predicted by the formula. This discrepancy was explained physically by

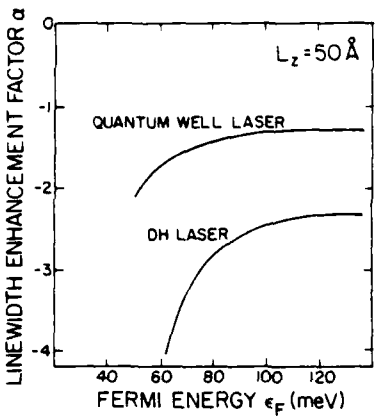

Fig. 7. The linewidth enhancement factor α as a function of the conduction band quasi-Fermi energy level in a conventional double heterostructure laser and a quantum well laser with 50 Å well thickness.

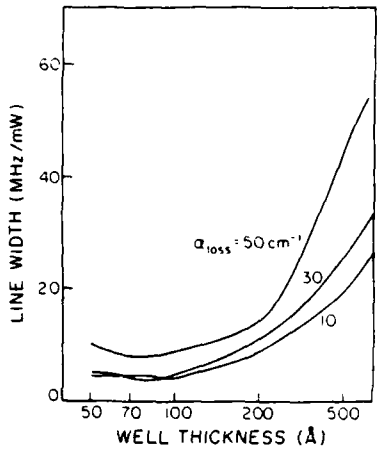

Fig. 8. The spectral linewidth in a quantum well laser as a function of the well thickness. The number of quantum wells is optimized for each quantum well thickness.

Henry [60], and a new theory was developed by Vahala *et al.* [61], [62]. They showed that the expected broadening enhancement is a factor $(1 + \alpha^2)$ where α is named the linewidth enhancement factor. The basic explanation is that phase fluctuations can result from index variations during relaxation oscillations after a spontaneous event, as well as by direct spontaneous emission events. For reducing the linewidth, the use of an external mirror, coupled cavity laser, and distributed feedback laser have been investigated. Another approach for reducing the linewidth is to modify the density of states. In this section, we indicate how the linewidth (or α) is reduced through the use of QW structures [10]–[12], [63].

The spectral linewidth $\Delta\nu$ can be expressed by [60], [61], [64]

$$\Delta\nu = \frac{v_g h\nu \Gamma_g R_m n_{sp}}{\pi P}(1 + \alpha^2) \tag{18}$$

$$\alpha = \frac{\partial\chi_R(E_l, n)/\partial n}{\partial\chi_I(E_l, n)/\partial n}. \tag{19}$$

R_m, v_g, $h\nu$, Γ, g, n_{sp}, and P are the mirror loss, the group velocity of light, the photon energy, the optical confinement factor, the bulk gain at threshold, the spontaneous emission factor, and the laser output power, respectively. $\chi_R(E, n)$ is the real part of the complex susceptibility and

$$\chi_R(E, n) = \int \sum_{n=0}^{\infty} \sum_{j=l,h} \rho^j_{\mathrm{red}_n}(\epsilon)(f_c(E_{c_n}) - f_v(E_{v_n}))\, \hat{\chi}_R^{n,j}(E, \epsilon)\, d\epsilon$$

$$\hat{\chi}_R^{n,j}(E, \epsilon) = \frac{\pi e^2 h}{m_0^2 c n_r E_g} |M_{n,j}(\epsilon)|^2_{\mathrm{ave}} \frac{E - \epsilon}{(E - \epsilon)^2 + (\hbar/\tau_{\mathrm{in}})^2}. \tag{21}$$

α reflects the strong amplitude-phase coupling of the lasing field in a semiconductor laser resulting from the highly detuned optical gain spectrum. Equation (18) indicates that $\Delta\nu$ depends on the electronic density of states through α and n_{sp}.

The denominator of (19) is proportional to $g'(E_l, n)$. Therefore, from the results of the previous section, an increase of the denominator can be expected with the use of QW's. The numerator in (19), however, is also enhanced in QW structures. Therefore, it is difficult to predict the behavior of α in these structures without numerical calculations. Fig. 7 gives a calculation of α as a function of ϵ_{F_c} for conventional DH lasers and QW lasers. In this figure, the thickness of the QW's is equal to 50 Å. These calculation indicate first that α depends strongly on ϵ_{F_c} (or equivalently, on the level of injection which is determined by optical gain required for laser oscillation), its magnitude decreasing for larger ϵ_{F_c}. (This result has been observed experimentally for conventional DH lasers [65].) Second, this reduction of $|\alpha|$ with increasing excitation is larger in QW lasers than in conventional DH lasers. Therefore, a smaller number of QW's leads to a smaller value of $|\alpha|$ because a laser with a smaller number of QW's requires higher Fermi energy levels for a given modal gain.

The linewidth $\Delta\nu$ also contains the spontaneous emission factor n_{sp} which decreases monotonically with the increase of ϵ_{F_c} and converges to 1. This n_{sp} is the ratio of the spontaneous emission rate into the lasing mode to the stimulated emission rate and is given by

$$n_{sp} = \frac{\int \sum_{n=0}^{\infty} \sum_{j=l,h} \rho^j_{\mathrm{red}_n}(\epsilon) f_c(E_{c_n})(1 - f_v(E_{v_n}))\, \hat{\chi}_I^{n,j}(E, \epsilon)\, d\epsilon}{\int \sum_{n=0}^{\infty} \sum_{j=l,h} \rho^j_{\mathrm{red}_n}(\epsilon)\, (f_c(E_{c_n}) - f_v(E_{v_n}))\, \hat{\chi}_I^{n,j}(E, \epsilon)\, d\epsilon}. \tag{22}$$

If the energy broadening due to the intraband relaxation is extremely small, we can approximate n_{sp} at the photon energy E_l by

$$n_{sp} \approx \frac{1}{1 - \exp((E_l - \epsilon_{F_c} + \epsilon_{F_c})/kT)}. \tag{23}$$

As shown in this equation, n_{sp} is a monotonically decreas-

ing function of ϵ_{F_c}. Therefore, for a fixed loss (i.e., Γ_g is constant), it is advantageous to operate with a high ϵ_{F_c} to attain a reduction in $\Delta\nu$. With regard to the number of QW's, this means that, in contrast to f_r, the SQW active layer is the optimum choice for phase noise reduction. Fig. 8 gives the minimum attainable $\Delta\nu$ as a function of L_z with various α_{loss}. We notice that $\Delta\nu$ is reduced greatly for a thin active layer. $\Delta\nu$ is minimum around $L_z = 80$ Å because there is the current region in which α of $L_z = 80$ Å is smaller than that of $L_z = 50$ Å in the case of $\alpha_{loss} = 10\ cm^{-1}$. Since the value $\Delta\nu$ for a DH laser (0.1 μm active layer) is calculated to be 60 MHz/mW with $\alpha_{total} = 30\ cm^{-1}$, $\Delta\nu$ can be substantially reduced with a thin QW structure by a factor of $\frac{1}{10}$ compared to $\Delta\nu$ for DH lasers. For all L_z, $\Delta\nu$ increases monotonically when the number of QW's increases.

B. Experiments

Recently, Ogasawara *et al.* [66] measured the α parameter of MQW lasers experimentally. The active layer consisted of four 40 Å thick GaAs wells and four 50 Å thick $Al_{0.3}Ga_{0.7}As$ barriers. They measured the change in $\partial\chi_R(E_l, n)/\partial n$ and $\partial\chi_I(E_l, n)/\partial n$ separately. $\partial\chi_R(E_l, n)/\partial n$ is measured from the wavelength shift of a Fabry–Perot mode with pulsed current injection below threshold and $\partial\chi_I(E_l, n)/\partial n$ is measured from the depth of modulation in the spontaneous emission intensity. Although their measurement is not a direct measurement and the measured α is obtained below threshold, their result supports our prediction. Their experiment suggests that α of a QW laser is smaller by a factor of $\frac{1}{2}$ compared to that of a conventional DH laser with the same carrier concentration.

V. New Optical Devices Using Quantum Wells

A. New Optical Devices Using QW Structures

As discussed above, the QW laser is a promising light source for various applications, and considerable effort has been devoted to developing high-quality QW lasers. In addition, other new optical devices based on QW structures have been proposed and demonstrated. These include optical modulators [67], [68], optical bistable devices [69], tunable p-i-n QW photodetectors [70], [71], size effect modulation light sources [74], Q-switching laser light sources [9], and modulation-doped detectors [72], [73]. The first three devices utilize the quantum-confined Stark effects [84], [85] described as follows. The room-temperature absorption spectrum of MQW displays enhanced absorption at the band edge, with a double-peaked structure caused by excitons whose binding energy is enhanced by the two-dimensional confinement. When an electric field is applied to the QW's perpendicular to the layers, the exciton absorption peak shifts to lower energy. This effect is much larger than the Franz-Keldysh effect seen in bulk materials. The dominant mechanism is the decrease in confinement energies, resulting in a red shift of the excitonic absorption energy.

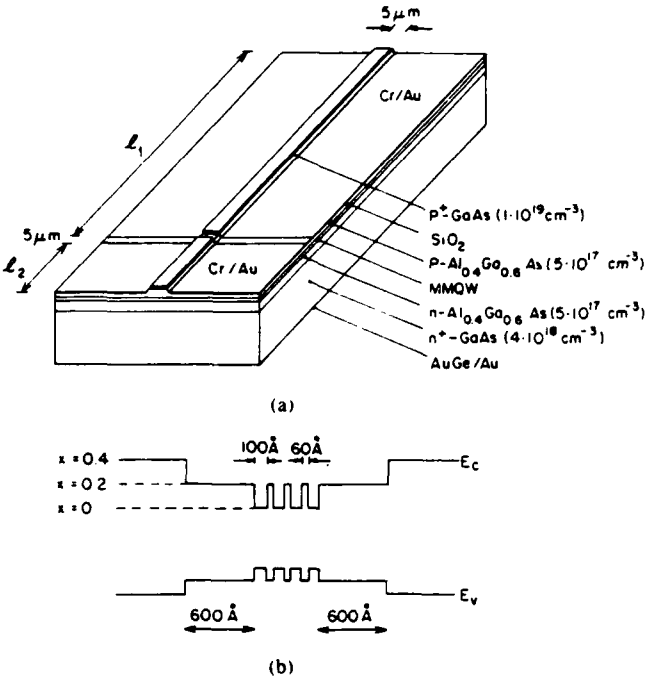

Fig. 9. (a) Perspective view of the two-segment quantum well laser. The lengths of the amplifier section l_1 and the modulator section l_2 were 250 and 50 μm, respectively. (b) The associated energy band diagram of the active layer.

The band discontinuities prevent the ionization of the exciton, allowing excitonic resonances to be observed at room temperature with large applied fields ($> 10^5$ V/cm).

The concept of the size effect modulation proposed by Yamanishi *et al.* [74] also utilizes the application of electric field. This causes the spatial displacement of the electron distribution and hole distribution in a well, which leads to the modulation of the matrix elements.

B. Q Switching in an MQW Laser with an Internal Loss Modulation

Picosecond pulse generation technology in semiconductor laser diodes is important for high-speed optical communication systems [75]–[83]. In Q-switching lasers, in contrast to mode-locked lasers, no external mirror is needed [80], [81] and lower modulation power is required compared to gain switching systems [82], [83]. Recently, effective active Q switching was successfully demonstrated by Arakawa *et al.* [13] in a GaAs/AlGaAs MQW laser with an intracavity monolithic electroabsorption loss modulator. The physical phenomena utilized are the quantum confined Stark effect in the modulation section and the enhanced carrier-induced band shrinkage effect [86] in the optical amplifier section. Optical pulses as narrow as 18.6 ps full width at half maximum (FWHM), assuming a Gaussian waveform, are generated.

Fig. 9(a) illustrates the two-segment MQW laser consisting of an optical amplifier section and an electroabsorption loss modulator section. The device structure was grown by molecular beam epitaxy. The associated energy band diagram is shown in Fig. 9(b). A 5 μm wide sepa-

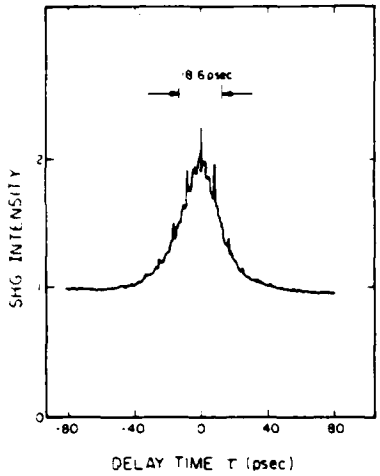

Fig. 10. Intensity autocorrelation trace obtained from second harmonic generation widht 1.5 GHz modulation frequency and 0 V bias. The current injected into the optical amplifier section is 170 mA.

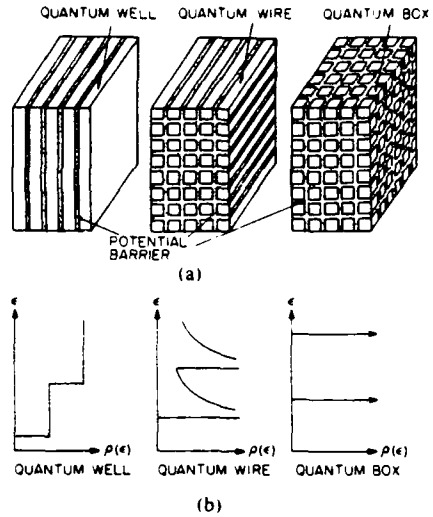

Fig. 11. (a) Illustration of the active layer with a multiquantum well structure, a multiquantum wire structure, and a multiquantum box structure. (b) Density of states of electrons in a DH structure, a multiquantum well structure, a multiquantum wire structure, and a multiquantum box structure.

ration was selectively etched in the p^+-GaAs between the two segments for electrical isolation. The lengths of the amplifier section l_1 and the modulator section l_2 were 250 and 50 μm, respectively.

In the amplifier section, the carrier-induced band shift occurs. This effect is enhanced in MQW lasers compared to conventional DH lasers, resulting in a decrease of the lasing photon energy by about 17 meV [86] compared to the absorption edge. Therefore, with no electronic field, the absorption loss is small at the lasing photon energy, which results in extremely large loss changes induced by the application of an electrical field with the quantum-confined Stark effects to the modulation section.

Q switching was obtained by applying both a dc bias voltage V_b and a microwave signal to the modulator. Fig. 10 shows an intensity autocorrelation trace obtained from the second harmonic generation under the condition of 1.5 GHz modulation frequency and $V_b = 0$. The autocorrelation FWHM is 26.3 ps, which corresponds to a pulse full width at half maximum $\Delta\tau_{1/2}$ of 18.6 ps if a Gaussian waveform is assumed.

The efficient Q switching in the two-segment MQW laser results from the following mechanisms. In the Q-switching regime, a large loss change and a high differential gain (the derivative of the gain with respect to carrier concentration) will lead to a narrow pulse width. In this device, a large loss change is realized with the quantum-confined Stark effect in the modulator section and the band shrinkage effect in the optical amplifier section. On the other hand, a high differential gain is also expected in the quasi-two-dimensional electronic system in an MQW structure [10], [11]. Thus, by the use of an MQW structure, the two-segment laser satisfies both requirements for the generation of narrow optical pulses.

The modulation frequency response (i.e., repetition rate) of the laser was also measured. We observed the fundamental spectrum as well as harmonic spectrum lines in the spectrum analyzer display. At the present stage, the maximum repetition rate which still leads to regular pulse generation is 5.2 GHz.

VI. Quantum Wire and Quantum Box Lasers and Their Experimental Demonstration

A. Concepts of Quantum Wire Laser and Quantum Box Laser

The QW structure has proved to be very promising for application to semiconductor lasers, which is due mainly to the two-dimensional properties of the carriers [9]. Arakawa *et al.* [9] proposed the concept of quantum wire lasers or quantum box lasers with, respectively, a one-dimensional or/and a zero-dimensional electronic system. They predicted a reduction in the temperature dependence of the threshold current due to the peaked structure of the density of states. In addition, the gain characteristics [87] and the dynamic properties were also investigated [10]. Although Petroff tried to fabricate quantum wire structures [88], no satisfactory quantum wire structure has been fabricated for optical devices or electronic devices [89] to date. Another approach for realizing the one- or two-dimensional effects experimentally is the use of magnetic fields [9], [90]–[95]. One-dimensional electronic systems can be formed by placing a conventional DH laser in a high magnetic field. If we place a quantum well laser in a high magnetic field so that the quantum well plane is perpendicular to the field, a zero-dimensional electronic system is realized. In this section, we discuss the possible properties obtained in quantum wire lasers and quantum box lasers theoretically and then demonstrate these effects in high magnetic field experiments.

Fig. 11(a) shows simple illustrations of the active layer in multiquantum well, multiquantum wire, and multiquantum box lasers. By making such multidimensional microstructures, the freedom of the carrier motion is re-

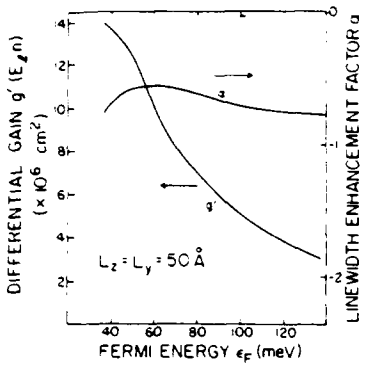

Fig. 12. The differential gain and α as a function of the conduction band quasi-Fermi energy level in a quantum wire laser with 50 Å quantum dimensions.

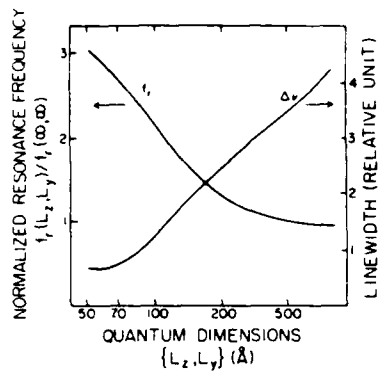

Fig. 13. The relaxation resonance frequency and the linewidth in a quantum wire laser as a function of the wire thickness. The number of quantum wells and quantum wires is optimized at each quantum well thickness.

duced to one or zero. The density of states of electrons in these structures is expressed as

$$\rho_c^{\text{wire}}(\epsilon) = \left(\frac{m_c}{2\hbar^2\pi^2}\right)^{1/2} \sum_{l,m} \frac{1}{\sqrt{\epsilon - \epsilon_l - \epsilon_m}}$$

for the quantum wire laser (24)

$$\rho_c^{\text{box}}(\epsilon) = \sum_{l,m,k} \delta(\epsilon - \epsilon_l - \epsilon_m \epsilon_k)$$

for the quantum box laser (25)

where ϵ_l, ϵ_m, and ϵ_k are the quantized energy levels of a quantum wire laser and a quantum box laser. As shown in Fig. 11(b), the density of states has a more peaked structure with the decrease of the dimensionality. This leads to a change in the gain profile, a reduction of threshold current density, and a reduction of the temperature dependence of the threshold current. Furthermore, improvements of the dynamic properties are also expected.

The narrower gain profile due to the peaked density of states leads to a high differential gain. One curve in Fig. 12 shows the differential gain as a function of the Fermi energy level for quantum wire lasers. A comparison of this figure to Fig. 5 reveals two important results. One is that a higher differential gain can be obtained with the use of quantum wire structures. The second one is that the dependence of the differential gain on the Fermi energy level is enhanced for quantum wire lasers compared to quantum well lasers. A higher differential gain, therefore, is obtained in a quantum wire laser with a large number of quantum wires, and the sensitivity of the differential gain to the number is more enhanced for quantum wire lasers compared to the quantum well lasers.

One curve in Fig. 13 shows the f_r as a function of the dimension of the quantum wires. In this calculation, it is assumed that the two quantum dimensions are equal and that the number of quantum wires is optimized for each quantum dimension. This result indicates that f_r is enhanced by a factor of 3 with the use of thin quantum wires compared to the conventional DH. The spectral properties of the quantum wire laser are also improved. The second curve in Fig. 12 shows the dependence of α on the Fermi energy level. As shown in this figure, the dependence of α in a quantum wire laser is not as enhanced and is almost constant in the whole range. The second curve in Fig. 13 shows $\Delta\nu$ as a function of the thickness of the quantum wells. This indicates that α is reduced with the decrease of the thickness.

The α parameter of quantum box lasers should be noted. If we can ignore higher subbands' effect, the density of states is a δ function-like. Therefore, the photon energy with the maximum gain coincides with the energy levels, which leads to the disappearance of the detuning and the real part of the complex susceptibility becomes zero. Consequently, α is expected to be extremely small in a quantum box laser with a simultaneous improvement of f_r.

B. Magnetic Field Experiment

A quasi-quantum wire effect in a semiconductor laser can be realized through the use of high magnetic fields [8], [9], in which case electrons can move freely only in the direction of the magnetic field. The motion of such electrons is quantized in the two transverse directions (x, y), forming a series of Landau energy subbands. The density of states for the system $\rho_c(\epsilon)$ can be expressed as

$$\rho_c(\epsilon) = (\hbar\omega_c)\left(\frac{2m_c}{\hbar^2}\right)^{3/2} \sum_{j=0}^{\infty} \frac{1}{\sqrt{\epsilon - (j + \frac{1}{2})\hbar\omega_c}} \quad (26)$$

where ω_c and m_c are the cyclotron cc r frequency and the effective mass of electrons. When $\hbar\omega_c$ is large enough (i.e., the B field is large enough), only the first Landau subband is occupied, resulting in a true one-dimensional electronic system. In the actual system, the carrier relaxation effect should also be considered.

Fig. 14 shows the measured spectral linewidth at 190 K for various magnetic fields (B = 0, 11, 16, 19 tesla) as a function of the reciprocal mode power $1/P$ [94]. A GaAlAs buried heterostructure laser grown by liquid phase epitaxy was operated in a stationary magnetic field of up to 19 tesla at 190 K. The test laser (an ORTEL Corporation experimental model) has a 0.15 μm active region thickness, 3 μm stripe width, and was 300 μm long. As

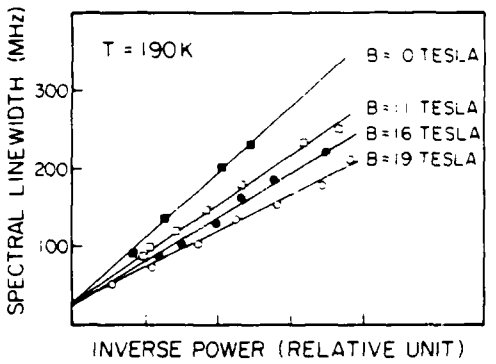

Fig. 14. The measured spectral linewidth as a function of the reciprocal of output power (in relative units) for magnetic fields of $B = 0$, 11, 16, and 19 tesla at 190 K.

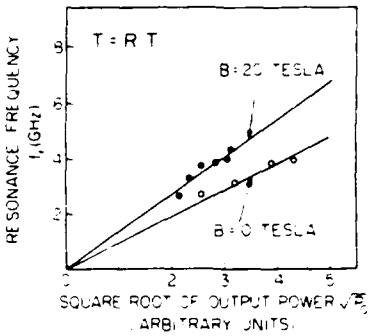

Fig. 15. The measured relaxation resonance frequency as a function of the square root of output power (in relative units) for magnetic fields of $B = 0$, 20 tesla at room temperature.

shown in the figure, the measured linewidth for each magnetic field varies linearly with the reciprocal mode power. Such a variation indicates that the linewidth results from quantum broadening (spontaneous emission). The experimental results indicate that this power-dependent linewidth is substantially reduced with the increase of the magnetic field. At 19 tesla, the linewidth decreases by a factor of 0.6 compared to the linewidth without a magnetic field. This improvement of the power-dependent linewidth is believed to be due mainly to quantum wire effects through the formation of a quasi-one-dimensional electronic system as discussed above.

One important difference between "true" quantum wire structures and the quasi-quantum wires due to magnetic fields is that the optical confinement factor for true quantum wire structures can be controlled by varying the number of quantum wires. Theoretical predictions indicate that a higher Fermi energy level for laser oscillation leads to lower α and n_{sp} [7]. Therefore, in the true quantum wire case, it should be possible to decrease n_{sp} and α by reducing the number of quantum wires while maintaining the one-dimensional electronic properties. This would allow one to reap the benefits of quantum wires in terms of smaller α's without paying a penalty in n_{sp}. The overall reduction of linewidth $\Delta\nu$ would then be much larger than demonstrated here.

f_r was also measured at room temperature [93]. Fig. 15 shows the measured f_r with and without a magnetic field of 20 tesla as a function of the square root of the output power P_0. Open circles ($B = 0$) and closed circle ($B = 20$ tesla) indicate the measured f_r. The straight lines in the figure are drawn by the least square error method. Since, as shown in (16), f_r is proportional to $\sqrt{P_0}$, f_r should lie on a straight line. The variation of the slope of this line will mainly reflect the change in differential gain g' which has resulted from the applications of the magnetic field. We notice that f_r with $B = 20$ tesla is enhanced 1.4 times compared to f_r with $B = 0$. From this change, we can estimate that g' ($B = 20$ tesla) is 1.9 times larger than g' ($B = 0$).

Quantum box effects (i.e., full quantization) were also investigated by Arakawa *et al.* [95] by placing a GaAs/GaAlAs quantum well laser in a high magnetic field. If a magnetic field is applied perpendicular to the quantum well plane as shown in Fig. 16(a), electrons are confined by the quantum well potential as well as the Lorentzian force, being in zero-dimensional electronic states. In this case, the density of states is described by the following formula:

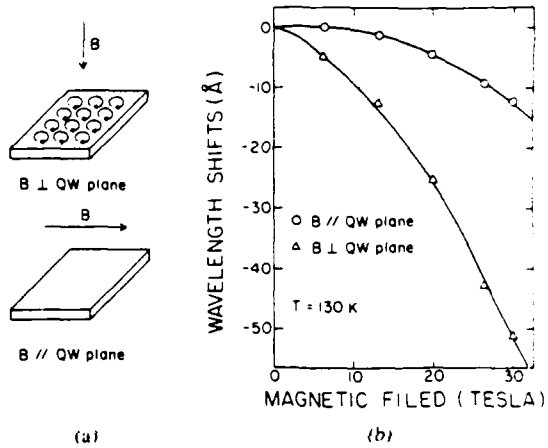

Fig. 16. (a) Electron motions confined by the quantum well potential as well as Lorentzian force, being in zero-dimensional electronic states. (b) Experimental results of the wavelength shift of the spontaneous emission spectrum as a function of the pulsed magnetic field up to 30 tesla.

$$\rho_c(\epsilon) = (\hbar\omega_c)\left(\frac{2m_c}{\hbar^2}\right)\sum_{k=0}^{\infty}\sum_{j=l,h}\sum_{n=1}^{\infty} \cdot \delta\left(\epsilon - \epsilon_{c_n}^{j} - \left(k + \frac{1}{2}\right)\hbar\omega_c\right). \quad (27)$$

The evidence of the formation of the full quantized effects was obtained by measuring anistropic properties of the spectral shift with the increase of the magnetic field. If a magnetic field is applied parallel to the QW plane, the cyclotron motion is interrupted by the QW potentials. Therefore, as long as the magnetic field is not extremely strong, the spectral peak shift is suppressed. On the other hand, with the perpendicular magnetic field, the spectral peak shift occurs towards a shorter wavelength through the increase of the Landau energy level. Fig. 16(b) is the experimental results of the wavelength shift of the spon-

taneous emission spectrum as a function of the pulsed magnetic field up to 30 tesla. The results clearly indicate the anisotropic properties, which is the evidence of the formation of the zero-dimensional electron states.

VII. Conclusions

We have discussed a number of interesting theoretical and experimental results of quantum well lasers with emphasis on the basic physical phenomena involved in the gain, the spectral fields, and the modulation response. The results reveal that an optimized use of the quantum well structure can lead to substantial improvement in most of the important properties of these devices.

References

[1] L. Esaki and R. Tsu, "Superlattice and negative differential conductivity in semiconductor lasers," *IBM. J. Res. Develop.*, vol. 14, pp. 61-68, 1970.

[2] R. Dingle, A. C. Gossard, and W. Wiegmann, "Direct observation of super lattice formation in a semiconductor heterostructure," *Phys. Rev. Lett.*, vol. 34, pp. 1327-1330, 1975.

[3] J. P. van der Ziel, R. Dingle, R. C. Miller, W. Wiegmann, and W. A. Nordland Jr., "Laser oscillation from quantum well states in very thin GaAl-$Al_{0.2}Ga_{0.8}As$ multilayer structures," *Appl. Phys. Lett.*, vol. 26, pp. 463-465, 1975.

[4] N. Holonyak, Jr., R. M. Kolbas, R. D. Dupuis, and P. D. Dapkus, "Quantum-well heterostructure lasers," *IEEE J. Quantum Electron.*, pp. 170-181, 1980.

[5] W. T. Tsang, "Extremely low threshold (AlGa)As modified multiquantum well heterostructure lasers grown by molecular beam epitaxy," *Appl. Phys. Lett.*, vol. 39, pp. 786-788, 1981.

[6] T. Fujji, S. Yamakoshi, K. Nanbu, O. Wada, and S. Hiyamizu, "MBE growth of extremely high-quality GaAs-AlGaAs GRIN-SCH lasers with a superlattice buffer layer," *J. Vac. Sci. Technol.*, vol. 2, pp. 259-261, 1984.

[7] R. Chin, N. Holonyak, Jr., B. A. Bojak, K. Hess, R. D. Dupuis, , and P. D. Dapkus, "Temperature dependence of threshold current for quantum well $Al_xGa_{1-x}As$-GaAs heterostructure laser diodes," *Appl. Phys. Lett.*, vol. 36, pp. 19-21, 1979.

[8] K. Hess, B. A. Bojak, N. Holonyak, Jr., R. Chin, and P. D. Dapkus, "Temperature dependence of threshold current for a quantum-well heterostructure laser," *Solid-State Electron.*, vol. 23, pp. 585-589, 1980.

[9] Y. Arakawa and H. Sakaki, "Multiquantum well laser and its temperature dependence of the threshold current," *Appl. Phys. Lett.*, vol. 40, pp. 939-941, 1982.

[10] Y. Arakawa, K. Vahala, and A. Yariv, "Quantum noise and dynamics in quantum well and quantum wire lasers," *Appl. Phys. Lett.*, vol. 45, pp. 950-952, 1984.

[11] Y. Arakawa, and A. Yariv, "Theory of gain, modulation response, and spectral linewidth in AlGaAs quantum well lasers," *IEEE J. Quantum Electron.*, vol. QE-21, pp. 1666-1674, 1985.

[12] Y. Arakawa, K. Vahala, and A. Yariv, "Dynamic and spectral properties in semiconductor lasers with quantum well and wire effects," presented at the 2nd Int. Conf. Modulated Semiconductor Structures, Kyoto, Japan, 1985.

[13] Y. Arakawa, A. Larsson, J. Paslaski, and A. Yariv, "Active *Q*-switching in a multiquantum well laser with an internal loss modulation," submitted to *Appl. Phys. Lett.*

[14] H. Kromer and H. Okamoto, "Some design consideration for multiquantum-well lasers," *Japan. J. Appl. Phys.*, vol. 23, pp. 970-972, 1984.

[15] A. Yariv, C. Lindsey, and U. Sivan, "Approximate analytic solution for electronic wave function and energies in coupled quantum wells," *J. Appl. Phys.*, vol. 58, pp. 3669-3671, 1985.

[16] R. Lang and K. Nishi, "Electronic localization in a semiconductor superlattice.," *Appl. Phys. Lett.*, vol. 45, pp. 98-100, 1984.

[17] D. Kasemset, C. S. Hong, N. B. Patel, and D. Dapkus, "Graded barrier single quantum well lasers—Theory and experiment," *IEEE J. Quantum Electron.*, vol. QE-19, pp. 1025-1030, 1983.

[18] A. Sugimura, "Threshold current for AlGaAs quantum well lasers," *IEEE J. Quantum Electron.*, vol. QE-20, pp. 336-343, 1984.

[19] P. T. Landsberg, M. S. Abrahams, and M. Olsinski, "Evidence of no *k*-selection in gain spectra of quantum well AlGaAs laser diodes," *IEEE J. Quantum Electron.*, vol. QE-21, pp. 24-28, 1985.

[20] N. K. Dutta, "Calculated threshold current of GaAs quantum well lasers," *J. Appl. Phys.*, vol. 53, pp. 7211-7214, 1982.

[21] ——, "Current injection in multiquantum well lasers," *IEEE J. Quantum Electron.*, vol. QE-19, pp. 794-797, 1983.

[22] M. Yamada, S. Ogita, M. Yamagishi, and K. Tabata, "Anisotropy and broadening of optical gain in a GaAs/AlGaAs multiquantum-well laser," *IEEE J. Quantum Electron.*, vol. QE-21, pp. 640-645, 1985.

[23] M. Yamada, K. Tabata, S. Ogita, and M. Yamagishi, "Calculation of lasing gain and threshold current in GaAsAlGaAs mutiquantum well lasers," *Trans. IECE Japan*, vol. E68, pp. 102-108, 1984.

[24] Y. Arakawa, H. Sakaki, M. Nishioka, J. Yoshino, and T. Kamiya," Recombination lifetime of carriers in GaAs-GaAlAs quantum wells near room temperature," *Appl. Phys. Lett.*, vol. 46k, pp. 519-521, 1985.

[25] N. K. Dutta, R. L. Hartman, and W. T. Tsang, "Gain and carrier lifetime measurement in AlGaAs single quantum well lasers," *IEEE J. Quantum Electron.*, vol. QE-19, pp. 1243-1246, 1983.

[26] Casey and Panish, *Heterostructure Lasers, Part A*. New York: Academic, 1978.

[27] H. Kobayaski, H. Iwamura, T. Saku, and K. Otsuka, "Polarization dependent gain-current relationship in GaAs-AlGaAs MQW laser diodes," *Electron. Lett.*, vol. 19, pp. 166-168, 1983.

[28] M. Asada, A. Kameyama, and Y. Suematsu, "Gain and intervalenceband absorption in quantum-well lasers," *IEEE J. Quantum Electron.*, vol. QE-20, pp. 745-753, 1984.

[29] M. Yamanishi and I. Suemune, "Comments on polarization dependent momentum matrix elements in quantum well lasers," *Japan. J. Appl. Phys.*, vol. 23, pp. L35-L36, 1984.

[30] E. O. Kane, "Band structure of indium antimonide," *J. Phys. Chem. Solids*, pp. 249-269, 1957.

[31] A. Sugimura, "Auger recombination effect on threshold current of InGaAsP quantum well lasers," *IEEE J. Quantum Electron.*, vol. QE-19, pp. 932-941, 1983.

[32] N. K. Dutta, "Calculation of Auger rates in a quantum well structure and its application to InGaAsP quantum well lasers," *J. Appl. Phys.*, vol. 54, pp. 1236-1245, 1983.

[33] L. C. Chiu and A. Yariv, "Auger recombination in quantum-well InGaAsP heterostructure lasers," *IEEE J. Quantum Electron.*, vol. QE-18, pp. 1406-1409, 1982.

[34] C. Smith, R. A. Abram, and M. G. Burt, "Auger recombination in long wavelength quantum-well lasers," *Electron. Lett.*, 1984.

[35] Y. Arakawa, A. Larsson, M. Mittelstein, and A. Yariv," Observation of gain flattening and second subband laser oscillation in a single quantum well laser," unpublished.

[36] R. D. Dupis, P. D. Dapkus, N. Holonyak, Jr., E. A. Rezek, and R. Chin, "Room-temperature laser operation of quantum well $Ga_{1-x}Al_xAs$-GaAs laser diodes by metal organic chemical vapor deposition," *Appl. Phys. Lett.*, vol. 32, pp. 292-297, 1978.

[37] W. T. Tsang, C. Weisbuch, R. C. Miller, and R. Dingle, "Curent injection GaAS-$Al_xGa_{1-x}As$ multiquantum well heterostructure lasers prepared by molecular beam epitaxy," *Appl. Phys. Lett.*, vol. 35, pp. 673-675, 1979.

[38] W. T. Tsang, "A graded-index waveguide separate-confinement laser with very low threshold and a narrow Gaussian beam," *Appl. Phys. Lett.*, vol. 39, pp. 134-136, 1981.

[39] P. Blood, E. D. Fletcher, and K. Woodbridge, "Dependence of threshold current on the number of wells in AlGaAs-GaAs quantum well lasers," *Appl. Phys. Lett.*, vol. 47, pp. 193-195, 1985.

[40] S. D. Harsee, M. Baldy, P. Assenat, B. de Cremoux, and J. P. Duchemin," Very low threshold GRIN-SCH GaAs/AlGaAs laser structure grown by OM-VPE," *Electron. Lett.*, vol. 18, pp. 1095-1097, 1982.

[41] D. R. Scifres, R. D. Burham, and W. Streifer, "High power coupled multiple strip quantum well injection lasers," *Appl. Phys. Lett.*, pp. 118-120, 1982.

[42] J. P. van der Ziel, H. Temkin, and R. D. Dupis, "High-power picosecond pulse generation in GaAs multiquantum well phase-locked laser arrays using pulsed current injection," *IEEE J. Quantum Electron.*, vol. QE-20, pp. 1236-1242, 1984.

[43] O. Wada, T. Sanada, M. Kuno, and T. Fujii, "Very low threshold current ridge-waveguide AlGaAs/GaAs single-quantum-well lasers," *Electron. Lett.*, 1985.

[44] E. A. Rezek, N. Holonyak, Jr., and B. K. Fuller, "Temperature dependence of threshold current for coupled multiple quantum well $In_{1-x}Ga_xP_{1-y}As_y$-InP heterostructure laser diodes," *J. Appl. Phys.*,

vol. 51, pp. 2402-2405, 1980.

[45] H. Temkin, K. Alavi, W. R. Wagner, T. P. Pearsall, and A. Y. Cho, "1.5-16 μm $Ga_{0.47}In_{0.53}As/Al_{0.48}$ multiquantum well laser grown by molecular beam epitaxy," *Appl. Phys. Lett.*, vol. 42, pp. 845-847, 1983.

[46] T. Yanase, Y. Kato, I. Mito, M. Yamaguchi, K. Nishi, K. Kobayashi, and R. Lang, "1.3 μm InGaAsP/InP multiquantum-well laser grown by vapour-phase epitaxy," *Electron. Lett.*, vol. 19, pp. 700-701, 1983.

[47] N. K. Dutta, T. Wessel, N. A. Olsson, R. A. Logan, R. Yen, and P. J. Anthony," Fabrication and performance characteristics of InGaAsP ridge-guide distributed-feedback multiquantum-well lasers," *Electron Lett.*, vol. 21, pp 571-573, 1985.

[48] Y. Kawamura, H. Asahi, and K. Wakita, "InGaAs/InGaAlAs/InAlAs/InP SCH-MQW laser diodes grown by molecular beam epitaxy," *Electron Lett.*, vol. 20, pp. 459-460, 1984.

[49] Y. Ohmori, Y. Suzuki, and H. Okamoto, "Room temperature CW operation of GaSb/AlGaSb MQW laser diodes grown by MBE," *Japan. J. Appl. Phys.*, vol. 24, pp. L657-659, 1985.

[50] A. Larsson, M. Mittelstein, Y. Arakawa, and A. Yariv," High efficiency broad area single quantum well laser with narrow single-lobed far-field patterns prepared by molecular beam epitaxy," *Electron. Lett.*, vol. 22, pp. 79-81, 1986.

[51] T. Ikegami and Y. Suematsu, "Direct modulation semiconductor junction lasers," *Electron. Commun. Japan*, vol. B51, pp. 51-58, 1968.

[52] T. P. Paoli and J. E. Ripper, "Direct modulation of semiconductor lasers," *Proc. IEEE*, vol. 58, p. 1457, 1970.

[53] K. Y. Lau, N. Bar-Chaim, I. Ury, C. Harder, and A. Yariv, "Direct amplitude modulation of short cavity lasers up to *X*-band frequency," *Appl. Phys. Lett.*, vol. 43, pp. 1-3, 1983.

[54] K.Y. Lau, N. Bar-Chaim, I. Ury, and A. Yariv, "An 11 GHz direct modulation bandwidth GaAlAs window laser on semi-insulating substrate operating at room temperature," *Appl. Phys. Lett.*, vol. 45, pp. 345-347, 1984.

[55] K. Y. Lau and A. Yariv, "Ultra-high speed semiconductor lasers," *IEEE J. Quantum Electron.*, vol. QE-21, p. 121, 1985.

[56] K. Vahala and A. Yariv, "Detuned loading in couple cavity semiconductor lasers—Effects on quantum noise and dynamics," *Appl. Phys. Lett.*, vol. 45, pp. 501-503, 1984.

[57] K. Uomi, N. Chinone, T. Ohyoshi, and T. Kajimura, "High relaxation oscillation freqeuncy (beyond 10 GHz) of GaAlAs multiquantum well lasers," *Japan. J. Appl. Phys.*, vol 24, pp. L539-L541, 1985.

[58] K. Kobayashi, H. Iwamura, T. Saku, K. Otsuka, and H. Okamoto," Dynamic behavior of a GaAs-AlGaAs MQW laser diode," *Electron. Lett.*, vol. 19, pp. 166-167, 1983.

[59] M. W. Fleming and A. Mooradian, "Fundamental line broadening of single mode (GaAl)As diode lasers," *Appl. Phys. Lett.*, vol. 38, pp. 511-513, 1981.

[60] C. Henry, "Theory of the linewidth of semiconductor," *IEEE J. Quantum Electron.*, vol. QE-18, pp. 259-264, 1982.

[61] K. Vahala and A. Yariv, "Semiclassical theory of noise in semiconductor lasers—Part I," *IEEE J. Quantum Electron.*, vol. QE-18, pp. 1096, 1101, 1982.

[62] ——, "Semiclassical theory of noise in semiconductor lasers—Part II, "*IEEE J. Quantum Electron.*, vol. QE-18, pp 1102-1109, 1982.

[63] M. G. Burt, "Linewidth enhancement factor for quantum well laser," *Electron. Lett.*, vol. 20 pp. 27-28, 1984.

[64] K. Vahala, L. C. Chiu, S. Margalit, and A. Yariv," On the linewidth enchancement factor α in semiconductor injection lasers," *Appl Phys. Lett.*, vol. 42, pp. 531-633, 1983.

[65] Y. Arakawa and A. Yariv, "Fermi energy dependence of linewidth enhancement factor," *Appl. Phys. Lett.*, vol. 47, pp. 905-907, 1985.

[66] N. Ogasawara, R. Itoh, and R. Morita, "Linewidth enhancement factor in GaAs/AlGaAs multiquantum well lasers," *Japan. J. Appl. Phys.*, vol. 24, pp. L519-L521, 1985.

[67] T. H. Wood, C. A. Burrus, D. A. B. Miller, D. S. Chemla, T. C. Damen, A. C. Gossard, and W. Wiegmann," High-speed optical modulation with GaAs/GaAlAs quantum wells in a p-i-n diode structure," *Appl Phys. Lett.*, vol. 44, pp. 16-18, 1984.

[68] T. H. Wood, C. A. Burrus, R. S. Tucker, J. S. Weiner, D. A. B. Miller, D. S. Chemla, T. C. Damen, A. C. Gossard, and W. Wiegmann, *Electron. Lett.*, vol. 21, pp. 693-695, 1985.

[69] D. A. B. Miller, D. S. Chemla, T. C. Damen, A. C. Gossard, W. Wiegmann, T. H. Wood, and C. A. Burrus," Novel hybrid optically bistable switch: The quantum well self-optic effect device," *Appl Phys. Lett.*, vol. 45, pp. 13-15, 1984.

[70] T. H. Wood, C. A. Burrus, A. H. Gnauck, J. M. Wiesenfeld, D. A. B. Miller, D. S. Chemla, and T. C. Damen," *Appl. Phys. Lett.*, vol. 47, pp. 190-192, 1985.

[71] A. Larsson, A. Yariv, R. Tell, J. Maserjian, and S. T. Eng, "Spectral and temporal characterisitcs of AlGaAs/GaAs superlattice p-i-n photodetectors," *Appl. Phys. Lett.*, vol. 47, pp. 866-868, 1985.

[72] C. Y. Chen, "New minority hole sinked photoconductive detector," *Appl. Phys. Lett.*, vol. 43, pp. 1115-1117, 1983.

[73] K. Kaede, Y. Arakawa, P. Derry, J. Papaslaski, and A. Yariv," High speed GaAs/AlGaAs photoconductive detector using a p-modulation doped superlattice," *Appl. Phys. Lett.*, vol. 48, pp. 1096-1097, 1986.

[74] M. Yamanishi and M. Suemune, "Quantum mechanical size effect modulation light source—A new field effect semiconductor laseror light emitting diode," *Japan. J. Appl. Phys.*, vol. 22, p. L22, 1983.

[75] K. Tsukada and C. L. Tang, "*Q*-switching of semiconductor lasers," *IEEE J. Quantum Electron.*, vol. QE-13, pp. 37-43, 1977.

[76] M. Yamanishi, K. Ishii, M. Ameda, and T. Kawamura, "High speed repetitive *Q*-switching in acoustic distributed feedback lasers," *Japan. J. Appl. Phys.*, suppl. 17, pp. 359-363, 1978.

[77] D. Z. Tsang, J. N. Walpole, S. H. Groves, J. J. Hsieh, and J. P. Donnelly, "Intracavity loss modulation of GaInAsP diode lasers," *Appl. Phys. Lett.*, vol. 38, p. 120, 1981.

[78] D. Z. Tsang and J. N. Walpole, "*Q*-switched semiconductor diode lasers," *IEEE J. Quantum Electron.*, vol. QE-19, p. 145, 1983.

[79] D. Z. Tsang, J. N. Walpole, Z. L. Liau, S. H. Groves, and V. Diadiuk, "*Q* switching of low threshold buried heterostructure diode laser at 10 GHz," *Appl. Phys. Lett.*, vol. 45, p. 204, 1984.

[80] P. T. Ho, L. A. Glasser, E. P. Ippen, and H. A. Haus, "Picosecond pulse generation with a CW GaAlAs laser diodes," *Appl. Phys. Lett.*, vol. 33, pp. 241-242, 1978.

[81] J. P. van der Ziel, R. A. Logan, and R. M. Mikulyak, "Generation of subpicosecond pulse from an actively mode locked GaAs laser in an external ring cavity," *Appl. Phys. Lett.*, vol. 39, pp. 867-869, 1981.

[82] H. Ito, H. Yokoyama, S. Murata, and H. Inaba, "Picosecond optical pulse generation from r.f. modulated AlGaAs DH diode laser," *Electron. Lett.*, vol. 15, p. 738, 1979.

[83] G. J. Aspin, J. E. Carrol, and R. G. Plumb," The effect of cavity length on picosecond pulse generation with high rf modulated AlGaAs double heterostructure lasers," *Appl. Phys. Lett.*, vol. 39, p. 860, 1981.

[84] D. A. B. Miller, D. S. Chemla, T. C. Damen, A. C. Gossard, W. Wiegmann, T. H. Wood, and C. A. Burrus," Bandedge electroabsorption in quantum well structure: The quantum confined Stark effect," *Phys. Rev. Lett.*, vol. 53, pp. 2173-2177, 1984.

[85] J. S. Weiner, D. A. B. Miller, D. S. Chemla, T. C. Damen, C. A. Burrus, T. H. Wood, A. C. Gossard, and W. Wiegman, *Appl. Phys. Lett.*, vol. 47, p. 1148, 1985.

[86] S. Tarucha, H. Kobayashi, Y. Horikoshi, and X. Okamoto, "Carrier induced energy-gap shrinkage in current injection GaAs AlGaAs MQW heterostructures," *Japan. J. Appl. Phys.*, vol. 23, pp. 874-881, 1984.

[87] Asada and Suematsu, *Japan. J. Appl. Phys.*, vol. 24, pp. L93-L95, 1985.

[88] Petroff, "Toward quantum well wires: Fabrication and optical properties," vol. 41, pp 635-637, 1982.

[89] H. Sakaki, "Scattering suppression and high mobility effect of single quantum electrons in ultrafine semiconductor wire structure," *Japan J. Appl. Phys.*, vol. 20, pp. L91-L93, 1981.

[90] Y. Arakawa, H. Sakaki, M. Nishioka, and N. Miura, "Two dimensional quantum-mechanical confinement of electrons in semiconductor lasers by strong magnetic fields," *IEEE J. Quantum Electron.*, vol. QE-18, pp. 10-17, 1983.

[91] ——, "Two-dimensional quantum-mechanical confinement of electrons in light emitting diodes by strong magnetic fields," *IEEE Trans Electron Devices*, vol. ED-30, pp. 330-338, Apr. 1983.

[92] H. J. A. Bluyssen and L. J. van Ruyven, "Operation of a double heterojunction GaAs/AlGaAs injection laser with a p-type active layer in a strong magnetic field," *IEEE J. Quantum Electron.*, vol. QE-16, pp. 29-33, 1983.

[93] Y. Arakawa, K. Vahala, A. Yariv, and K. Lau, "Enhanced modulation bandwidth of GaAlAs double heterostructure lasers in high magnetic fields: Dynamic response with quantum wire effects," *Appl Phys. Lett.*, vol. 47, pp. 1142-1144, 1985.

[94] ——, "Reduction of the spectral linewidth of semiconductor lasers

with quantum wire effects—Spectral properties of GaAlAs double heterostructure lasers," *Appl. Phys. Lett.*, vol. 48, pp. 384-386, 1986.
[95] Y. Arakawa, H. Sakaki, M. N. Nishioka, H. Okamoto, and N. Miura, "Spontaneous emission characteristics of quantum well lasers in strong magnetic fields—An approach to quantum box light source," *Japan. J. Appl. Phys.*, vol. 22, pp. L804-L806, 1985.

Yasuhiko Arakawa (S'77-M'80) was born in Aichi Prefecture, Japan, on November 26, 1952. He received the B.S., M.S., and Ph.D. degrees in electrical engineering from the University of Tokyo, Tokyo, Japan, in 1975, 1977, and 1980, respectively.

In the graduate school, he conducted research on optical communication theory. In 1980, he joined the Institute of Industrial Science, University of Tokyo, as an Assistant Professor and is currently an Associate Professor. After 1980, he extended his speciality to optical device research. His current research includes dynamic and noise properties of quantum well lasers, basic investigation of quantum wire and quantum box lasers using high magnetic fields, and fabrication of new optical devices using quantum well structures. From 1984 to 1986, he was Visiting Scientist at the California Institute of Technology, Pasadena, doing research in collaboration with Professor A. Yariv.

In 1980 Dr. Arakawa was awarded the Niwa Memorial Prize. In 1981 and 1983, he was also awarded the Excellent Paper Award and the Young Scientist Award, respectively, from Institute of Electronics and Communication Engineers of Japan. He is a member of the Institute of Electronics and Communication Engineers of Japan and the Japan Society of Applied Physics.

Amnon Yariv (S'56-M'59-F'70), for a photograph and biography, see p. 448 of the March 1986 issue of this JOURNAL.

Unclassified
SECURITY CLASSIFICATION OF THIS PAGE

REPORT DOCUMENTATION PAGE

Form Approved
OMB No. 0704-0188

1a. REPORT SECURITY CLASSIFICATION Unclassified	1b. RESTRICTIVE MARKINGS
2a. SECURITY CLASSIFICATION AUTHORITY 2b. DECLASSIFICATION / DOWNGRADING SCHEDULE	3. DISTRIBUTION / AVAILABILITY OF REPORT Approved for public release; distribution unlimited.
4. PERFORMING ORGANIZATION REPORT NUMBER(S) N00014-85-K-0211	5. MONITORING ORGANIZATION REPORT NUMBER(S) 696-002
6a. NAME OF PERFORMING ORGANIZATION California Institute of Technology 6b. OFFICE SYMBOL (If applicable)	7a. NAME OF MONITORING ORGANIZATION Office of Naval Research
6c. ADDRESS (City, State, and ZIP Code) Pasadena, California 91125	7b. ADDRESS (City, State, and ZIP Code) 565 S. Wilson Pasadena, California 91106-3212
8a. NAME OF FUNDING / SPONSORING ORGANIZATION Office of Naval Research 8b. OFFICE SYMBOL (If applicable)	9. PROCUREMENT INSTRUMENT IDENTIFICATION NUMBER
8c. ADDRESS (City, State, and ZIP Code) 800 N. Quincy Street Arlington, VA 22217	10. SOURCE OF FUNDING NUMBERS PROGRAM ELEMENT NO. / PROJECT NO. / TASK NO / WORK UNIT ACCESSION NO.

11. TITLE (Include Security Classification)
Intermodal Stability of a Coupled-Cavity Semiconductor Laser

12. PERSONAL AUTHOR(S)
R. Lang and A. Yariv

13a. TYPE OF REPORT	13b. TIME COVERED	14. DATE OF REPORT (Year, Month, Day)	15. PAGE COUNT
Reprint	FROM _____ TO _____		

16. SUPPLEMENTARY NOTATION The view, opinions and/or findings contained in this report are those of the author(s) and should not be construed as an official Department of the Navy position, policy, or decision unless so designated by other documentation.

17. COSATI CODES			18. SUBJECT TERMS (Continue on reverse if necessary and identify by block number)
FIELD	GROUP	SUB-GROUP	Coupled-Cavity Semiconductor Laser

19. ABSTRACT (Continue on reverse if necessary and identify by block number)

We present an analysis of the steady-state operation of a two-element coupled-cavity laser near a mode hop. The equations of motion for the two cavities and two relevant modes of a longitudinally coupled-cavity laser are reduced to a system of nondimensional nonlinear ordinary differential equations which describe a general two-element laser. The equations are then solved and the stability of their solutions is analyzed. Depending upon the fill factors for the two modes there exists an intrinsically multimode oscillation for operating conditions under which it was previously thought that no steady state existed. Under conditions where the multimode state is unstable, both of the single-mode states are stable with bistable transitions occurring only on the boundaries of the unstable multimode regimes.

20. DISTRIBUTION / AVAILABILITY OF ABSTRACT ☐ UNCLASSIFIED/UNLIMITED ☐ SAME AS RPT. ☐ DTIC USERS	21. ABSTRACT SECURITY CLASSIFICATION
22a. NAME OF RESPONSIBLE INDIVIDUAL	22b. TELEPHONE (Include Area Code) / 22c. OFFICE SYMBOL

DD Form 1473, JUN 86 Previous editions are obsolete. SECURITY CLASSIFICATION OF THIS PAGE

Surface Science 174 (1986) 155–162
North-Holland, Amsterdam

DYNAMIC AND SPECTRAL PROPERTIES OF SEMICONDUCTOR LASERS WITH QUANTUM-WELL AND QUANTUM-WIRE EFFECTS

Y. ARAKAWA *, K. VAHALA and A. YARIV
California Institute of Technology, Pasadena, California, USA

Received 29 July 1985; accepted for publication 15 October 1985

Our recent studies of the dynamic and spectral properties of semiconductor lasers with quantum-well or quantum-wire structures are described. We have predicted a two-fold increase in the modulation corner frequency of a multiquantum-well laser as compared to the conventional laser: a threefold increase in this quantity is predicted for the multiquantum-wire laser. Improvement of the spectral linewidth in the single quantum-well and single quantum-wire cases is also predicted. Enhancement of the modulation corner frequency in a quantum-wire laser is experimentally demonstrated by operation of a conventional laser in magnetic fields up to 20 Tesla. A corner frequency enhancement of 1.5× has been observed.

1. Introduction

An understanding of the modulation and noise properties of semiconductor lasers is of fundamental importance in certain applications of these devices. At the present time these properties are fairly well understood in conventional double heterostructure semiconductor lasers. Although quantum-well lasers have proven to be attractive light sources because of their low threshold-current density [1], little effort has been directed towards understanding how the dynamic and noise properties of these devices differ from the conventional case. The quantum-wire laser is even less studied owing to difficulties in fabrication of such a device. Two important quantities which in part characterize modulation dynamics and noise in a semiconductor laser are the relaxation oscillation corner frequency, f_r, which sets the useful direct modulation bandwidth of the device, and the field spectrum linewidth, $\Delta\nu$, which gives a direct measure of the phase noise in the light output for single-mode operation. In this paper we describe our recent theoretical and experimental results concerning these quantities in semiconductor lasers having quantum-well and quantum-wire effects.

* On leave from the University of Tokyo, Tokyo, Japan.

0039-6028/86/$03.50 © Elsevier Science Publishers B.V. (North-Holland Physics Publishing Division) and Yamada Science Foundation

2. Direct modulation bandwidth in quantum-well and quantum-wire lasers

The relaxation oscillation corner frequency, f_r, gives the useful direct modulation bandwidth of a semiconductor laser. Small-signal analysis of the rate equations yields the following expression for this quantity [2]

$$f_r = \frac{1}{2\pi}\left(\frac{g'(E_l,n)P_0}{\tau_p}\right)^{1/2}, \tag{1}$$

where P_0 is the steady-state photon density in the cavity, τ_p is the photon lifetime, $g'(E, n)$ is the differential gain (i.e., $g'(E, n) = \partial g(E, n)/\partial n$), and E_l is the photon energy at which laser oscillation occurs. Eq. (1) suggests several ways to improve f_r; larger $g'(E_l, n)$, smaller τ_p, and larger P_0. The reduction of τ_p and the increase of P_0 are realized with the use of short cavity lasers [2] and window-type lasers [3]. To increase $g'(E_l, n)$ operation at low temperatures [4] and the use of coupled cavity lasers [5,6] have been studied.

The basic quantum-mechanical expression for $g'(E, n)$ suggests yet another way to increase $g'(E, n)$: changing the electron density of states with the use of quantum-well or quantum-wire structures [7,8]. Since the gain $g(E, n)$ is proportional to the imaginary part, $\chi_I(E, n)$, of the complex susceptibility function $\chi(E, n) = \chi_R(E, n) + i\chi_I(E, n)$, $g'(E, n)$ can be expressed by the following equation:

$$g'(E,n) = \frac{\partial}{\partial n}\left(\frac{\omega}{n_r^2}\chi_I(E,n)\right) = \frac{\partial}{\partial n}\left(\frac{\omega}{n_r^2}\int \rho_{red}(E-\epsilon)\,(f_c - f_v)\,\hat{\chi}_I(\epsilon)\,d\epsilon\right), \tag{2}$$

where $\hat{\chi}_I(\epsilon)$ is the imaginary part of the susceptibility contributed by an electron–hole pair with energy difference ϵ, $\rho_{red}(\epsilon)$ is the reduced density-of-states function, ω is the lasing frequency, n_r is the non-resonant contribution to the refractive index, and f_c (f_v) is the Fermi–Dirac function giving the occupancy of a state in the conduction (valence) band. It is easily seen from this equation that the density of states plays an important role in determining the properties of $g'(E, n)$.

The electronic density-of-states functions for electrons in quantum-well and quantum-wire structures are given by [7]

$$\rho_2(\epsilon) = \frac{m_c}{\pi\hbar^2}\sum_l H[\epsilon - \epsilon_l] \quad \text{for the quantum well laser,} \tag{3}$$

$$\rho_1(\epsilon) = \left(\frac{m_c}{2\hbar^2\pi^2}\right)^{1/2}\sum_{l,m}\frac{1}{(\epsilon - \epsilon_{l,m})^{1/2}} \quad \text{for the quantum wire laser,} \tag{4}$$

where m_c is the electron effective mass, $\hbar$ is Planck's constant, $H[x]$ is the

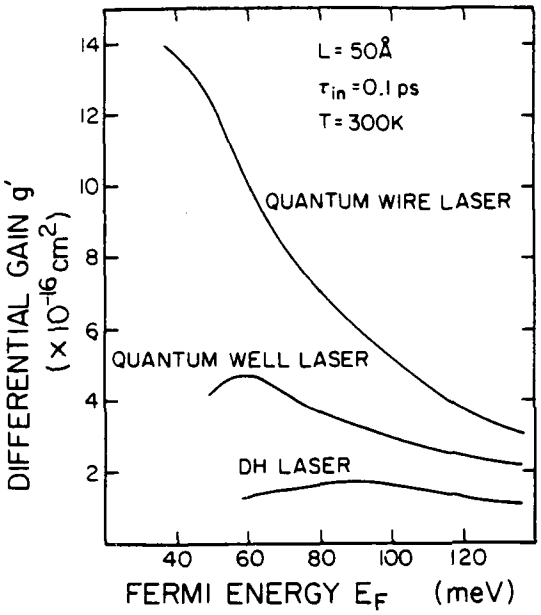

Fig. 1. The differential gain as a function of the conduction-band quasi-Fermi energy level in a conventional double heterostructure laser, a 50 Å well thickness quantum-well laser, and a 50 Å × 50 Å quantum-wire laser.

Heaviside function ($H[x]=0$ for $x<0$, $H[x]=1$ for $x \geqslant 0$), ϵ_l and $\epsilon_{l,m}$ are the subband edge energies for an electron in a quantum well and a quantum wire (or wells and wires as the case may be). In these structures the density-of-states functions have stepped and peaked behaviors. This effectively narrows the gain spectrum as compared to the bulk thereby increasing $g'(E, n)$.

Fig. 1 shows the calculated differential gain $g'(E_1, n(E_F))$ for the conventional double heterostructure (DH) laser, the quantum-well laser, and the quantum-wire laser as a function of the conduction band quasi-Fermi energy level, E_F (measured from the lowest subband energy level). The quantum dimensions (e.g., thickness of the quantum-well structures) are all equal to $L = 50$ Å. The quasi-Fermi energy level for the holes is determined by the charge neutrality condition. The result predicts an enhancement of g' for the quantum-well active layer. Further improvement is predicted with the quantum-wire active layer. Note that since $g'(E_1, n)$ is a bulk parameter, it is independent of the number of quantum wells and quantum wires.

Fig. 1 also shows that $g'(E_1, n(E_F))$ depends strongly on E_F (i.e. necessary excitation for laser oscillation), particularly for the quantum-well and quantum-wire cases [8]. This Fermi energy dependence of $g'(E_1, n)$ means there is an optimum number, N, of quantum wires in a laser structure which causes

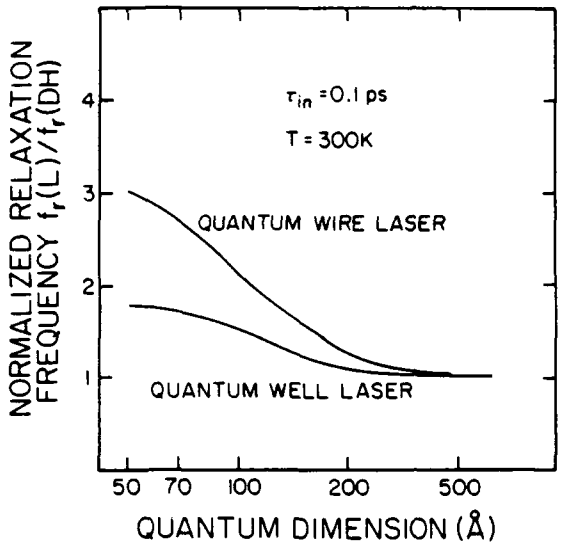

Fig. 2. The relaxation resonance frequency in a quantum-well laser and a quantum-wire laser as a function of the well thickness. The number of quantum wells and quantum wires is optimized at each quantum-well thickness.

greatest enhancement of f_r. To see this consider the threshold condition for lasing in such structures,

$$\Gamma(N)g(E_1, n(E_F)) = \alpha_{\text{total}}, \tag{5}$$

where $\Gamma(N)$ is the optical confinement factor which is a monotonically increasing function of N and α_{total} is the total loss. For simplicity, we ignore the dependence of α_{total} on the structure. Since the gain is a monotonically increasing function of E_F, the required E_F for laser oscillation decreases monotonically with the increase of N. Consequently, there exits an optimum N for realizing $E_F^{\max}$, defined to yield the maximum $g'(E_1, n)$. It is easily shown that the lasing threshold E_F for $N = 1$ is much larger than $E_F^{\max}$. Therefore the largest g' values and fastest modulation speeds are achieved for the multi-quantum-well and multiquantum-wire cases ($N \geqslant 2$).

Fig. 2 shows the calculated f_r as a function of L (the quantum-well and quantum-wire width). At each L the number of wells or wires is optimized and f_r is normalized by the f_r of a conventional DH laser. The results suggest that by optimizing N, f_r can be enhanced by $2\times$ in thin quantum-well lasers and by $3\times$ in thin quantum-wire lasers.

The experimental demonstration of the quantum-wire effect on the dynamic properties can be realized by using a high magnetic field [7,9]. When a semiconductor laser is immersed in a high magnetic field, electrons move freely only along the flux lines. The motion of such electrons is quantized in the two

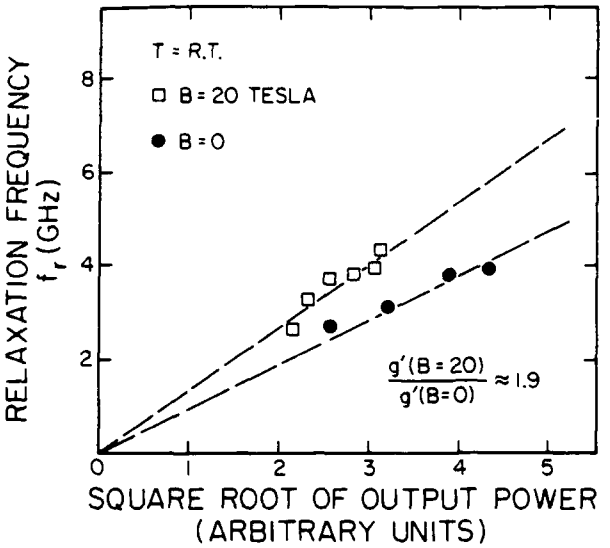

Fig. 3. The measured modulation corner frequencies with and without magnetic field as a function of the square root of the output power.

transverse directions and forms a series of Landau energy levels. With a sufficiently intense field, the electrons behave as a quasi-one-dimensional gas. Note that if we place a quantum-well laser in a high magnetic field, quantum box effects can be realized (i.e. confinement in all three spatial dimensions).

We have operated LPE-grown GaAlAs buried heterostructure lasers in stationary magnetic-fields up to 20 Tesla at room temperature. The measured modulation corner frequency with and without a magnetic field is shown in fig. 3 as a function of the square root of the output power P_0. Open circles ($B = 0$) and closed circle ($B = 20$ Tesla) indicate the measured f_r. The straight lines in the figures are drawn by the least-square-error method. Since, as shown in eq. (1), the resonant frequency is proportional to $P^{1/2}$, the f_r should lie on a straight line. The variation of the slope of these lines will mainly reflect the change in the differential gain $g'(E_1, n)$ which has resulted from the application of the magnetic field. We notice that the f_r with $B = 20$ Tesla is enhanced by 1.5 × compared to the f_r with $B = 0$. From this change we can estimate that $g'(E_1, n, B = 20 \text{ Tesla})$ is 1.9 times larger than $g'(E_1, n, B = 0)$.

3. Spectral noise properties in quantum-well and quantum-wire lasers

Recently the spectral linewidth of single-mode semiconductor lasers has received considerable attention [11–14]. This quantity gives a direct measure of the phase noise present in the output of a semiconductor laser and is therefore

an important consideration in the application of these devices to coherent communication systems. The spectral linewidth $\Delta\nu$ can be expressed by [14]

$$\Delta\nu = \frac{v_g h\nu(\Gamma g) R_m n_{sp}}{8\pi P}(1+\alpha^2), \tag{6}$$

$$\alpha = \frac{\partial\chi_R(E_1,n)/\partial n}{\partial\chi_I(E_1,n)/\partial n}. \tag{7}$$

R_m, v_g, $h\nu$, Γ, g, n_{sp}, and P are the mirror loss, the group velocity of light, the photon energy, the optical confinement factor, the bulk gain at threshold, the spontaneous emission factor, and the laser output power, respectively. Expression (6) differs from the well-known Schawlow–Townes linewidth formula through a linewidth enhancement factor involving the quantity α. α reflects a strong amplitude–phase coupling of the lasing field in a semiconductor laser resulting from the highly detuned optical gain spectrum. This coupling causes a phase noise (linewidth) enhancement which was only observed recently [11]. This formula indicates that $\Delta\nu$ depends on the electronic density of states $\rho_{red}(\epsilon)$ through α and n_{sp}.

The denominator of eq. (7) is proportional to $g'(E_1, n)$. Therefore, from the results of the previous section, an increase of the denominator can be expected with the use of quantum-well and quantum-wire structures. The numerator in (7), however, is also enhanced in the quantum-well and quantum-wire structures. Therefore it is difficult to predict the behavior of α in these structures

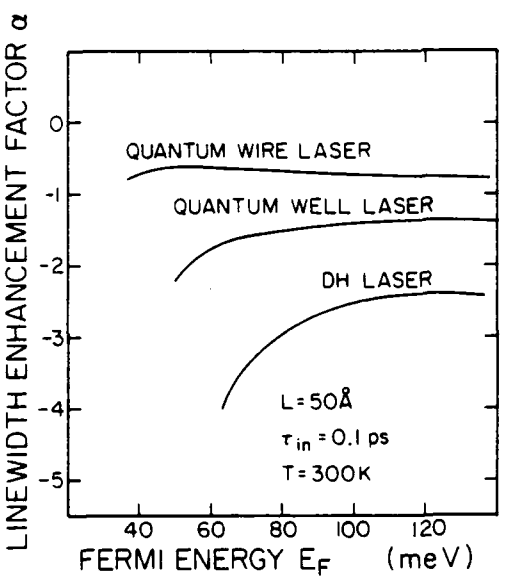

Fig. 4. The linewidth enhancement factor α as a function of the conduction-band quasi-Fermi energy level in a conventional double heterostructure laser, a 50 Å well thickness quantum-well laser, and a 50 Å × 50 Å quantum-wire laser.

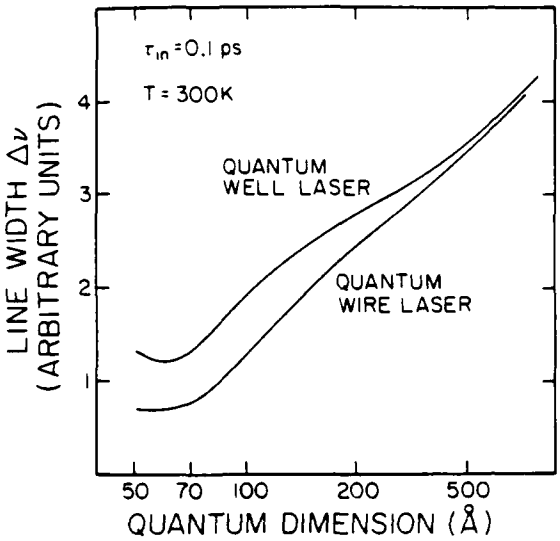

Fig. 5. The spectral linewidth in a quantum-well laser and a quantum-wire laser as a function of the well thickness. The number of quantum wells and quantum wires is optimized at each quantum well thickness.

without numerical calculation. Fig. 4 gives a calculation of α as a function of E_F for conventional DH lasers, quantum-well lasers, and quantum-wire lasers. In this figure, the quantum dimensions are all equal to $L = 50$ Å. The results indicate first, that α depends strongly on E_F (or equivalently the optical gain required for laser oscillation), its magnitude decreasing for larger E_F. (This result has been observed experimentally for conventional DH lasers [15].) Second, this reduction of $|\alpha|$ with increasing excitation is larger in quantum-well and quantum-wire lasers.

The linewidth $\Delta\nu$ also contains the spontaneous emission factor, n_{sp}, which decreases monotonically with the increase of E_F and converges to 1. Therefore, for a fixed loss (i.e. Γg constant), it is advantageous to operate with a high E_F to attain reductions in $\Delta\nu$. With regards to well- or wire-number selection, this means that, in contrast to f_r, single quantum-well and quantum-wire active layers are the optimum choice for phase noise reduction. Fig. 5 gives $\Delta\nu$ as a function of L with $N = 1$. This result shows that a thin quantum well and a thin quantum wire are effective for reducing $\Delta\nu$. The demonstration of the quantum-wire effect for improving phase noise properties has also been done using a high magnetic field and is described elsewhere.

4. Conclusion

The spectral and dvnamic properties of quantum-well and quantum-wire lasers have been investigated and compared with these properties in conven-

tional DH lasers. Calculations and preliminary experimental results indicate that these structures may exhibit superior dynamic and spectral performance if designed properly. More detailed experimental results are described elsewhere.

Acknowledgements

We express our thanks to Dr. Kam Lau for fruitful discussions and supplying lasers. This work was supported by the Air Force Office of Scientific Research, the Office of Naval Research, I.T.T. Corporation, and the Japanese Society for the Promotion of Science. Part of this work was performed at the Francis Bitter National Magnet Laboratory at M.I.T.

References

[1] W.T. Tsang, Appl. Phys. Letters 39 (1981) 134.
[2] K.Y. Lau, N. Bar Chaim, I. Ury, C. Harder and A. Yariv, Appl. Phys. Letters 43 (1983) 1.
[3] K.Y. Lau, N. Bar-Chaim, I. Ury and A. Yariv, Appl. Phys. Letters 45 (1984) 345.
[4] K.Y. Lau and A. Yariv, IEEE J. Quantum Electron. QE-21 (1985) 106.
[5] K. Vahala and A. Yariv, Appl. Phys. Letters 45 (1984) 501.
[6] K. Vahala, J. Paslaski and A. Yariv, Appl. Phys. Letters 44 (1985) 1025.
[7] Y. Arakawa and H. Sakaki, Appl. Phys. Letters 40 (1982) 490.
[8] Y. Arakawa, K. Vahala and A. Yariv, Appl. Phys. Letters 45 (1984) 950.
[9] Y. Arakawa, K. Vahala, A. Yariv and K. Lau, Appl. Phys. Letters (1985), in press.
[10] Y. Arakawa and A. Yariv, IEEE J. Quantum Electron. QE-21 (1985), in press.
[11] M.W. Fleming and A. Mooradian, Appl. Phys. Letters 38 (1981) 511.
[12] C.H. Henry, IEEE J. Quantum Electron. QE-18 (1982) 259.
[13] K. Vahala and A. Yariv, IEEE J. Quantum Electron. QE-19 (1983) 1096.
[14] K. Vahala and A. Yariv, IEEE J. Quantum Electron. QE-19 (1983) 1102.
[15] Y. Arakawa and A. Yariv, Appl. Phys. Letters (1985), in press.

Unclassified
SECURITY CLASSIFICATION OF THIS PAGE

REPORT DOCUMENTATION PAGE

Form Approved
OMB No. 0704-0188

1a. REPORT SECURITY CLASSIFICATION Unclassified	1b. RESTRICTIVE MARKINGS
2a. SECURITY CLASSIFICATION AUTHORITY 2b. DECLASSIFICATION / DOWNGRADING SCHEDULE	3. DISTRIBUTION / AVAILABILITY OF REPORT Approved for public release; distribution unlimited.
4. PERFORMING ORGANIZATION REPORT NUMBER(S) N00014-K-0211	5. MONITORING ORGANIZATION REPORT NUMBER(S) 696-002
6a. NAME OF PERFORMING ORGANIZATION California Institute of Technology 6b. OFFICE SYMBOL (If applicable)	7a. NAME OF MONITORING ORGANIZATION Office of Naval Research
6c. ADDRESS (City, State, and ZIP Code) Pasadena, California 91125	7b. ADDRESS (City, State, and ZIP Code) 565 S. Wilson Pasadena, California 91106-3212
8a. NAME OF FUNDING / SPONSORING ORGANIZATION Office of Naval Research 8b. OFFICE SYMBOL (If applicable)	9. PROCUREMENT INSTRUMENT IDENTIFICATION NUMBER P00001
8c. ADDRESS (City, State, and ZIP Code) 800 N. Quincy Street Arlington, VA 22217	10. SOURCE OF FUNDING NUMBERS PROGRAM ELEMENT NO. / PROJECT NO. / TASK NO / WORK UNIT ACCESSION NO.

11. TITLE (Include Security Classification)
Theory of Gain, Modulation Response and Spectral Linewidth in AlGaAs Quantum Well Lasers

12. PERSONAL AUTHOR(S)
Y. Arakawa and A. Yariv

13a. TYPE OF REPORT	13b. TIME COVERED	14. DATE OF REPORT (Year, Month, Day)	15. PAGE COUNT
Reprint	FROM _____ TO _____	1985 October	9

16. SUPPLEMENTARY NOTATION The view, opinions and/or findings contained in this report are those of the author(s) and should not be construed as an official Department of the Navy position, policy, or decision unless so designated by other documentation.

17. COSATI CODES			18. SUBJECT TERMS (Continue on reverse if necessary and identify by block number)
FIELD	GROUP	SUB-GROUP	Quantum Well Lasers

19. ABSTRACT (Continue on reverse if necessary and identify by block number)

We investigate theoretically a number of important issues related to the performance of AlGaAs quantum well (QW) semiconductor lasers. These include a basic derivation of the laser gain, the linewidth enhancement factor α, the the differential gain constant in single and multiple QW structures. The results reveal the existence of gain saturation with current in structures with a small number of wells. They also point to a possible two-fold increase in modulation bandwidth and a ten-fold decrease in the spectral laser linewidth in a thin QW laser compared to a conventional double heterostructure laser.

20. DISTRIBUTION / AVAILABILITY OF ABSTRACT ☐ UNCLASSIFIED/UNLIMITED ☐ SAME AS RPT ☐ DTIC USERS	21. ABSTRACT SECURITY CLASSIFICATION
22a. NAME OF RESPONSIBLE INDIVIDUAL	22b. TELEPHONE (Include Area Code) / 22c. OFFICE SYMBOL

DD Form 1473, JUN 86 Previous editions are obsolete. SECURITY CLASSIFICATION OF THIS PAGE

Theory of Gain, Modulation Response, and Spectral Linewidth in AlGaAs Quantum Well Lasers

YASUHIKO ARAKAWA, MEMBER, IEEE, AND AMNON YARIV, FELLOW, IEEE

Abstract—We investigate theoretically a number of important issues related to the performance of AlGaAs quantum well (QW) semiconductor lasers. These include a basic derivation of the laser gain, the linewidth enhancement factor α, and the differential gain constant in single and multiple QW structures. The results reveal the existence of gain saturation with current in structures with a small number of wells. They also point to a possible two-fold increase in modulation bandwidth and a ten-fold decrease in the spectral laser linewidth in a thin QW laser compared to a conventional double heterostructure laser.

I. Introduction

THE application of semiconductor lasers for optical communication requires low-noise characteristics and high-frequency dynamic performance. These properties have received considerable attention in conventional double heterostructure (DH) lasers [1]–[5]. Recently the detuned loading by the use of coupled-cavity DH lasers was proposed for improving these properties [6]. In this structure, the differential gain g' and the linewidth enhancement factor α which determine, respectively, the dynamic performance and noise characteristics, are varied by detuning the lasing frequency away from the loss peak. The basic quantum mechanical expressions for g' and α suggest yet another way to improve α and g' through changes in the density of states which occur in quantum well (QW) structures. Although QW lasers have proven to be attractive light sources because of their low threshold current densities and the low temperature sensitivity of the threshold current [7]–[11], little effort has been directed towards measurement or calculation of these noise characteristics and high-modulation performance [12]–[14].

In this paper, we investigate theoretically the effects of QW structure parameters such as the number and the thickness of QW's on the dynamic response and quantum noise, and consider the optimum QW structure for realizing low-noise characteristics and/or high-dynamic performance. In the analysis, we also consider the important issue of the use of multiquantum well structures in order to avoid the phenomenon of gain saturation with current, as well as for improving the noise and dynamic performance. The effect of the structural parameters such as the thickness and the number of QW's on the threshold current have been considered before [15], [16], although the gain saturation effect was not explicitly treated. In Section III the fundamental properties of differential gain are discussed, and then the effects of QW structure parameter on the laser dynamics are investigated. In Section IV, the linewidth enhancement factor α and the spontaneous emission factor are studied and the attainable reduction of the linewidth by the use of the optimum QW structures is considered. The results indicate that the modulation bandwidth (relaxation resonance frequency) is enhanced by a factor of ~ 2 in the multiquantum well (MQW) laser and the laser linewidth (FM noise) is found to be significantly suppressed, by $\sim \frac{1}{10}$, in a single thin QW (SQW) laser compared to a conventional double heterostructure laser. In order to clarify achievable limits of these properties with quantum well effects, we will consider AlGaAs quantum well lasers which are almost free from nonradiative processes, such as the Auger recombination at room temperature.

Manuscript received February 8, 1985; revised May 13, 1985. This work was supported by the Air Force Office of Scientific Research, the Office of Naval Research, the ITT Corporation, and the Japan Society for Promotion of Science

The authors are with the California Institute of Technology, Pasadena, CA 91125.

II. Linear Gain and Threshold Current

A. Density of States

In the QW structures [7], a series of energy levels and associated subbands are formed owing to the quantization of electrons in the direction of the quantum well thickness. The density of states (per unit energy per unit area) of such confined electrons in the nth subband is given by

$$\rho_{c_n}(E) = \frac{m_c}{\pi\hbar^2} H(E - \epsilon_{c_n}) \tag{1}$$

where $H(x)$, m_c, $\hbar$, L_z, and ϵ_{c_n} are the Heaviside function, the effective mass of electrons, Planck's constant (h) divided by 2π, the QW thickness, and the quantized level of electrons in the nth subband of the QW structures, respectively. When the barrier height is sufficiently big and the barrier thickness is sufficiently large, ϵ_{c_n} is equal to $(n\pi\hbar)^2/(2m_c L_z^2)$. On the other hand, if the barrier is thin or its barrier height is small so that coupling between adjacent wells exists, the degeneracy of the individual well quantized energy levels dissappears and each single-well level splits into N different energy levels. In order to simplify the discussion in this paper, we will consider the weak coupling limit of QW structures in which energy broadening due to coupling is sufficiently small compared to the energy broadening (usually more than 5 meV) due to intraband relaxation time.

0018-9197/85/1000-1666$01.00 © 1985 IEEE

B. Linear Gain and Threshold Current

When the recombination is dominated by band-to-band radiative process, the linear bulk gain derived under k-selection rule is given by

$$g(E) = \int A(\epsilon) \sum_{j=h,l} \sum_{n=1}^{\infty} \frac{\rho^j_{\mathrm{red}_n}(\epsilon)}{L_z} (f_c(E_{c_n}) - f_v(E^j_{v_n})) \frac{(\hbar/\tau_{in})}{(E-\epsilon)^2 + (\hbar/\tau_{in})^2} d\epsilon. \quad (2)$$

The bulk gain is the gain exercised by an electromagnetic field if it were completely confined to the quantum well. E is the photon energy, j designates either light holes (l) or heavy holes (h), $\rho^j_{\mathrm{red}_n}$ is the reduced density of states which is defined by $\rho^j_{\mathrm{red}_n} = ((\rho_{c_n})^{-1} + (\rho^j_{v_n})^{-1})^{-1}$, $\rho^j_{v_n}$ is the density of states of light holes ($j = l$) or heavy holes ($j = h$), $f_c(f_v)$ is the Fermi-Dirac distribution function for electrons (holes) in the conduction band (the valence band) with the Fermi-energy $\epsilon_{F_c}(\epsilon_{F_v})$, τ_{in} is the intraband relaxation time. E_{c_n} and $E^j_{v_n}$ are equal to $(m_c\epsilon^j_{v_n} + m^j_v E + m^j_v\epsilon_{c_n})/(m_c + m^j_v)$, and $(m_c\epsilon^j_{v_n} - m_c E + m^j_v\epsilon_{c_n})/(m_c + m^j_v)$, respectively, where m^j_v and $\epsilon^j_{v_n}$ are the effective mass and the energy level of the nth subband of heavy holes ($j = h$) or light holes ($j = l$). $A(\epsilon)$ is the coefficient related to the square of the dipole matrix element $|M|^2_{\mathrm{ave}}$ as given by

$$A(\epsilon) = \frac{\pi e^2 h}{m_0^2 c n_r E_g} |M|^2_{\mathrm{ave}} \quad (3)$$

where n_r is the refractive index of GaAs, e is the electron charge, m_0 is the mass of electrons, c is the light velocity, E_g is the band-gap, and h is the Planck's constant. In quantum well structures, the gain depends on the polarization of the light. The dipole matrix element $|M|^2_{\mathrm{ave}}$ which is different from that of the double heterostructure was discussed by Asada *et al.* [16]. For instance the dipole matrix element for TE mode due to an electron-heavy hole transition is given by

$$|M|^{2\mathrm{TE}}_{\mathrm{ave}} = |M_0|^2_{\mathrm{ave}} (1 + E/(\epsilon_{c_n} - \epsilon^h_{v_n})) \quad (4)$$

where $|M_0|^2_{\mathrm{ave}}$ is the square of the dipole matrix with the conventional double heterostructure lasers and is approximately equal to 1.33 $m_0 E_g$. The quasi-Fermi energy ϵ_{F_c} and ϵ_{F_v} are determined by both the charge neutrality condition and the condition that the modal gain $g_{\mathrm{mod}}(E) = \Gamma g(E)$ at the photon energy E_l for laser oscillation is equal to the total losses α_{total} as follows:

$$g_{\mathrm{mod}}(E_l) = \Gamma g(E_l) = \alpha_{\mathrm{total}} = \Gamma\alpha_{ac} + (1-\Gamma)\alpha_{ex} + L^{-1}\ln(1/R) \quad (5)$$

where α_{ac}, α_{ex}, R, and L are the loss in the active region, the loss in the cladding layer, the reflectivity, and the cavity length. The optical confinement factor Γ depends on the structure strongly. In this paper, we assume a multiquantum well (MQW) structure composed of thin GaAs well layers, $Ga_{0.75}Al_{0.25}As$ barrier layers, and $Ga_{0.75}Al_{0.25}As$ waveguide layers. The dimension of the waveguide layers is determined so that the total thickness, including QW wells, barrier layers, and waveguide layers, is equal to 2000 Å. The cladding layers are a p-$Ga_{0.6}Al_{0.4}As$ layer, and n-$Ga_{0.6}Al_{0.4}As$ layer, respectively. In particular, when the number of QW is equal to 1, we call this structure a single QW (SQW) structure, hereafter. In these MQW structures the Γ is given approximately by [15]

$$\Gamma = 0.3\, N(L_z/L_0) \quad (6)$$

where L_0 is equal to 1000 Å, N is the number of QW's.

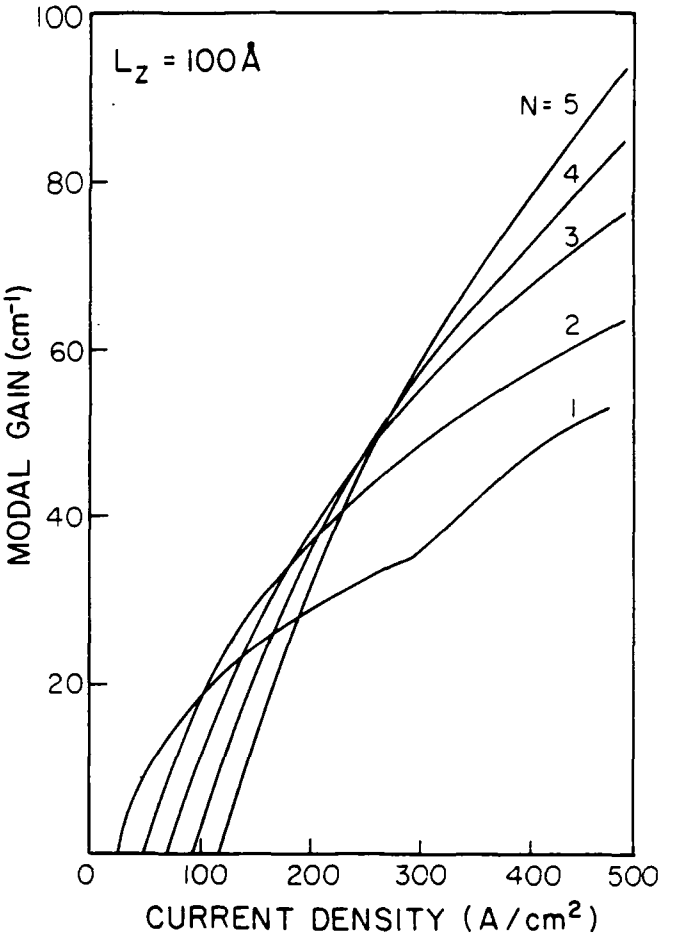

Fig. 1. The modal gain g_{mod} ($=\Gamma_e$) as a function of the injected current density J with the various number of quantum wells N. In this case, the quantum well thickness L_z is assumed to be 100 Å.

Fig. 1 shows the maximum gain g_{mod} (E_l) exercised by the laser mode as a function of the injected current density J for different number of QW's. The injected current J is given by

$$J = eL_zN\left(\iint \frac{8\pi n_r^2 E_g^2}{c^2 h} A(\epsilon) \sum_{j=h,l} \sum_{n=1}^{\infty} \frac{\rho^j_{\mathrm{red}_n}(\epsilon)}{L_z} f_c(E_{c_n}) \cdot (1 - f_v(E^j_{v_n})) \frac{(\hbar/\tau_{in})}{(E-\epsilon)^2 + (\hbar/\tau_{in})^2} d\epsilon\, dE\right). \quad (7)$$

The term surrounded by parenthesis is the total emission rate. In this calculation, the QW thickness L_z and τ_{in} are

assumed to be 100 Å and 0.2 ps. The energy band-gap discontinuity ΔE_c and ΔE_v of the conduction band and the valence band at the interface of GaAs and $Al_{0.3}Ga_{0.7}As$ are set 0.8 ΔE and 0.2 ΔE, respectively, where ΔE, which is the total band discontinuity, is assumed to be 333 meV. We notice a very marked flattening ("saturation") of the gain at high injected currents, especially in a single well ($N = 1$). This gain saturation is due to the step-like shape of the density of state functions, and the fact that penetration of the quasi-Fermi levels into the conduction band or valence band takes place at high current injection. The product $\rho_{red}(\epsilon)[f_c(E_c) - f_v(E_v)]$, which determines the gain, becomes a constant and no longer increases with current. The maximum gain $g_{mod}(E_l)$ available with N QW's is thus N times larger than $g_{mod}(E_l)$ with $N = 1$ since each well can now provide its saturation gain, which is equal to that of a SQW laser. We can consequently avoid the saturation effect by increasing the number of QW's although the injected current to achieve this maximum gain also increases by N times. Owing to this gain saturation effect there exists an optimum number of QW's for minimizing the threshold current for a given total loss α_{total}. From Fig. 1 we see that, for low losses, the injected threshold current is minmimum in the case of $N = 1$. On the other hand, if the $\alpha_{total} > 20\ cm^{-1}$, the threshold current with $N = 1$ is larger than that of $N = 2$. At higher values of α_{total}, which call for large laser modal gain g_{mod}, a larger number of wells are needed. From Fig. 1 we see that for $\alpha_{loss} > 50\ cm^{-1}$ a five-well structure ($N = 5$) will have the lowest threshold current.

In order to clarify these situations, in Fig. 2 the threshold current as a function of the QW number with various total loss is shown. This figure indicates that when the α_{total} is low, $N = 1$ is optimum, whereas the optimum number N is larger than 1 for higher α_{loss}. Thus the gain saturation which is enhanced in a SQW structure causes the significant dependence of the optimum number N on the α_{total} for reducing threshold current.

There remains another important structural parameter, the quantum well thickness. Fig. 3 shows the threshold current change as a function of the QW thickness. In this calculation, the number of QW's with each QW thickness is optimized so that the threshold current is minimum. The results indicate that the threshold current of thinner QW lasers ($L_z = 50 \sim 100$ Å) is much lower than that of thicker QW lasers. We also notice that the threshold current is minimized with $L_z \sim 60$ Å when α_{loss} is low ($\alpha_{loss} = 10, 30\ cm^{-1}$). This is mainly due to the fact that the current for transparency (gain is just equal to zero), which corresponds approximately to threshold current with extremely low loss, is minimized at the thickness of $L_z \sim 60$ Å in the case of $N = 1$ and also due to the fact that the optimum N at each QW is 1 in the case of low α_{loss} for thin quantum well structures. Since the gain saturation is more enhanced for smaller L_z, the optimum N of thinner QW's is larger than that of thicker QW's. For $\alpha_{loss} = 50\ cm^{-1}$, $N_{opt}(L_z = 50\ Å) = 4$, while $N_{opt}(L_z = 100\ Å) = 2$ and $N_{opt}(L_z = 200\ Å) = 1$.

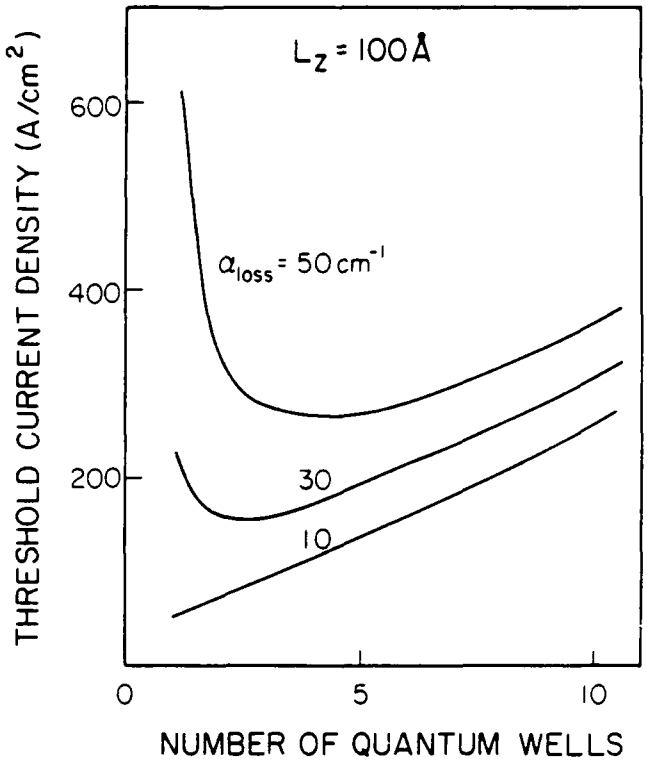

Fig. 2. The threshold current change as a function of the number N of quantum wells with the various total loss α_{loss}. In this case, the quantum well thickness L_z is assumed to be 100 Å.

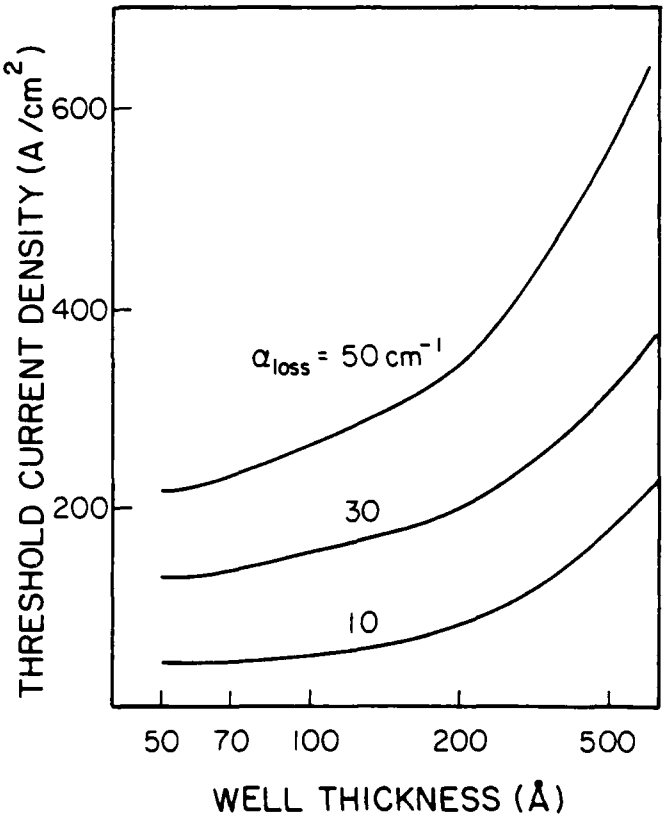

Fig. 3. The threshold current change as a function of the quantum well thickness L_z with various total loss α_{loss}. The number N of quantum wells which is optimized so that threshold current is minimum.

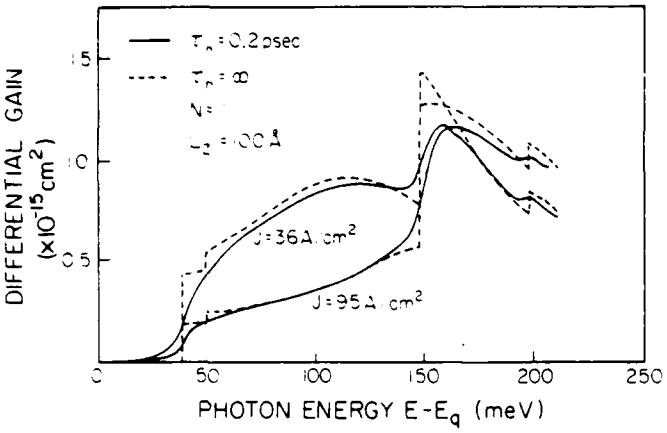

Fig. 4. The differential gain $g'(E)$ with several injected currents as a function of the photon energy substracted the band-gap energy of GaAs ($E - E_g$). In this calculation τ_{in} is assumed to be 0.2 ps (solid curve) and ∞ s (broken curve). The number of the quantum wells is 1 and the thickness is 100 Å.

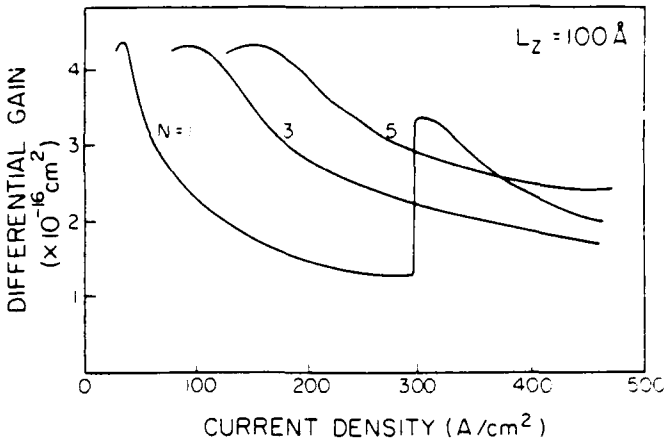

Fig. 5. The differential gain $g'(n, E_l)$, at which the gain is maximum, is shown as a function of the injected current J with various number of quantum wells. The thickness of quantum wells is 100 Å.

III. Differential Gain and Modulation Bandwidth

A. Differential Gain

In this section, we investigate the properties of the differential gain and calculate the modulation bandwidth of the quantum well laser. The differential gain $g'(n, E)$ at a photon energy E is defined as the derivative of the bulk gain with respect to carrier concentration, i.e., ($g'(n, E) \equiv dg(n, E)/dn$). Since it figures in the modulation response of the semiconductor laser through the expression $f_r = \frac{1}{2}\pi\sqrt{g'(n, E)(n_r/c)(P_0/\tau_p)}$ (where f_r is the relaxation frequency conventionally used as a measure of the upper useful modulation frequency [1], P_0 is the photon density in the active region and τ_p is the photon lifetime in the passive cavity), $g'(n, E)$ contains the "physics" of the semiconductor laser. The derivation of f_r will be discussed in the next section. In order to emphasize the carrier dependence of the gain, we describe the gain as a function of both E and n. When we take broadening effects due to intraband relaxation into consideration the differential gain is given by

$$g'(n, E)\frac{dg(n, E)}{dn} = \int A(\epsilon) \sum_{j=h,l} \sum_{n=1}^{\infty} \frac{\rho^{j}_{\mathrm{red}_n}(\epsilon)}{L_z} \cdot \left(\frac{df_c(\epsilon_{cn})}{dn} - \frac{df_v(\epsilon^{j}_{vn})}{dn}\right) \cdot \frac{(\hbar/\tau_{in})}{(E-\epsilon)^2 + (\hbar/\tau_{in})^2}\, d\epsilon. \tag{8}$$

Fig. 4 shows the differential gain $g'(n, E)$ as a function of the excess photon energy ($E - E_g$) (E_g = band-gap energy) at two injected current densities (J = 36, 95 A/cm^{-2}) in SQW laser with a QW thickness of L_z = 100Å. The solid curve is that of $g'(n, E)$ with τ_{in} = 0.2 ps and the broken line represents $g'(n, E)$ with $\tau_{in} = \infty$ (i.e., no energy broadening). We call $g'(n, E)$ without energy broadening the differential gain profile, hereafter. This differential gain profile is 0 below 39 meV which corresponds to the energy difference between the first subband of electrons and heavy holes ($\epsilon_{c1} - \epsilon^{h}_{v1} - E_g$). The abrupt small change near 50 meV is due to the onset of the electron-light hole transition of the first subband. We also note other abrupt changes in the $g'(E, n)$ near 150 meV and 190 meV. These changes correspond to the electron-heavy hole, and electron-light hole transitions of the second subband, respectively. In the case of the more realistic τ_{in} = 0.2 ps curves, the energy broadening of the abrupt features, by ($\hbar/\tau_{in}$), causes a lowering of $g'(n, E)$. In this case we can still observe dips at the onset of higher order transitions. Since the photon energy E_l that maximizes the gain, is near 40–50 meV in both cases of the injected current, this figure indicates that differential gain at E_l seems to decrease with the increase of the injected current.

In order to clarify the injected current dependence of the differential gain, we show in Fig. 5 the differential gain $g'(n, E_l)$ at maximum gain photon energy E_l as a function of the injected current in a MQW laser with various numbers of QW's. The results show that $g'(n, E_l)$ has a peaked structure, which is due to the gain saturation effects discussed in Section II. Since $g'(n, E_l)$ is a bulk parameter, it does not change with the increase of the number of QW's as long as the Fermi energy is fixed, whereas the injected current increases by a factor of N. Consequently, the $g'(E, n)$ curve is stretched in the direction of the current axis with an increase of N. Note that the second peak appears at $J \sim 300$ mA. In the current region below the second peak ($J < 300$ mA), E_l is located near the first subband. When E_l jumps from the first subband to the second subband, this second peak appears.

The differential gain also depends on the QW thickness. Fig. 6 shows the differential gain at E_l as a function of the injected current in a SQW laser with the various QW thickness (50 Å, 100 Å, and 200 Å). The results indicate two important properties of the $g'(n, E)$. First is that the thinner QW laser achieves higher differential gain. This is mainly due to the fact that the contribution of the injected current to the increment of the gain by the next higher subband is enhanced when the QW thickness is larger, and that happens at the expense of gain at E_l. Sec-

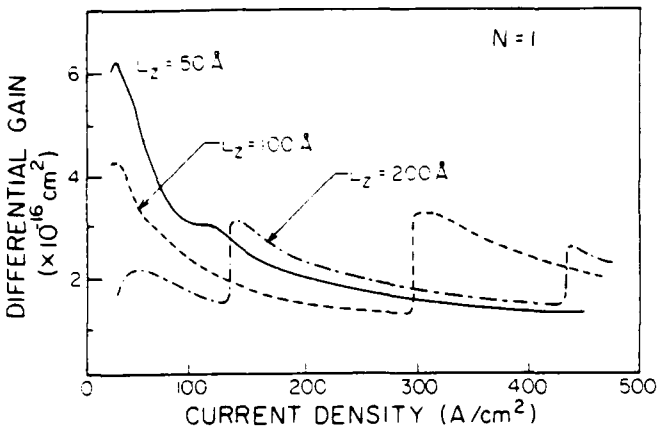

Fig. 6. The differential gain $g'(n, E_l)$, at which the gain is maximum, is shown as a function of the injected current with various quantum well thickness L_z. The number of quantum wells is equal to 1.

ond is that the $g'(n, E)$ has many peaks when $L_z = 200$ Å. Note that the values of the second and third peak of $g'(n, E)$ are comparable to that of the first peak. When E_l jumps from the first (second) subband to the second (third) subband, the second peak (third peak) appears. Since thicker QW's have more peaks in the density of states, the jumps appear more frequently with the increase of the L_z. In the limiting case of thick QW's, $g'(n, E)$ increases gradually with the increase of J.

B. Modulation Resonance Frequency

On the basis of the discussion concerning $g'(n, E)$ in the previous subsection, we will investigate modulation dynamics in QW lasers. The rate equation for laser dynamics can be described as follows.

$$\frac{dn}{dt} = \frac{J(t)}{eL_z} - \frac{n_r}{c} g(n, E_l) P - \frac{n}{\tau_s}$$

$$\frac{dP}{dt} = \Gamma \frac{n_r}{c} g(n, E_l) P + \beta \frac{n}{\tau_s} - \frac{P}{\tau_p} \tag{9}$$

where P is the photon density (cm^{-3}), β is the spontaneous emission coefficient into the lasing mode, τ_s is the carrier lifetime, $J(t)$ (cm^{-2}) is the injected current density, n is the carrier concentration, and $g(n, E_l)$ (cm^{-1}) is the bulk gain, while $\Gamma g(n, E_l)$ is the modal gain as a function of the carrier density n (cm^{-3}) at the lasing photon energy E_l. When we discuss the carrier density in the quantum well structure we usually use the density per cm^2, however, the proper "bookkeeping" of photons and carriers requires that n stands for carrier density per unit volume. The relaxation resonance frequency f_r is determined by a small-signal analysis of (9). The results can be simply expressed by [1]

$$f_r = \frac{1}{2\pi} \sqrt{\frac{n_r g'(n, E_l)}{c} \frac{P_o}{\tau_p}}, \tag{10}$$

where P_o is the photon density in the cavity at stationary states. Note that τ_p is related to the total loss as follows.

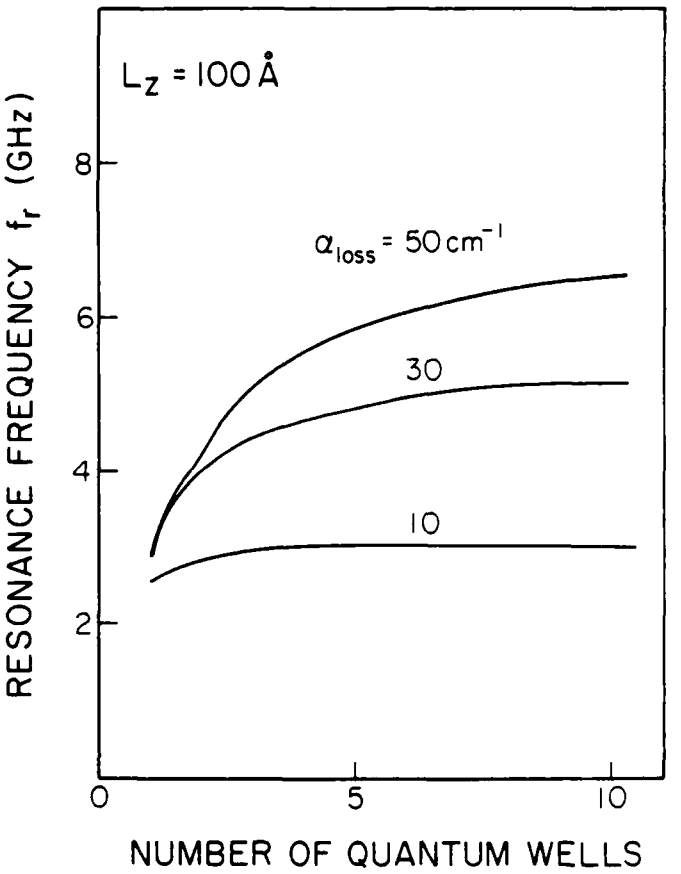

Fig. 7. The calculated results of the resonant frequency f_r as a function of N with various total loss α_{loss}, with quantum well thickness $L_z = 100$ Å.

$$\tau_p = \frac{n_r}{c\alpha_{loss}}. \tag{11}$$

It follows from (10) that an increase of the differential gain and of P_o, together with a decrease of τ_p, is required in order to increase the modulation bandwidth. The increase of P_o is usually limited by catastrophic mirror damage, while τ_p is determined by the total loss α_{total}. Thus P_o and τ_p depend strongly on the laser geometry. On the other hand, the differential gain $g'(n, E_l)$ depends on the properties of the QW's and on the injected current at threshold as discussed in connection with Figs. 5 and 6. Fig. 7 shows the calculated result of the resonance frequency f_r of MQW lasers with $L_z = 100$ Å as a function of N with α_{loss} (photon lifetime) as a parameter taking (11) into consideration. As shown in this figure, there is the optimum N which is, usually, not equal to 1 for obtaining high f_r. This can be explained as follows. When the number of QW's is small, the threshold current J_{th} is larger than the current J^N_{max} which gives the maximum differential gain because of the gain saturation effects, leading to lower differential gain. On the other hand, the differential gain increases with the increase of N, since J_{th} approaches J^N_{max}. However, once J_{th} becomes smaller than J^N_{max}, with the further increase of N, the differential gain decreases again. Therefore there exists an optimum number N_{opt} at which $J_{max} \sim J_{th}$. Since J^N_{max} increases with the increase

of α_{loss} with the same N, the N_{opt} increases for higher α_{loss}.

In Fig. 8, the maximum resonance frequency f_r, which can be attained by optimizing N as a function of L_z with various α_{loss}, is shown by a solid curve. This result indicates that for the range of losses (α_{loss}) considered, the resonance frequency increases with the reduction of the QW thickness: the resonance frequency f_r with L_z = 50 Å is enhanced by 1.8 compared to the f_r of the double heterostructure laser.

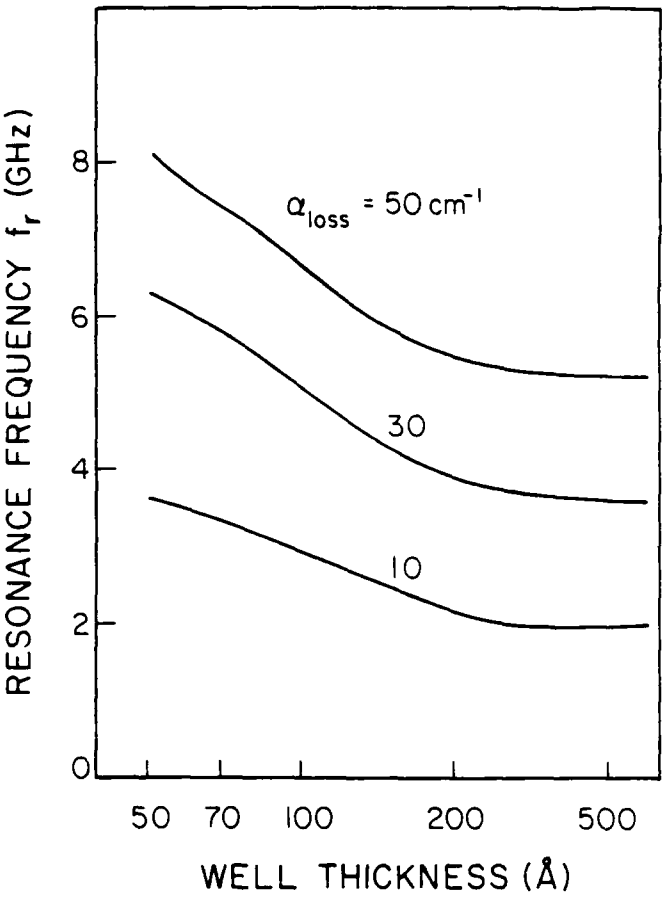

Fig. 8. The maximum resonant frequency, which is achieved by optimizing the number of quantum wells, as a function of the quantum well thickness L_z with various total loss α_{loss}.

IV. Laser Linewidth

A. Spontaneous Emission Factor

In this section, we analyze the spectral linewidth broadening in the QW lasers and show how a substantial reduction of the linewidth can be obtained with an optimization of the quantum well structures.

The power-dependent linewidth in semiconductor lasers occurs due to the spontaneous emission that modulates the laser field both in intensity and in frequency (phase). This linewidth involves the Schawlow—Townes linewidth that is due to the instantaneous-phase fluctuation as well as to the delayed-phase fluctuation that occurs as the laser intensity returns to its steady states (amplitude phase coupling). The reduced linewidth is [3], [4]

$$\Delta\nu = \frac{v_g^2 h\nu(\Gamma g(E_l))\,(L^{-1} ln\,(1/R))\,n_{sp}}{8\pi P_1}(1 + \alpha^2) \quad (12)$$

where P_1 is the output photon density, α is the linewidth enhancement factor, v_g is the group velocity of light in the active layer, $h\nu$ is the photon energy, and n_{sp} is defined as the spontaneous emission rate divided by total stimulated emission rate given by

$$n_{sp}(E) = \frac{\int A(\epsilon) \sum_{j=h,l} \sum_{n=1}^{\infty} \rho^j_{red_n}(\epsilon) f_c(1 - f_v) \frac{(\hbar/\tau_{in})}{(E - \epsilon)^2 + (\hbar/\tau_{in})^2}}{\int A(\epsilon) \sum_{j=h,l} \sum_{n=1}^{\infty} \rho^j_{red_n}(\epsilon)\,(f_c - f_v) \frac{(\hbar/\tau_{in})}{(E - \epsilon)^2 + (\hbar/\tau_{in})^2}\,d\epsilon}. \quad (13)$$

If energy broadening is extremely small we can approximate n_{sp} at the photon energy E_l at which the gain is maximum ($E = E_l$) by

$$n_{sp} \approx (1 - \exp\,(E_1 - \Delta\epsilon_F))^{-1} \quad (14)$$

where $\Delta\epsilon_F$ is the difference between the quasi-Fermi energy of electrons and that of holes ($\epsilon_{F_c} - \epsilon_{F_v}$). Equation (14) shows that n_{sp} at E_l increases substantially with the approach of $\Delta\epsilon_F$ to E_l (i.e., the total loss decreases), since E_l is fixed near ($\epsilon_{c1} - \epsilon_{v1}$) (the photon energy which corresponds to the lowest subband) in the QW lasers. Finally, n_{sp} at E_l becomes infinite when the injected current is equal to the current J_{tr} at which transparency occurs ($\Delta\epsilon_F \rightarrow E_l$). In Fig. 9, we show the calculated results of n_{sp} at E_l as a function of the injected current with a various numbers of QW's. The QW thickness is assumed to be 100 Å and τ_{in} is assumed to be 0.2 ps. The observed dip corresponds to the jump of E_l from the electron-hole transition of the first subband to the electron-hole transition of the second subband.

Fig. 10 shows the n_{sp} at E_l as a function of the injected current with various QW thicknesses. In this calculation, the number of QW's is 1 and τ_{in} = 0.2 ps. We notice that the approach of n_{sp} to 1, with the increase of the injected current, occurs more rapidly when the QW thickness is smaller. We also notice that two dips appear in the case of L_z = 200 Å. These dips appear when E_l jumps from the electron-hole transition of the first (second) subband to the electron-hole transition of the second (third) subband.

B. Linewidth Enhancement Factor

The linewidth enhancement factor α of (12), which represents the spectral broadening due to the coupling between AM linewidth and FM noise, is given by [17]

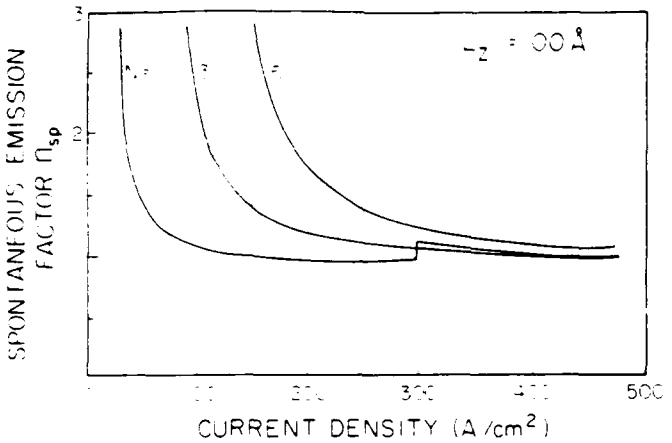

Fig. 9. The spontaneous emission factor n_{sp} as a function of the injected current, at which the gain is maximum, is shown as a function of the injected current J with various number of quantum wells. The thickness of quantum wells is 100 Å.

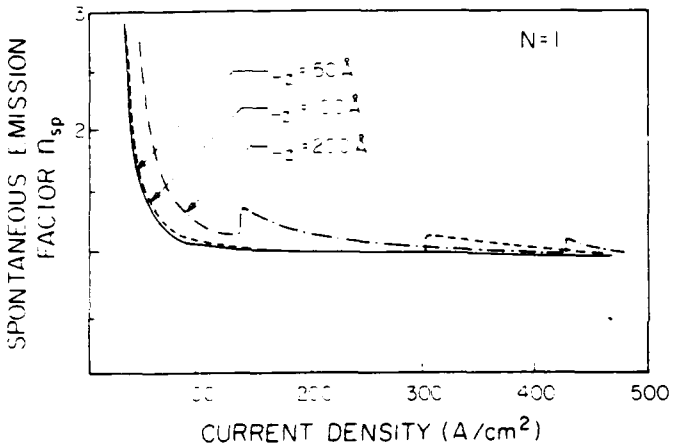

Fig. 10. The spontaneous emission factor n_{sp} as a function of the injected current, at which the gain is maximum, is shown as a function of the injected current J with various quantum well thickness. The number of quantum wells N is equal to 1.

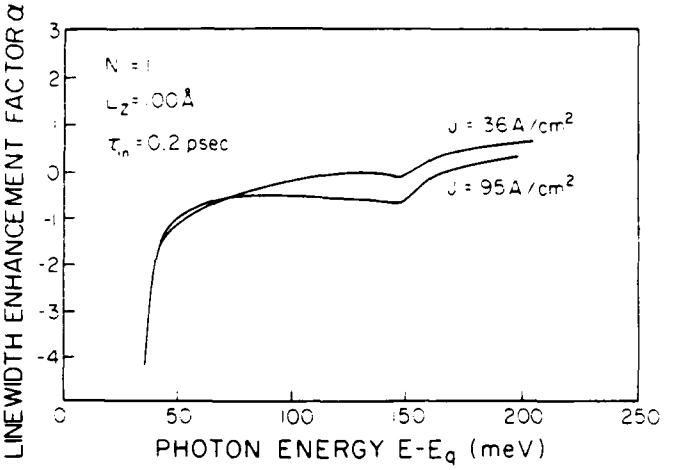

Fig. 11. The linewidth enhancement factor α with various injected currents as a function of the photon energy substracted by the band-gap energy of GaAs ($E - E_g$).

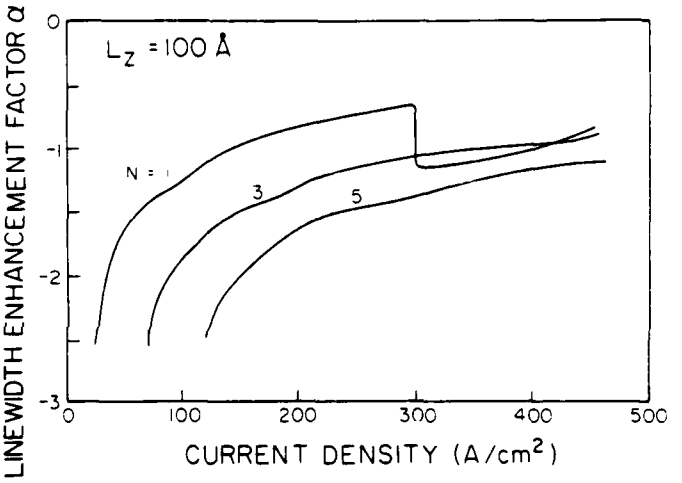

Fig. 12. The linewidth enhancement factor α as a function of the injected current at photon energy, at which the gain is maximum with various N. The thickness of quantum wells is 100 Å.

$$\alpha = \frac{\int A(\epsilon) \sum_{j=jh,l} \sum_{n=1}^{\infty} \rho^{j}_{\mathrm{red}_n}(\epsilon) \left(\frac{df_c(\epsilon_{cn})}{dn} - \frac{df_v(\epsilon^{j}_{vn})}{dn} \right) \frac{(E-\epsilon)}{(E-\epsilon)^2 + (\hbar/\tau_{in})^2} d\epsilon}{\int A(\epsilon) \sum_{j=h,l} \sum_{n=1}^{\infty} \rho^{j}_{\mathrm{red}_n}(\epsilon) \left(\frac{df_c(\epsilon_{cn})}{dn} - \frac{df_v(\epsilon^{j}_{vn})}{dn} \right) \frac{(\hbar/\tau_{in})}{(E-\epsilon)^2 + (\hbar/\tau_{in})^2} d\epsilon}. \tag{15}$$

Fig. 11 shows the α parameter as a function of $(E - E_g)$ (the photon energy minus the band-gap energy) for injected currents of $J = 36 A/\mathrm{cm}^{-2}$, and $J = 95\ A/\mathrm{cm}^{-2}$, respectively. We notice that α increases with the increase of the photon energy and also changes its sign from minus to plus. This is due to the change in the sign of the numerator of (15) from minus to plus, since the differential gain profile has a peaked structure as indicated in Fig. 4. Fig. 12 shows α at the maximum gain photon energy E_l as a function of the injected current for various N's. In this calculation the QW thickness and τ_{in} are assumed to be 100 Å, and 0.2 ps, respectively. Since α is a bulk parameter, the value of α is independent of the number of quantum wells N, so that the injected current to achieve a given value of α is proportional to N, and the currents for $N = 1, 3, 5$ differ only in their horizontal scale. We find that the absolute value of α ($|\alpha|$) decreases with the increases of the injected current. Therefore we can reduce the value of $|\alpha|$ by the use of high loss α_{loss} although this leads to high-threshold current.

Fig. 13 shows the α parameter as a function of the injected current with various QW thickness at E_l. The value of N is taken as unity. We notice a tendency that the smaller L_z is, the smaller α is.

C. Spectral Linewidth

Fig. 14 shows the laser spectral width $\Delta\nu$ calculated from (11) as a function of the number of QW's with various total loss ($\alpha_{\mathrm{total}} = 10, 30, 50\ \mathrm{cm}^{-1}$). We find that the

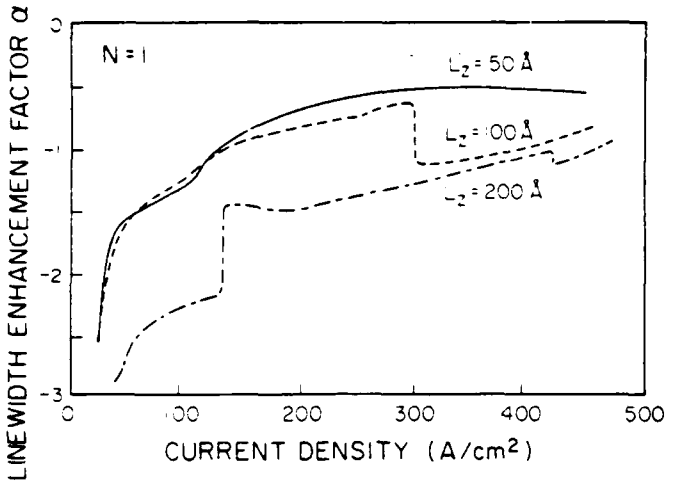

Fig. 13. The linewidth enhancement factor α as a function of the injected current with various quantum well thickness. The thickness of quantum wells is 100 Å.

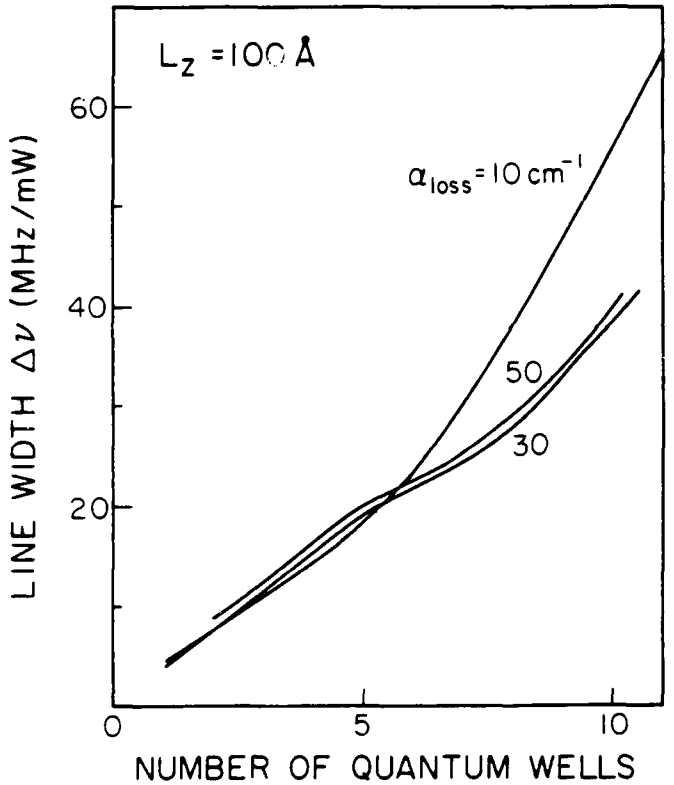

Fig. 14. The spectral linewidth Δν as a function of the number of quantum wells with various total loss α_{loss}.

Δν increases monotonically with the increase of the number of QW's. This is due to the fact that both ∝ and n_{sp} are reduced with the increase of $\Delta\epsilon_F$ which is enhanced with small number of N. Therefore, in order to reduce Δν, a SQW laser should be used rather than a MQW laser. The substantial change in Δν with the increase of N is due to the fact that the abrupt change in α occurs in the low injected-current region. Note that this change is enhanced with low α_{loss}.

The spectral width Δν is also a function of the thickness L_z. Fig. 15 shows the minimum attainable Δν as a function

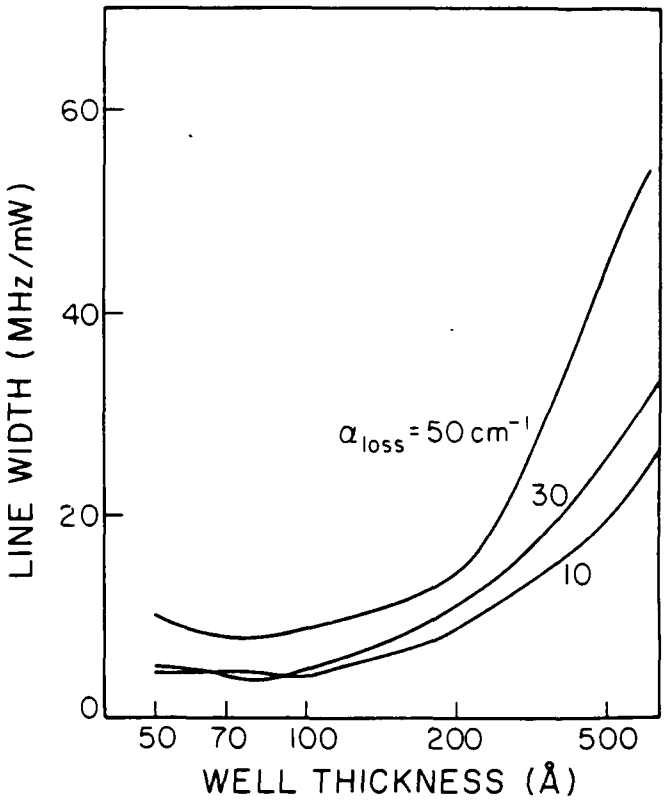

Fig. 15. The minimum spectral linewidth Δν as a function of the quantum well thickness with various total loss. The number of quantum wells is optimized.

of the QW thickness with various α_{loss}. Generally speaking, we notice that Δν is reduced greatly in the region of thin active layer. In the case of α_{loss} = 10 cm^{-1}, Δν is minimum arround L_z = 80 Å. This is due to the fact that there is the current region in which ∝ of L_z = 100 Å is smaller than that of L_z = 50 Å, as shown in Fig. 13. Since the value Δν for a DH laser (0.1 μm active layer) is calculated to be 60 MHz/mW with α_{loss} = 30 cm^{-1}, the Δν can be substantially reduced with a thin QW structure by factor of ~ 1/10 compared to DH lasers. For all L_z, the Δν increases monotonically when the number of QW's increases.

V. Conclusions

We investigate theoretically the effects of quantum well (QW) structure parameters such as the number and the thickness of QW's on the gain, the dynamic response and quantum noise of QW lasers. We have considered the issues of optimum conditions for realizing low-noise characteristics and high-dynamic performance. We have found that the gain in structures with a small number of layers tends to saturate with current. The differential gain and linewidth enhancement factor of QW lasers are also discussed. The results indicate that the modulation bandwidth can be enhanced by a factor of ~2 in the multiquantum well laser, and linewidth is found to be significantly suppressed by 1/10 in a single thin QW laser compared to the conventional double heterostructure laser.

References

[1] K. Y. Lau, N. Bar Chaim, I. Ury, Ch. Harder, and Y. Yariv, "Direct amplitude modulation of short-cavity GaAs lasers up to X-band frequency," *Appl. Phys. Lett.*, vol. 43, pp. 1-3, 1983.

[2] M. W. Fleming and A. Mooradian, "Fundamental line broadening of single mode (GaAl)As diode lasers," *Appl. Phys. Lett.*, vol. 38, pp. 511-513, 1981.

[3] C. Henry, "Theory of the linewidth of semiconductor lasers," *IEEE J. Quantum Electron.*, vol. QE-18, pp. 259-254, 1982.

[4] K. Vahala and A. Yariv, "Semiclassical theory of noise in semiconductor lasers—Part 1," *IEEE J. Quantum Electron.*, vol. QE-18, pp. 1096-1101, 1982.

[5] K. Vahala and A. Yariv, "Semiclassical theory of noise in semiconductor lasers—Part 2," *IEEE J. Quantum Electron.*, vol. QE-18, pp. 1102-1109, 1982.

[6] K. Vahala and A. Yariv, "Detuned loading in coupled cavity semiconductor lasers—Effects on quantum noise and dynamics," *Appl. Phys. Lett.*, vol. 45, pp. 501-503, 1984.

[7] N. Holonyak, Jr., R. M. Kolbas, R. D. Dupuis, and P. D. Dapkus, "Quantum-well heterostructure lasers," *IEEE J. Quantum Electron.*, vol. QE-16, p. 170, 1980.

[8] R. D. Dupuis, P. D. Dapkus, N. Holonyak, Jr., E. A. Rezek, and R. Chin, "Room-temperature laser operation of quantum-well $Ga_{1-x}Al_xAs$-GaAs laser diodes by metalorganic chemical vapor deposition," *Appl. Phys. Lett.*, vol. 32, pp. 295-297, 1978.

[9] W. T. Tsang, C. Weisbuch, R. C. Miller, and R. Dingle, "Current injection GaAs-$Al_xGa_{1-x}As$ multiquantum well heterostructure lasers prepared by molecular beam epitaxy," *Appl. Phys. Lett.*, vol. 35, pp. 673-675, 1979.

[10] W. T. Tsang, "A graded-index waveguide separate-confinement laser with very low threshold and a narrow Gaussian beam," *Appl. Phys. Lett.*, vol. 39, pp. 134-136, 1981.

[11] W. T. Tsang, "Extremely low threshold (AlGa)As modified multiquantum well heterostructure lasers grown by molecular beam epitaxy," *Appl. Phys. Lett.*, vol. 39, pp. 786-788, 1981.

[12] Y. Arakawa, K. Vahala, and A. Yariv, "Quantum noise and dynamics in quantum well and quantumwire lasers," *Appl. Phys. Lett.*, vol. 45, pp. 950-952, 1984.

[13] M. G. Burt, "Linewidth enhancement factor for quantum well lasers," *Electron. Lett.*, vol. 20, pp. 27-28, 1984.

[14] Kobayashi, H. Iwamura, T. Saku, K. Otsuka, and H. Okamoto, "Dynamic behavior of a GaAs-AlGaAs MQW laser diode," *Electron. Lett.*, vol. 19, pp. 166-167, 1983.

[15] A. Sugimura, "Threshold current for AlGaAs quantum well lasers," *IEEE J. Quantum Electron.*, vol. QE-20, no. 4, pp. 336-343, 1984.

[16] M. Asada, A. Kameyama, and Y. Suematsu, "Gain and intervalence band absorption in quantum-well lasers," *IEEE J. Quantum Electron.*, vol. QE-20, no. 7, pp. 745-753, 1984.

[17] K. Vahala, L. C. Chiu, S. Margalit, and A. Yariv, "On the linewidth enhancement factor α in semiconductor injection lasers," *Appl. Phys. Lett.*, vol. 42, pp. 631-633, 1983.

Yasuhiko Arakawa (S'77-M'80) was born in Aichi Prefecture, Japan, on November 26, 1952. He received the B.S., M.S., and Ph.D. degrees in electrical engineering from the University of Tokyo, in 1975, 1977, and 1980, respectively. In the graduate school, he conducted research on optical communication theory.

In 1980, he joined the Institute of Industrial Science, University of Tokyo, as an Assistant Professor and is now an Associate Professor. After 1980, he extended his speciality to optical device research. His current research includes dynamic and noise properties of quantum well lasers, basic investigation of quantum wire and quantum box lasers using high magnetic fields, and fabrication of new optical devices using quantum well structures. From 1984 to 1986, he will be a Visiting Scientist at the California Institute of Technology, Pasadena, doing research in collaboration with Professor A. Yariv.

Dr. Arakawa is a member of the Institute of Electronics and Communication Engineers of Japan and Japan Society of Applied Physics. In 1981, he was awarded the Excellent Paper Award for "the proposal of a new type transmission code for digital optical communication" from Institute of Electronics and Communication Enginners of Japan. For this work, he was also awarded Niwa Memorial Prize in 1980. In 1983, he was awarded the Young Scientist Award for "study on the light emission from one-dimensional electronic systems" from the Institute of Electronics and Communication Engineers of Japan.

Amnon Yariv, (S'56-M'59-F'70), for a photograph and biography, see p. 138 of the February 1985 issue of this JOURNAL.

Unclassified
SECURITY CLASSIFICATION OF THIS PAGE

REPORT DOCUMENTATION PAGE

Form Approved
OMB No. 0704-0188

1a. REPORT SECURITY CLASSIFICATION Unclassified	1b. RESTRICTIVE MARKINGS
2a. SECURITY CLASSIFICATION AUTHORITY	3. DISTRIBUTION/AVAILABILITY OF REPORT Approved for public release; distribution unlimited.
2b. DECLASSIFICATION/DOWNGRADING SCHEDULE	
4. PERFORMING ORGANIZATION REPORT NUMBER(S) N00014-K-0211	5. MONITORING ORGANIZATION REPORT NUMBER(S) 696-002
6a. NAME OF PERFORMING ORGANIZATION California Institute of Technology 6b. OFFICE SYMBOL (If applicable)	7a. NAME OF MONITORING ORGANIZATION Office of Naval Research
6c. ADDRESS (City, State, and ZIP Code) Pasadena, California 91125	7b. ADDRESS (City, State, and ZIP Code) 565 S. Wilson Pasadena, California 91106-3212
8a. NAME OF FUNDING/SPONSORING ORGANIZATION Office of Naval Research 8b OFFICE SYMBOL (If applicable)	9. PROCUREMENT INSTRUMENT IDENTIFICATION NUMBER P00001
8c. ADDRESS (City, State, and ZIP Code) 800 N. Quincy Street Arlington, VA 22217	10 SOURCE OF FUNDING NUMBERS PROGRAM ELEMENT NO. / PROJECT NO. / TASK NO / WORK UNIT ACCESSION NO.

11. TITLE (Include Security Classification)
Intermodal Stability of a Coupled-Cavity Semiconductor Laser

12. PERSONAL AUTHOR(S)
R. Lang and A. Yariv

13a. TYPE OF REPORT	13b. TIME COVERED	14. DATE OF REPORT (Year, Month, Day)	15. PAGE COUNT
Reprint	FROM _____ TO _____	1986 May	6

16. SUPPLEMENTARY NOTATION The view, opinions and/or findings contained in this report are those of the author(s) and should not be construed as an official Department of the Navy position, policy, or decision unless so designated by other documentation.

17. COSATI CODES			18. SUBJECT TERMS (Continue on reverse if necessary and identify by block number)
FIELD	GROUP	SUB-GROUP	Coupled-Cavity Semiconductor Laser

19. ABSTRACT (Continue on reverse if necessary and identify by block number)

We present an analysis of the steady-state operation of a two-element coupled cavity laser near a mode hop. The equations of motion for the two cavities and two relevant modes of a longitudinally coupled-cavity laser are reduced to a system of nondimensional nonlinear ordinary differential equations which describe a general two-element laser. The equations are then solved and the stability of their solutions is analyzed. Depending upon the fill factors for the two modes, there exists an intrinsically multimode oscillation for operating conditions under which it was previously thought that no steady state existed. Under conditions where the multimode state is unstable, both of the single-mode states are stable with bistable transitions occurring only on the boundaries of the unstable multimode regimes.

20 DISTRIBUTION/AVAILABILITY OF ABSTRACT ☐ UNCLASSIFIED/UNLIMITED ☐ SAME AS RPT ☐ DTIC USERS	21. ABSTRACT SECURITY CLASSIFICATION
22a NAME OF RESPONSIBLE INDIVIDUAL	22b TELEPHONE (Include Area Code) / 22c. OFFICE SYMBOL

DD Form 1473, JUN 86 Previous editions are obsolete. SECURITY CLASSIFICATION OF THIS PAGE

Intermodal Stability of a Coupled-Cavity Semiconductor Laser

ROBERT J. LANG, STUDENT MEMBER, AND AMMON YARIV, FELLOW, IEEE

Abstract—**We present an analysis of the steady-state operation of a two-element coupled-cavity laser near a mode hop. The equations of motion for the two cavities and two relevant modes of a longitudinally coupled-cavity laser are reduced to a system of nondimensional nonlinear ordinary differential equations which describe a general two-element laser. The equations are then solved and the stability of their solutions is analyzed. Depending upon the fill factors for the two modes, there exists an intrinsically multimode oscillation for operating conditions under which it was previously thought that no steady state existed. Under conditions where the multimode state is unstable, both of the single-mode states are stable with bistable transitions occurring only on the boundaries of the unstable multimode regimes.**

I. Introduction

COUPLED-CAVITY lasers have recently become the subject of much study because of their potential for single-mode operation under high-speed current operation [1], [2]. In addition, they, like many other two-element lasers [3], have been shown to exhibit bistable behavior. Such behavior makes them suitable for digital optical read/write operations or candidates for elements of an optical logic system [4]. Although there have been several analyses of longitudinally coupled-cavity lasers (e.g., a C^3 laser) at varying levels of approximation [5]–[8], none has treated the problems associated with operation near a mode boundary. Yet, when the current supplied to one of the two cavities is modulated, crossing a mode boundary is almost inevitable [8]. Recently, in a steady-state analysis, Henry and Kazarinov made the claim that there existed regimes of operation near a mode boundary where no steady-state solutions were stable (although they left open the question of what happened in such a regime). In this paper, we analyze the behavior of a two-element coupled-cavity laser near a mode boundary. Although we choose the specific geometry of a longitudinally coupled pair of cavities, the nondimensional equations of motion are equally applicable to any two-element laser (e.g., a laterally coupled cavity [9]). In Section II, we give a brief development of the equations of motion of the laser, using a slowly varying complex frequency approximation [10]. In Section III, we expand around a mode hop in the carrier density plane and develop a set of nondimensional equations which describe the dynamical behavior of the laser. We solve for the dc solutions of the equations and perform a stability analysis upon the solutions. We show that in all regimes of operation, there exists at least one stable solution, and sometimes two; we identify a sufficiency condition for bistable behavior, and we solve for the lines of instability on which a bistable transition occurs. In Section IV, we summarize the important results of the analysis.

Manuscript received July 29, 1985; revised November 7, 1985. This work was supported by Rockwell International and the Office of Naval Research. The work of R. J. Lang was supported by the National Science Foundation.

The authors are with the California Institute of Technology, Pasadena, CA 91125.

IEEE Log Number 8607703.

II. Equations of Motion

We begin by deriving the eigenvalue equation for the modes of a longitudinally coupled-cavity laser illustrated schematically in Fig. 1. It consists of two cavities of length L_1 and L_2, separated by a small gap D. Although in actual practice one would control the currents j_1 and j_2 supplied to each of the two sections, for the purposes of analysis, it is more convenient to treat the carrier densities n_1 and n_2 as free parameters, solve for the lasing frequency ω, and then find the currents necessary to support that operating point at a given power level. We choose our time factor as $e^{j\omega t}$. Then a roundtrip self-reproduction condition imposed upon the field in the laser yields the secular equation [5]

$$\left[\frac{\exp\left[-\gamma_1(n_1)\,L_1 + 2j\omega\mu_1(n_1)\,L_1/c\right]}{R_1} - 1\right] \cdot \left[\frac{\exp\left[-\gamma_2(n_2)\,L_2 + 2j\omega\mu_2(n_2)\,L_2/c\right]}{R_2} - 1\right] - K_s = 0 \tag{1}$$

where $\gamma_i(n_i)$ is the linear gain constant for the ith cavity, $\mu_i(n_i)$ is the index of refraction, R_i is the reflectivity of the outside mirrors, and K_s is a coupling factor which characterizes the gap (taking into account the length and reflectivity of the mirrors bounding the gap) [5]. Equation (1) can be considered [10] an implicit equation for complex ω as a function of n_1 and n_2. For any fixed pair (n_1, n_2), there exists an infinite number of complex ω solutions; each solution corresponds to a different spatial (longitudinal) mode of the structure. We are not interested in the phase of the optical field, so we can ignore the real part of ω, but the dynamics of the power depend upon the imaginary part. The time evolution of the average photon

0018-9197/86/0500-0631$01.00 © 1986 IEEE

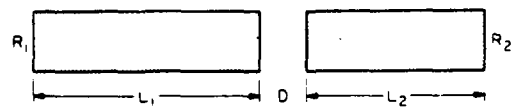

Fig. 1. Schematic of a longitudinally coupled-cavity laser.

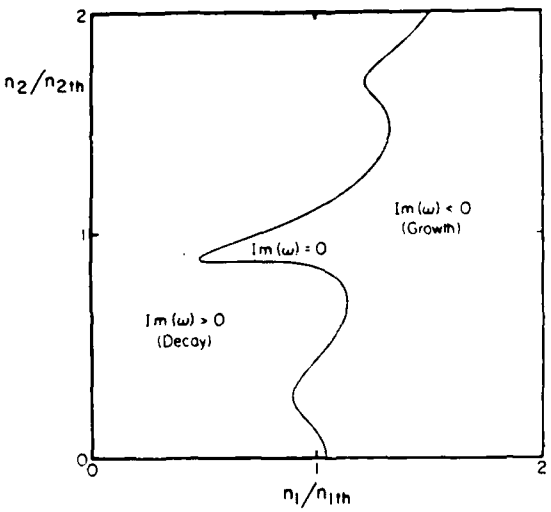

Fig. 2. Plot of the line Im (ω) = 0 for a single mode in the carrier density plane (normalized to threshold values for the uncoupled lasers) for a laser with L_1 = 200 μm, L_2 = 20 μm, D = 1.5 wavelengths.

density p_i in the ith mode obeys

$$\dot{p}_i = -2 \text{ Im } (\omega_i)\, p_i + \frac{1}{\tau_s} \sum_j \beta_{ij} n_j \tag{2}$$

where n_j is the carrier density in the jth cavity, τ_s is the spontaneous lifetime, and β_{ij} are coefficients representing the fraction of spontaneous emission coupled into the optical field. For a single mode, the line determined by the requirement Im (ω) = 0 (Fig. 2) corresponds to a quasi-steady-state mode which neither grows nor decays in time (that is, a true steady-state mode). For Im (ω) < 0, the quasi-steady-state mode grows without limit, and for Im (ω) > 0, it decays to zero. When spontaneous emission [which was not included in (1)] is considered, the carrier densities of the laser are clamped just to the left of the Im (ω) = 0 line (in the absence of spontaneous emission, they are clamped onto it).

As we said, there are an infinite number of solutions Im (ω) = 0 to (1), each corresponding to a different longitudinal mode; we plot a set of them in Fig. 3. Consider a point well to the left of any of the lines, e.g., point A in Fig. 3. Then Im (ω) > 0 for all the modes in the set; any excitation will decay away and no lasing state exists for that pair of carrier densities. On the other hand, a point on the curve's leftmost boundary (point B) is on the steady-state curve for one mode and in the Im (ω) > 0 region for the rest; consequently, the one mode will lase (and since Im (ω) = 0, neither grow nor decay) while all others decay away. An operating point at the intersection of two curves (point C) could conceivably have two lasing modes. However, a point to the right of any of the mode curves (point D) does not corresond to a physically

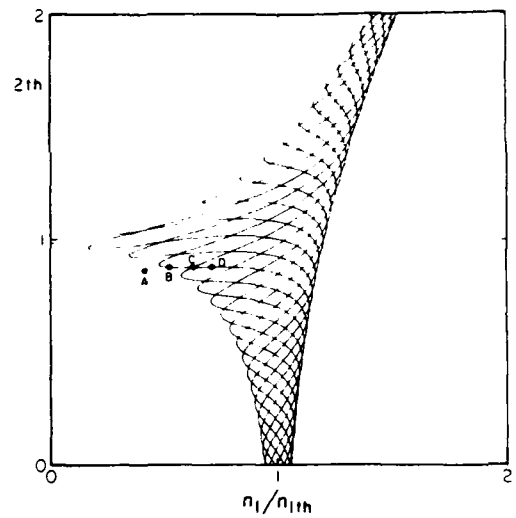

Fig. 3. Plot of ten modes in the carrier density plane.

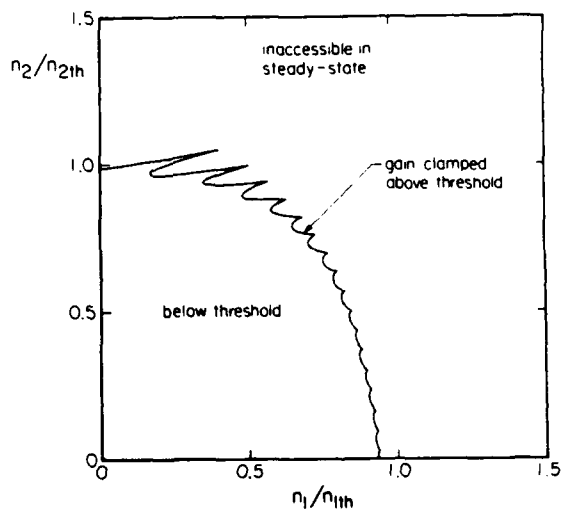

Fig. 4. Accessible regions of the carrier density plane. Above threshold, the carrier density is clamped onto the threshold carrier density line. Each cusp on the curve indicates a mode hop.

realizable steady state. It is in the Im (ω) < 0 regime for one or more modes, and those modes will thus grow exponentially without limit. This region is, of course, accessible on a transient basis—but if one drives the device into the Im (ω) < 0 region for a particular mode, the optical power in that mode will build up over time and saturate the gain back down to a point somewhere on the lowest curve. These arguments justify the division of the (n_1, n_2) plane into regions below and above threshold as in Fig. 4. Between any two cusps, the curve corresponds to the Im (ω) = 0 line of the lowest lying mode. The cusps correspond to mode hopping. Above lasing threshold, the carrier density is clamped onto the threshold line (although it is free to shift along the line).

In practice, one controls the currents supplied to the two sections, not the carrier densities. The question of multistability refers to the existence of multiple operating points (n_1, n_2) for the same pump current densities (j_1,

j_2). We must also consider the carrier density equations

$$\dot{n}_i = \frac{j_i}{qd} - \frac{n_i}{\tau_s} - g_i(n_i) \sum_j \Gamma_{ij} p_j \tag{3}$$

where q is the electronic charge, d is the thickness of the active layer, $g_i(n_i)$ is the gain constant, and Γ_{ij} are fill factors defined by

$$\Gamma_{ij} \equiv \{\text{the proportion of optical power of the } j\text{th mode in the } i\text{th cavity}\}.$$

In steady state, we can write this equation as

$$\frac{j_i}{qd} = \frac{n_i}{\tau_s} + g_i(n_i) \sum_j \Gamma_{ij} p_j. \tag{4}$$

Thus, for a given operating point (n_1, n_2) and a given set of photon densities p_j, the currents are exactly determined. As we have seen, for all operating points well away from a mode boundary, only a single mode lases, so we can set the photon density for that mode equal to the total power density and set all of the other photon densities to 0. For $p_{tot} = 0$, the allowable currents are precisely equal to the threshold carrier densities (with a scaling factor of qd/τ_s), and for $p_{tot} > 0$, we can use (4) to replot the carrier density curves at any desired power level.

A modification occurs when we are at a cusp, since two lasing modes are possible. Let the two modes have power levels

$$p_1 = xp_{tot}, \; p_2 = (1 - x)\, p_{tot} \tag{5}$$

so that x is the relative fraction of optical power in mode 1; then the current relations can be written as

$$\frac{j_i}{qd} = \frac{n_i}{\tau_s} + g_i(n_i)\, [x\Gamma_{i1} + (1 - x)\, \Gamma_{i2}]\, p_{tot}. \tag{6}$$

It is clear from (6) that as x is varied from 0 to 1, the current (and mode) changes linearly from that of purely mode 1 to that of purely mode 2. Hence, as we increase the power, the cusps which exist at threshold move out into the current plane and become straight line segments which join the single-mode curves. There are two qualitively different ways in which this situation manifests itself, both illustrated in Fig. 5 for a constant p_{tot} (they usually do not occur together; both are shown on the same graph for illustrative purposes only). The line segment labeled "modes 1 & 2" is one of a family which fills the region of the current plane claimed [5] to possess no stable solution. The segment labeled "modes 2 & 3" which completes the loop shows that multiple (in this case, three) steady-state solutions exist (the three solutions at three different power levels for the same (j_1, j_2) are shown explicitly in Fig. 6). A steady-state analysis cannot tell us anything about the stability of such states, however. In the next section, we will transform the equations of motion near the mode hop to a simple system of nonlinear ordinary differential equations which incorporate all of the relevant physics, yet allow simple analytic solutions and thus an unmistakeable interpretation of the physics of the device.

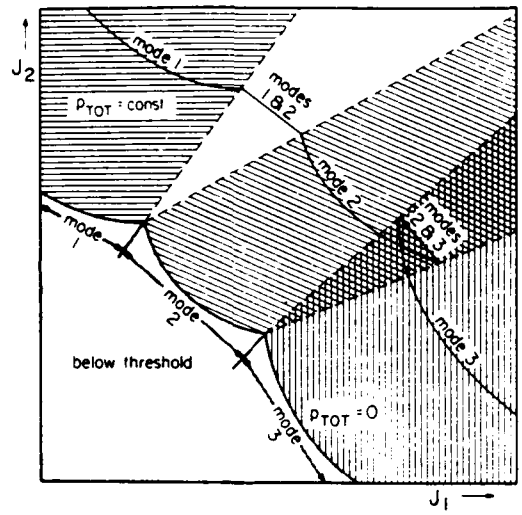

Fig. 5. Schematic of constant power curves in the current plane (arbitrary units). The $p_{tot} = 0$ curve is identical to the threshold gain curve in the (n_1, n_2) plane (within a scaling factor). The straight line segments joining the curves for fixed $p_{tot} \geq 0$ are the mixed state (two simultaneously oscillating modes).

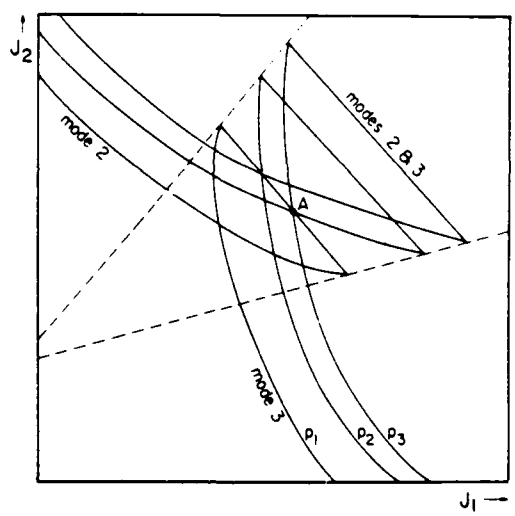

Fig. 6. Illustration of a single point in the current plane which possesses three steady-state solutions at different power levels (multimode at p_1, mode 2 at p_2, mode 3 at p_3).

III. Nondimensional Equations and Stability

The problem as posed is strongly nonlinear; in particular, the variation of Im (ω_j) with n_i must be analyzed numerically. However, we can put (2) and (3) in nondimensional form valid near a mode boundary which carries all physical information without recourse to numerical techniques. The results we derive will be applicable to any two-element laser and not exclusively to a longitudinally coupled-cavity laser.

We begin by putting (3) and (2) in matrix form:

$$\dot{\tilde{N}} = \frac{1}{qd}\tilde{J} - \frac{1}{\tau_s}\tilde{N} - \tilde{\tilde{G}}(\tilde{N})\,\tilde{\tilde{\Gamma}}\tilde{P} \tag{7}$$

$$\dot{\tilde{P}} = \tilde{\tilde{W}}\tilde{P} + \tilde{\tilde{B}}\tilde{N}. \tag{8}$$

The ith element of $\tilde{N}$ is $\{n_i\}$, the elements of $\tilde{J}$ are $\{j_i\}$, the elements of $\tilde{\tilde{\Gamma}}$ are $\{\Gamma_{ij}\}$, the elements of $\tilde{\tilde{W}}$ are $\{\delta_{ij}\,\mathrm{Im}\,(\omega_i)\}$, the elements of $\tilde{\tilde{B}}$ are $\{\beta_i\delta_{ij}/\tau_s\}$, and the elements of $\tilde{P}$ are $\{p_i\}$. We now transform to the coordinate system $\tilde{M}$ illustrated in Fig. 7. If we linearize the mode lines about the mode crossing, then there exists a transformation matrix $\tilde{\tilde{R}}$ such that

$$\tilde{M} = \tilde{\tilde{R}}(\tilde{N} - \tilde{N}^{(0)}) \tag{9}$$

where the elements of $\tilde{N}^{(0)}$ are $\{n_i^{(0)}\}$, the coordinates of the mode crossing. (Note that $\tilde{\tilde{R}}$ is only unique to within a constant scaling matrix $\left(\begin{smallmatrix} a & 0 \\ 0 & b \end{smallmatrix}\right)$ with $a, b > 0$; this ambiguity does not affect the analysis.) To lowest order, the system of matrix equations becomes

$$\dot{\tilde{M}} = \frac{1}{qd}\tilde{\tilde{R}}\left(\tilde{J} - \frac{qd}{\tau_s}\tilde{N}^{(0)}\right) - \frac{1}{\tau_s}\tilde{M} - \tilde{\tilde{R}}\tilde{\tilde{G}}(\tilde{N}^{(0)})\,\tilde{\tilde{\Gamma}}\tilde{P} \tag{10}$$

$$\dot{\tilde{P}} = \tilde{\tilde{K}}\tilde{\tilde{M}}\tilde{P} + \tilde{\tilde{B}}\tilde{N}^{(0)} \tag{11}$$

where the elements of $\tilde{\tilde{K}}$ are $\{-2(\partial\mathrm{Im}(\omega_i)/\partial m_j)\}$ and $\tilde{\tilde{M}}$ is the 2×2 matrix with the elements of $\tilde{M}$ on the diagonal. The virtue of choosing the axes $\{m_i\}$ is that (to the same order of approximation as the linearization) $\tilde{\tilde{K}}$ is diagonal. It is also important to note that with the axes so defined, det $\tilde{\tilde{R}} > 0$ (if the axes were reversed, the sign would change). Now, we define dimensionless variables by taking

$$t \equiv \tau_s\tau, \qquad \tau \text{ is the new time variable} \tag{12a}$$

$$\tilde{E} \equiv \tilde{\tilde{K}}\tilde{M} \tag{12b}$$

$$\tilde{I} \equiv \frac{\tau_s}{qd}\tilde{\tilde{K}}\tilde{\tilde{R}}\tilde{J} - \tilde{\tilde{K}}\tilde{\tilde{R}}\tilde{N}^{(0)} \tag{12c}$$

$$\tilde{\tilde{H}} \equiv \tilde{\tilde{K}}\tilde{\tilde{R}}\tilde{\tilde{G}}(\tilde{N}^{(0)})\,\tilde{\tilde{\Gamma}} \tag{12d}$$

$$\tilde{D} \equiv \tilde{\tilde{B}}\tilde{N}^{(0)} \tag{12e}$$

which reduces (10) and (11) to the simple system

$$\tilde{E} = \tilde{I} - \tilde{E} - \tilde{\tilde{H}}\tilde{P}$$

$$\tilde{P} = \tilde{\tilde{E}}\tilde{P} + \tilde{D}. \tag{13}$$

In component form,

$$\dot{e}_i = i_i - e_i - \sum_j h_{ij}p_j \tag{14}$$

$$\dot{p}_j = e_jp_j + d_j. \tag{15}$$

Equations (14) and (15) are several levels removed from the original system, so it is helpful to review the terms in each equation and identify them with a physical mechanism. $\{e_i\}$ are carrier densities, $\{i_i\}$ are pump currents, $\{p_i\}$ are the modal power densities, $\{h_{ij}\}$ are the fill factors (the proportion of mode j in carrier pool i), and $\{d_i\}$ are the spontaneous emission rates. Thus, the three terms on the right side of (14) correspond to pump current, spontaneous emission, and stimulated emission, respectively; the two terms on the right of (15) are stimulated emission and spontaneous emission, respectively. Examination of (12d) reveals that det H is of the same sign as det Γ (because the determinants of all of the intervening matrices is positive). This is indicative of the fact that in transforming from the $\{n_i\}$ representation to the $\{e_i\}$ representation, we "stretched" the axes, but did not flip them over. Also, we note that the spontaneous emission rate is typically quite small ($\beta_i \approx 10^{-4}$) so that $\{d_i\}$ are also of the same small order.

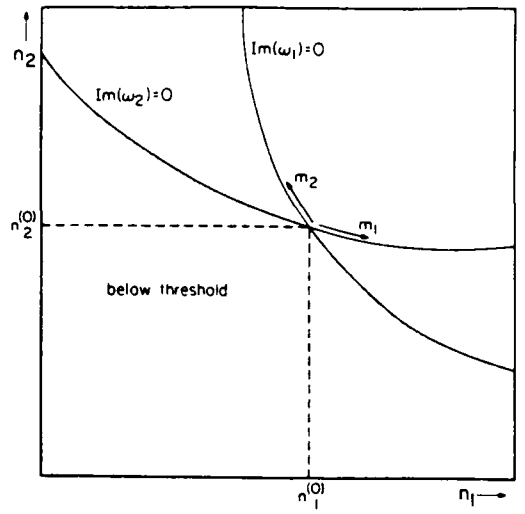

Fig. 7. Schematic of a single mode crossing in the carrier density plane (arbitrary units). The transformed variables $\{m_i\}$ are measured along the two intersecting mode lines.

The steady-state solutions of (14) and (15) are plotted in the current plane for a fixed p_{tot} in Fig. 8 (subject to the physical constraint $p_i \geq 0$). The solutions in the absence of spontaneous emission ($d_i = 0$) are apparent by inspection (one virtue of the dimensionless system of equations). They are

$$\{p_1 = 0,\ e_2 = 0,\ e_1 \text{ free}$$

or

$$\{p_2 = 0,\ e_1 = 0,\ e_2 \text{ free}$$

or

$$\{e_1 = e_2 = 0,\ p_2 = p_{tot} - p_1,\ p_1 \text{ free}. \tag{16}$$

If we include spontaneous emission and define x as the free parameter (restricted to $x \in [0, 1]$), the solutions are

$$\begin{cases} p_1 = xp_{tot},\ p_2 = (1 - x)\,p_{tot}, \\ e_1 = \dfrac{-d_1}{xp_{tot}},\ e_2 = \dfrac{-d_2}{(1 - x)\,p_{tot}}. \end{cases} \tag{17}$$

Equation (17) is more exact than (16); however, the shape of the curves is not as obvious from the equations.

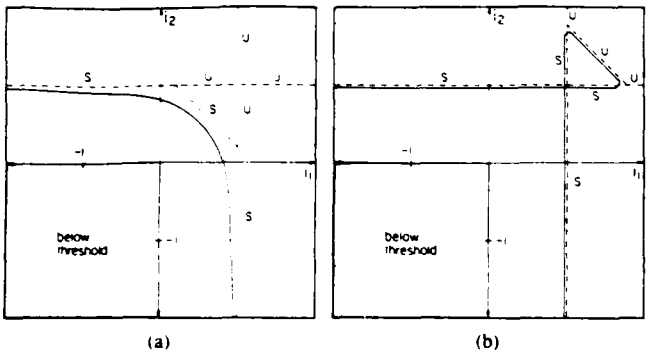

Fig. 8. Steady-state modes in the transformed current plane for fixed total output power $p_{tot} = 1$. Dotted lines are solutions in the absence of spontaneous emission ($d_i = 0$), solid lines are solutions including spontaneous emission ($d_1 = d_2 = 0.05$). (a) $h_{11} = h_{22} = 1$, $h_{12} = h_{21} = 0.2$, so det $H \geq 0$. (b) $h_{11} = h_{22} = 1$, $h_{12} = h_{21} = 1.8$, so det $H \leq 0$.

With or without spontaneous emission, we still must prove that these steady-state solutions are stable. We do this by performing a second linearization of (14) and (15) and determining the boundedness of the response of the homogeneous system to a perturbation.

$$e_i \to e_i + \epsilon_i,\ p_i \to p_i + \rho_i \tag{18}$$

giving

$$\dot{\epsilon}_i = -\epsilon_i - \sum_j h_{ij}\rho_j$$

$$\dot{\rho}_j = \epsilon_j p_j + e_j \rho_j. \tag{19}$$

These can be put into matrix form as

$$\begin{pmatrix} \dot{\epsilon}_1 \\ \dot{\epsilon}_2 \\ \dot{\rho}_1 \\ \dot{\rho}_2 \end{pmatrix} = \begin{pmatrix} -1 & 0 & -h_{11} & -h_{21} \\ 0 & -1 & -h_{12} & -h_{22} \\ p_1 & 0 & e_1 & 0 \\ 0 & p_2 & 0 & e_2 \end{pmatrix} \begin{pmatrix} \epsilon_1 \\ \epsilon_2 \\ \rho_1 \\ \rho_2 \end{pmatrix}. \tag{20}$$

The solution to (20) is bounded only if all of the eigenvalues of the square matrix have nonpositive real parts. The secular equation for the eigenvalue λ is

$$(\lambda + 1)^2 (\lambda - e_1)(\lambda - e_2) + (\lambda + 1)(\lambda - e_2) p_1 h_{11} + (\lambda + 1)(\lambda - e_1) p_2 h_{22} + p_{12} \det H = 0. \tag{21}$$

We shall first solve for the case with no spontaneous emission.

Case I—$e_2 = p_1 = 0$ (Only Mode 2 Lasing): Equation (21) reduces to

$$(\lambda + 1)(\lambda - e_1)[\lambda(\lambda + 1) + p_2 h_{22}] = 0. \tag{22}$$

The roots are $\lambda = -1$, $\lambda = e_1$, $\lambda = -(\frac{1}{2}) \pm [\frac{1}{4} - p_2 h_{22}]^{1/2}$, so the solution is stable if $e_1 \leq 0$.

Case II—$e_1 = p_2 = 0$ (Only Mode 1 Lasing): By switching subscripts we see that $e_2 \leq 0$ is necessary for stability.

Case III—$e_1 = e_2 = 0$ (Multimode State):

$$(\lambda + 1)^2 \lambda^2 + (p_1 h_{11} p_2 h_{22}) \lambda(\lambda + 1) + p_1 p_2 \det H = 0. \tag{23}$$

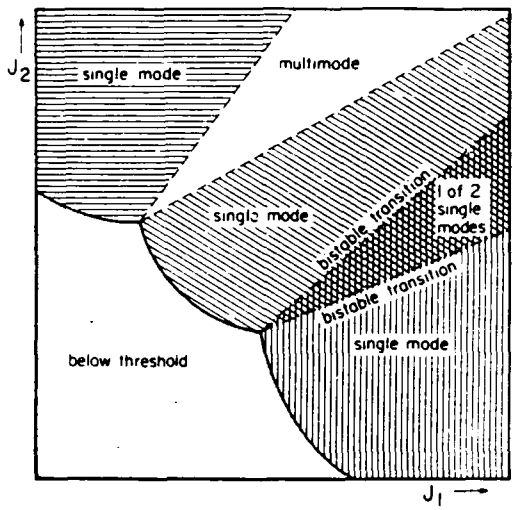

Fig. 9. Division of the current plane into regions of subthreshold lasing, multimode operation, single-mode operation, and bistable operation. Lines of instability on which bistable transitions take place are indicated.

Define $x \equiv \lambda(\lambda + 1)$. Then

$$\lambda = -\tfrac{1}{2} \pm [\tfrac{1}{4} + x]^{1/2} \tag{24}$$

so x must have a negative real part for stability. The equation for x is

$$x^2 + (p_1 h_{11} + p_2 h_{22}) x + p_1 p_2 \det H = 0. \tag{25}$$

From inspection, we can see that x has a negative real part only if det $H \geq 0$. In Fig. 8, we have plotted representative cases in the (i_1, i_2) plane for the two possible signs of det H. Case I yields the vertical dashed lines, Case II yields horizontals, and Case III yields the diagonal line; det $H \geq 0$ in Fig. 8(a) and det $H \leq 0$ in Fig. 8(b). Thus, the multimode state (Case III) is stable in Fig. 8(a), while it is unstable in Fig. 8(b). All of the steady-state solutions in Fig. 8 are labeled (S = stable, U = unstable) according to these rules. While one can work out the roots for the case including spontaneous emission numerically, there is no need; as the spontaneous emission goes to zero, the solution lines and the roots of (21) must collapse onto those of no spontaneous emission. Therefore, the labelings are valid for the curves which include spontaneous emission.

One important point is that the portions of the single-mode curves in Fig. 8(b) which overlap each other (and consequently yield multiple solutions) are stable; bistable transitions can only occur at their endpoints (where they become unstable). Furthermore, we have proven the stability of the mixed state of Fig. 8(a). It remains to relate this nondimensional problem to the physical problem with which we started. This is accomplished by noting that the point $(e_1, e_2) = (0, 0)$ is the crossing of the two mode lines in Fig. 5. Since (as we pointed out earlier) det H and det Γ have the same sign, the stability criterion for the mixed state is that det $\Gamma \geq 0$. The different states and their stability are summarized in Fig. 9. The current plane will, in general, divide into regions of single-mode operation; the boundaries will either consist of bimodal re-

gions (two simultaneous lasing modes) where det $\Gamma \geq 0$ or bistable regions (two possible single-mode states) where det $\Gamma \leq 0$. This is contrary to the assertions of [5]. One final point of interest: the stable mixed state [Fig. 8(a)] is a multimode state that persists in the absence of spontaneous emission. This is to be contrasted with the more usual multimode behavior where the intensity of side modes is proportional to the spontaneous emission rate. (It should be pointed out that with insufficient selectivity between modes, any laser—including coupled cavity—will run multimode due to the spontaneous emission.)

There are several features of this behavior which would be of interest from a systems viewpoint. Every point in the bimodal region corresponds to the same set of carrier densities $\{e_1 = e_2 = 0\}$. Therefore, the carrier density is fixed, and so the gain and resonant refractive index are effectively clamped (which is *not* the case in a single-mode region). Consequently, if one modulates the laser entirely within the multimode region, there is no direct frequency modulation of either of the two modes. With the addition of a notch filter to remove one of the two modes from the optical output, the device becomes a chirpless modulator. Also the response time of a laser diode is dependent upon the total optical power present. By modulating the diode in the bimodal region, the optical power is merely switched from one mode to another (as in a push-pull amplifier); consequently, even though the amplitude of the desired mode may approach zero, the *total* power present remains constant and the response time of the device remains short.

On the other hand, if the cavity were tuned such that det $\Gamma \leq 0$ at the mode hop, the device possesses electrical bistability and the inherent noise immunity associated with bistability. Examination of (4) shows that an external beam of light impinging upon one of the cavities shifts the entire set of tuning curves up and down (or side to side) in the current plane. Hence, all-optical bistability is equally feasible.

IV. Conclusions

In summary, we have analyzed the steady-state operation of a two-element coupled-cavity semiconductor laser near a mode boundary. We showed how the equations of motion for a specific system of a longitudinally coupled-cavity laser can be reduced to a nondimensional set of nonlinear differential equations which describe the behavior of a general two-element coupled-cavity laser near a mode boundary. We showed that a multimode state which was previously unexplained exists whenever the determinant of the matrix of fill-factor coefficients is nonzero. The multimode state varies continuously between the two involved single modes regardless of the level of spontaneous emission.

If the determinant is greater than zero, the multimode state is stable. Otherwise, it is unstable, but there are two stable single-mode states. Bistable transitions occur on the boundaries of the unstable multimode state. Large bistabilities are desirable from the point of optical storage and hysteretic devices; consequently, the relation between the bistable region and the size of the determinant of the fill-factor matrix is a useful design criterion for such devices.

References

[1] W. T. Tsang and N. A. Olsson, "High speed direct single-frequency modulation with large tuning rate and frequency excursion in cleaved-coupled-cavity semiconductor lasers," *Appl. Phys. Lett.*, vol. 42, pp. 650-652, 1983.

[2] K. J. Ebeling, L. A. Coldren, B. I. Miller, and J. A. Rentschler, "Single-mode operation of coupled-cavity GaInAsP/InP semiconductor lasers," *Appl. Phys. Lett.*, vol. 42, pp. 6-8, 1983.

[3] I. H. White, J. E. Carroll, and R. G. Plumb, "Closely coupled twin-stripe lasers," *Proc. IEE*, vol. 129, pp. 291-293, 1982.

[4] Ch. Harder, K. Y. Lau, and A. Yariv, "Bistability and negative resistance in semiconductor lasers," *Appl. Phys. Lett.*, vol. 40, pp. 124-126, 1982.

[5] C. H. Henry and R. F. Kazarinov, "Stabilization of single frequency operation of coupled cavity lasers," *IEEE J. Quantum Electron.*, vol. QE-20, pp. 733-744, 1984.

[6] D. Marcuse and T.-P. Lee, "Rate equation model of a coupled-cavity laser," *IEEE J. Quantum Electron.*, vol. QE-20, pp. 166-176, 1984.

[7] K. J. Ebeling and L. A. Coldren, "Analysis of multielement semiconductor lasers," *J. Appl. Phys.*, vol. 54, pp. 2962-2969, 1983.

[8] W. Streifer, D. Yevick, T. L. Paoli, and R. D. Burnham, "An analysis of cleaved coupled-cavity lasers," *IEEE J. Quantum Electron.*, vol. QE-20, pp. 754-764, 1984.

[9] J. Salzman, R. J. Lang, and A. Yariv, "Laterally coupled cavity semiconductor laser," *Appl. Phys. Lett.*, vol. 47, pp. 195-197, 1985.

[10] R. J. Lang and A. Yariv, "Analysis of the dynamic response of multielement semiconductor lasers," *IEEE J. Quantum Electron.*, vol. QE-21, pp. 1683-1688, 1985.

Robert J. Lang (S'83), for a photograph and biography, see p. 448 of the March 1986 issue of this Journal.

Amnon Yariv (S'56-M'59-F'70), for a photograph and biography, see p. 448 of the March 1986 issue of this Journal.

Unclassified
SECURITY CLASSIFICATION OF THIS PAGE

REPORT DOCUMENTATION PAGE

Form Approved
OMB No. 0704-0188

1a. REPORT SECURITY CLASSIFICATION Unclassified	1b. RESTRICTIVE MARKINGS
2a. SECURITY CLASSIFICATION AUTHORITY	3. DISTRIBUTION/AVAILABILITY OF REPORT Approved for public release; distribution unlimited.
2b. DECLASSIFICATION/DOWNGRADING SCHEDULE	
4. PERFORMING ORGANIZATION REPORT NUMBER(S) N00014-K-0211	5. MONITORING ORGANIZATION REPORT NUMBER(S) 696-002
6a. NAME OF PERFORMING ORGANIZATION California Institute of Technology 6b. OFFICE SYMBOL (If applicable)	7a. NAME OF MONITORING ORGANIZATION Office of Naval Research
6c. ADDRESS (City, State, and ZIP Code) Pasadena, California 91125	7b. ADDRESS (City, State, and ZIP Code) 565 S. Wilson Pasadena, California 91106-3212
8a. NAME OF FUNDING/SPONSORING ORGANIZATION Office of Naval Research 8b. OFFICE SYMBOL (If applicable)	9. PROCUREMENT INSTRUMENT IDENTIFICATION NUMBER P00001
8c. ADDRESS (City, State, and ZIP Code) 800 N. Quincy Street Arlington, VA 22217	10. SOURCE OF FUNDING NUMBERS PROGRAM ELEMENT NO. / PROJECT NO. / TASK NO / WORK UNIT ACCESSION NO.

11. TITLE (Include Security Classification)
Active Q switching in a GaAs/AlGaAs multiquantum well laser with an intracavity monolithic loss modulator

12. PERSONAL AUTHOR(S)
Y. Arakawa, A. Larsson, J. Paslaski and A. Yariv

13a. TYPE OF REPORT	13b. TIME COVERED	14. DATE OF REPORT (Year, Month, Day)	15. PAGE COUNT
Reprint	FROM _____ TO _____	1986 March	3

16. SUPPLEMENTARY NOTATION The view, opinions and/or findings contained in this report are those of the author(s) and should not be construed as an official Department of the Navy position, policy, or decision unless so designated by other documentation.

17. COSATI CODES			18. SUBJECT TERMS (Continue on reverse if necessary and identify by block number)
FIELD	GROUP	SUB-GROUP	quantum well lasers

19. ABSTRACT (Continue on reverse if necessary and identify by block number)

Active Q switching in a GaAs/AlGaAs multiquantum well laser with an intracavity electroabsorption monolithic loss modulator is demonstrated. In this device, an efficient loss modulation is achieved through the quantum confined Stark effect in a modulator section and the enhanced carrier induced band shrinkage effect in an optical amplifier section. It is found that a picosecond pulse as narrow as 18.6 ps full width at half-maximum is generated and a high repetition rate of more than 3 GHz is obtained.

20. DISTRIBUTION/AVAILABILITY OF ABSTRACT ☐ UNCLASSIFIED/UNLIMITED ☐ SAME AS RPT ☐ DTIC USERS	21. ABSTRACT SECURITY CLASSIFICATION
22a. NAME OF RESPONSIBLE INDIVIDUAL	22b. TELEPHONE (Include Area Code) / 22c. OFFICE SYMBOL

DD Form 1473, JUN 86 Previous editions are obsolete. SECURITY CLASSIFICATION OF THIS PAGE

Active Q switching in a GaAs/AlGaAs multiquantum well laser with an intracavity monolithic loss modulator

386

Y. Arakawa,[a] A. Larsson,[b] J. Paslaski, and A. Yariv
California Institute of Technology, Pasadena, California 91125

(Received 16 December 1985; accepted for publication 6 January 1986)

Active Q switching in a GaAs/AlGaAs multiquantum well laser with an intracavity electroabsorption monolithic loss modulator is demonstrated. In this device, an efficient loss modulation is achieved through the quantum confined Stark effect in a modulator section and the enhanced carrier induced band shrinkage effect in an optical amplifier section. It is found that a picosecond pulse as narrow as 18.6 ps full width at half-maximum is generated and a high repetition rate of more than 3 GHz is obtained.

Picosecond pulse generation technology in semiconductor laser diodes is important for high-speed optical communication systems. For this purpose, Q-switching systems are of great interest,[1-5] because no external mirror is needed in contrast to mode-locked systems,[6,7] and lower modulation power is required compared to gain switching systems.[8,9] Recently, active Q switching at 10 GHz rate was demonstrated by Tsang *et al.* in InGaAsP/InP lasers with an intracavity electroabsorption loss modulator.[3-5] In their device the Franz–Keldysh effect is used for loss modulation in the cavity.

In this letter we report on the demonstration of efficient active Q switching in a GaAs/AlGaAs multiquantum well (MQW) laser with a monolithic intracavity electroabsorption loss modulator. The physical phenomena utilized are the quantum confined Start effect[10,11] in the modulator section and the enhanced carrier induced band shrinkage effect[12] in the optical amplifier section. Optical pulses as narrow as 18.6 ps full width at half-maximum (FWHM), assuming a Gaussian waveform, are generated and a high modulation bandwidth of more than 3 GHz is obtained.

Figure 1(a) illustrates the two-segment MQW laser consisting of an optical amplifier section and an electroabsorption loss modulator section. The device structure was grown by molecular beam epitaxy in a Riber 2300 R&D system. The following layers were sequentially grown on a (100) oriented n^+-GaAs substrate doped to 2×10^{18} cm^{-3}: a 0.5 μm n^+-GaAs buffer layer (4×10^{18} cm^{-3}), a 1.5 μm n-$Al_{0.4}Ga_{0.6}As$ cladding layer (5×10^{17} cm^{-3}), a 0.06 μm n-$Al_{0.2}Ga_{0.8}As$ waveguide layer (5×10^{17} cm^{-3}), an undoped active region consisting of four 100 Å GaAs wells separated by 60 Å $Al_{0.2}Ga_{0.8}As$ barriers, a 0.06 μm p-$Al_{0.2}Ga_{0.8}As$ waveguide layer (5×10^{17} cm^{-3}), a 1.5 μm p-$Al_{0.4}Ga_{0.6}As$ cladding layer (5×10^{17} cm^{-3}), and a 0.2 μm p^+-GaAs contact layer (1×10^{19} cm^{-3}). The associated energy-band diagram is shown in Fig. 1(b). After this growth, a ridge waveguide structure with a 5 μm width and a 1.2 μm height was formed by wet chemical etching. SiO_2 was used to confine the current injection to the ridge. A 5-μm-wide separation was selectively etched in the p^+-GaAs between the two segments for electrical isolation and separate Cr/Au contacts were defined by liftoff. The lengths of the amplifier section l_1 and of the modulator section l_2 were 250 and 50 μm, respectively. The measured resistance between the segments was 5 kΩ. Since no critical process technology such as a precise control of a Zn diffusion is used in the fabrication process, the device is expected to be reproducible.

The modulator section makes use of the quantum confined Stark effect. This effect has recently been investigated for optical bistable switches,[13] wavelength selective optical detectors,[14,15] and optical modulators.[16,17] The room-temperature absorption spectrum of MQW displays enhanced absorption at the band edge, with a double-peaked structure, caused by excitons whose binding energy is enhanced by the two-dimensional confinement. When an electric field is applied to the quantum wells perpendicular to the layers, the exciton absorption peak shifts to lower energy. This effect is much larger than the Franz–Keldysh effect seen in bulk materials. The dominant mechanism is the decrease in confinement energies, resulting in a red shift of the excitonic absorption energy. The band discontinuities prevent the ionization of the exciton, allowing excitonic resonances to be observed at room temperature with large applied fields ($>10^5$ V/cm). In addition, the carrier induced band shrinkage effect is enhanced in MQW lasers compared to conventional double heterostructure lasers, resulting in a decrease of the lasing photon energy by about 20 meV (Ref. 12) compared to the intrinsic absorption edge. Consequently, the band-gap shrinkage which occurs in the amplifier section and the enhanced electroabsorption in the modulator section results in extremely large loss changes which are induced by the application of an electric field to the modulation section.

Figure 2 shows the measured threshold current I_{th} which is injected in the optical amplifier section under pulsed conditions (2 μs, 50 kHz), plotted as a function of the dc modulator bias V_b. In this figure, $I_{th}(V_b)$ is normalized by $I_{th}(V_b=0)$ which is 115 mA. As a result of the pn junction, a built-in electric field exists in the active region even with $V_b=0$. Therefore, a nearly flatband condition is obtained with a forward bias voltage. As shown in the figure, $I_{th}(V_b=-2\text{ V})$ is larger by a factor of 2.5 compared to $I_{th}(V_b=1\text{ V})$. This increase of threshold current is larger than that of a device with conventional double heterostruc-

[a] Present address: University of Tokyo, Roppongi, Minato-ku, Tokyo 106, Japan.

[b] Present address: Chalmers University of Technology, S-41296 Goteborg, Sweden.

 0003-6951/86/090561-03$01.00 © 1986 American Institute of Physics

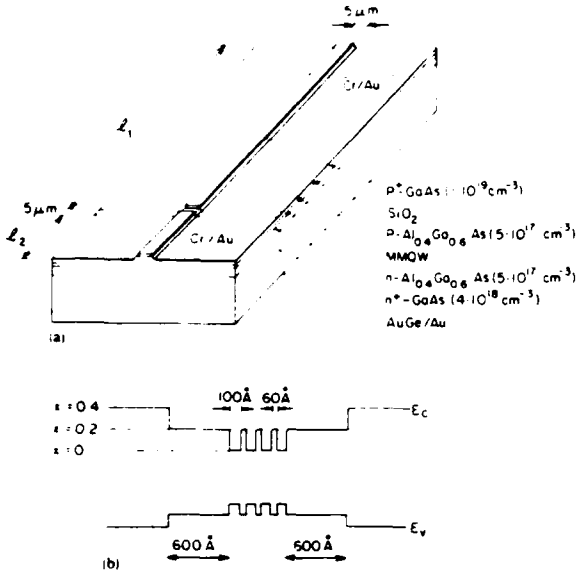

FIG. 1. (a) Perspective view of the two-segment quantum well laser. The lengths of the amplifier section l_1 and the modulator section l_2 were 250 and 50 μm, respectively. (b) Associated band-gap diagram of the active layer.

tures,[4] which suggests that an efficient electroabsorption loss modulation is realized in the MQW modulator section. A preliminary estimation shows that the internal loss is 3000 cm^{-1} at $V_b = 1$ V, whereas the loss is 12 000 cm^{-1} at $V_b = -1$ V. A more detailed discussion of the electroabsorption loss change will be given elsewhere. An optical self-pulsation is observed in the bias region between 0.2 and 0.7 V. This is the result of an optoelectronically generated negative resistance.[18] However, under the Q-switching operation with microwave modulation, such pulsation does not occur and the output pulse is synchronized with the modulation frequency.

Q switching was obtained by applying both a dc bias voltage and a microwave signal to the modulator. The device was modulated at rates between 100 MHz and 3.2 GHz. The optical pulse from the laser was collected by a collimating lens and divided into two beams. One beam is fed to an autocorrelator system which uses the second harmonic generation in a $LiIO_3$ crystal and a photomultiplier (RCA 4830). The other beam is focused on a GaAs *pin* photodiode (Ortel Corporation) with less than 50 ps FWHM response time. The detector output was connected to a spectrum analyzer (HP-3450A and HP34569A plug-in) for observation of the repetition rate and higher order spectrum.

Figure 3 shows an intensity autocorrelation trace obtained from the second harmonic generation under the condition of 1.5 GHz modulation frequency and $V_b = 0$. The injected current into the optical amplifier section, I_{in}, is 170 mA [$= 1.5I_{th}(V_b = 0)$]. Note that this is the first measurement of the picosecond pulse width from an actively Q-switched laser diode. The autocorrelation FWHM is 26.3 ps, which corresponds to a pulse FWHM $\Delta\tau_{1/2}$ of 18.6 ps if a Gaussian waveform is assumed. For semiconductor lasers without external mirrors, $\Delta\tau_{1/2} = 15$ ps has been reported so far[8] in a gain switched laser with a very short cavity (100 μm). Our result is comparable to this result with less modulation power, higher repetition rate, and an ordinary device length (300 μm). A narrower pulse generation can be expected by optimizing structure parameters.

The efficient Q switching in the two-segment MQW laser results from the following mechanisms. In Q-switching operation, a large loss change and a high differential gain (the derivative of the gain with respect to carrier concentration) will lead to a narrow pulse width. In our device, a large loss change is realized with the quantum confined Stark effect in the modulator section and the band shrinkage effect in the optical amplifier section. On the other hand, a high differential gain is also expected in the quasi-two-dimensional

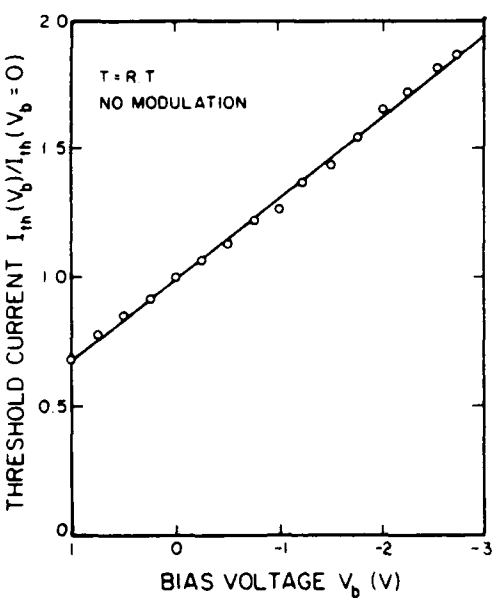

FIG. 2. Threshold current I_{th} as a function of the bias voltage V_b. I_{th} is normalized by $I_{th}(V_b = 0)$.

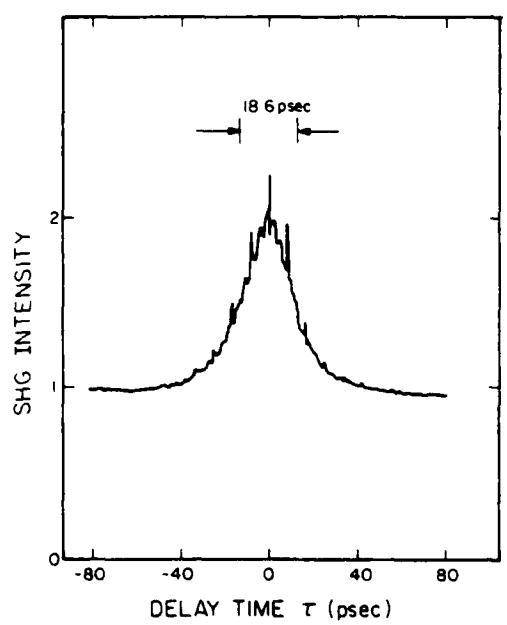

FIG. 3. Intensity autocorrelation trace obtained from second harmonic generation with 1.5 GHz modulation frequency and $I_{in} = 170$ mA ($= 1.5I_{th}$). The autocorrelation FWHM is 26.3 ps which corresponds to a pulse FWHM $\Delta\tau_{1/2}$ of 18.6 ps if a Gaussian waveform is assumed.

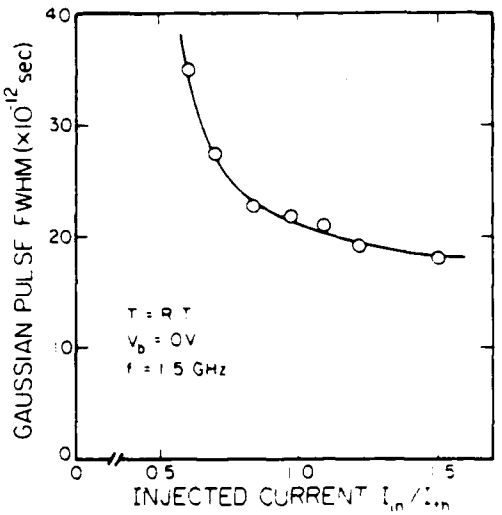

FIG. 4. Estimated pulse width, assuming a Gaussian waveform, as a function of the injected current I_{in} with 1.5 GHz modulation frequency. The I_{in} is normalized to the threshold current I_{th} with no modulation power.

electronic system in a MQW structure.[19] Thus, by the use of a MQW structure, the two-segment laser satisfies both requirements for the generation of narrow optical pulses.

The pulse width $\Delta\tau_{1/2}$ depends on the current I_{in} which is injected into the amplifier section. Figure 4 shows the dependence of $\Delta\tau_{1/2}$ on I_{in} under the conditions of 1.5 GHz modulation frequency and 0 V dc bias. This result shows that $\Delta\tau_{1/2}$ decreases with the increase of the injected current, converging to a certain value under our measurement conditions. In the region of lower I_{in}, $\Delta\tau_{1/2}$ increases drastically with the decrease of I_{in}.

The modulation frequency response (i.e., repetition rate) of the laser was measured in a preliminary fashion. We observed the fundamental spectrum as well as harmonic spectrum lines in the spectrum analyzer display. At present stage, the maximum repetition rate which still leads to regular pulse generation is 3.2 GHz. No attempt at optimization was made so that the expectation of a considerably higher pulse rate is reasonable. The pulse width $\Delta\tau_{1/2}$ was found to be nearly independent of the modulation frequency, changing from 19 to 22 ps when the modulation frequency was changed from 500 MHz to 3.2 GHz (I_{in} = 150 mA).

In conclusion, efficient active Q switching is demonstrated in a GaAs/AlGaAs MQW laser with an intracavity monolithic electroabsorption loss modulator. The efficient loss modulation achieved through the quantum confined Stark effect and the carrier induced band shrinkage effect, as well as a high differential gain, lead to the generation of narrow optical pulses. The results indicate that a picosecond pulse as narrow as 18.6 ps FWHM is generated and a high repetition rate of more than 3 GHz is obtained. Optimization of the structure for generating narrower pulses is now under study.

The authors wish to express their thanks to Dr. N. Bar Chaim at Ortel Corporation for his cooperation. This work was supported by the Air Force Office of Scientific Research, the Office of Naval Research, I.T.T. Corporation, the Japan Society for the Promotion of Science, and the National Aeronautics and Space Administration (NAS7-918).

[1] T. Tsukada and C. L. Tang, IEEE J. Quantum Electron. QE-13, 37 (1977).
[2] M. Yamanishi, K. Ishii, M. Ameda, and T. Kawamura, Jpn. J. Appl. Phys. Suppl. 17, 359 (1978).
[3] D. Z. Tsang, J. N. Walpole, S. H. Groves, J. J. Hsieh, and J. P. Donnelly, Appl. Phys. Lett. 38, 120 (1981).
[4] D. Z. Tsang and J. N. Walpole, IEEE J. Quantum Electron. QE-19, 145 (1983).
[5] D. Z. Tsang, J. N. Walpole, Z. L. Liau, S. H. Groves, and V. Diadiuk, Appl. Phys. Lett. 45, 204 (1984).
[6] P. T. Ho, L. A. Glasser, E. P. Ippen, and H. A. Haus, Appl. Phys. Lett. 33, 241 (1978).
[7] J. P. van der Ziel, R. A. Logan, and R. M. Mikulyak, Appl. Phys. Lett. 39, 867 (1981).
[8] H. Ito, H. Yokoyama, S. Murata, and H. Inaba, Electron. Lett. 15, 738 (1979).
[9] G. J. Aspin, J. E. Carrol, and R. G. Plumb, Appl. Phys. Lett. 39, 860 (1981).
[10] D. A. B. Miller, D. S. Chemla, T. C. Damen, A. C. Gossard, W. Wiegmann, T. H. Wood, and C. A. Burrus, Phys. Rev. Lett. 53, 2173 (1984).
[11] J. S. Weiner, D. A. B. Miller, D. S. Chemla, T. C. Damen, C. A. Burrus, T. H. Wood, A. C. Gossard, and W. Wiegmann, Appl. Phys. Lett. 47, 1148 (1985).
[12] S. Tarucha, H. Kobayashi, Y. Horikoshi, and H. Okamoto, Jpn. J. Appl. Phys. 23, 874 (1984).
[13] D. A. B. Miller, D. S. Chemla, T. C. Damen, A. C. Gossard, W. Wiegmann, T. H. Wood, and C. A. Burrus, Appl. Phys. Lett. 45, 13 (1984).
[14] T. H. Wood, C. A. Burrus, A. H. Gnauck, J. M. Wiesenfeld, D. A. B. Miller, D. S. Chemla, and T. C. Damen, Appl. Phys. Lett. 47, 190 (1985).
[15] A. Larsson, A. Yariv, R. Tell, J. Maserjian, and S. T. Eng, Appl. Phys. Lett. 47, 866 (1985).
[16] T. H. Wood, C. A. Burrus, D. A. B. Miller, D. S. Chemla, T. C. Damen, A. C. Gossard, and W. Wiegmann, Appl. Phys. Lett. 44, 16 (1984).
[17] T. H. Wood, C. A. Burrus, R. S. Tucker, J. S. Weiner, D. A. B. Miller, D. S. Chemla, T. C. Damen, A. C. Gossard, and W. Wiegmann, Electron. Lett. 21, 693 (1985).
[18] C. Harder, K. Y. Lau, and A. Yariv, IEEE J. Quantum Electron. QE-18, 1351 (1982).
[19] Y. Arakawa and A. Yariv, IEEE J. Quantum Electron. QE-21, 1666 (1985).

Unclassified
SECURITY CLASSIFICATION OF THIS PAGE

REPORT DOCUMENTATION PAGE

Form Approved
OMB No. 0704-0188

1a. REPORT SECURITY CLASSIFICATION Unclassified	1b. RESTRICTIVE MARKINGS
2a. SECURITY CLASSIFICATION AUTHORITY	3. DISTRIBUTION/AVAILABILITY OF REPORT Approved for public release; distribution unlimited.
2b. DECLASSIFICATION/DOWNGRADING SCHEDULE	
4. PERFORMING ORGANIZATION REPORT NUMBER(S) N00014-K-0211	5. MONITORING ORGANIZATION REPORT NUMBER(S) 696-002
6a. NAME OF PERFORMING ORGANIZATION California Institute of Technology 6b. OFFICE SYMBOL (If applicable)	7a. NAME OF MONITORING ORGANIZATION Office of Naval Research
6c. ADDRESS (City, State, and ZIP Code) Pasadena, California 91125	7b. ADDRESS (City, State, and ZIP Code) 565 S. Wilson Pasadena, California 91106-3212
8a. NAME OF FUNDING/SPONSORING ORGANIZATION Office of Naval Research 8b. OFFICE SYMBOL (If applicable)	9. PROCUREMENT INSTRUMENT IDENTIFICATION NUMBER P00001
8c. ADDRESS (City, State, and ZIP Code) 800 N. Quincy Street Arlington, VA 22217	10. SOURCE OF FUNDING NUMBERS PROGRAM ELEMENT NO. / PROJECT NO. / TASK NO / WORK UNIT ACCESSION NO.

11. TITLE (Include Security Classification)
High quality molecular beam epitaxial growth on patterned GaAs substrates

12. PERSONAL AUTHOR(S)
J. S. Smith, P. L. Derry, S. Margalit and A. Yariv

13a. TYPE OF REPORT	13b. TIME COVERED	14. DATE OF REPORT (Year, Month, Day)	15. PAGE COUNT
Reprint	FROM _____ TO _____	85 October	4

16. SUPPLEMENTARY NOTATION The view, opinions and/or findings contained in this report are those of the author(s) and should not be construed as an official Department of the Navy position, policy, or decision unless so designated by other documentation.

17. COSATI CODES			18. SUBJECT TERMS (Continue on reverse if necessary and identify by block number)
FIELD	GROUP	SUB-GROUP	
			laser arrays

19. ABSTRACT (Continue on reverse if necessary and identify by block number)

In this letter we describe a procedure for high quality molecular beam epitaxy (MBE) growth over finely patterned GaAs substrates which is suitable for device fabrication requiring lateral definition of small (∿1-2μm) dimension. This method was used for the fabrication of index guided laser arrays. Yields of individual lasers exceeded 90%, and the thresholds were uniform to 10%. Temperature and flux ratio dependence of faceting during MBE growth over patterned substrates is shown for temperatures ranging from 580 to 700°C and for As/Ga flux ratios from 1.4:1 to 4:1. The real index guided structure, which can be formed by a single MBE growth over a ridged substrate, is discussed. This technique should prove useful in the fabrication of devices which take advantage of unique features formed during regrowth by MBE.

20. DISTRIBUTION/AVAILABILITY OF ABSTRACT ☐ UNCLASSIFIED/UNLIMITED ☐ SAME AS RPT ☐ DTIC USERS	21. ABSTRACT SECURITY CLASSIFICATION
22a. NAME OF RESPONSIBLE INDIVIDUAL	22b. TELEPHONE (Include Area Code) / 22c. OFFICE SYMBOL

DD Form 1473, JUN 86 Previous editions are obsolete. SECURITY CLASSIFICATION OF THIS PAGE

High quality molecular beam epitaxial growth on patterned GaAs substrates

John Stephen Smith, Pamela L. Derry, Shlomo Margalit, and Amnon Yariv
California Institute of Technology, Pasadena, California 91125

(Received 12 March 1985; accepted for publication 3 July 1985)

In this letter we describe a procedure for high quality molecular beam epitaxy (MBE) growth over finely patterned GaAs substrates which is suitable for device fabrication requiring lateral definition of small (~ 1–$2\ \mu$m) dimension. This method was used for the fabrication of index guided laser arrays. Yields of individual lasers exceeded 90%, and thresholds were uniform to 10%. Temperature and flux ratio dependence of faceting during MBE growth over patterned substrates is shown for temperatures ranging from 580 to 700 °C and for As/Ga flux ratios from 1.4:1 to 4:1. The real index guided structure, which can be formed by a single MBE growth over a ridged substrate, is discussed. This technique should prove useful in the fabrication of devices which take advantage of unique features formed during regrowth by MBE.

Growth over patterned substrates has been proposed as a useful technique to increase the flexibility of the molecular beam epitaxy (MBE) process,[1] allowing fabrication of devices which have three-dimensional structure[2] or the integration of devices which have different epitaxial layer requirements.[3] However, the low tolerance of MBE to contamination of the substrate has limited these growths to structures with surface features on the order of 10 μm or more, which can be cleaned by techniques which etch the original surface extensively. Methods which allow the use of MBE to grow epilayers with lateral definition include mechanical masks,[4] masking with dielectric layers,[1] and growth over etched[2,5] or previously grown layers.[3] However, except for regrowths over coarsely featured substrates,[3,6] few electrical or optical properties, or devices which use these techniques have been presented in the literature, presumably because of difficulty with the quality of the epitaxial layers.

The following describes a procedure for MBE growth over finely detailed surfaces, including a surface preparation technique which removes comparatively little material. Laser arrays showing good uniformity and high yield were fab-

 0003-6951/85/190712-04$01.00 © 1985 American Institute of Physics

ricated by epitaxial growth over finely corrugated substrates prepared by this technique. Photographs are presented of multilayer stuctures grown over patterned substrates, showing the dependence of the facet formation during MBE on the As/Ga flux ratio and substrate temperature.

The cleaning procedure is a modification of one described by Cho[7] with the etching times reduced, the bromine/methanol polishing solution at a much lower dilution, and the use of a specially designed Pyrex apparatus which continuously distilled trichloroethylene (TCE) and flowed it over the surface of the wafer.

The wafers were patterned using conventional photolithography, and etched for 10–20 s in 1:8:8 (H_2SO_4,H_2O_2,H_2O) to form grooves of the desired depth. The patterned wafers were boiled in TCE for 10 min and placed in the TCE distillation apparatus for 24 h. The wafer were then lightly hand polished on a lens tissue soaked in a very dilute bromine/methanol solution (~ 1 min in a 0.005% solution by volume) and dip etched in 4:1:1 (H_2SO_4,H_2O_2,H_2O) for 10 s which removes $\sim 0.4\,\mu m$ of material. They were then soaked in HCl for 2 min, and a protective oxide was grown in a de-ionized water bath.[7] The samples were then rinsed and mounted for growth.

The growths were carried out in a Riber 2300 MBE with continuous rotation of the wafer at 12 rpm. Rotation prevents the asymmetrical growth noted in earlier papers.[2,5,6] It can be shown that for a rotating subtrate, the flux on a facet with a tilt of θ is proportional to $\cos\theta$ for all of the Knudsen cells, provided the angles of the facets are not large enough to cause shadowing during some part of the rotation.

The faceting properties of MBE growth over small structures and their dependence on temperature and Ga/As flux ratio can be seen in Figs. 1 and 2 and in Table I. The wafers shown were produced by etching grooves with a 9-μm period in the $[0\bar{1}\bar{1}]$ direction and the $[0\bar{1}1]$ direction, respectively, on (100) substrates. After cleaning by the above procedure, alternating 4500 Å layers of GaAs and 500 Å marker layers of $Ga_{0.8}Al_{0.2}As$ were grown.

The relative growth of adjacent facets can be accurately determined by the propagation angle of their vertex. If the tilt angles of two adjacent facets are taken as α_1 and α_2, and θ is the angle of propagation of their intersection during the growth,

$$\frac{x_1}{x_2} = \frac{\cos\phi_1}{\cos\phi_2} = \frac{\cos(\alpha_1 - \theta)}{\cos(\alpha_2 + \theta)}, \qquad (1)$$

where x_1/x_2 is equal to the ratio of their growth rates, as shown in Fig. 3.

Using this result and a similar one for a convex vertex, from Figs. 1 and 2 we can determine the relative growth rates of small facets. Their growth rates, normalized for the incident flux, are ordered as follows:

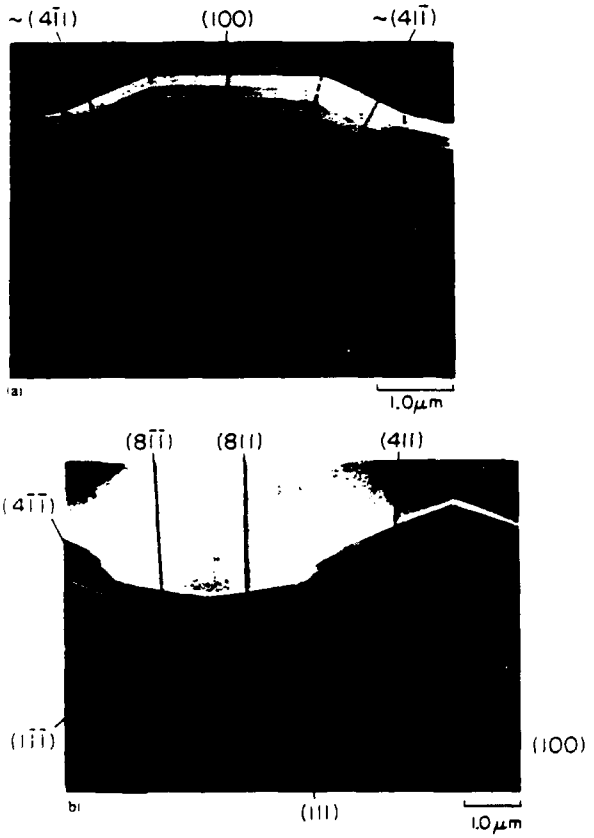

FIG. 1. SEM of 1000-Å alternating layers of $GaAs/Ga_{0.3}Al_{0.7}As$ grown over a (100) substrate ridged in the (a) $[0\bar{1}\bar{1}]$ direction and (b) the $[0\bar{1}1]$ direction, at a substrate temperature of 680 °C and a As/Ga flux ratio of 2, with facet indices marked.

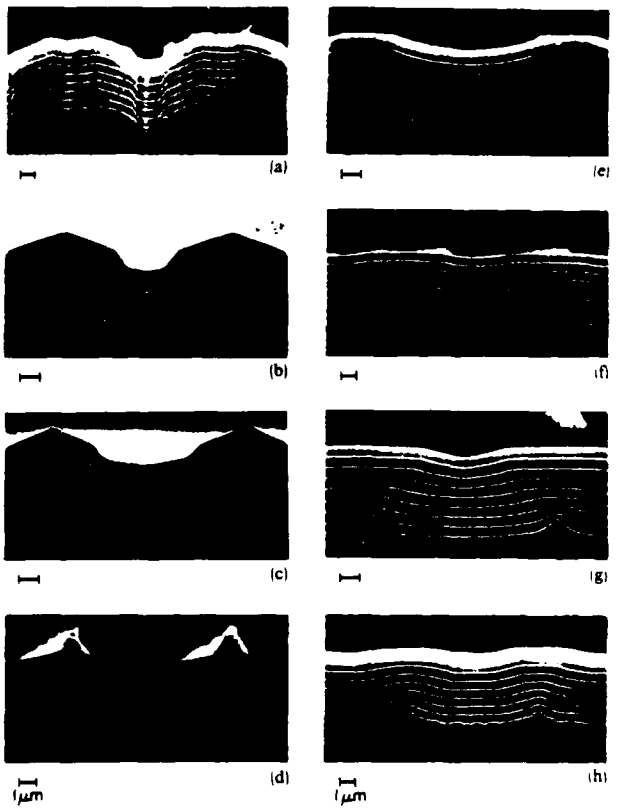

FIG. 2. Photographs showing facet propagation and step propagation as a function of temperature. The samples are composed of 4500-Å GaAs layers and 500-Å marker layers of $Ga_{0.8}Al_{0.2}As$ grown over substrates ridged with a 9-μm period. Samples (a)–(d) were ridged in the $[0\bar{1}\bar{1}]$ direction, grown at substrate temperature 580, 620, 660, and 700 °C, respectively, at a As/Ga flux ratio of 2. Samples (e)–(h) were ridged in the $[0\bar{1}1]$ direction, and grown at the same temperatures and As flux.

TABLE I. Relative growth rates for various facets formed by MBE growth under the states conditions. The range indicated allows for errors in measurements of the photographs. The bottom pairs of figures in each case are normalized for the cos θ dependence of the flux.

Temp	As/Ga ratio	$4\bar{1}1$ vs 100	$4\bar{1}\bar{1}$ vs 100	$1\bar{1}\bar{1}$ vs $4\bar{1}\bar{1}$	$8\bar{1}\bar{1}$ vs $1\bar{1}\bar{1}$
580	2	1.01 ± 0.01	0.90 ± 0.03	0.59 ± 0.02	1.79 ± 0.03
		1.07 ± 0.01	0.97 ± 0.03	0.95 ± 0.02	1.07 ± 0.03
620	2	1.20 ± 0.08	0.78 ± 0.02	0.55 ± 0.02	2.0 ± 0.1
		1.27 ± 0.08	0.83 ± 0.02	0.89 ± 0.04	1.2 ± 0.1
660	2	1.24 ± 0.04	<0.5	0.41 ± 0.06	2.9 ± 0.5
		1.31 ± 0.04	<0.5	0.67 ± 0.10	1.7 ± 0.3
700	2	1.11 ± 0.05	<0.5	0.21 ± 0.04	5.3 ± 0.8
		1.18 ± 0.05	<0.5	0.35 ± 0.05	3.3 ± 0.5
660	1.4	1.12 ± 0.02	0.81 ± 0.02	0.59 ± 0.01	1.83 ± 0.05
		1.18 ± 0.02	0.86 ± 0.02	0.95 ± 0.01	1.10 ± 0.03
660	4	1.14 ± 0.04	<0.5	0.57 ± 0.01	1.86 ± 0.07
		1.21 ± 0.04	<0.5	0.92 ± 0.01	1.11 ± 0.04

$$\left\{\begin{matrix}(111)\\(1\bar{1}\bar{1})\end{matrix}\right\} < \left\{\begin{matrix}(411)\\(4\bar{1}\bar{1})\end{matrix}\right\} < \{(100)\} < \left\{\begin{matrix}(811)\\8\bar{1}\bar{1})\end{matrix}\right\} \tag{2}$$

and

$$\{(100)\} < \left\{\begin{matrix}(4\bar{1}1)\\(41\bar{1})\end{matrix}\right\}. \tag{3}$$

Table I indicates the relative growth rates for these facets over a range of temperatures and pressures. Higher temperatures increase the differential growth rates, while a high As flux decreases it to some extent. The enhancement of the growth rate over the $(4\bar{1}1)$ facet can be taken advantage of in the formation of waveguides, as shown in Fig. 4.

Using this technique, arrays of double heterostructure lasers were grown over a substrate with ridges etched in the $[1\bar{1}1]$ direction with a 9-μm period. The growth consisted of a 0.1-μm GaAs n^+ buffer layer, a 1.3-μm $Ga_{0.7}Al_{0.3}As$ n^+ lower cladding layer, a 1500-Å GaAs active layer, a 1.3-μm $Ga_{0.7}Al_{0.3}As$ p^+ upper cladding layer, and a 0.1-μm p^+ GaAs contact layer. A 150-μm-wide Cr/Au contact was applied, and the wafer was cleaved into bars 350 μm long. The laser cross section is shown in Fig. 5(a) and the spontaneous emission near field is shown in Fig. 5(b). The 1.5× threshold near field is shown in Fig. 5(c) with 15 adjacent pairs of devices of the single contact array lasing, each pair formed on either side of a ridge. The typical threshold current for these arrays was 50–60 mA per element. The elements of the arrays are index guided due to the greater thickness of the active layer over the $(4\bar{1}\bar{1})$ facets as shown in Fig. 4. In the 9-μm ridged array, individual pairs of lasers were phase locked and typically operated in a single longitudinal mode, but the individual pairs oscillated independently. Arrays grown with a 4-μm period phase lock between the pairs as well.

In summary, a technique for growing high quality GaAs/GaAlAs epilayers over patterned substrates has been presented. Laser device yields of greater than 90% have been achieved. We have included detailed scanning electron microscopy photographs of multiple layers grown over wafers with etched ridges a few microns in extent, which allow visualization of the faceting properties of MBE growth. This technique should prove useful in the fabrication of other devices which take advantage of the geometric features of regrowth by MBE and fabrication of integrated structures.

The research reported in this letter is supported through

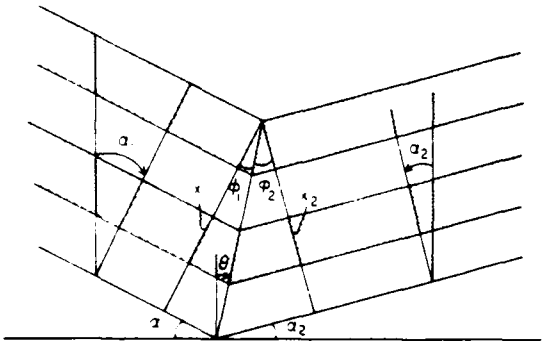

FIG. 3. Diagram relating growth rates of two adjacent facets to the propagation of their vertex.

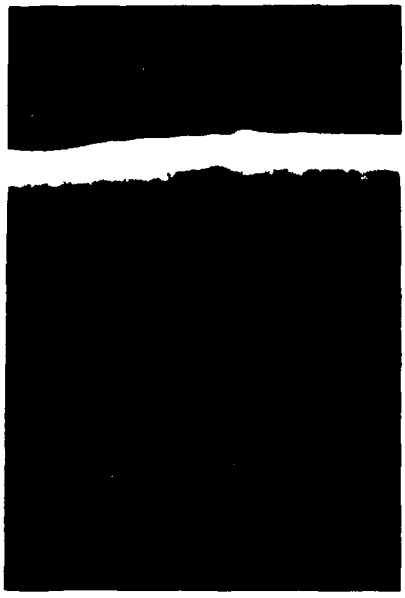

FIG. 4. Photographs of waveguide formed by enhanced growth rate over the $(4\bar{1}1)$ facet.

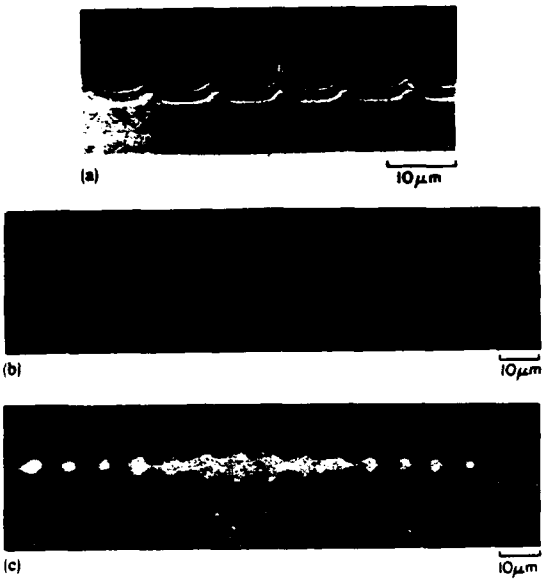

FIG. 5. (a) Cross section of laser array; (b) near field of laser array below threshold; (c) near field of laser array at 1.5× threshold.

contracts with the National Science Foundation, the Office of Naval Research, and the Air Force Office of Scientific Research. J. S. Smith gratefully acknowledges the support of the Fannie and John Hertz Foundation.

[1]A. Y. Cho and W. C. Ballamy, J. Appl. Phys. **46**, 783 (1975).
[2]W. T. Tsang and A. Y. Cho, J. Appl. Phys. **30**, 293 (1977).
[3]T. Sanada, S. Yamakoshi, O. Wada, T. Fujii, T. Sakurai, and M. Sasaki, Appl. Phys. Lett. **44**, 325 (1984).
[4]A. Y. Cho and F. K. Reinhart, Appl. Phys. Lett. **21**, 355 (1972).
[5]S. Nagata, T. Tanaka, and M. Fukai, Appl. Phys. Lett. **30**, 505 (1977).
[6]Y. H. Wu, M. Werner, K. L. Chen, and S. Wang, Appl. Phys. Lett. **44**, 834 (1984).
[7]A. Y. Cho, H. C. Casey, Jr., C. Radice, and P. W. Foy, Electron. Lett. **16**, 72 (1980).

Spatially resolved luminescence near dislocations in In-alloyed Czochralski-grown GaAs

 © 1985 American Institute of Physics

END

6-89

DTIC